PROJECT HYREUS

MARS SAMPLE RETURN MISSION UTILIZING *IN SITU* PROPELLANT PRODUCTION

FINAL REPORT

Space Systems Design, AA 420/421
NASA/USRA Advanced Design Program

Prepared By

Anita Abrego
Chris Bair
Anthony Hink
Jae Kim
Amber Koch
Ross Kruse
Dung Ngo
Heather Nicholson
Laurie Nill
Craig Perras
Susan Peter-Thompson
Peter Sawyer
Heidi Schubert
Eric Schug
Kwong Shek
Brian Smith
Keith Stokke
Gretchen Swanson
Patrick Sweeney
Elsayed Talaat
Lee Thrush
Dave Van Noy
Thu Vu
Leo Warmuth
Richard Warwick
Andre Williams
Michael Wu
Mark Yee

Instructor: Prof. Adam P. Bruckner

Teaching Assistant: Brian Thill

University of Washington
Department of Aeronautics and Astronautics FS-10
Seattle, Washington 98195

July 31, 1993

ABSTRACT

Project Hyreus is an unmanned Mars sample return mission that utlizes propellants manufactured *in situ* from the Martian atmosphere for the return voyage. A key goal of the mission is to demonstrate the considerable benefits of using indigenous resources and to test the viability of this approach as a precursor to manned Mars missions. The techniques, materials, and equipment used in Project Hyreus represent those that are currently available or that could be developed and readied in time for the proposed launch date in 2003. Project Hyreus includes such features as a Mars-orbiting satellite equipped with ground-penetrating radar, a large rover capable of sample gathering and detailed surface investigations, and a planetary science array to perform on-site research before samples are returned to Earth. Project Hyreus calls for the Mars Landing Vehicle to land in the Mangala Valles region of Mars, where it will remain for approximately 1.5 years. Methane and oxygen propellant for the Earth return voyage will be produced using carbon dioxide from the Martian atmosphere and a small supply of hydrogen brought from Earth. This process is key to returning a large Martian sample to Earth with a single Earth launch.

PREFACE

This report is the ninth in a series that began in 1985, when the University of Washington was invited by NASA to participate in what evolved into the highly successful NASA/USRA Advanced Design Program. Under this program our students have examined various innovative design problems related to the critical needs of space prime power, propulsion, and transportation, most based on ongoing research in our Department of Aeronautics and Astronautics.

Last year, based on ideas originally proposed by Robert Zubrin at Martin Marietta, our design project delved into the topic of a manned Mars mission which would make use of *in situ* resources, namely the Martian atmosphere, to manufacture the propellant necessary for the return trip to Earth. This concept makes possible a "direct-to-Mars" scenario that circumvents any need to perform on-orbit assembly of the spacecraft that travel to and from Mars, thus reducing the overall mission costs by nearly an order of magnitude. The growing interest in this mission approach motivated us this year to study the feasibility of an unmanned Mars mission based on indigenous propellant production, with a view to demonstrating the mission-enhancing capabilities of this technology at much lower cost and risk than that of a manned mission. Accordingly, our 1993 design project was chosen to be a rover sample return mission, which we called Project Hyreus. Initially, we focused on the production of methane and oxygen from the reaction of carbon dioxide from the Martian atmosphere with seed hydrogen brought from Earth, but later also examined the alternative of producing carbon monoxide and oxygen directly from the atmosphere, without recourse to any feedstock gases brought from Earth. We found that with either scenario *in situ* resource utilization (ISRU) offers striking benefits compared to conventional sample return mission scenarios, enabling the return of Martian soil and rock samples in quantities two orders of magnitude greater than otherwise possible.

At the NASA/USRA ADP Summer Conference in Houston, in June, several members of NASA Johnson Space Center's New Initiatives Office were present at our students' presentation and invited us to JSC to do a detailed briefing. I am pleased to report that our design study was very well received at JSC, as it was at the Mars Forum II held a few weeks later at the NASA Ames Research Center. Our work was also published as Paper No. AIAA 93-2242 at the AIAA/SAE/ASME/ASEE 29th Joint Propulsion Conference this June, where it generated considerable interest. (For the convenience of the reader the paper is included in this report as Appendix F).

Based on our own work and that of others, we have come to firmly believe that *in situ* resource utilization is the only logical approach to future planetary exploration on a scale that will ultimately lead to humans on Mars and other solar system destinations. Currently, ISRU research and mission analysis is underway at several institutions, including Martin Marietta, NASA LeRC and JSC, the University of Arizona, and the University of Washington. Although much work remains to be done to develop and implement the technology of ISRU, we feel that it can be accomplished at modest cost and on a relatively short time scale. It is not too bold to predict that an ISRU-based mission to Mars could be launched early in the next decade.

Adam P. Bruckner
Professor of Aeronautics and Astronautics
July 31, 1993

ACKNOWLEDGMENTS

The authors are deeply indebted to the NASA/USRA Advanced Design Program (ADP) for the grant that supports the AA420/421 Space Systems Design course at the University of Washington. The USRA ADP staff has provided valuable assistance with various administrative issues related to our program and has helped us with identifying sources of information or data needed for our project. Vicki Johnson, Jack Sevier, and Barbara Rumbaugh deserve special mention. Thanks are also due to our Center Mentor, Frank Swalley, at the Marshall Space Flight Center, for his interest and support.

Many people have provided valuable information and help that contributed in a major way to the successful completion of this design project. Special thanks go to Robert Zubrin at Martin Marietta for his enthusiastic support and for providing information and advice on numerous aspects of *in situ* resource utilization. Diane Linne and Mary Wadel of NASA Lewis Research Center were invaluable for their help with information on rocket engines designed for using indigenous propellants. Tom Callahan, Phil Ginser, and Mike Holquin of General Dynamics provided copious and prompt data on the Titan Centaur. Ed Parsons of the Air Force Public Affairs Office and Capt. Kevin Klonoski of the Titan IV Program Office were extremely helpful and Lt. Tim Dickinson even provided his home number in the event we needed to reach him after hours. Peter Nolan of the University of Arizona provided much useful information about indigenous propellant plants.

We are very grateful to Dana Andrews and Jeff Cannon of Boeing for their advice at our preliminary design review. Their dose of reality was instrumental in improving our design. Thanks are also due to John Jordan of Boeing, who was able to fill in the gaps of our knowledge about the Russian Energia launch vehicle. Robert Hartmann of General Electric promptly sent information about the MOD-RTG space power system. Clarence Quan of McDonnell Douglas

was able to answer all our questions about modifications to the Titan payload fairing, and Tim Voght of Martin Marietta provided the Titan IV launch simulations we requested. We are also deeply indebted to everyone else who provided technical assistance to this project.

Many thanks are due to Dean J. Ray Bowen for helping to make possible our travel to the NASA/USRA Advanced Design Summer Conference in Houston, and to the Department of Aeronautics and Astronautics for its support of the project.

Finally, we would like to express our special gratitude to Professor Adam Bruckner and to our teaching assistant, Brian Thill, both of whom made this class one of our best experiences at the University of Washington.

The AA420/421 Space Systems Design Class
July 31, 1993

TABLE OF CONTENTS

1. INTRODUCTION AND MISSION OVERVIEW 1.1

2. VEHICLE CONFIGURATION AND DESIGN 2.1

3. LAUNCH SYSTEM 3.1

4. ASTRODYNAMICS 4.1

5. ATMOSPHERIC ENTRY AND AEROBRAKING 5.1

6. *IN SITU* PROPELLANT PRODUCTION 6.1

7. MARS SCIENCE 7.1

8. MARS ROVER 8.1

9. SATELLITE OBSERVATION AND COMMUNICATION AT MARS 9.1

10. EARTH RETURN SCENARIO 10.1

11. CONCLUSIONS 11.1

APPENDIX A: THE TALE OF HYREUS A.1

APPENDIX B: MATERIAL SELECTION B.1

APPENDIX C: LAUNCH VEHICLE ANALYSIS C.1

APPENDIX D: CARBON MONOXIDE PRODUCTION D.1

APPENDIX E: MARS BALLOON E.1

APPENDIX F: AIAA PAPER NO. 93-2242 ..... F.1

1.0 INTRODUCTION AND MISSION OVERVIEW

Amber Koch

Andre Williams

TABLE OF CONTENTS

1.1 INTRODUCTION 1.1

1.2 BACKGROUND 1.1

1.2.1 Past and Present Missions 1.1

1.2.2 *In Situ* Propellant Production 1.3

1.3 MISSION GOALS 1.4

1.4 MISSION SUMMARY 1.5

1.5 REPORT ORGANIZATION 1.6

REFERENCES 1.7

FIGURES 1.8

1.1 INTRODUCTION
(Amber Koch)

Project Hyreus is an unmanned Mars sample return mission that utilizes *in situ* propellant production to reduce the amount of mass that needs to be launched from Earth. In other words, the propellant necessary for the return trip is produced using materials from the Martian environment. The demonstration of propellant production from indigenous sources is an important precursor for manned missions to Mars. In addition, the unmanned return of Martian soil and rock samples would prove invaluable for scientific discovery.

1.2 BACKGROUND
(Amber Koch)

Mars is not the nearest planetary neighbor to Earth. However, the red planet has the closest approximation to an Earth-like climate and has historically stimulated the greatest expectations and speculations with regard to extraterrestrial life forms. From the time when the first human eye set view on the Martian surface through a telescope, to the excellent surveys performed by the Mariner and Viking missions, both the scientific community and the general public have held a sincere interest in Mars.

1.2.1 Past and Present Missions

The success of Project Hyreus depends critically upon indigenous propellant production, which in turn depends upon the knowledge of planetary resources. Past missions have contributed greatly to knowledge about the Martian environment. Future missions will contribute even more. The U.S. began exploring Mars with the Mariner

program [1]. Mariner 4 (1965) produced the first photographs of Mars, revealing a landscape similar to the Earth's moon. Additional photographs were taken by Mariners 6 and 7 (1969),which showed that Mars has distinct features such as volcanic mountains, large chasms, and broad terrain. Mariner 9 followed in 1971 and produced a complete map of the Martian surface. The U.S. Viking missions followed in 1976 with the Viking 1 and 2 landers, which successfully conducted surface science, meteorological measurements, detailed surface photography, and exobiological experiments. The Mariner and Viking era of Mars exploration has fortunately provided an excellent knowledge base for all future missions to Mars [2].

Currently, a new phase in Mars exploration is underway, beginning with the Mars Observer (MO) mission which is scheduled to arrive at Mars in August 1993. The main mission objectives of MO are to measure Mars' gravitational and magnetic fields, conduct climatological studies, and produce the highest resolution images ever taken of the surface (1.4 m/pixel). Data obtained from MO will contribute substantially to both current and future missions [2,3].

Russia's Mars '94 is the next mission in line, set for launch in October 1994. This mission will not only carry the first experiments to the Martian surface in nearly twenty years but will also carry the U.S. Mars oxidant experiment (MOX) on board [3].

The next logical step in Mars exploration is to have a global network mission that follows MO and Russia's Mars '94. Two such missions designed to accomplish this step are Mars Environmental Survey (MESUR) and ESA Marsnet (a Mars Network of Surface Stations). Both of these presently slated missions are designed to globally distribute landers on the Martian surface, in order to perform both short and long term observations of the atmosphere and surface. MESUR and Marsnet will assist greatly in laying ground-work for the advancement of future manned and unmanned missions to Mars [2,3].

1.2.2 *In Situ* Propellant Production

The future of Mars exploration is primarily constrained by high cost. The key to reducing mission cost is to use a simplified and streamlined mission architecture. However, the main issue in reducing cost is decreasing Earth launch mass. One method of accomplishing this is to incorporate low mass components into mission architecture, while another is to use *in situ* propellant production [4,5]. While lowering the mass of components has always been important in reducing launch mass, *in situ* propellant production could set precedent for future missions. This method could drastically reduce mission costs, thus expediting a manned mission to Mars.

The concept behind using planetary resources to manufacture propellant is relatively simple. A plant for propellant production is brought from Earth, and upon arrival begins producing propellant from planetary resources. As propellant is manufactured, the return vehicle tanks are filled. The plant may also be used as a refueling station for other mission operations such as surface rovers.

While the feasibility of producing propellant on Mars has been investigated considerably since the early 1970's, the most significant advancements towards incorporating this technology into an actual mission scenario have been in the 1990's [6-9]. R. Zubrin of Martin Marietta first suggested the use of indigenous propellant production as a way to reduce launch mass and increase payload in 1990 [6]. The mission architecture examined by Zubrin uses a Mars-direct conjunction class trajectory, and does not require in-space construction, the use of the Space Shuttle, or the existence of Space Station Freedom [7,8].

In 1992, the NASA/USRA design team at the University of Washington presented the Project Minerva proposal [9]. This proposal called for a series of manned expeditions

to Mars which would rely on propellant produced from the Martian atmosphere and a supply of seed hydrogen carried from Earth. A cost analysis of this mission design indicated that its cost would be approximately 10% of that of the conventional missions that NASA has been studying. Even the much reduced cost of the Minerva manned Mars mission would represent a very large national investment in terms of money, resources, time, and personnel. Therefore, a precursor unmanned mission based as much as possible on existing hardware, should be performed to prove the viability of this mission architecture. Project Hyreus is our proposal for such a mission. Project Hyreus takes the technology of *in situ* propellant production and places it in a cost-effective mission scenario that lays the ground work for future missions to Mars.

1.3 MISSION GOALS
(Amber Koch, Andre Williams)

The primary mission goal of project Hyreus is to demonstrate that *in situ* propellant production can be used as a critical mission element, thus setting the stage for manned exploration of Mars. Another significant goal of the mission is to successfully deliver a Martian soil sample, on the magnitude of 25 to 30 kg, to Earth. Conventional sample returns are envisioned to be of the order of magnitude of 1/4 kg, therefore bringing back upwards of 25 kg would sustain scientific inquiries about Martian material composition for a long time. In addition to the primary mission goals, several other secondary goals exist. These include:

1) Locate water deposits

2) Investigate top soil, underground soil, rock, and lava

3) Investigate surface composition

4) Investigate the existence of life on Mars

5) Investigate volcanic activity

1.4 MISSION SUMMARY
(Amber Koch, Andre Williams)

The mission scenario (Fig.1) begins with a Titan IV launch of the spacecraft and Centaur upper stage into low Earth orbit (LEO). The Centaur then injects the Mars Landing Vehicle (MLV) into a conjunction-class transfer orbit to Mars. The MLV is equipped with a raked-cone aerobrake. The vehicle is captured into an elliptical Mars polar orbit through aerobraking maneuvers, during which the satellite is released into Mars orbit. Additional aerobraking maneuvers are used to initiate descent to the Martian surface. Parachutes and retro-rockets are used to softly land the vehicle in the Mangala Valles region.

Once the MLV is in place, the surface portion of the mission, which lasts for 1.5 years, can proceed. The propellant production plant is activated and begins producing fuel and oxidizer for the rover and return trip. Through a coupled Sabatier and electrolysis process, methane and oxygen are produced by reacting carbon dioxide from the Martian atmosphere with seed hydrogen imported from Earth [3]. The product gases are liquefied and stored in the initially empty tanks of the Earth Return Vehicle (ERV).

The Project Hyreus mission goals are accomplished through the following: a rover is placed on Mars to explore the area around the landing site. The rover, using a variety of attachments such as a "scoobber" on a remote manipulator arm, collects samples for the return to Earth. Using methane produced with indigenous resources for its methane-burning thermophotovoltaic power system, the rover collects 25 to 30kg of soil and rock samples. Additional scientific instruments, which conduct investigations in exobiology, meteorology, and seismology, are mounted directly on the Mars Landing Vehicle (MLV). A satellite, equipped with a ground penetrating radar (GPR), is placed in a near-polar orbit around Mars during the aerobraking maneuvers. The GPR is used to explore the Martian subsurface landscape and detect potential water and ice deposits. In addition, the satellite's

payload includes a communication system and a wide angle camera. The former provides a communication link between the rover and lander when the rover is out of the lander's line-of-sight. The camera system serves as a weather monitoring system, used to warn mission operators of impeding weather conditions, such as dust storms.

The return to Earth begins with the ERV launching from the MLV support structure. The ERV is a single-stage vehicle which first ascends into Low Mars Orbit (LMO) and then performs a burn that places it in an Earth transfer orbit. In the vicinity of the Earth, the Sample Return Capsule (SRC), fitted with an aerobrake, detaches from the ERV and performs an aerocapture maneuver to place it in a Low Earth Orbit (LEO). The ERV continues on a hyperbolic trajectory back to deep space. Once in LEO, the samples can be retrieved by the Space Shuttle (or space station, if operable).

1.5 REPORT ORGANIZATION
(Amber Koch)

Project Hyreus' mission architecture and main components are presented in what follows in the following format: The MLV design and configuration are discussed first. Next, the launch system, astrodynamics, and aerobraking/landing aspects of the mission are presented. Then Martian operations are discussed: propellant production, planetary science, rover, and satellite. Lastly, the Earth return scenario and conclusions are given.

REFERENCES

1. McKay, C.P., *The Case For Mars II*, Umvelt Incorporated, 1984, pp. 99-119.

2. Pritchard, B., "Mars, Past, Present, and Future", *Progress in Aeronautics and Astronautics*, Vol. 145, AIAA Inc., Washington D.C., 1992, Ch 4-7,17-19.

3. Asker, J.R., "Cheaper, Faster Mars Missions in Sight" *Aviation Week & Space Technology*, Vol. 138, April 12, 1993, pp. 50-53.

4. Ash, R.L. and Dowler, W.L, "Feasibility of Rocket Propellant Production on Mars," *Acta Astronautica*, Vol 5, 1983 pp. 705-724.

5. Ramohalli, K., Lawton, E., and Ash, R.L. "Recent Concepts in Missions to Mars: Extraterrestrial Processes," *Journal of Propulsion and Power*, Vol. 5, March-April 1989, pp. 181-187.

6. Zubrin, R.M. and Baker, D., "Humans to Mars in 1990," *Aerospace America*, August 1990, pp. 30-41.

7. Zubrin, R.M., Baker, D., and Gwynne, O., "Mars Direct: A Simple, Robust, and Cost Effective Architecture for the Space Exploration Initiative," AIAA Paper 91-0326, 29th Aerospace Sciences Meeting, Reno, NV, Jan. 7-10, 1991.

8. Zubrin, R. M., "In-Situ Propellant Production: The Key Technology Required for the Realization of a Coherent and Cost-Effective Space Exploration Initiative," AIAA Paper 91-668, 42nd Congress of the International Astronautical Federation, Montreal, Canada, October 1991.

9. *Project Minerva: A Low Cost Manned Mars Mission based on Indigenous Propellant Production,* Final Report, AA420/421 Space System Design, NASA/USRA Design Program, Department of Aeronautics and Astronautics, University of Washington, Seattle, WA, June 1992.

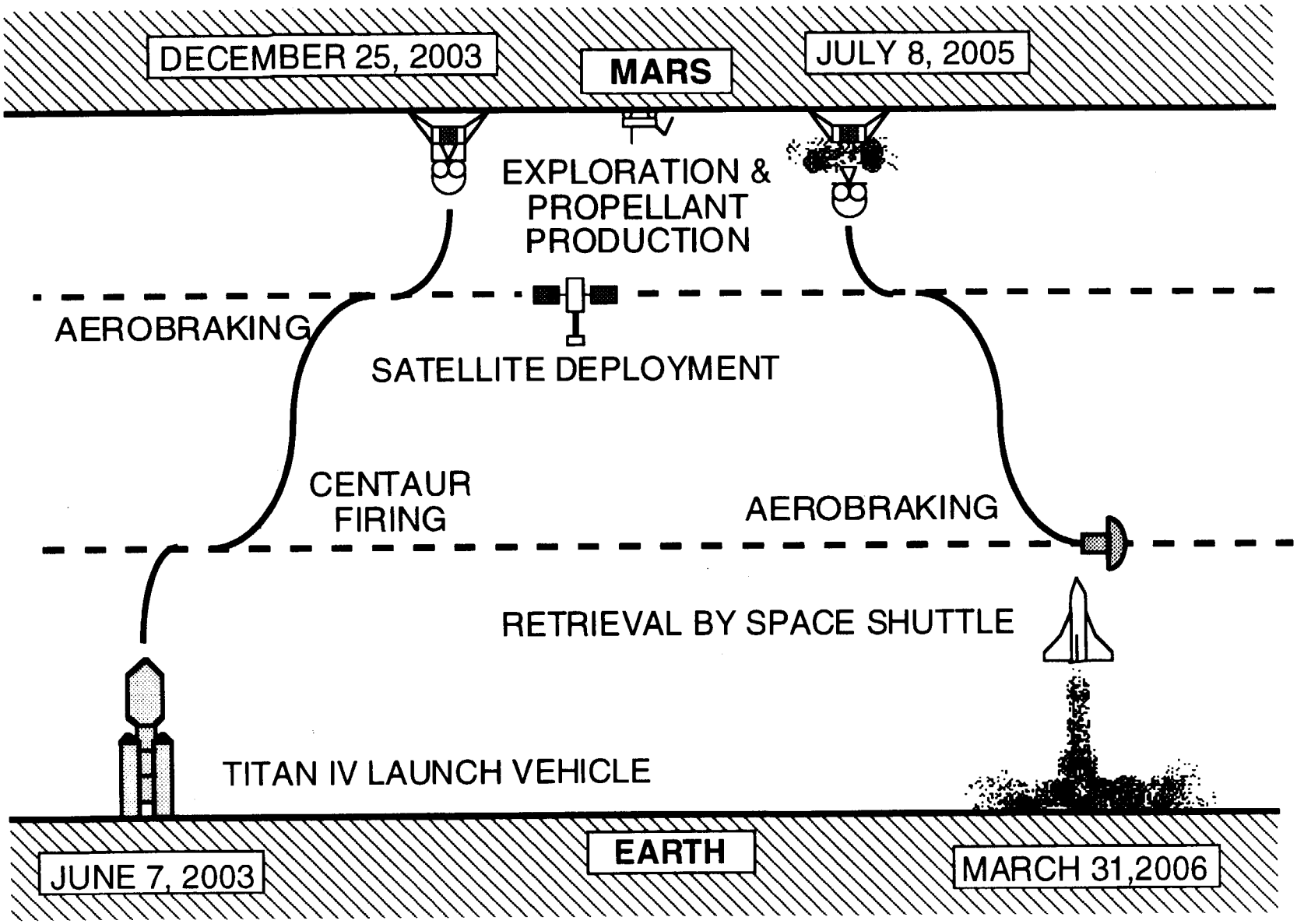

Fig. 1.1 Hyreus mission scenario

2.0 VEHICLE CONFIGURATION AND DESIGN

Ross A. Kruse

Keith A. Stokke

Mark C.C. Yee

Susan Peter-Thompson

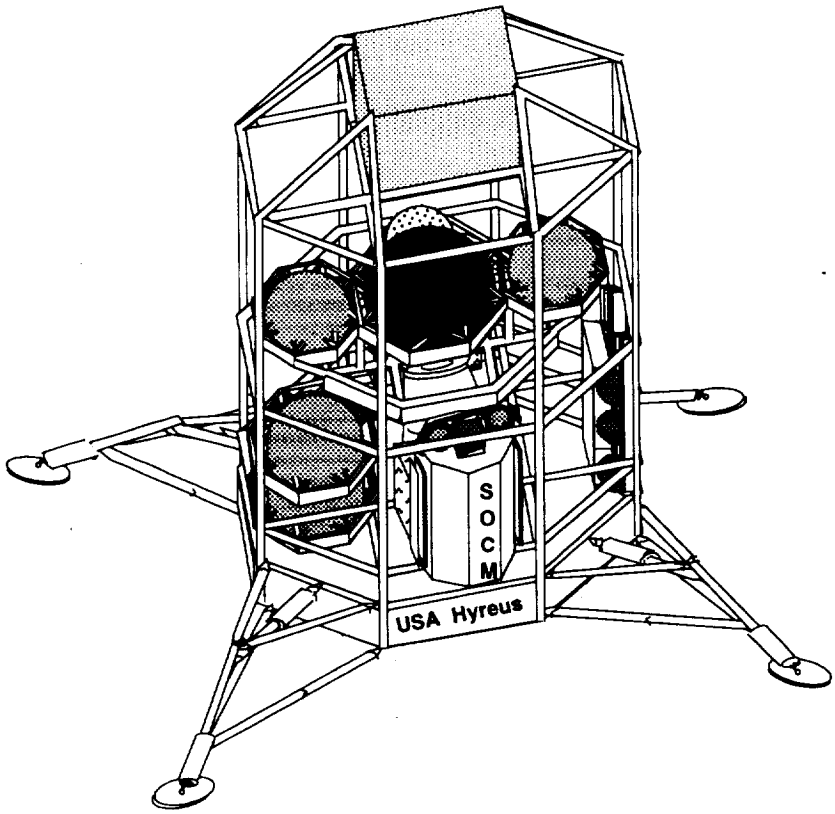

TABLE OF CONTENTS

2.1 INTRODUCTION 2.1

2.2 MLV/ERV CONFIGURATION 2.2

2.2.1 Payload Sizing And Location 2.2

2.2.2 Deployability 2.3

2.23 Aerobrake Location 2.4

2.2.4 Fairing Size 2.4

2.2.5 ERV Design 2.4

2.2.6 Center of Mass Location 2.5

2.3 STRUCTURAL DESIGN 2.7

2.3.1 MLV Structure 2.7

MLV Truss Frame 2.7

MLV Thrust Structure 2.8

Centaur Adapter 2.9

Landing Gear Configuration 2.10

2.3.2 ERV Structure 2.12

2.3.3 Propellant Tank Design 2.13

Tank Structural Analysis Methodology 2.13

Propellant Tank Support Struts 2.19

Propellant Tank Orientation 2.20

2.4 DEPLOYMENT AND LOADING MECHANISMS 2.21

2.4.1 Satellite Deployment 2.21

2.4.2 Aerobrake and Parachute Detachment 2.21

2.4.3 Rover Deployment 2.22

2.4.4 ERV Separation and Sample Capsule Detachment 2.22
2.4.5 Sample Return Loading 2.23
2.5 METHANE ROCKET ENGINE DESIGN 2.23
2.5.1 Existing Technology 2.24
2.5.2 Engine Design 2.26
2.6 LANDING ENGINES AND REACTION AND CONTROL SYSTEM 2.28
2.6.1 Landing and RCS Engine Selection 2.28
2.6.2 Landing and RCS Engine Location 2.30
2.7 VEHICLE MASS INVENTORY 2.31
2.8 CONCLUSION 2.32
NOMENCLATURE 2.34
REFERENCES 2.36
FIGURES 2.38

2.1 INTRODUCTION
(Keith Stokke)

The structure of a spacecraft is very critical in that it must be as lightweight as possible, yet still be strong enough to withstand a variety of often unpredictable loading throughout its lifetime, without maintenance or opportunity for repair. The vehicles used to meet the mission objectives of project Hyreus are designed keeping this in mind.

There are two vehicles used in this project, the Mars Landing Vehicle (MLV) and the Earth Return Vehicle (ERV). The MLV carries all of the payload to Mars and is mounted above the Centaur during Earth launch using the Centaur adapter, which is discussed in Section 2.3. After aerobraking and parachuting is complete (discussed in Chapter 5), the MLV will land on the Martian surface using retro-firing. The ERV is mounted within the MLV until it is time for the return trip to Earth. At this point it will separate from the MLV and launch into its transfer orbit. The Mars launch is discussed in Chapter 3. The payload of the ERV consists mainly of the samples to be returned to Earth and the necessary propellant tanks. Figure 2.1 shows the two nestled vehicles with the MLV landing legs in the deployed position.

This chapter explains the configuration of the two spacecraft, the structural design and integration of structural components, the deployment mechanisms, the materials used, and the propulsion systems. It is divided into the following five subsections: MLV/ERV configuration, structural design, deployment mechanisms, methane engine design, and landing engines and reaction and control system.

2.2 MLV/ERV CONFIGURATION
(Ross Kruse)

The configurations of the Mars Landing Vehicle (MLV) and Earth Return Vehicle (ERV) shown in Fig. 2.1, are based upon seven criteria. Each criterion was treated with equal weight in the overall final configuration. The seven criteria that govern our configuration are:

- sizing and locating each payload component
- any necessary deployment of payload
- fitting the raked cone aerobrake
- fitting the entire structure in an existing fairing
- stability of launch of the ERV.
- horizontal location of the center of mass (c.m.)
- vertical location of the center of mass (c.m.)

The MLV and ERV configurations are shown in Figs. 2.2 and 2.3 respectively. Each of the design criteria are discussed in greater detail in the following sections.

2.2.1 Payload Sizing and Location

The purpose of this criterion is to make certain that components that need to be close to each other or apart from each other are. The propellant plant is located close to the hydrogen, methane, and oxygen tanks to minimize the distance for fuel transfer. Also, the propellant plant needs to be accessible to the rover. The propellant plant has radiators that are located on the outside of the MLV for cooling purposes. The rover will need to refuel periodically, hence the propellant plant is located close to the exterior of the MLV vehicle for refueling purposes. The seed hydrogen tank needs to be as far as possible from the Dynamic Isotope Power System (DIPS) for launch safety reasons. The

DIPS radiators also are located on the outside of the MLV. The Mars science equipment is located near the side of the MLV so that the rover can access the equipment. In addition, the science equipment will also be taking soil samples directly from the spacecraft using a large retractable arm, therefore the science equipment is located near the ground also. The Mars science equipment is located directly beneath the sample return capsule to allow transport of the soil samples from the Mars science equipment and the rover using the same retractable arm. Figure 2.1 and Fig 2.3 show the orientation of the various payload components.

2.2.2 Deployability

This criterion is not as flexible as other criteria are. Certain items of payload are located in particular locations so that they can be deployed properly. The satellite needs to be deployed first, so it is located on the side of the MLV. The only other possibility is to locate it on top of the MLV. However, this presents problems because the satellite has a large mass and shifts the center of mass too high if it is positioned at the top.

The parachute canister needs to be located at the top of the MLV so that when the parachutes are deployed, the MLV will be oriented with the landing gear toward the surface. In addition, the parachute canister also has to be located horizontally over the center of mass.

The rover is oriented vertically, as shown in Figs. 2.1 and 2.3, attached to a pair of deployable channels, as shown. These two wheel-channels are attached to the exterior truss struts of the MLV. Once the vehicle lands, the channels swing out and down simultaneously, providing a ramp for the rover to descend to the Martian surface, as illustrated in Fig. 2.4.

2.2.3 Aerobrake Location

The aerobrake is very cumbersome because it is 2 m wider and 4 m taller than the MLV. It also comprises approximately 15% of the mass of the MLV. To maintain the mass symmetry of the vehicle, the other components are shifted slightly toward the side opposite of the aerobrake. The sides of the aerobrake are also folded in to accommodate the fairing size. Section 5.5.1 shows how the aerobrake is oriented. A requirement that the aerobrake has is that the center of mass of the MLV after Centaur separation be located at a point 2.7 m above the bottom of the MLV thrust structure for the purpose of aerodynamic stability during the aerobrake maneuvers. The center of mass during aerobraking is calculated by subtracting the mass of the Centaur adapter from the original center of mass determination. A full description of the aerobrake design and maneuvers is presented in Section 5.

2.2.4 Fairing Size

The fairing required for enclosing the MLV atop its launch vehicle is the largest one that has been used to date for the Titan IV launch vehicle [1]. It is important not to exceed this size requirement, in order to keep launch costs down. If a larger fairing were used, then new tooling could need to be designed for manufacture, thus inflating the cost of the mission. Figure 2.2 shows how all of the payload fits into the 7 m diameter fairing.

2.2.5 ERV Design

The ERV, Fig. 2.2, is located within the MLV, as shown in Figs. 2.1 and 2.2, because as its propellant tanks are filled on Mars, the mass of the MLV will almost double and it is desirable for the center of mass of the MLV to stay close to its original landing location. It is important that the center of mass not be allowed to move much while on Mars, because if it were to, it could cause the MLV to become unstable,

possibly resulting in the entire vehicle leaning to one side. The ERV payload is symmetric with respect to an axis that runs through the center of the ERV and also through the centerline of the methane ascent engine. This symmetry provides greater stability on launch from the Martian surface because when the methane engine is directly beneath the center of mass of the ERV it is able to utilize its thrust vectoring system. It is also vital for control purposes that the center of mass of the ERV be located in the center of the vehicle. A full description of the methane return engine and its means of control is presented in Section 2.5.

2.2.6 Center of Mass Location

The horizontal location of the center of mass is important for launch control and structural support. The payload is configured in several layers. Each layer is designed so that the center of mass is at the center axis of the MLV. The payload in each layer is close to symmetric with respect to the axis originating from the center of each layer. Fig 2.2 shows plane cuts of the MLV and the symmetry in each layer. The horizontal center of mass needs to be as close to the center as possible, to allow for more uniform structural support and to minimize the difficulties in controlling the MLV during launch. In addition, the center of mass upon launch can be a maximum of 0.2 meters (8 inches) off center horizontally. This is a requirement of the Titian IV and Centaur launch vehicle combination [1]. As designed, the center is located 0.002 m (0.1 in) in the x-direction (horizontal) and 0.012 m (0.46 in) in the negative z-direction (aft). The reference origin is located in the center of the MLV. The horizontal location of the center of mass is denoted in Fig. 2.5.

The vertical location of the center of mass is important for launch from Earth. There is a maximum vertical center of mass location for launching a particular payload mass. Our maximum center of mass location is 4.2 m (168 in) above the Centaur

interface plane [1]. If the center of mass is higher than this, then either a structural upgrade for the Centaur or a decrease in the mass of payload would be required. The structural upgrade would increase the cost of the mission. Alternatively, if the mass of the payload were to be decreased instead then not all mission objectives might be met. To keep the center of mass as low as possible, the widest payload fairing available has been chosen. Thus the payload is distributed horizontally rather than vertically, lowering the overall center of mass. The height of the center of mass is located 4.18 meters (164 inches) above the interface between the Centaur and Centaur adapter. Figure 2.5 shows the location of the center of mass with respect to the Centaur interface plane.

Table 2.1 Center of masses throughout the mission

Configuration	Vertical Location of the Center of Mass (m)	Horizontal Location of the Center of Mass (m)	Forward (pos-x) or Aft (neg-x) Location of the Center of Mass (m)
Launch from Earth Before any Payload is Deployed	4.18 m	0.002 m	0.01 m
After the Centaur Adapter is Detached	2.65 m	0.002 m	0.01 m
After Satellite is Deployed	2.76 m	0.002 m	0.18 m
After Aerobrake is Jettisoned	2.35 m	0.003 m	0.13 m
After Parachutes are Detached	2.08 m	0.003 m	0.14 m

It is necessary that the location of the center of mass be known at various points during the mission. Table 2.1 gives a compilation of masses at points during the mission after various items of payload are detached or deployed. From the point at which the

Centaur is released, the vertical location of the origin is changed to the bottom of the MLV. Therefore all of the center of mass locations except at launch from Earth are measured from the base of the thrust structure on the MLV.

2.3 STRUCTURAL DESIGN

(Ross Kruse, Keith Stokke)

Structural design includes structural analysis, fabrication, and assembly of structural components as well as the integration of the various components. There are several structural components that must be designed and assembled to form the overall spacecraft structure. The structural design is organized into the following sections: MLV structure, ERV structure, and propellant tanks. The following subsections explain the structural analysis and assembly of each of these items.

2.3.1 MLV Structure

The structure of the MLV is organized into sections for the main structural components. These components are the truss (primary) frame, the MLV thrust structure, the Centaur adapter, and the landing gear.

Truss (Primary) Frame

The frame of the MLV is primarily a truss-frame with support struts to hold various equipment and tanks in place. Skin is not used, except where it is needed for shielding purposes in some places. The method of the structural analysis is outlined below.

The first step is to design a preliminary structure based on elementary static truss analysis. After a reasonable preliminary design is developed, a more advanced structural

analysis can be performed. The next step is to do a finite element analysis of the structure, using a program called FRED, developed by K. Holsapple at the University of Washington. There are several important design criteria which are followed. These criteria include simplicity (few members), high strength, low mass, and low cost. Having as few members as possible not only yields a mass savings but also provides easier assembly because fewer joints are needed.

The truss frame is shown in Fig. 2.6. It consists of five octagonal rings with vertical members at the corners and diagonal cross-members for additional stiffness. Between the thrust structure and the bottom ring of the truss frame both internal and external cross-members are used, because a majority of the payload is located here. Above the ERV no internal cross-members are used (except to attach the parachute), in order to leave open space for the ERV to be launched. The structural members are aluminum-lithium 2090 tubing with a 4 cm OD and a 3.6 cm ID. The joints are welded. The frame structure was developed using a 68 node, 200 element finite element model that assumes three degrees of freedom per node, with uniaxial rod elements. Analysis was done for both static loading with 10 g's due to launch, which is considerably more than what is actually seen, and for aerodynamic loading from aerobraking. In both cases the nodal displacements were found to be quite small, on the order of 0.1 mm.

MLV Thrust Structure

The thrust structure for the MLV must support the primary truss frame and serve as the attachment point for the landing engines. Also, the Centaur interface structure, discussed next, must be joined to this structure until it is jettisoned at the appropriate time. Because of this, this thrust structure must be strong enough to handle the thrust loads of the landing engines and the Centaur. The thrust structure used for the MLV, shown in Fig. 2.7, is a modified Boeing thrust structure. It consists of eight 5.5 m long

beams attached to the inside of an octagonal ring. The beams are made of conventional stiffened web and chord construction made of aluminum 7075 alloy [2]. The landing, reaction, and control engines are arranged in four clusters and mounted on the cross-members. These engines are discussed in Section 2.6.

Centaur Adapter

The Centaur adapter is a temporary structure that is used to mount the MLV to the Centaur during launch and orbital maneuvers, before it is jettisoned. There are two methods of attaching a spacecraft to the Centaur: using a spacecraft-peculiar adapter or using a truss adapter [1]. The spacecraft-peculiar adapter method, or 8-hard point interface, has been selected because it is more flexible and allows the thrust structure to have a larger diameter than the interface surface, which is about 3 m.

The adapter, which must withstand the Centaur thrust of 73 kN, is comprised of a small ring that attaches to the Centaur, a larger octagonal ring that attaches to the MLV, and diagonal truss members which connect the two. Figure 2.8 shows the adapter. The small ring is fabricated of aluminum-lithium 120° angle stock, and has a 120° cross-section and an inside diameter of 2.95 m. A 2.84 m bolt circle is drilled in this ring for attachment to the Centaur interface surface. The large ring is about the same size as the MLV thrust structure octagonal ring but is made from 30° angle stock. This ring is attached to the MLV thrust structure with pyrotechnic bolts in order to separate the adapter from the MLV after Centaur burn. The upper and lower rings are attached to each other by 16 aluminum-lithium 2090 rectangular struts. The struts are 1.7 m long, 6 cm wide, and 1 cm thick. The struts are designed to not buckle under the applied compressive load even if any two of the other struts fail. The cross-sectional area is determined from the moment of inertia necessary to satisfy Euler's buckling equation:

$$I = \frac{Fl^2}{E\pi^2} \tag{2.1}$$

where F = Force in each member

I = Moment of inertia

E = Modulus of elasticity

l = length of member

Landing Gear Configuration and Structure

The landing gear of the MLV, shown in Fig. 2.9, is designed to withstand a 10 Martian-g impact load per leg [5]. The impact force is calculated using 2650 kg as the mass of the MLV when it lands, thus, a 10 Martian-g impact load is equal to 24,850 N. The majority of this impact force is absorbed by a shock absorber on each leg. The position of the shock absorber can be seen in Fig. 2.9. In addition, the landing gear is designed to support the static load resulting from the weight of the spacecraft. The wet mass of the MLV before the ERV is launched back to Earth is 6970 kg. Hence, each leg can support a 6500 N static load.

The landing gear consists of six hollow cylindrical truss members, a shock absorber, a screw actuator, and a foot pad. The 3 cm OD and 2.8 cm ID circular truss members are made of aluminum-lithium 2090. The members are connected together using titanium hinge joints. Screw actuators are used to deploy the landing gear before landing. Screw actuators were chosen because when the legs are fully deployed the actuators can act as load bearing members. Once on Mars the screw actuators will also be used to level the ship. The landing gear is in a retracted position during the trip to Mars. The two lower landing gear support struts telescope to enable the landing gear to be stowed in a compact position. The deployed and retracted landing gear positions can be seen in Fig. 2.9. When the landing gear is in its fully deployed position, it gives a 1 m

clearance between the bottom of the MLV and the Martian surface. The reason for this clearance is to avoid landing the MLV on a rock that could do damage to the MLV structure or cause the MLV to skew and possibly tip over. To support any lateral loads on the landing the landing gear outer strut is designed to have a 60° angle. Also, each landing pad is located 1.6 m horizontally from the vehicle. This provides the MLV with the needed stability to run science experiments, to produce propellant, and to increase its overall mass as the propellant tanks are filled. Each foot pad is made out of a honeycomb composite material [5]. These pads can compress upon landing to further absorb the shock of landing.

The mass of each landing gear member is a function of the various axial loads that exist in each leg. The force in each member was calculated using static and dynamic loading methods [5]. Each member was designed to withstand compression loading so that the legs would be rigid in their design. Once the force in each leg was found, the cross-sectional area could be calculated using the following equations.

For members in compression:

$$I = \frac{Fl^2}{\pi^2 E} \tag{2.1}$$

$$I = \frac{\pi r^4}{4} \tag{2.2}$$

$$A_c = \pi r^2 \tag{2.3}$$

where:

A_c = Cross-sectional area

F = Force in each member

σ = Allowable yield stress for aluminum-lithium 2090

I = Moment of inertia

E = Modulus of elasticity

r = radius of each circular member

Using the cross-sectional area the mass of each member is found using the following equations:

$$m = \rho A_c l \tag{2.4}$$

ρ = Density of aluminum lithium 2090

A_c = Cross-sectional area

l = length of the member

The total mass of each leg is 15.5 kg. Of the 15.5 kg the screw actuator and shock absorber make up 9 kg.

2.3.2 ERV Structure

The structure of the ERV is of fairly simple design. It consists of only a thrust structure, which is discussed below, with support struts as needed to attach the propellant tanks and the sample return capsule with its aerobrake. The support struts are made of aluminum-lithium tubing with an OD of 4 cm and an ID of 3.6 cm.

The ERV thrust structure is different from that of the MLV for a few reasons. It is smaller because it must support only the mass of the return propellant tanks and the sample return package, and needs only to withstand a thrust of 24 kN from the methane ascent engine (see Section 2.5). Another difference is that the methane engine must be attached in a different manner from the landing engines because it must be connected to a gimbal in order to vector its thrust.

The ERV thrust structure, Fig. 2.10, is composed of two main parts, a main payload bearing ring and a thrust frame. The ring is octagonal and is made of aluminum-lithium 2090 I-beams. The I-beams are 10 cm high and 5 cm wide with a web thickness of 1 cm. The thrust frame is made up of eight members which are made of aluminum-lithium 2090 tubing. Each member has an OD of 4 cm and an ID of 3 cm. The members

are welded together at the joints. The cross-sectional area of the members is determined using the same buckling criteria as discussed previously. The gimbal assembly is attached to the gimbal point as shown in Fig. 2.10. The thrust frame is welded onto the inside of the main ring at four points.

2.3.3 Propellant Tank Design

The propellant tank configuration is essential in determining the size and available space on the return vehicle. Propellant tanks are needed for oxygen and methane for the return trip, as well as for the seed hydrogen needed for propellant production. A structural analysis was done based on the required amount of propellant. The method is described below.

Tank Structural Analysis Methodology

The first step in designing the propellant tanks is to determine the amount of volume that is needed to store the propellant and oxidizer for the return trip. The storage conditions used for methane, oxygen, and hydrogen for the calculations are listed in Table 2.2.

Table 2.2 Storage condition and properties for propellants

Fuel	Pressure (atm)	Temperature (K)	Density (kg/m^3)
Methane	10	135	445
Oxygen	7.1	108.2	1068
Hydrogen	10	15	72.3

The total amount of propellant that is needed for the return trip is 2300 kg. The ratio of fuel to oxidizer mass is 1:4. To find the total volume of each tank, an ullage

volume, boil-off volume, and trapped volume must be added to the usable volume needed for the propellant. The ullage volume is 2.5% of the sum of the trapped volume and the usable volume [3]. To a good approximation the boil-off volume is 8% of the usable volume [3]. The total volume, V_t, is found using the following equation [3]:

$$V_t = V_o + T + B + U_o \tag{2.5}$$

where:
- V_o = usable propellant volume calculated from propulsion-system requirements
- T = trapped-propellant volume
- B = boiled-off propellant volume
- U_o = tank ullage volume

All of the tanks are designed to withstand both the pressure needed to keep the propellants in a liquid state and the axial and lateral loads due to launch. First, the thickness needed for a tank to withstand its given storage condition is determined. This thickness is then compared to the thickness needed to withstand the axial and lateral loads due to launch. The greater of the two thicknesses is used for each tank. The thickness of the cylindrical tank portion of a cylindrical tank with spherical or elliptical ends may be different from that of the ends. An appropriate material is chosen for the tank structures. The safety factors used are 2 for ultimate stress and 1.6 for yield stress, corresponding to a condition for no structural test [4].

The size and number of tanks that are needed for a particular tank configuration needs to be decided first. Then the thickness needed for a particular-sized tank to withstand its storage pressure can be determined. The equations for determining the thickness depend on what type of tank it is. Three types of tanks were considered in the design process; spherical, cylindrical with spherical ends, and cylindrical with elliptical

ends. The equations used for determining the thicknesses of the walls of these tanks are shown below [3]:

$$t_s = \frac{p_t r}{2 S_w e_w} \tag{2.6}$$

$$t_k = \frac{K p_t r}{S_w e_w} \tag{2.7}$$

$$t_{cr} = \frac{p_t R}{2 S_w e_w} \tag{2.8}$$

$$t_e = \frac{(t_k + t_{cr})}{2} \tag{2.9}$$

$$t_c = \frac{p_t r}{S_w e_w} \tag{2.10}$$

where:

t_s = spherical wall thickness

t_e = elliptical and spherical end wall thickness

t_k = wall thickness at knuckle

t_{cr} = wall thickness at the crown

t_c = cylindrical wall thickness

p_t = maximum tank operating pressure

r = tank radius

S_w = maximum allowable operating stress of material

e_w = weld efficiency

R = tank end crown radius

K = stress factor

The crown thickness of a cylindrical tank is located where the axis crosses the spherical or elliptical end. The knuckle thickness of a cylindrical tank is located where the cylinder joins the spherical or elliptical end. Figure 2.11 illustrates this nomenclature [3]. The weld efficiency is a measure of how well two pieces of metal are welded together. The stress factor a design safety factor which accounts for discontinuities, it is a function of

ellipse ratio, membrane stress, discontinuity stress, and local-bending stress, and is obtained from Fig. 2.12 [3].

It is not necessary to consider the loads due to launch at Earth for the return tanks because they contain no propellant and are pressurized during Earth launch. The thickness that is needed for the seed hydrogen tank to withstand axial and lateral loads due to launch must be calculated. The wall thickness required for this tank to withstand launch accelerations can be found from the following equations [3]:

$$t_c = \frac{P_{eq,c}}{2\pi r S_w} \tag{2.11}$$

$$t_e = \frac{P_{eq,e}}{4\pi r S_w} \tag{2.12}$$

$$P_{eq,c} = P_{axial} + \frac{2M}{r} \tag{2.13}$$

$$P_{eq,e} = P_{axial}$$

where:

t_c	=	spherical or elliptical wall thickness
t_e	=	cylindrical wall thickness
r	=	tank radius
S_w	=	maximum allowable operating stress of material
P_{eq}	=	equivalent load produced by axial force and bending moment
P_{axial}	=	vertical load on tank
M	=	bending moment

The distributed axial or vertical load on the tank is found by multiplying the weight of the propellant by the total acceleration at launch. The axial load is a combination of steady-state and dynamic accelerations. These accelerations can be found from launch vehicle data. The spherical ends need only to withstand the axial force.

Once the wall thickness of the tank has been decided, the corresponding mass of the tank can be determined. When deciding on a particular tank configuration it is important to consider both the weight and the volume. In addition, the amount of insulation needed to hold the tank at a certain temperature should also be considered. These factors were considered and implemented into the configuration design process. The tank insulation analysis is discussed in Section 3.3.1. The mass of the tanks is calculated using the following equations [3]:

$$m_s = 4\pi r^2 t_s \rho \tag{2.14}$$

$$m_c = 2\pi r l_c t_c \rho \tag{2.15}$$

$$m_e = \frac{\pi r^2 t_e E' \rho}{2k} \tag{2.16}$$

where:

m_s = mass of spherical tank or spherical tank ends

m_c = mass of cylindrical tank

m_e = mass of elliptical tank ends

r = radius of the tank

t_s = thickness of spherical tank or tank ends

t_c = thickness of cylindrical tank

t_e = thickness of elliptical ends

l_c = length of cylindrical portion of the tank

E' = design factor (function of ellipse ratio)

k = tank-end ellipse ratio (minor axis length / major axis length)

ρ = density of the tank material

The critical pressure allowable for exterior loading was also calculated. The critical pressure is the amount of exterior loading pressure from support struts that a particular tank design can withstand. This is important to take into consideration when

choosing a thickness of a particular tank. If the exterior loading pressure exceeds the critical pressure calculated for a certain tank thickness, then the thickness of the tank must be increased. The following equations are used to calculate the critical pressures of the tanks [3]:

$$P_{cr,c} = \frac{Et_c^3}{4(1-\nu^2)r^3} \tag{2.17}$$

$$P_{cr,e} = \frac{C_b 2Et_e^2}{R^2} \tag{2.18}$$

$$P_{cr,s} = \frac{0.342Et_s^2}{r^2} \tag{2.19}$$

where:

$P_{cr,c}$ = critical pressure on cylinder

$P_{cr,e}$ = critical pressure on elliptical end

$P_{cr,s}$ = critical pressure on spherical end

r = tank radius

R = tank-end crown radius

E = modulus of elasticity

C_b = buckling coefficient

ν = Poison's ratio

t_c = thickness of cylinder

t_e = thickness of ellipsoidal end

t_s = thickness of spherical end

The buckling coefficient is a constant that is used in design to account for the buckling of the propellant tanks. The buckling coefficient is a function of the ratio of radius to tank end wall thickness. It ranges from 0.05 to 0.1 [3].

The characteristics of the various propellant tanks for the selected configuration have been compiled into Table 2.3 for both Aluminum 2219 and Weldalite-049. The selected material is Weldalite-049; the other alloy is shown as a comparison only. The configuration of the tanks is shown in Figs. 2.1 and 2.3. It consists of a cylindrical tank with spherical ends for the seed hydrogen and spherical tanks for both oxygen and methane. The methane is divided into two spherical tanks in order to help make the ERV symmetrically balanced.

Table 2.3 Methane, oxygen, and hydrogen tank characteristics.

Propellant	Type of Tank	Radius (m)	Length (m)	Wall Thickness (mm)	Mass (kg)	Critical Pressure (Pa)
		Weldalite™-049 (Al-Li alloy)				
Methane	Spherical (2 tanks)	0.55	-----	1.1	22.1	1.01×10^6
Oxygen	Spherical	0.79	-----	1.1	23.5	5.11×10^5
Hydrogen	Cylindrical	0.7	0.63	2.7	40.7	9.58×10^3
	Spherical Ends	0.7	-----	1.2		8.58×10^4
		Aluminum 2219-T81				
Methane	Spherical (2 tanks)	0.55	-----	1.5	32.0	1.82×10^5
Oxygen	Spherical	0.79	-----	1.5	33.8	9.16×10^5
Hydrogen	Cylindrical	0.7	0.63	3.9	61.1	1.62×10^5
	Spherical Ends	0.7	-----	3.1		1.54×10^4

Propellant Tank Support Struts

The spherical oxygen and methane tanks are held in place in the ERV using octagonal rings, as shown in Fig. 2.3. These rings are attached to vertical struts, which in

turn attach to the thrust frame of the ERV. The cylindrical hydrogen tank is attached to the MLV using two octagonal rings. The hydrogen tank attachment is the same as that of the methane and oxygen tanks, except for the hydrogen tank there are two. The octagonal rings are connected to the MLV using vertical and horizontal tubular truss struts.

Propellant Tank Orientation

The oxygen tank, when full, has the highest mass of any component on the MLV or the ERV. It was placed in the center of the ERV to minimize the lateral loads due to launch for the return trip from Mars. The methane propellant was separated into two separate tanks, in order to make the ERV as symmetric as possible. It was important to have the ERV symmetric during its filling period on Mars and for purposes of controlling the ERV during launch. The methane and oxygen tank locations are shown in Fig. 2.3. The hydrogen tank is located in close proximity to the propellant plant on the MLV and far from the DIPS, as shown in Fig. 2.2.

2.4 DEPLOYMENT AND LOADING MECHANISMS

(Ross Kruse, Keith Stokke)

There are five items that are deployed at various times during the mission. First, the satellite is detached during the aerocapture and landing maneuvers at Mars. Next, when the aerobrake has completed all of its necessary passes, it is jettisoned from the MLV. The MLV then deploys its parachutes for the second stage of deceleration in the Martian atmosphere. When the parachutes have served their function they are detached along with their casing. Once the MLV is on the Martian surface, the rover is deployed. Upon launch back to Earth, the ERV separates from the MLV. Once the ERV reaches Earth orbit, the sample return capsule is jettisoned from the ERV. All of the detachment,

deployment, separation, and jettisoning of the various components is achieved by using pyrotechnic fasteners.

2.4.1 Satellite Deployment

The satellite (see Chapter 9) is the first item of payload to be deployed. During transit the satellite is stored on the side of the MLV as shown in Figs. 2.1 and 2.2. This allows for easy detachment in Mars orbit. The aerobrake is positioned on the opposite side of the MLV so that it will not interfere with the satellite deployment. Once in the correct Martian orbit for the satellite, it is released using pyrotechnic bolts. The points of detachment can be seen in Fig. 2.13. The satellite uses its own thrusters to place itself in its required circular orbit.

2.4.2 Aerobrake and Parachute Detachment

The aerobrake is the first stage in slowing down the MLV during the landing maneuvers. Once the aerobrake is no longer needed, it is detached using pyrotechnic bolts. Following detachment, the parachutes are deployed, lifting the MLV away from the aerobrake. When the parachutes have served their purpose, they are jettisoned along with their storage canister. This is also done using pyrotechnic bolts. The detachment points of the aerobrake and parachutes are shown in Fig. 2.13.

2.4.3 Rover Deployment

The rover is stored vertically in the lower portion of the MLV. The rover wheels are prohibited from rolling in the two channel tracks by using pins which extend into the wire mesh wheels. A tension cable is used to attach the rover to the MLV truss frame. This cable supports the majority of loads during to launch and descent. The transit storage position can be seen in Fig. 2.2 and Fig. 2.4. Once on Mars, the two channel

tracks are released allowing them and the attached rover to be lowered to the ground. The pyrotechnic detachment points for the ends of the track channels can be seen in Fig. 2.13. The channels are 2.6 m long and, upon landing, the base of the MLV is 1 m above the surface. Hence, in the deployed position the channels are at a 30° angle to the surface of Mars. The deployed position of the rover is shown in Fig. 2.4. After the channels are deployed, the pins holding the wheels in place are retracted from the wire mesh rover wheels and the tension cable is released from the rover. If one or both of the channels land on a large rock during deployment the channels are raised and swiveled to avoid the rock.

2.4.4 ERV Separation and Sample Return Capsule Detachment

When the ERV is ready for its return flight back to Earth it separates from the MLV. The separation occurs along the base of the ERV thrust structure, using pyrotechnic bolts. The separation points are seen in Fig. 2.13. Once the ERV reaches the vicinity of Earth, the sample return capsule and its aerobrake are jettisoned away from the ERV. This is accomplished using pyrotechnic bolts and small thrusters on the sample return capsule. The detachment points for the sample return are also shown in Fig. 2.13.

2.4.5 Sample Return Loading

The payload bay for the sample return is located relatively high above the planet surface because it has to be mounted aboard the ERV, above its engine. Therefore, it is necessary to provide a means for a surface rover to load the samples into the ERV. Several methods for loading the samples were considered. Two methods in particular were given the most serious consideration. One of these methods is to have the sample return rack located near the bottom of the vehicle where it can easily be loaded directly from the rover. After the rack is full, it would be lifted up to the ERV where it would be

placed inside the sample return container for the return voyage. The problem with this method is that if the lift were to fail for some reason none of the samples would be able to be returned to Earth. In the other loading method the samples would be loaded directly from the rover to the sample return container by a remote manipulator arm (RMA). In order to keep a relatively short arm, the base of the arm is attached to a vertical pole and is able to travel up and down on the pole in order to successfully load samples. With this method there is a good chance that at least some samples can be returned even in the case of the failure of the RMA at some point during the surface stay. For this reason this method was selected.

2.5 Methane Rocket Engine Design
(Mark Yee)

In the past, methane and other light hydrocarbons have been examined for their applicability in Earth-to-orbit vehicles [6]. The last two years have seen an increased interest in methane's potential for Mars in situ propellant production missions [2,7]. To exploit this potential is currently the major motivation of a liquid-methane/liquid-oxygen (LCH_4/LOX) rocket engine design.

Light hydrocarbon rocket engine research goes back more than 28 years [8]. For potential use in Earth-to-orbit engines, light hydrocarbons were proposed as a bipropellant combination with LOX. Research later showed that an increase in performance and efficiency could be achieved by the addition of LH_2 in the combustion chamber; thus creating the tripropellant engine [9]. For Mars in situ propellant production missions, though, a tripropellant engine is impractical since any imported hydrogen can be better utilized to create the methane fuel and LOX oxidizer. In Section 6, this utilization is demonstrated through the design of a plant to produce 420 kg of CH_4 from 158 kg of H_2. The reduced performance of a bipropellant CH_4/LOX engine is more than compensated for by the increase in the amount of methane.

The engine used for the Earth Return Vehicle (ERV) is required to satisfy certain criteria:

- Thrust Level Comparable to Estimated ERV Mars weight
- Ability to Restart
- Record of Reliability
- Existing Technology

Because there are no existing spaceworthy LCH_4/LOX engines known to have been built to date that satisfy these criteria, the methane engine used for project Hyreus is a new design, but it utilizes as much existing and proven technology as possible.

2.5.1 Existing Technology

The methane engine designed for project Hyreus operates on an expander cycle. This cycle was chosen for its simplicity, proven technology [10], and potential for adaptability to a throttleable engine. The expander cycle is used in such engines as Pratt & Whitney's RL-10 [11]. Because oxygen has better heat transfer characteristics than methane [12], it is used as the regenerative coolant in the LCH_4/LOX rocket engine proposed here.

Because LH_2/LOX engines already exist, a LOX turbopump can be easily designed for use in a methane engine. A turbopump for methane was designed, fabricated, and tested successfully in 1989 by Rockwell International [13].

There has been some concern about carbon deposition inside the engine when burning hydrocarbons. For the heavier hydrocarbons such as RP-1 this has been the case, but methane is able to burn cleaner and hence results in a minimal amount of carbon accumulation[14]. A study by Pratt & Whitney shows that methane generates 30% less solid carbon by weight than RP-1 [15].

Copper is preferred for use in the combustion chambers of most rockets, since its high heat conductivity aids the cooling of the chamber [16]. The Space Shuttle Main Engine has a copper lined combustion chamber. It has been shown that at high temperatures CH_4 can cause serious erosion and/or corrosion of copper surfaces [14]. Copper has also been shown to catalyze the decomposition of many hydrocarbon fuels [15]. Since dissolved copper is a known contributor to fuel fouling in aircraft gas turbine engines burning JP-4 and JP-5 [15], the same fouling is likely to occur in a methane engine if copper is used in the combustion chamber. While CH_4 has proven to be resistant to decomposition by copper [15], a material that does not react with copper at all is preferred. A graphite-lined regeneratively cooled chamber was tested with LOX/LCH_4 and is described as having worked, "...very successfully in the test program...," [17].

Injectors for LOX/LCH_4 have been designed by three different companies at different times. All designs were coaxial, a geometry that has been shown to provide inherently stable combustion and is presently used in such engines as the RL-10 [15]. Coaxial injectors are able to inject both fuel and oxidizer axially into the combustion chamber from one faceplate. The RL-10 coaxial injector is shown in Fig. 2.14. Pratt & Whitney, in 1965, built and tested injectors for light hydrocarbons, including methane. Using a coaxial design with a chamber pressure of 3447 kPa (500 psia), dynamically stable combustion was achieved [15]. Aerojet TechSystems Company, in 1979, built their own LOX/LCH_4 coaxial injector and tested it at Marshall Space Flight Center (MSFC) at 20.6 MPa (3000 psia) [18]. Rockwell International's Rocketdyne Division, in 1989, reported the successful testing of their injector at MSFC. Their design was also coaxial but was tested between 11.7 MPa (1700 psia) and 16.5 MPa (2400 psia) [14]. All the above-mentioned injectors achieved stable combustion; demonstrating the viability of injectors for LOX/LCH_4 engines.

The major constituents of a LCH_4/LOX engine have been researched and tested successfully. All that remains is to combine the existing technology to create the LCH_4/LOX engine needed for project Hyreus.

2.5.2 Engine Design

As stated previously, the methane engine for project Hyreus is a new design. Its is based on five assumptions/criteria:

- Thrust is 20,000 N.
- Propellants enter combustion chamber at their respective boiling temperatures.
- Combustion chamber pressure is 3447 kPa (500 psia).
- Exit pressure is 800 Pa.
- Stoichiometric Oxidizer to Fuel Ratio is 4:1.

The thrust level was selected to provide a thrust-to-Mars-weight ratio of 2.0 at liftoff. The exit pressure is approximately equal to Mars surface atmospheric pressure. Because regenerative cooling is used in an expander cycle engine [16], the heat flux into the coolant vaporizes the LOX. It is assumed that once the vaporized hot O_2 and cryogenic LCH_4 are injected into the combustion chamber, the specific enthalpy of the mixture is similar to that of CH_4 and O_2 at their respective boiling temperatures (111 K and 90 K for CH_4 and O_2 respectively). The chamber pressure of 3447 kPa (500 psia) was chosen as being similar to that of another expander cycle engine; Pratt & Whitney's RL-10 [1]. This chamber pressure is close to the upper limit of today's expander cycle engines.

From these assumptions, the chamber temperature, exhaust molecular weight, and exhaust heat capacity ratio were calculated using the computer program EQLBRM [19]. By assuming an isentropic nozzle and using common rocket engine

design relations, the characteristics of the LCH4/LOX engine were calculated. These are summarized in Table 2.4.

Table 2.4 LCH4/LOX rocket engine characteristics.

I_{sp}	371	sec
Thrust	20,000	N
Propellant Mass Flow	5.49	kg/s
Exhaust Velocity	3,643	m/s
Combustion Chamber Temperature	3,505	K
Nozzle Exit Temperature	1,214	K
Combustion Chamber Pressure	3,447	kPa
Nozzle Exit Pressure	800	Pa
Area Ratio of Nozzle	296	

The engine was assumed to occupy the approximate space of a circular cylinder inside the MLV to allow clearance during liftoff of the ERV. The dimensions of the cylinder were found in the following manner: The area of the throat and exit area were calculated using the mass flow and area ratio. A cylinder diameter slightly larger than the nozzle exit diameter was chosen to allow room to gimbal the engine. The diffuser section of the nozzle is a bell-shape whose optimized length can be approximated as 15% less than that of a 15° cone [16]. Since this is only the distance from the throat to the exit, the total length of the engine was approximated by scaling an RL-10 to a similar exit diameter and measuring the resulting height. The final dimensions of the methane rocket engine are shown in Table 2.5. and illustrated in Fig. 2.15.

Table 2.5 Methane rocket engine dimensions.

Throat Area	0.0028 m^2
Throat Diameter	0.030 m
Exit Area	0.839 m^2
Exit Diameter	1.03 m

The mass of the engine was estimated from the engines used by the Space Shuttle Orbital Maneuvering System (OMS). The OMS engines have a thrust comparable to the design thrust of the LCH_4/LOX engine, thus, the methane engine mass was approximated to be the same as that of a single OMS engine, 100 kg [20].

At Mars take-off the ERV will be following a gravity turn trajectory. Thrust vectoring by gimbaling the engine will be used to provide the necessary impulse for the tip-over maneuver of this trajectory and will provide some correctional control during ascent, in concert with the reaction control system described below.

2.6 LANDING ENGINES AND REACTION CONTROL SYSTEM

(Susan Peter-Thompson, Mark Yee)

The landing engines are used in the final phase of project Hyreus' Mars descent. The descent sequence is discussed in Chapter 5. Reaction control system (RCS) engines are used during all phases of the mission, including the descent.

2.6.1 Landing and RCS Engine Selection

For the landing engines and RCS, several different types were examined. The criteria used in selecting an engine package was:

- Propellant must be storable for the duration of the mission.
- Landing engines must have at least 16,000 N (4496 lbf) total thrust.
- Engines must be simple and reliable.
- Low mass and high specific impulse.
- Use same propellants in landing engine as in reaction control system.
- Existing Technology

The thrust level was selected to provide a thrust-to-Mars-weight ratio of 1.3 when the retro fire phase of Mars descent is begun. With these requirements in mind, the Marquardt R-40B and R-4D engines were selected [4, 21, 22]. Both are currently in production and both use the same propellants. The R-4D engine is used for the Space Shuttle RCS. Relevant engine specifications are shown in Table 2.6. With a nominal thrust of 4,000 N, four R-40B engines are needed to meet the required net thrust of 16,000 N for the Mars final descent.

Table 2.6 Landing and RCS engines

Engine	Nominal Thrust (N)	Thrust Range (N)	Specific Impulse (sec)	Propellant	Mass (kg)	Number Of Engines	Total Mass (kg)
R-40B	4000	2670-5780	303	N_2O_4/MMH*	7.26	4	58
R-4D	490	230-680	312	N_2O_4/MMH	3.75	16	60

* MMH is monomethyl hydrazine

2.6.2 Landing and RCS Engine Location

As shown in Fig. 2.16, the four R-40B landing engines are spaced evenly on the bottom of the MLV. Because the center of mass in the final descent configuration is not

perfectly centered in the vehicle, the landing engines must fire at different thrust levels to keep the MLV upright. The total thrust level must remain at 16,000 N, while exerting no net moment on the vehicle. Engines are located as far away from the central axis to allow the maximum moment arm for each engine. The envelope within which the center of mass must remain is also shown in Fig. 2.16. This envelope was calculated from the thrust range of the engines and their moment arm from a potential location of the center of mass. The MLV's center of mass in its final descent is well within this range.

The RCS is configured to allow control of the vehicle in as many degrees of freedom as possible. Both rotational effects and translational effects have been accounted for in the design.

Four R-4D thrusters are mounted in close proximity to the descent engines, as is also shown in Fig. 2.16. These RCS engines point out radially from the axis of the vehicle and provide maneuvering control during the descent. Other R-4D engines are placed on the exterior of the vehicle, as well as recessed in the aerobrake to complete the RCS, as shown in Fig. 2.17. Engines in the aerobrake are equipped with scarfed nozzles to remain flush with the surface of the aerobrake. The RCS engines are located to allow a maximum moment without exerting any translational forces on the vehicle. Engines are throttled down to induce a maximum angular acceleration of 5 deg/sec^2 [23]. Table 2.7 shows the location of the center of mass and moments of inertia in the two main phases of the MLV. The location of the center of mass shown here is measured from the same zero point as discussed in Section 2.2 and shown in Fig. 2.4.

2.7 VEHICLE MASS INVENTORY
(Keith Stokke)

One issue of great concern is the structural (or dead) mass of the spacecraft. Table 2.8 summarizes the mass inventory of all of the structural components and the

Table 2.7 Center of mass and moments of inertia for deep space and landing configurations of MLV. Center of mass location same as shown in Fig. 2.4.

		Deep Space	Landing
Center of Mass (m):	Vertically (z)	4.15	2.57
	Horizontally (x)	0.0	0.0
	Forward (y)	-0.01	0.09
Moment of Inertia (kg):	I_z	8,804	6,896
	I_x	25,253	56,205
	I_y	19,615	16,184

Table 2.8 Inventory of vehicle masses (not including payload)

Component	Mass (kg)	% of Total Structural Mass
MLV		
Thrust Frame	60	5.0
Truss Frame	700	58.8
Landing Gear	62	5.2
Landing Engines	75	6.3
N204/MMH	290	24.4
Total	1190	100
ERV (dry)		
Thrust Frame	72	29.4
Propellant Tanks	45	18.4
Misc. Supports	28	11.4
Ascent Engine	100	40.8
Total	245	100

engines discussed in the previous sections for both the MLV and the ERV. Percentages of total vehicle mass are included. The masses for the MLV do not include payload mass. A complete list of all of the component masses including the payload is included in Chapter 3.

2.8 CONCLUSION
(Keith Stokke, Mark Yee)

The MLV and the ERV for project Hyreus are designed to minimize mass, size and cost while still using technology that is currently available and well-tested. The configuration of the MLV and ERV, the design of the structures, the deployment mechanisms, and the propulsion systems have been described here.

In designing the configuration of the two spacecraft, it was necessary to meet several requirements. Among them are to keep a suitable center of mass, to keep the payload within the aerobrake's wake, and to keep as small of a fairing size as possible. The configuration designed meets all of these requirements.

The structure of the MLV and the ERV needed to be as lightweight as possible without sacrificing the necessary strength. For this reason, aluminum-lithium alloys were selected for almost every structural component - Aluminum-lithium 2090 for most frame components and support struts and Weldalite™ for the propellant tanks. A finite element analysis was also done in order to minimize the number of excess frame members.

Deployment and loading methods for this spacecraft are designed to be as simple as possible, to minimize the chance for failure. The satellite, parachute, aerobrake, and the ERV are all jettisoned with the use of pyrotechnic bolts. The rover is deployed using a wheel-channel ramp which allows the rover to travel directly down to the surface without the use of a lift or crane arm. The samples are loaded from the rover with the use

of a remote manipulator arm. This helps ensure that at least some of the Mars samples are returned to Earth.

The engines utilize as much existing technology as possible. The components of the methane engine have been well researched by industry and the design takes this research into account. All engines used for landing and the RCS exist today and have been used in previous missions. The use of existing technology minimizes development cost for the engines; usually one of the most expensive parts of a space vehicle.

NOMENCLATURE

A_c	Cross-sectional area of uniaxial rod member
B	boiled-off propellant volume
C_b	buckling coefficient
E	modulus of elasticity
E'	propellant tank design factor
e_w	weld efficiency
F	Force in uniaxial member
I	Moment of inertia
K	stress factor
k	tank-end ellipse ratio (minor axis length / major axis length)
l	length of uniaxial member
l_c	length of cylindrical portion of tank
M	bending moment
m_c	mass of cylindrical tank
m_e	mass of elliptical tank ends
m_s	mass of spherical tank or spherical tank ends
P_{axial}	vertical load on tank
$P_{cr,c}$	critical pressure on cylinder
$P_{cr,e}$	critical pressure on elliptical end
$P_{cr,s}$	critical pressure on spherical end
P_{eq}	equivalent load produced by axial force and bending moment
p_t	maximum tank operating pressure
R	tank end crown radius
r	tank radius or radius of uniaxial rod member
S_w	maximum allowable operating stress of material

T	trapped-propellant volume
t_c	cylindrical wall thickness
t_{cr}	wall thickness at the crown
t_e	elliptical and spherical end wall thickness
t_k	wall thickness at knuckle
t_s	spherical wall thickness
U_o	tank ullage volume
V_o	usable propellant volume calculated from propulsion-system requirements
ν	Poisson's ratio
ρ	density of the tank material
σ	Allowable yield stress

REFERENCES

1. *Titan IV/Centaur User's Guide*, General Dynamics, Oct. 1992.

2. "Project Minerva: A Low Cost Manned Mars Mission Based on Indigenous Propellant Production," Final Report, Space Systems Design, AA420/421, NASA/USRA Advanced Design Program, Department of Aeronautics and Astronautics, University of Washington, June 1992.

3. Huang, D. H. and Huzed, D. K., *Modern Engineering for Design of Liquid Propellant Rocket Engines, Progress in Aeronautics and Astronautics, Vol. 147,* AIAA; Washington, D.C., 1992, pp 285-298.

4. Larson, W.J., and Wertz, J.R., *Space Mission Analysis and Design*, Second Edition, Microcosm, Inc. and Kluwer Academic Publishers, 1992, pp. 430-468, 646, 657.

5. Davanay, L., Garner B., and Rigol, J., "Design of an Unmanned Lunar Cargo Lander That Reconfigures Into a Shelter for a Habitation Module or Disassembles into Parts Useful to a Permanent Manned Lunar Base," NASA Technical Report N90 25667, University of Texas at Austin, 1989.

6. Martin, J.A., "Hydrocarbon Rocket Engines for Earth-to-Orbit Vehicles," *Journal of Spacecraft and Rockets*, Vol.20, May-June 1983, pp. 249-256.

7. Zubrin, R.M., "In-Situ Propellant Production: The Key Technology Required for the Realization of a Coherent and Cost-Effective Space Exploration Initiative," Paper No. IAA 91-668, 42nd Congress of the International Astronautical Federation, Montreal, Canada, October 5-11, 1991.

8. Masters, A.I., "Investigation of Light Hydrocarbon Fuels with Flox Mixtures as Liquid Rocket Propellants - Final Report," NASA Paper CR-54445, Pratt & Whitney Aircraft Paper FR-1443, Sept. 1, 1965.

9. Martin, J.A., "Effects of Tripropellant Engines on Earth-to-Orbit Vehicles," *Journal of Spacecraft and Rockets*, Vol.22, Nov.-Dec. 1985, pp. 620-625.

10. Kramer, R., and Martin, J., "Undeveloped rocket Cycle Applications to Advanced Earth-to-Orbit Transportation," Paper No. AIAA 90-2438, IAA/SAE/ASME/ASEE 26th Joint Propulsion Conference, Orlando, FL, July 16-18, 1990.

11. *Titan/Centaur Evolution Plan 1993*, General Dynamics Space Systems Division, 1993.

12. Bailey, C.R., "RP-1 and Methane Combustion and Coding Experiments," NASA Technical Report N89-12650, NASA George C. Marshal Space Flight Center, p. 546.

13. Nielson, C.E. and Csomor, A., "Advanced Launch System Propulsion Focused Technology Liquid Methane Turbopump Technical Implementation Plan," NASA CR-183681, Rockwell International/Rocketdyne Division, May 25, 1989.

14. Cook, R.T., and Kirby, F.M., "LOX/Hydrocarbon Combustion and Cooling Survey," NASA Technical Report N89-12648, Rockwell International/ Rocketdyne Division, pp. 472-473.

15. Masters, A.I., Visek, W.A., and Carroll, R.G., "Survey of LOX/Hydrocarbon Combustion and Cooling," NASA Technical Report N89-126471, Pratt & Whitney Aircraft / United Technologies Corp., p. 445.

16. Sutton, G.P., *Rocket Propulsion Elements: An Introduction to the Engineering of Rockets*, Sixth Edition, John Wiley & Sons, Inc., 1992, p.93.

17. Mercer, S.D., and Rousar, D.C., "Aerojet TechSystems Company Contribution to LOX/HC Combustion and Cooling Technology," NASA Technical Paper N89-12646, Aerojet TechSystems Company, pp. 398, 404-405.

18. Valler, H.W., "Design, Fabrication, and Delivery of a High Pressure LOX-Methane Injector," Paper No. NAS 8-33205, Report 33205F, 1979.

19. Pratt, B.S., and Pratt, D.T., "An Interactive Code for Calculation of Gas Phase Chemical Equilibrium: EQLBRM," NASA CR-168337, Department of Mechanical Engineering, University of Washington, April 1984.

20. "Spacecraft Subsystems," NASA/USRA ADP Paper, Department of Aerospace Engineering and Engineering Mechanics, The University of Texas at Austin, Sept., 1991.

21. Griffin, M.D., and French, J.R., *Space Vehicle Design*, American Institute of Aeronautics and Astronautics, 1991, pp.172, 292-309.

22. *Rocket Engines and Propulsion Systems*, Kaiser Marquardt, Revised 1985.

23. Powell, R.W., Braun, R.D., "A 6-Degree of Freedom Guidance and Control Analysis of Mars Aerocapture," Paper AIAA 92-0736, 30th Aerospace Sciences Meeting and Exhibit, Reno, Nevada, January 6-9, 1992.

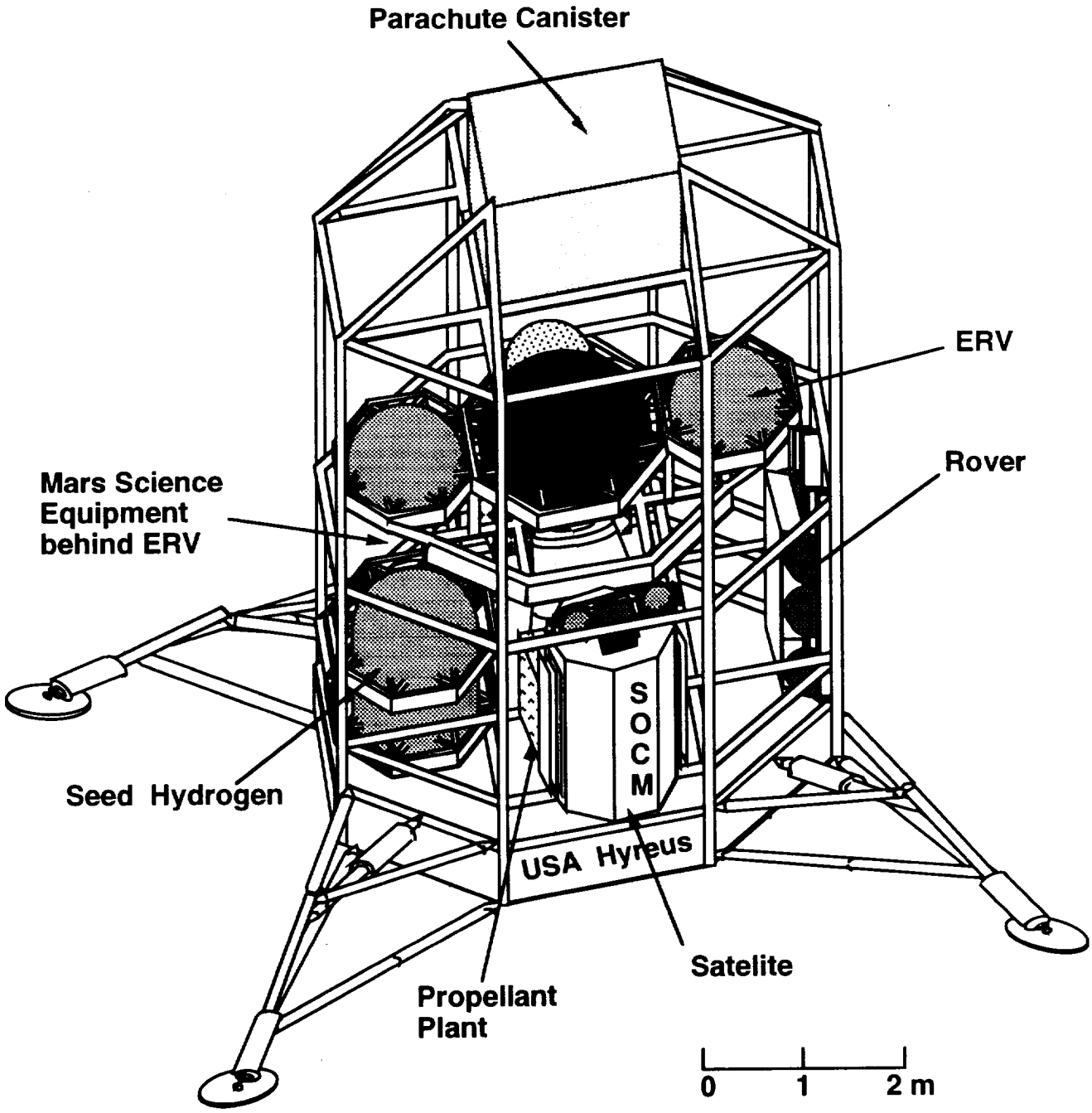

Fig. 2.1 Mars Landing Vehicle (MLV) and Earth Return Vehicle (ERV) three dimensional configuration. For clarity the aerobrake, support struts, ascent engines, hydrazine tanks, and Dynamic Isotope Power System (DIPS) are not shown.

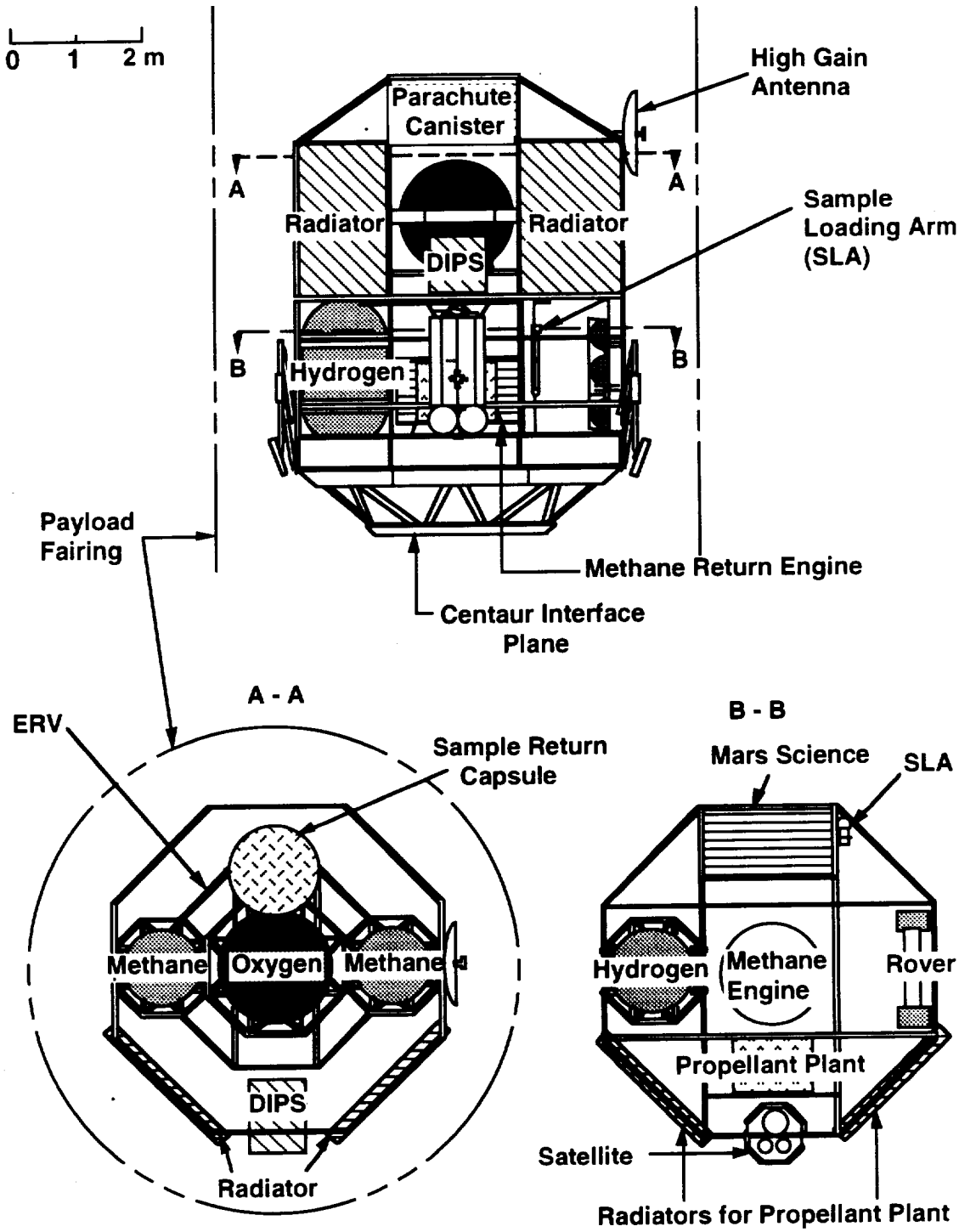

Fig. 2.2 MLV/ERV configuration. For clarity the aerobrake and the front views of the propellant plant radiators are not shown.

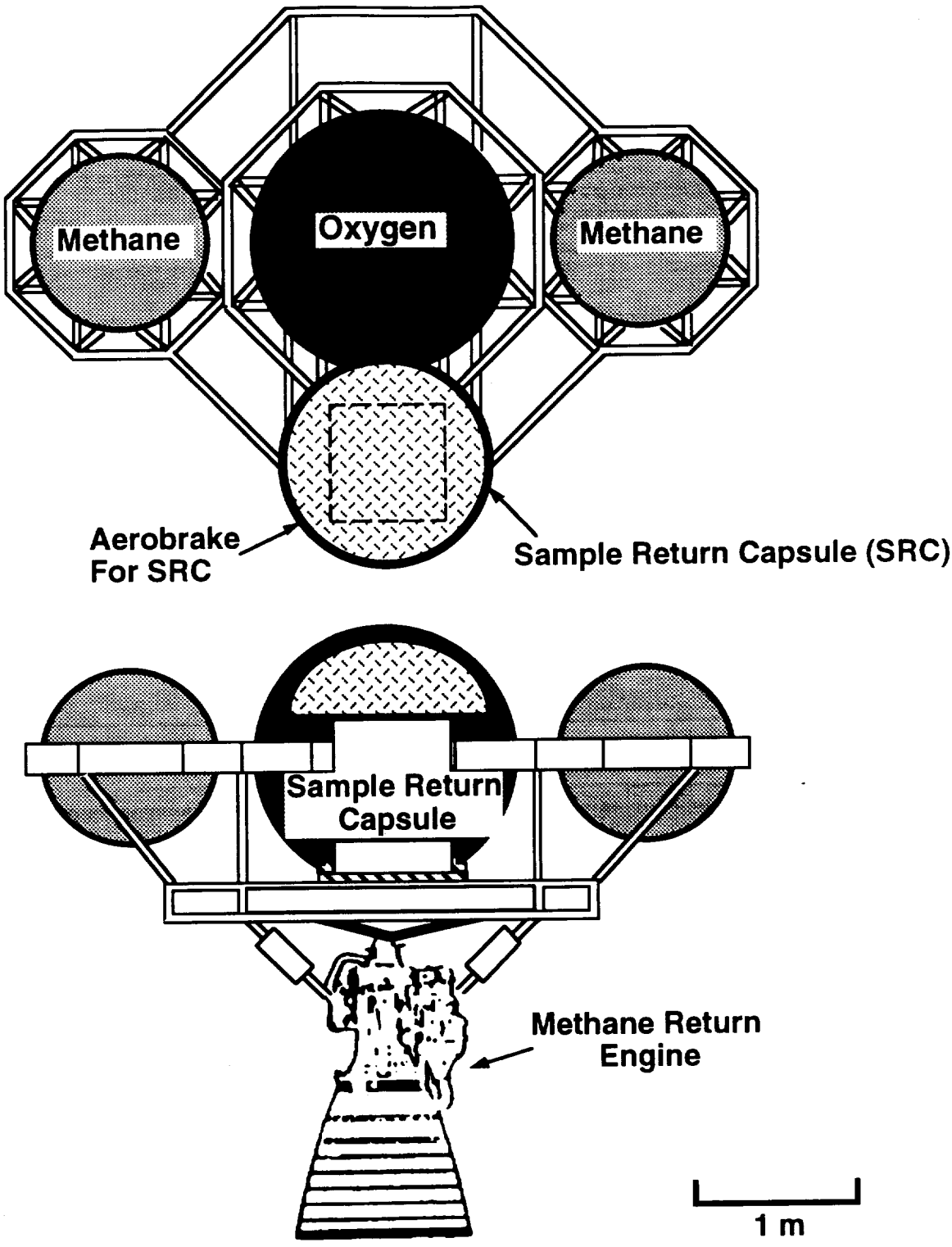

Fig. 2.3 ERV configuration.

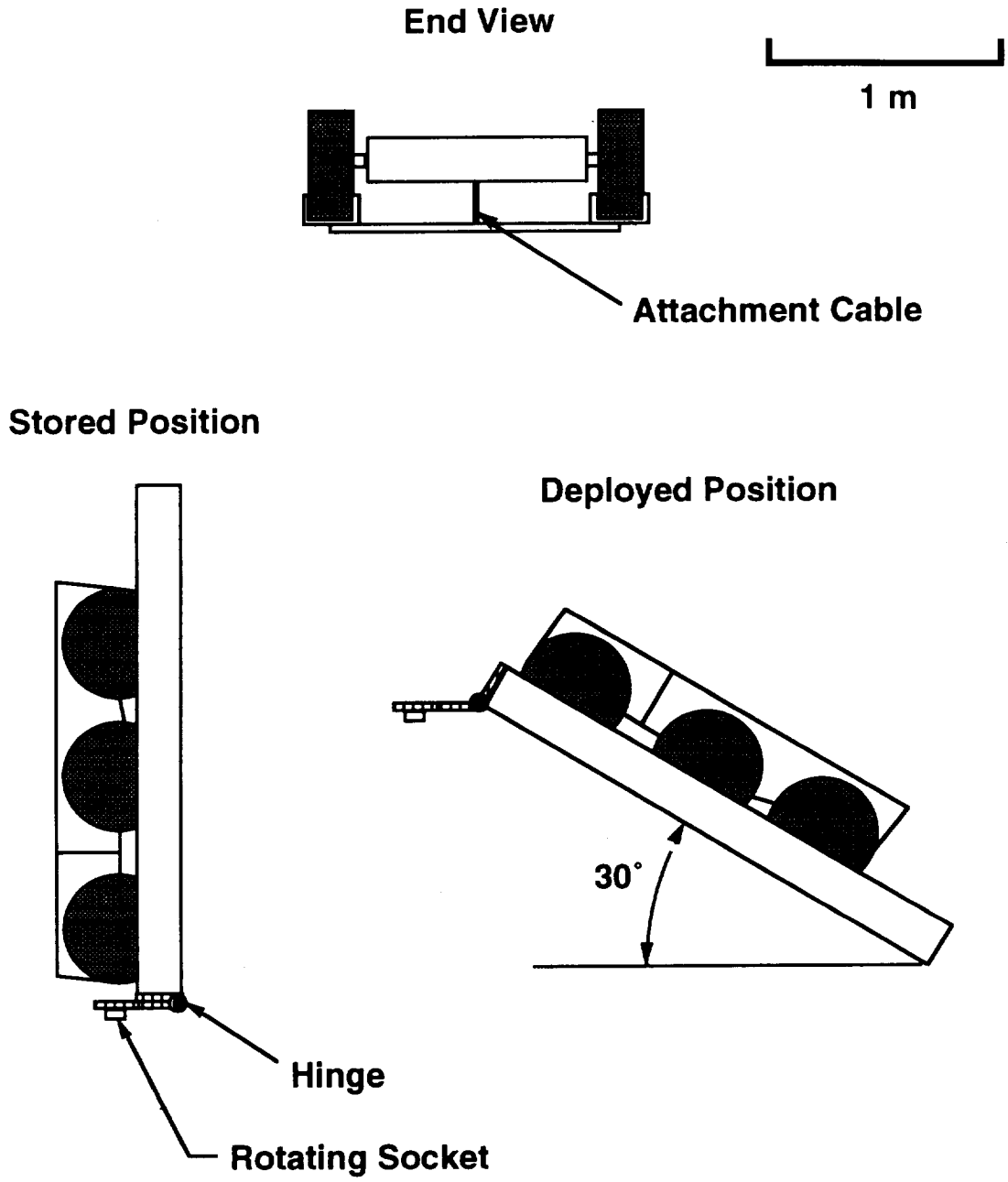

Fig. 2.4 Rover storage and deployment.

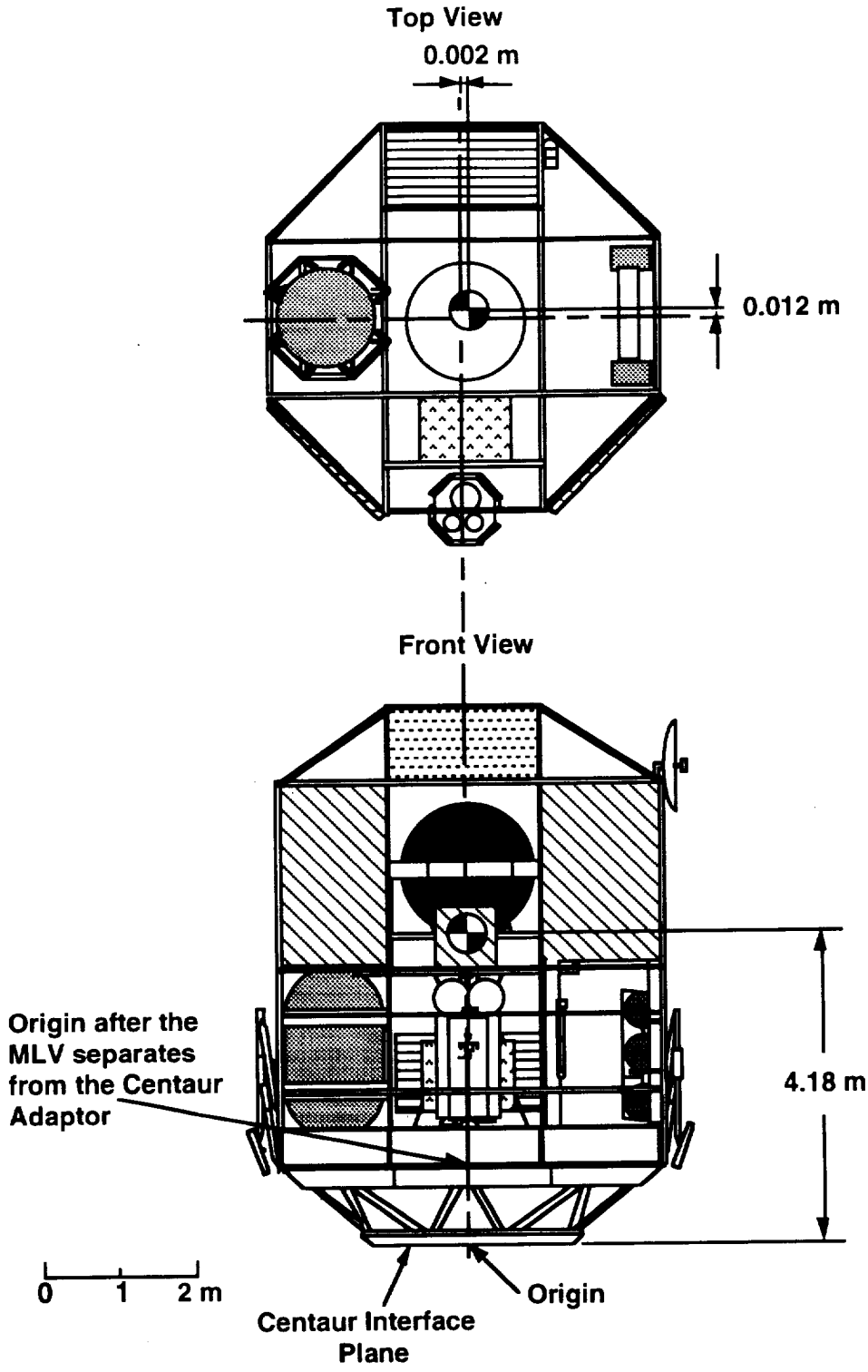

Fig. 2.5 Location of center of mass.

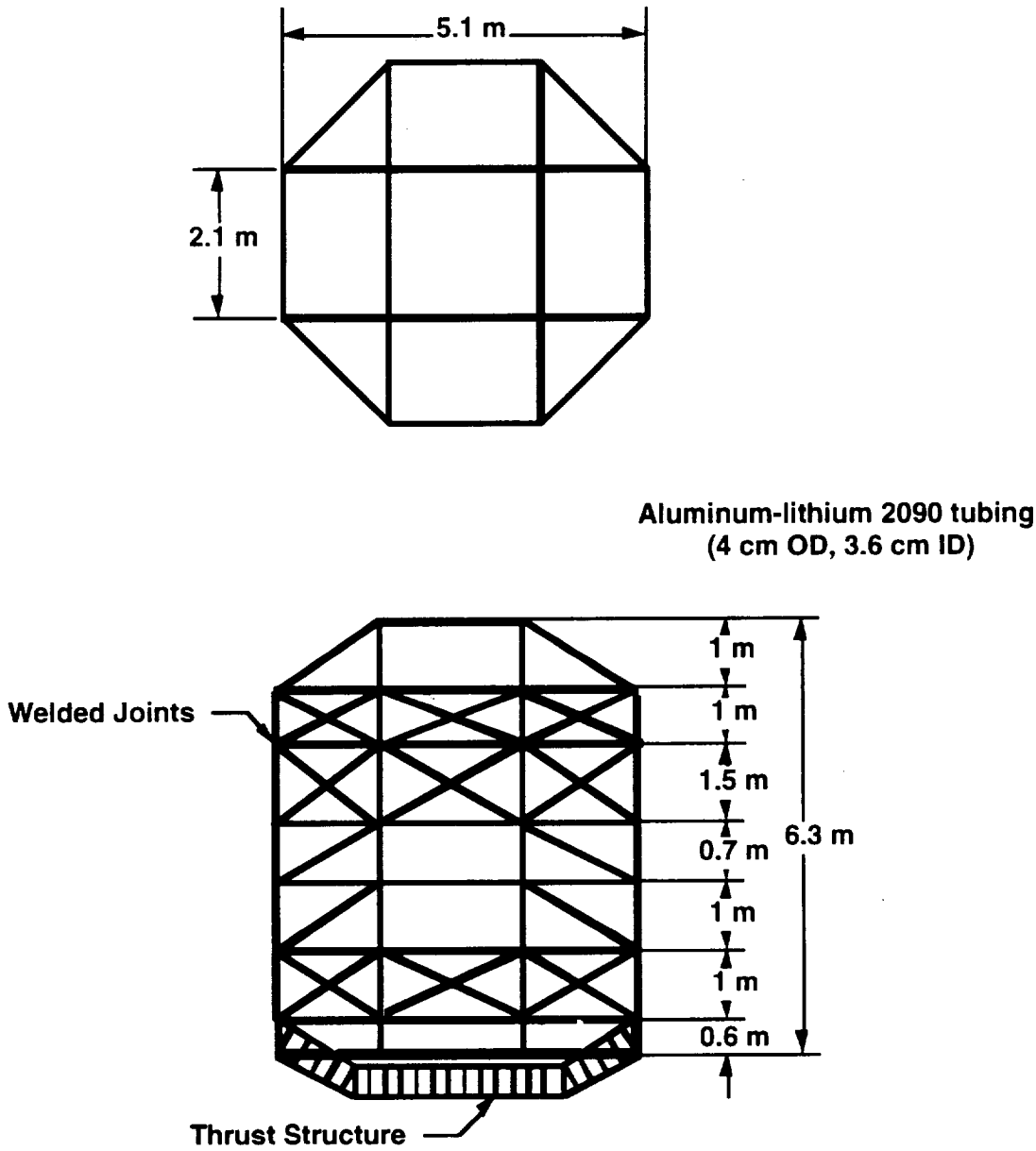

Fig. 2.6 MLV truss frame.

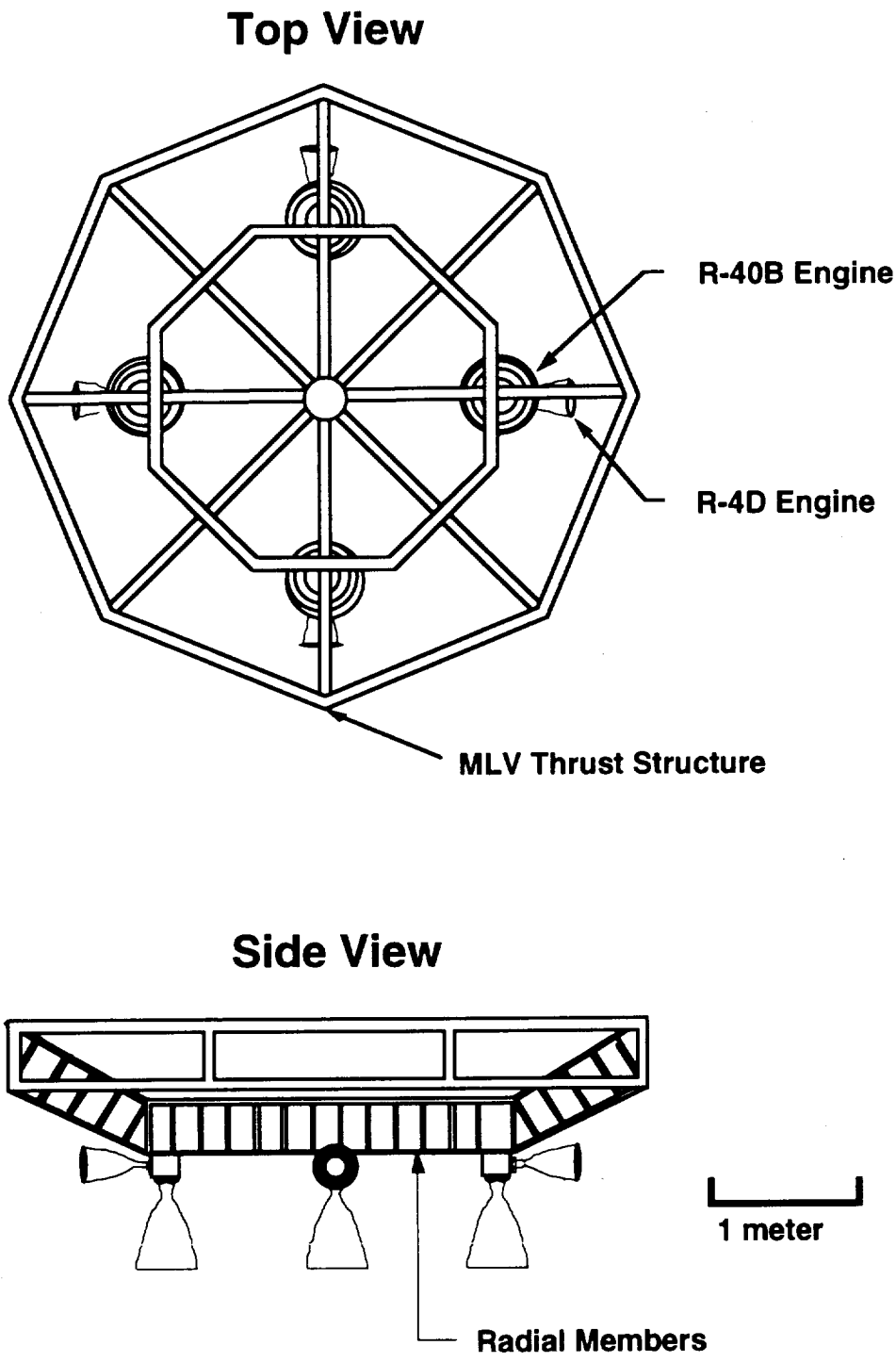

Fig. 2.7 MLV thrust structure.

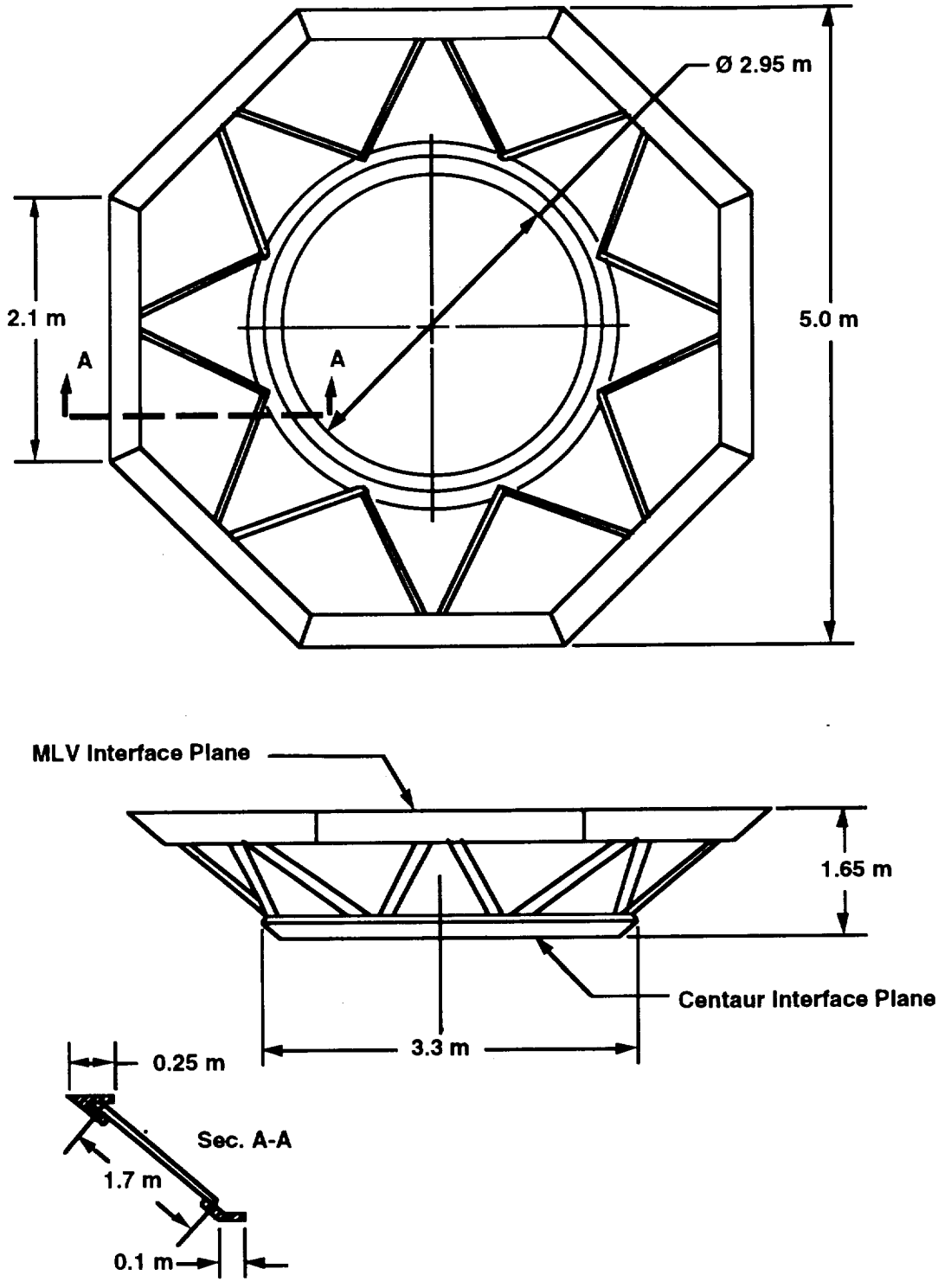

Fig. 2.8 Centaur adapter.

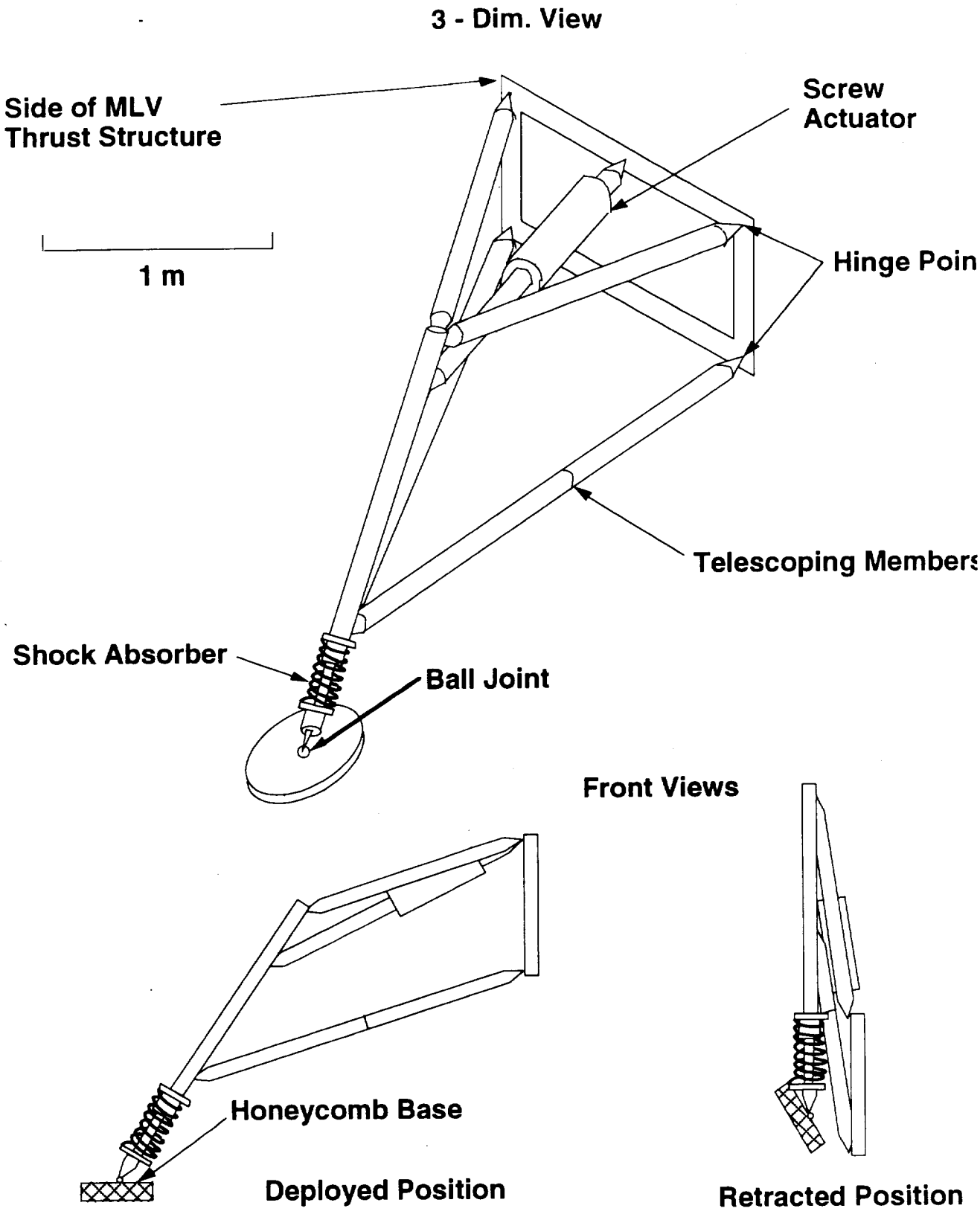

Fig. 2.9 Landing gear configuration and structure.

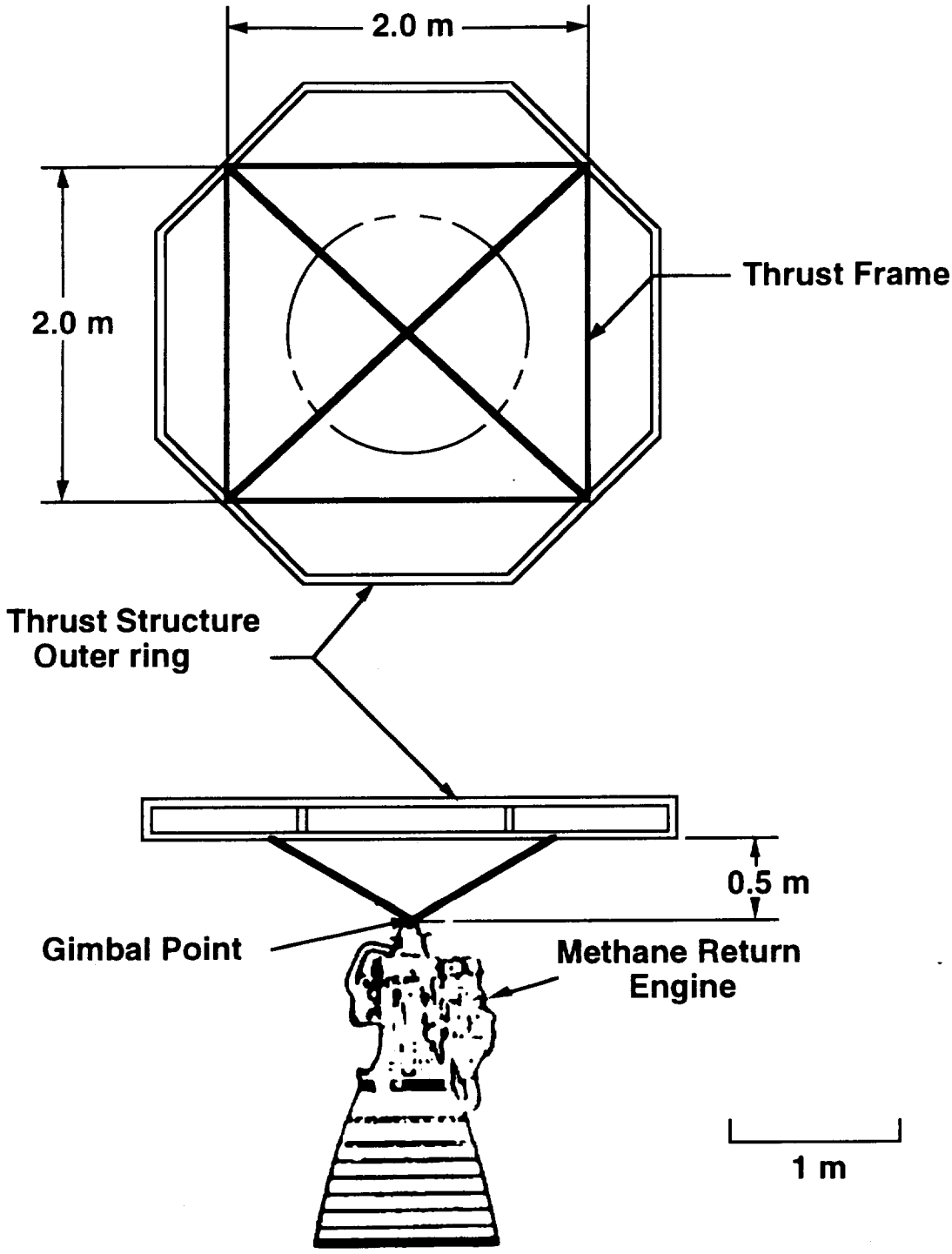

Fig. 2.10 ERV thrust structure.

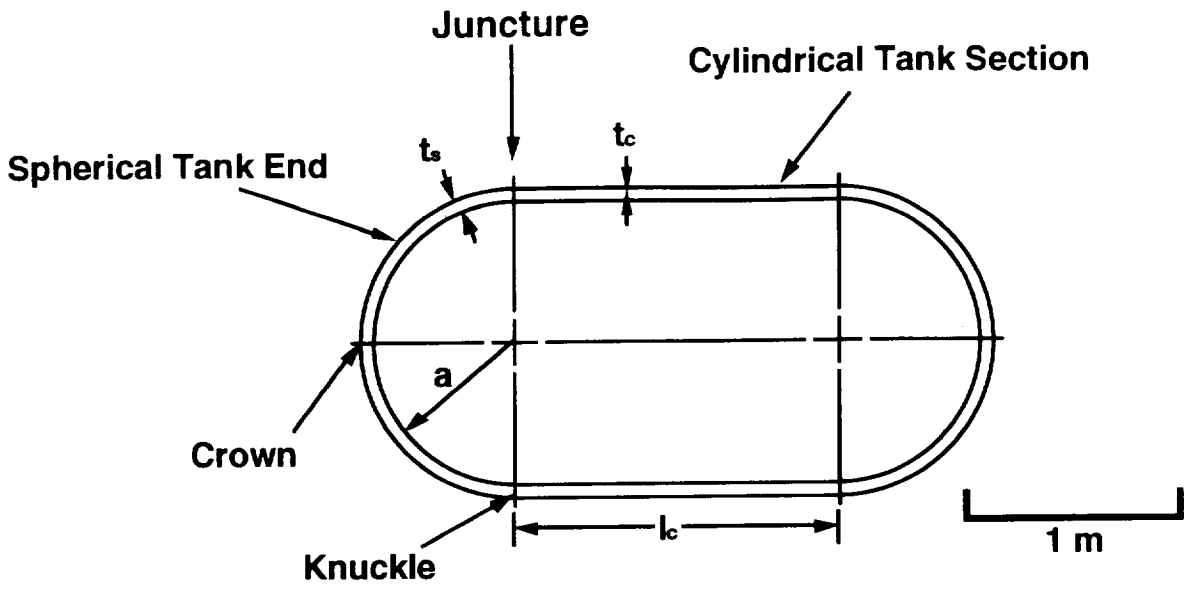

Fig. 2.11 Nomenclature of principal tank elements.

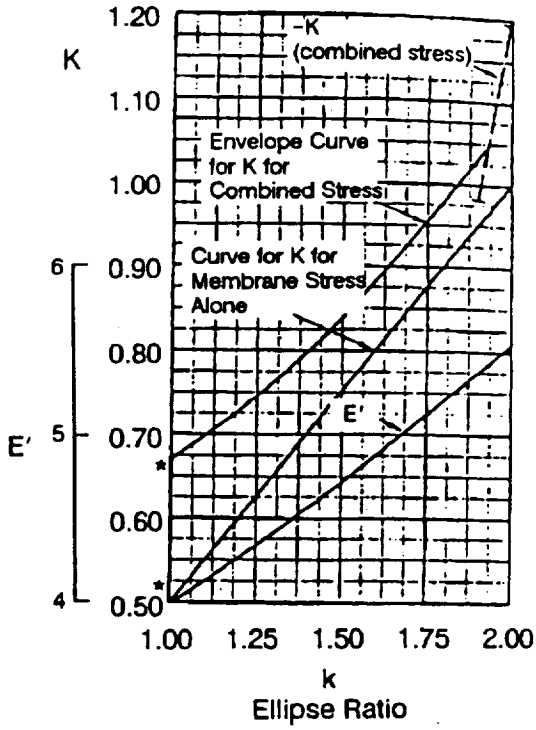

*For spherical tanks use K = 0.50 at k = 1.0
For spherical heads use K = 0.67 at k = 1.0

Fig. 2.12 Ellipse ratio k vs. knuckle factor K and compression stress.

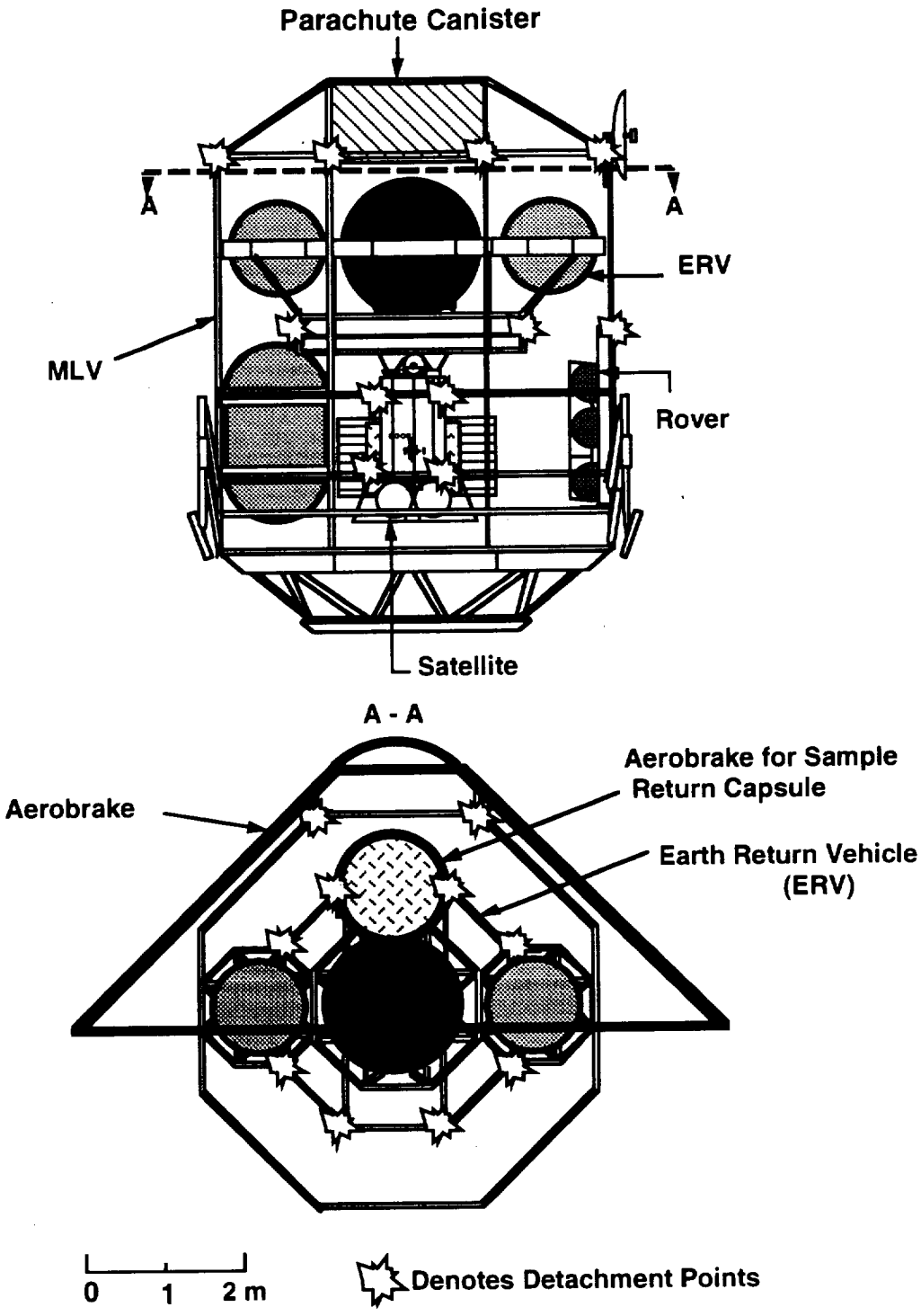

Fig. 2.13 Payload detachment points in the MLV. For the sake of clarity this figure shows mainly just the payload which is separating.

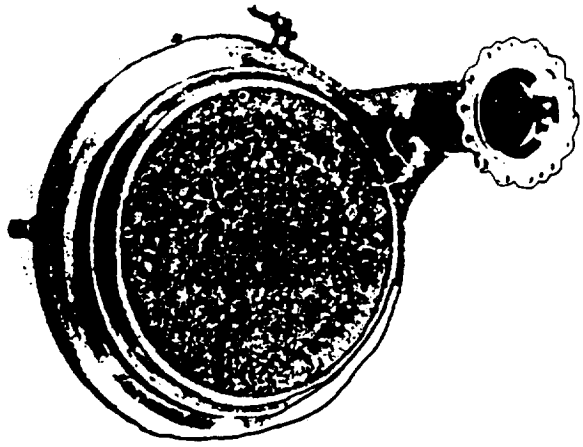

Fig. 2.14 RL-10 coaxial injector.

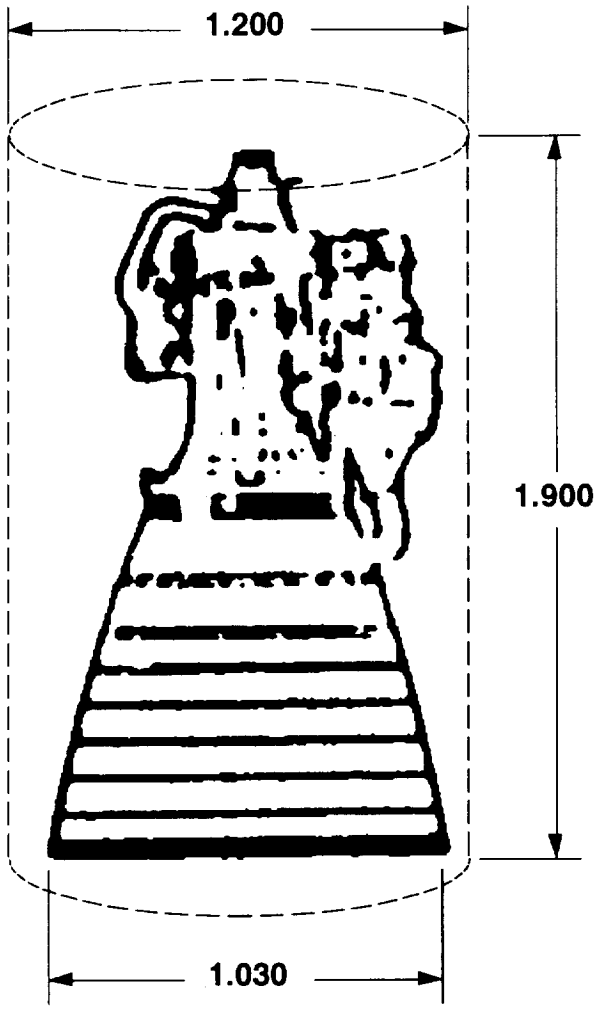

Fig. 2.15 Methane engine for Mars ascent showing dimensions of circumscribed cylinder.

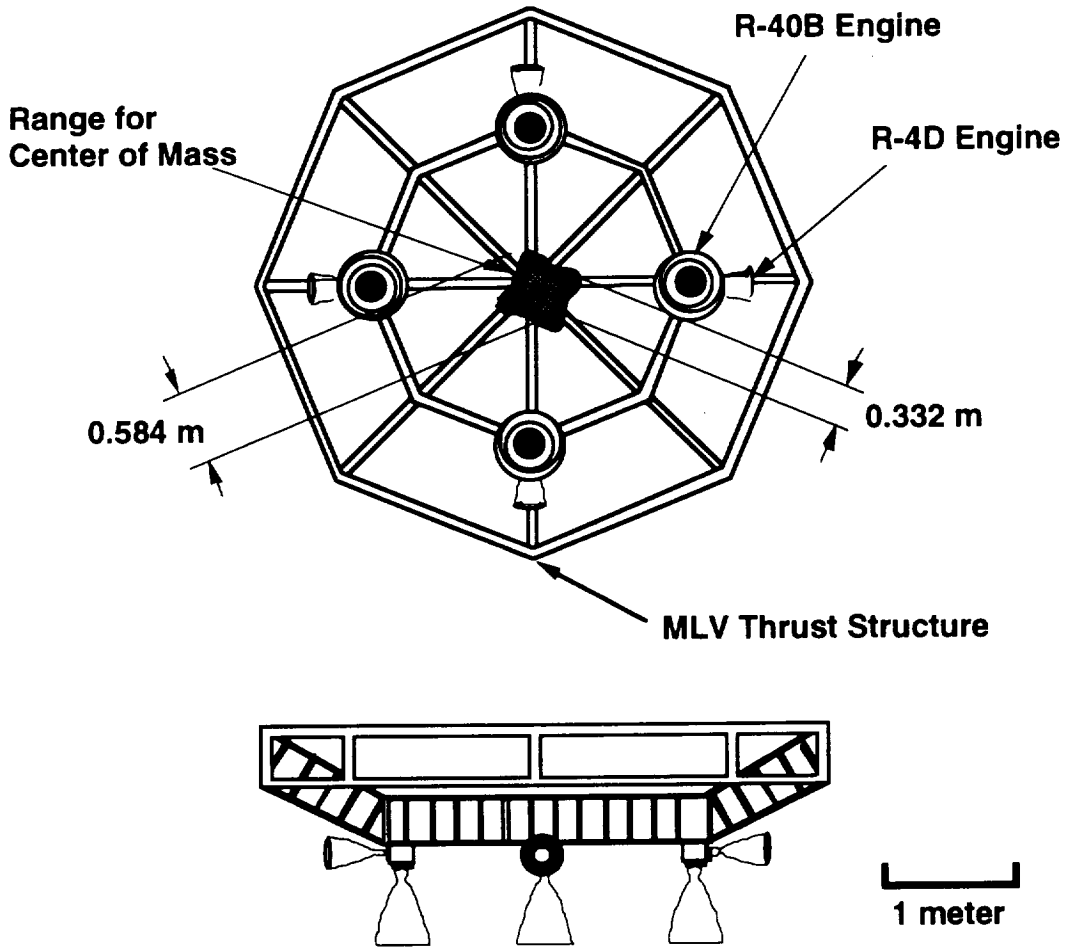

Fig. 2.16 Landing and RCS engine location on thrust structure. Center of mass variation area shown in view of MLV from bottom.

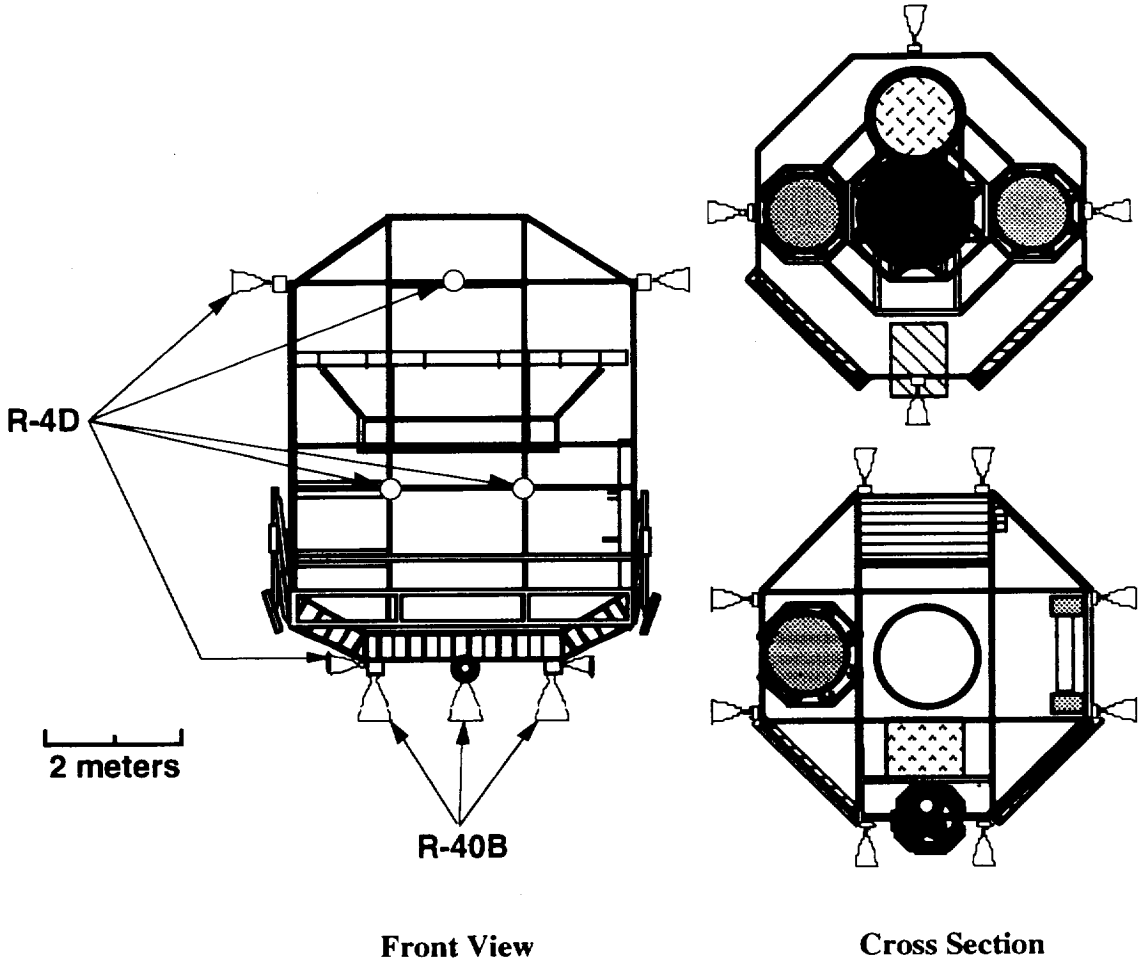

Fig. 2.17 Reaction control system engine location on MLV. Front view is shown on right. Cross sectional views are shown on the left. All engines shown in cross sectional views are R-4D.

3.0 LAUNCH SYSTEM

Richard Warwick

TABLE OF CONTENTS

3.1 INTRODUCTION 3.1

3.2 LAUNCH SYSTEM ANALYSIS 3.1

3.2.1 Titan III/TOS 3.1

3.2.2 Proton 3.1

3.2.3 Energia 3.2

3.2.4 Zenit 3.3

3.2.5 Ariane V 3.3

3.2.6 Space Shuttle 3.3

3.2.7 Delta 7925 ..... 3.4

3.2.8 Titan IV/Centaur 3.4

3.3 CONCLUSIONS 3.6

NOMENCLATURE 3.8

REFERENCES 3.9

FIGURES 3.10

3.1 INTRODUCTION

Project Hyreus does not have the large mass penalties associated with a manned launch, however, mass estimates place this project near the limits of most of the world's current launch vehicles. As a result, several launch systems were evaluated to determine which could be used by Hyreus. Once capable systems were identified, they were further analyzed with regard to cost, availability and reliability.

3.2 LAUNCH SYSTEM ANALYSES

Several launch systems were evaluated for this project; they included the Titan IV/Centaur, Titan III/TOS, the Space Shuttle, the Delta, the European Space Agency Ariane V, and the Russian Energia, Proton and Zenit. These are compared in Fig. 3.1 in terms of payload mass versus V capability. The data used to evaluate these systems were compiled from Ref 1 and each system's general capabilities were determined. The procedure involved step-by-step analysis of each segment of the launch sequence, as discussed in Appendix C. Gravity and drag losses were obtained from the manufacturers, if possible, or were estimated by linearly scaling time of flight and cross-sectional area.

3.2.1 Titan III/TOS

The Titan IIIE with a Transfer Orbit Stage (TOS) upper stage does not appear to be capable of launching the Hyreus spacecraft. The margin by which the Titan III falls short of the V requirement is the smallest of all systems evaluated, so future mission planners should reevaluate this vehicle.

3.2.2 Proton

The Russian Proton at a mere $70 M per launch is the most economic system capable of launching project Hyreus. However, several complications may prevent the use of the Proton. The largest diameter payload fairing available for the Proton is over 3 m too small. A fairing comparable in size to the fairing available with the Titan IV would incur an increase in mass of over 4000 kg. In addition, the fact that the Russian vehicles are integrated and fueled horizontally would require structural upgrades to the Hyreus vehicle and raise the mass of the payload to the point where the Proton could not launch it. Since available estimates suggest that a margin of less than 500 m/s already exists, such modifications would likely eliminate the Proton as a contender. Nevertheless, because cost is a major concern of all mission planners, the Proton is a serious contender.

3.2.3 Energia

The Energia has the highest V capability for a given payload of any system considered. However, the Energia has several drawbacks that could make the use of the system unfeasible. Because of its large cross-sectional area (four boosters, a tank and cargo module) and long burn time, Energia has the highest drag and gravity losses of all the systems. In addition, only launch pad No.1 at Baikonur Cosmodrome, in Khazakhstan, is outfitted to launch the payload carrier version of the Energia. Since Baikonur is at 45.6° latitude and the lowest orbit inclination available from there is 51.6° (to avoid overflights of China), an additional V may be required for a plane change. Another possible problem is the availability of upper stages for Energia. Only two launches of Energia have been confirmed [1]. The second flight was a successful unmanned test of the Soviet Buran space shuttle. The first flight carried a small version of the payload carrier, however, the upper stage failed and dumped the payload into the Pacific Ocean. Because of this, two upper stages, the Energia Upper Stage (EUS) and the Retro and Correction Stage (RCS) were to have been developed for use by 1993. The Energia's interplanetary mission called

for payload and both upper stages. These upper stages were supposed to be modifications of a Proton upper stage and an Energia Stage 2 [2]. Whether or not these stages have actually been built or tested has not been confirmed. If not, it has been suggested to simply use a Centaur with the Energia. While this may be feasible, the Centaur itself is structurally limited to a payload mass that is far below the lift capability of the Energia, defeating the entire purpose of using the Energia's heavy lift capability. The large version of the payload fairing has also apparently not been built [3]. An Energia launch also may not be politically feasible, as it may be difficult to persuade the U.S. Government and NASA to consider using a Russian rocket that must be launched from Khazakhstan. Nevertheless, the Energia is the second best choice.

3.2.4 Zenit

The Russian Zenit fell short of meeting the velocity increment required for Project Hyreus, as shown in Fig 3.1. Although the apparent lack of performance is largely due to gravity and drag losses that are not accurately known, it seems unlikely that the Zenit could launch Hyreus.

3.2.5 Ariane V

As can be seen from Fig. 3.1 the European Space Agency Ariane V also appears to be incapable of launching the Hyreus vehicle. Projected launch costs are around $110 M, and the first launch is not scheduled until 1995. Because it is a vehicle used by NASA's major competitor, the Ariane V was not considered further.

3.2.6 Space Shuttle

This scenario includes a Boeing IUS (Inertial Upper Stage). In 1986, Congress enacted a rule precluding the launch of any liquid fueled upper stage with the Space Shuttle. As a result, the Centaur G', which General Dynamics was developing for the Shuttle, was canceled. Reference 3 contains charts of added performance with OMS kits, which are

essentially additional fuel tanks for the OMS system, placed in the cargo bay to augment the existing OMS system [4]. Analysis suggests that the Space Shuttle is capable of launching Hyreus, and that the capability could be augmented by the OMS kits. A major problem with the Space Shuttle is that the payload bay is only 4.5 m in diameter. The aerobrake for Project Hyreus would have to be assembled by astronauts in orbit. Also, since the Shuttle is the most complex and costly ($300-$500 M for a dedicated launch) of all systems considered, and since the Hyreus vehicle will not fit into the payload bay, the Shuttle was eliminated as a contender.

3.2.7 Delta 7925

As is evident in Fig 3.1, the Delta fell short of meeting the requirement for Project Hyreus. It was evaluated to compare Hyreus to the Discovery class missions recently funded by NASA.

3.2.8 Titan IV/Centaur

Because of the preclusion of any liquid fueled upper stages on the Space Shuttle, the Titan IV/Centaur has the highest payload capacity for any U.S. launch vehicle at this time. Titan IV performance parameters and flight sequences have been analyzed, and pertinent data for the Titan IV/Centaur are shown in Table 3.1.

Table 3.1 Titan IV/Centaur performance ratings

Stage	Gross Mass (kg)	Propellant Mass (kg)	Vacuum Isp (sec)	Burn Time (sec)	Propellant
SRMU (each)	352,396	315,270	284.6	136.6	88% HTPB
1	169,457	154,450	301.45	187.73	N_2O_4/UDMH
2	39,000	34,636	316.55	226.91	N_2O_4/UDMH
Centaur	23,724	21,000	444.4	600	LH_2/LOX

The solid rocket motor upgrade (SRMU) has been used for this analysis. The SRMU has undergone two test firings already [5]. Two more are scheduled for 1993, after which the SRMU will be available for use with the Titan IV. The two test firings to date reveal that SRMU suffers from a reduction of vacuum specific impulse to approximately 284.6 from the design value of 286.5 [5]. Also, aluminum slag has been building up in the nozzle during test firing. Although this slag has not produced control problems, it effectively increases the mass, and thus decreases the performance. This performance defect should be compensated for by the removal of 1,082 kg of insulation and an increase in propellant mass of 1,947 kg [6]. The latest performance parameters of the Centaur were obtained from General Dynamics [7]. A modified payload fairing will be required because of the size of the aerobrake. McDonnell Douglas, the manufacturer of the fairing, can produce a five segment (8.38 m outer diameter) payload fairing that will weigh approximately 10,400 kg [8]. The largest version flown to date is a 5.08 m outer diameter fairing weighing 6,300 kg. Table 3.2 shows the Titan IV flight sequence. The flight sequence was provided by the Air Force Titan System Program Office [6].

Table 3.2 Flight sequence

Time (min:sec)	Event
00:00	SRMU ignition
02:15	Stage 1 ignition
02:26	SRMU separation
03:58	Payload fairing separation
05:22	Stage 2 ignition
05:23	Stage 1 separation
09:10	Stage 2 shutdown
09:21	Stage 2 jettison
09:33	Centaur 1st burn ignition (MES1)
11:10	Centaur 1st burn shutdown (MECO1)
11:11	RCS pressurization control
15:29	End RCS/Park orbit insertion
X (variable depending on launch holds)	Centaur 2nd burn ignition (MES2)
X+06:08	Centaur 2nd burn shutdown (MECO2)
X+06:18	Centaur separation/Transfer orbit insertion
X+012:18	Centaur CCAM*

*CCAM --Contamination and Collision Avoidance Maneuver

Table 3.3 shows the ΔV budget, which includes the required orbital velocity at burnout (see Section 4), the drag and gravity losses provided by a Martin Marietta launch simulation [9], the velocity required to send the Mars Landing Vehicle (MLV) into a hyperbolic escape orbit, and the velocity gained from the Earth's rotation by launching from Kennedy Space Center. To reduce mass, the Centaur is not well insulated. As a result, fuel boil-off may be significant depending on time spent in the coast phase of the final parking orbit. Launch azimuth and parking orbit inclination were derived as discussed in Section 4. A noon launch window best takes advantage of the rotational speed of the Earth by minimizing the inclination of the parking orbit. Only a few hours of launch window are available each day. If holds exceed the time limit, the launch will have to be delayed until the next day. For this reason, built in holds may be used late in the countdown to keep the parking orbit insertion and the escape orbit burn close together in order to minimize the Centaur fuel boiloff.

Table 3.3 ΔV budget for the Titan IV/Centaur

Velocity at parking orbit insertion	7898 m/s
Velocity penalty due to drag	68 m/s
Velocity penalty due to gravity	823 m/s
Transfer Orbit Injection (TOI) V	3649 m/s
Velocity gain from Earth rotation	− 407 m/s
TOTAL	12,031 m/s

From this information, it has been determined that the payload mass must be below 9290 kg. The Centaur, however, is structurally limited to a somewhat lower mass, depending on the position of the center of gravity of the payload from the interface between the payload and the Centaur (see Fig 3.2) [10]. Data from General Dynamics pertaining to the Centaur structural upgrades indicate that the modifications would incur a mass penalty of 210 kg and an additional cost of $28 million. Fortunately, the payload mass for this mission is below the structural limit of the Centaur.

3.3 CONCLUSIONS

Of the systems evaluated, only the Energia, the Space Shuttle, and the Titan IV launch vehicles are capable of launching the Hyreus spacecraft. The Space Shuttle was not selected because of its higher complexity, higher cost, and payload bay size limitations. The Energia was not chosen due to availability and reliability concerns. Several other less expensive vehicles could be used if the launch mass were reduced. Future mission planners should bear this in mind. For Project Hyreus, the Titan IV/Centaur was chosen for its reliability and availability. More detailed analysis confirmed the feasibility of using this launch vehicle.

NOMENCLATURE

CCAM	Contamination and Collision Avoidance Maneuver
EUS	Energia Upper Stage
IUS	Inertial Upper Stage
MECO1	Main Engine Cut-Off 1
MECO2	Main Engine Cut-Off 2
MES1	Main Engine Start 1
MES2	Main Engine Start 2
MLV	Mars Landing Vehicle
NASA	National Aeronautics and Space Administration
OMS	Orbital Manuevering System
RCS	Retro-Correction Stage (for Energia)
RCS	Reaction-Control System
SRMU	Solid Rocket Motor Upgrade
TOI	Transfer Orbit Injection
TOS	Transfer Orbit Stage

REFERENCES

1. Isakowitz, S. J., *International Reference Guide to Space Launch Systems*, American Institute of Aeronautics and Astronautics, Washington, DC, 1991.

2. Faranetta, C., Energia USA, Washington, DC, Personal communication, February 1993.

3. Jordan, J., Boeing Defense and Space Group, Seattle, WA, Personal communication, February 1993.

4. Griffin, M. D., French, J. R., *Space Vehicle Design*, Przemieniecki, J. S., Ed., American Institute of Aeronautics and Astronautics, Washington, DC, 1991.

5. Dornheim, M. A., "USAF May Pay Hercules for SRMU Loss", *Aviation Week and Space Technology*, March 1, 1993, p. 24.

6. Dickinson, Lt T., Air Force Titan Program Office, Los Angeles, CA, Personal communication, March 1993.

7. Callahan, T., General Dynamics, San Diego, CA, Personal communication, February 1993.

8. Quan, C., McDonnell Douglas, CA, Personal Communication, June 1993.

9. Vogt, T., Martin Marietta, Denver, CO, Personal Communication, April 1993.

10. General Dynamics Space Systems Division, *Titan IV/Centaur User's Handbook*, October, 1992.

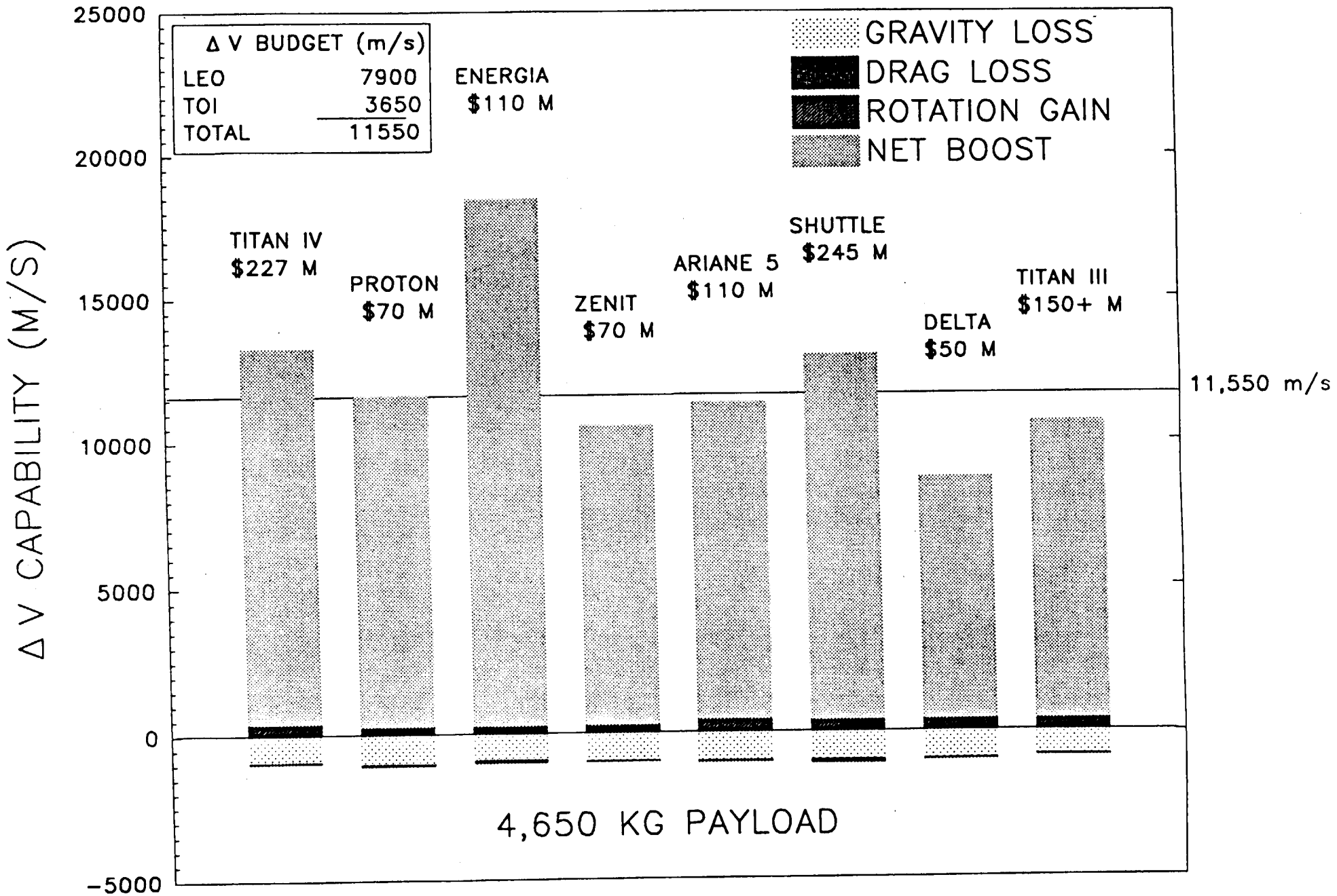

Figure 3.1 Launch System Analysis. ΔV capability of each system for the Hyreus spacecraft.

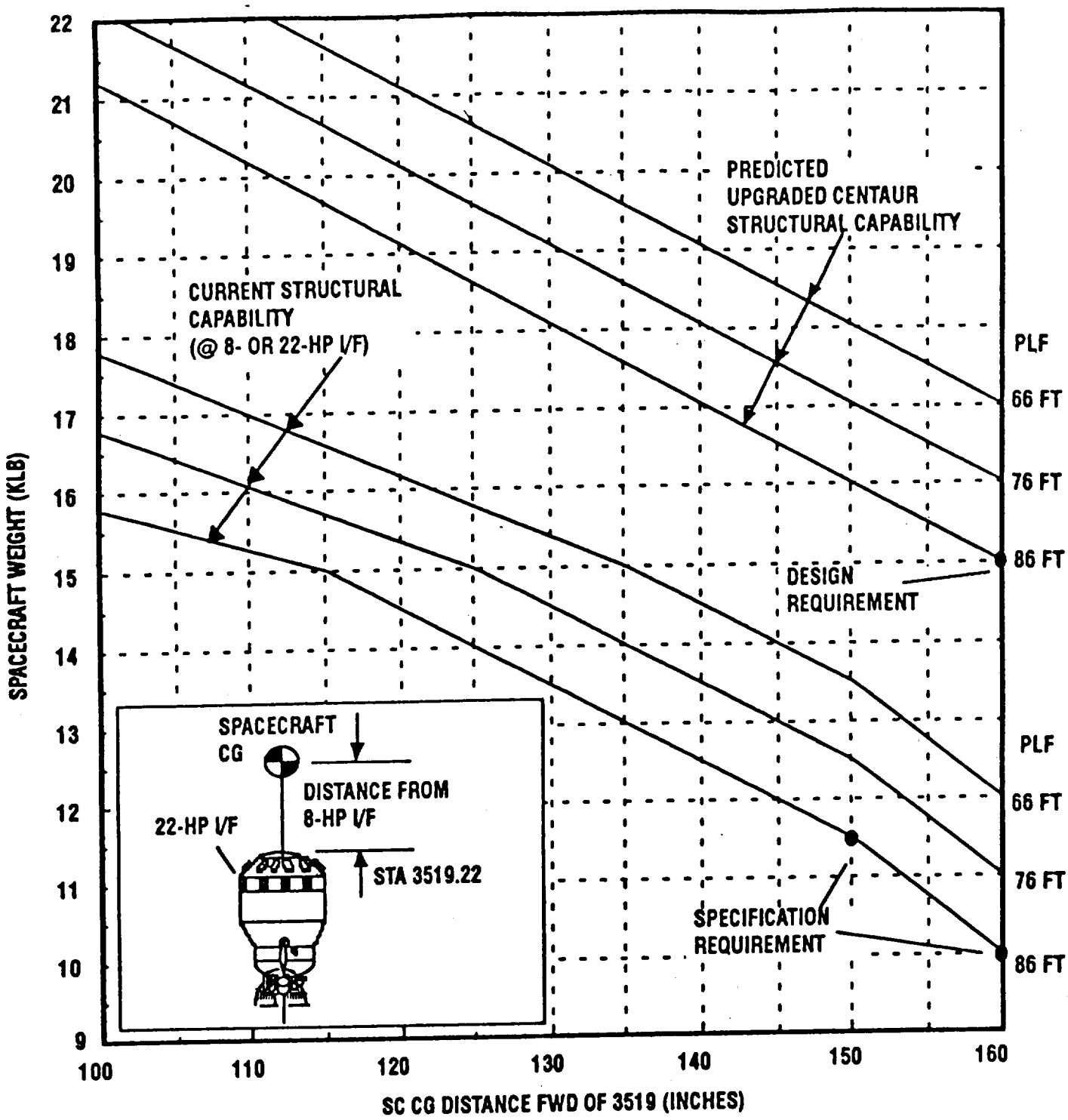

Figure 3.2 Centaur Structural Limit. Payload mass versus center of gravity position from the interface plane between the Centaur and the spacecraft. (This chart is from Ref. 10 and is in English units.)

4.0 ASTRODYNAMICS

Heather Nicholson

Elsayed Talaat

Lee Thrush

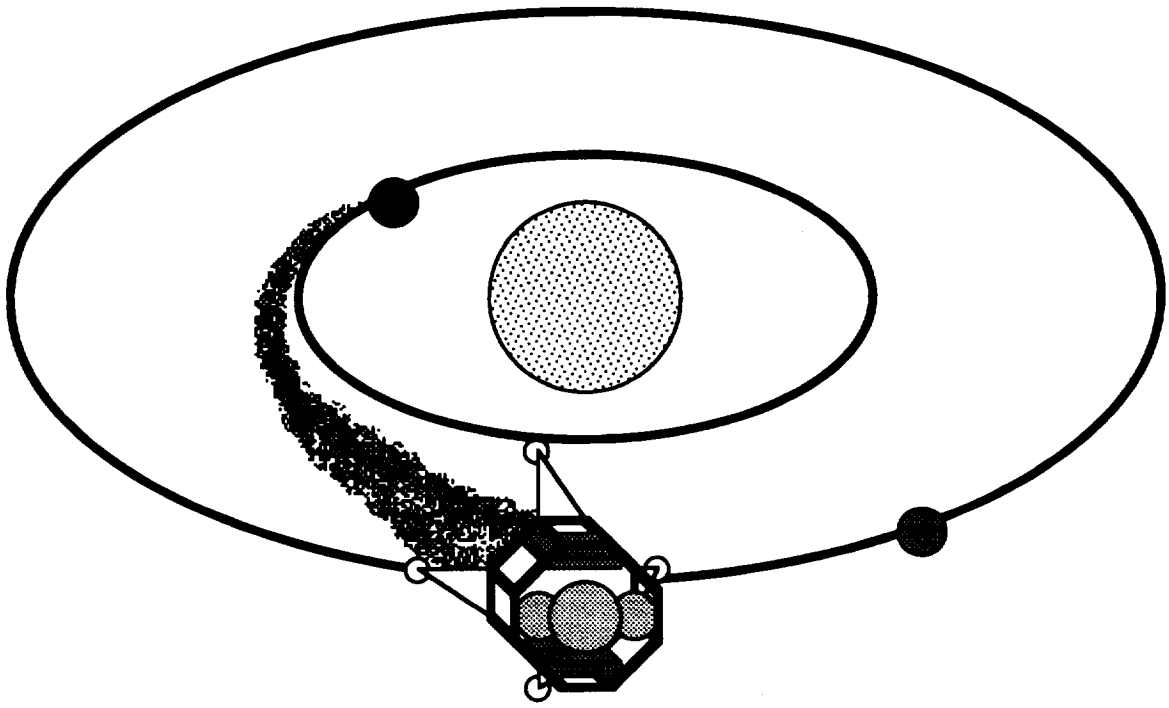

TABLE OF CONTENTS

4.1 **INTRODUCTION** 4.1

4.2 **MISSION CONSTRAINTS** 4.2

4.3 **MISSION WINDOWS** 4.3

4.4 **MISSION OVERVIEW** 4.5

4.4.1 Earth Launch and Escape 4.5

4.4.2 Earth-Mars Heliocentric Transfer Trajectory 4.7

4.4.3 Mars Arrival 4.8

4.4.4 Mars Surface Stay 4.9

4.4.5 Mars Escape 4.10

4.4.6 Mars-Earth Heliocentric Transfer Trajectory 4.11

4.4.7 Earth Capture 4.11

4.5 **CONCLUSIONS** 4.12

NOMENCLATURE 4.13

REFERENCES 4.15

FIGURES 4.16

4.1 INTRODUCTION

The Hyreus mission to Mars will consist of a single launch of an unmanned vehicle, assumed to occur in the year 2003. Mission windows and trajectory parameters have been specified using JPL Publication 82-43 [1], which is a handbook of plots, such as the one shown in Fig. 4.1, containing data on departure energies, hyperbolic excess velocities, times of flights, arrival hyperbolic excess velocities, and other transfer trajectory variables. Each transfer trajectory is uniquely specified by identifying pairs of departure and arrival dates. Because of the shape of the contours, these plots are referred to as "pork-chop" plots. The trajectory data contained in these plots are based on the Lambert method [1].

Trajectories are classified by the length of their transfer ellipse. As can be seen from Fig. 4.2, a vehicle will have a Type I trajectory if it travels less than 180° true anomaly around the sun. If it travels more than 180° true anomaly, the vehicle will have a Type II trajectory. Trajectories are also further subdivided into classes. A vehicle with a Class I trajectory will reach the target planet before apoapsis (for inbound missions, before periapsis). A vehicle with a Class II trajectory will reach the target planet after apoapsis (for inbound missions, after periapsis). This nomenclature is used as opposed to categorizing a trajectory as an opposition or conjuction class trajectory. An opposition class trajectory is defined as a high energy trajectory in which the positions of Earth at departure and the position of Mars at arrival are on generally the same side of the sun. A conjunction class trajectory is defined as one where the departure and arrival positions of Earth and Mars, respectively, are on generally opposite sides of the sun.

A Type I trajectory has the advantage of a shorter flight time, but there are drawbacks normally associated with this type of trajectory [2]. The energy of the trajectory is generally higher, thus the ΔV's required for injection into the transfer ellipse at Earth and for capture at Mars are high. This increases the amount of propellant necessary, which decreases the useful payload capacity. A Type II trajectory is generally a low energy transfer. This gives higher payload capacities for given energy expenditures.

It was found that an unusual case existed for the 2003 launch opportunity, in that the Type II trajectory from Earth to Mars actually required higher Earth departure energies. The 2005 Mars to Earth launch window was more typical and the Type II trajectory had lower energy requirements.

Since the primary concern for an unmanned mission of this kind is the maximization of payload, lower energy transfer orbits were used. A Type I trajectory was chosen for the flight to Mars and a Type II trajectory was selected for the return flight. The total trip time is approximately 2.8 years, with a Martian stay time of approximately 1.5 years.

4.2 MISSION CONSTRAINTS

The most important mission constraint is the necessity to minimize the transfer trajectory energy, in order to reduce the required overall ΔV for the mission. The lower the ΔV required, the lower the propellant expenditure and the higher the useful payload capacity of the mission. The trajectory energy must be minimized in order to reduce the required ΔV for the mission. The next mission constraint is the need to provide ample time to manufacture propellant and conduct planetary exploration and experiments.

4.3 MISSION WINDOWS

The mission will depart Earth in 2003 and depart the Martian surface 18.2 months later, in 2005. The launch window for Earth departure was specified by assuming a maximum departure energy and a constant date of arrival at Mars. The launch window for the return trip was specified in a similar manner. A computer program was used to specify the positions of Earth and Mars during the mission [3]. These positions are shown in Fig. 4.3.

The departure energy, C_3, is equal to the square of the hyperbolic excess velocity. The minimum value of C_3 for departure from Earth is 8.81 km^2/s^2 and occurs for a launch date of June 7, 2003 and an arrival date of December 25, 2003 [1]. The launch window for Earth departure is fully determined by assuming a maximum C_3 value of 10 km^2/s^2 and by keeping the arrival date constant at December 25, 2003.

The return trip will be launched from Mars in 2005. The minimum value of C_3 for the 2005 launch window from Mars is 13.197 km^2/s^2 and occurs for a launch date of July 8, 2005 and an Earth arrival date of March 31, 2006. The launch window for Mars departure is fully determined by assuming a maximum C_3 value of 14 km^2/s^2 and by keeping the arrival date at Earth constant at March 31, 2006.

Table 4.1 Launch window for Earth to Mars trajectory.

Window Opens	Window Closes	Min C_3 (km^2/s^2)	Max C_3 (km^2/s^2)	Arrival Date
May 22, 2003	June 20, 2003	8.81	10.00	Dec. 25, 2003

An alternate launch window for Mars departure exists in 2007. This launch window could be utilized if problems arise during the Martian stay time. For example, if the propellant production plant doesn't operate at the expected rate of output, the departure from Mars could be delayed until 2007, at which time enough propellant should be available for the return trip. The 2007 opportunity also requires a slightly lower C_3 value at departure, which would be advantageous in case of a failure in the propellant production plant before enough propellant for the 2005 launch is produced. The 2007 launch window has a minimum C_3 value of 10.20 km^2/s^2 and occurs for a launch date of July 21, 2007 and an Earth arrival date of April 29, 2008. The launch window is fully determined by assuming a maximum departure C_3 value of 14 km^2/s^2 and by keeping the Earth arrival date constant at April 29, 2008. Table 4.1 summarizes the launch window variables for the Earth to Mars trajectory. The variables for the Mars to Earth trajectory launch windows are summarized in Table 4.2.

Table 4.2 Launch windows for Mars to Earth trajectory.

Window Opens	Window Closes	Min C_3 (km^2/s^2)	Max C_3 (km^2/s^2)	Arrival Date
June 25, 2005	July 21, 2005	13.20	14.00	March 31, 2006
June 19, 2007	August 22, 2007	10.20	14.00	April 29, 2008

4.4 MISSION OVERVIEW

Of the many factors that influence the transfer trajectory choice, energy considerations are the most important. Minimizing the required energy for the flights to Mars and back to Earth results in less propellant needed and, therefore, an increase in payload capacity. The 2003 departure date from Earth was chosen due to its relatively low energy transfer trajectory and realistic mission date.

4.4.1 Earth Launch and Escape

The launch from Earth will occur from the Kennedy Space Center, which will result in an initial Low Earth Orbit (LEO) at 28.5° inclination to the Earth's equator [4]. A single burn will insert the transfer vehicle into the transfer trajectory from the initial LEO. The burn will occur over a relatively short time period and thus can be considered to be impulsive, as shown in Fig. 4.4.

The velocity, V_{ie}, at the injection point that the spacecraft must have in order to escape the Earth's sphere of influence and place intself on the correct trajectory asymptote to arrive at Mars is determined from the following equation:

$$C_3 = V_\infty^2 = V_{ie}^2 - 2\frac{\mu_e}{r_{ie}} \tag{4.1}$$

where: C_3 = departure energy

V_∞ = departure hyperbolic excess speed

V_{ie} = injection velocity

μ_e = Earth gravitational parameter, 3.986 X 10^5 km^3/s^2

r_{ie} = injection radius, $r_e + h_i$ = 6678 km

r_e = radius of Earth, 6378 km

h_i = height of injection, 300 km

For a maximum C_3 of 10 km^2/s^2, V_{ie} = 11.374 km/s.

For the purposes of the ΔV_{ie} calculations, it is assumed that the vehicle will depart from a 300 km cirular coast arc. The initial velocity of the vehicle can be calculated from:

$$V_{cs} = \sqrt{\frac{\mu_e}{r_{ie}}} = 7.726 \text{ km/s} \tag{4.2}$$

The maximum velocity increment required for insertion into the transfer trajectory, ΔV_{ie}, can be determined by subtracting V_{cs} from $V_{ie(max)}$, based on C_3 = 10 km^2/s^2.

$$\Delta V_{ie(max)} = V_{ie(max)} - V_{cs} = 3.648 \text{ km/s} \tag{4.3}$$

The minimum velocity increment required for Earth escape can be found by using the above method with the minimum value of C_3 of 8.81 km^2/s^2.

$\Delta V_{ie(min)}$ = 3.596 km/s

The launch / transfer orbit injection geometry is shown in Fig. 4.4. The direction of the departure hyperbolic excess velocity vector, with respect to the Earth Mean Equator and equinox of 1950.0 coordinate system is defined by the declination, δ_{∞}, and right ascension, α_{∞} [1]. The declination is the latitude of the outgoing asymptote. The right ascension is the equatorial east longitude from vernal equinox.

The ascent trajectory plane must contain the outgoing V_{∞} vector, the center of the Earth as one of the foci, and the injection point. The declination and right ascension are therefore necessary for determination of the initial orbit of the vehicle. For the given launch window, the declination varies from -6^{o} on May 22, 2003 to -10^{o} on June 20, 2003. The right ascension varies from 356^{o} on May 22, 2003 to 340^{o} on June 20, 2003.

4.4.2 Earth-Mars Heliocentric Transfer Trajectory

The heliocentric transfer trajectory from Earth to Mars was found from the JPL plots [1]. These plots are arrays of transfer arcs connecting Earth and Mars for specified pairs of Earth departure dates and Mars arrival dates. The algorithms used to obtain the contour plots are based on the Lambert method [1], which applies to restricted two-body orbital problems in which the primary body, the Sun, is so much more massive than the secondary body, the vehicle, that the system's gravitational attraction can be assumed to be concentrated at one point, the center of the Sun. The vehicle orbits the Sun in Keplerian orbits so that the Sun remains at one of the foci of the conic orbit. Once the departure and arrival dates are specified, the plots uniquely identify the transfer trajectory variables. The JPL plots give trajectories that require no mid-course plane changes. The trajectories are designed so that the vehicle departs the planet in the correct plane for target planet arrival. The Earth to Mars transfer trajectory variables are presented in Table 4.3.

Table 4.3 Earth to Mars transfer trajectory variables.

Launch Date	C_3 (km^2/s^2)	δ_∞ (deg)	α_∞ (deg)	Time of Flight (days)	ΔV_{ie} (km/s)
May 22, 2003	10.00	-6.0	356.0	217	3.648
June 7, 2003	8.81	-6.5	349.5	201	3.596
June 20, 2003	10.00	-10.0	340.0	188	3.648

4.4.3 Mars Arrival

The arrival hyperbolic excess velocity, VHP_m, is specified in the JPL plots. For the selected launch window, VHP_m is constant at 2.8 km/s. Knowing this value, the required velocity increment for capture into an orbit at Mars, ΔV_{cm}, can be calculated.

$$\Delta V_{cm} = \sqrt{VHP_m^2 + 2\frac{\mu_m}{r_p}} - \sqrt{\frac{2\mu_m r_a}{r_p(r_p + r_a)}} \qquad (4.4)$$

where: μ_m = Mars gravitational parameter 4.2828×10^4 km^3/s^2

r_p = radius of periapsis of capture orbit

r_a = radius of apoapsis of capture orbit

VHP_m= arrival hyperbolic excess velocity at Mars

C-2

For the purpose of aerobraking in the Martian atmosphere, a circular capture orbit of 500 km was used. This is discussed further in section 5. Thus, ΔV_{cm} is 2.147 km/s.

The velocity upon entrance into the Martian atmosphere, V_{en}, can also be calculated. This value determines how much velocity increment can be accomplished through aerobraking. For this calculation, it was assumed that the vehicle would first enter the Martian atmosphere at a height of 125 km. This is determned as follows:

$$V_{cm} = \sqrt{2\frac{\mu_m}{r_{en}} + VHP_m^2} = 5.69 \text{ km/s} \tag{4.5}$$

where: $r_{en} = R_m + h_e = 3497$ km

R_m = radius of Mars, 3380 km

$h_e = 125$ km

The vector of arrival at Mars is defined by the planetocentric right ascension of 59° and planetocentric declination of 5.5°.

4.4.4 Mars Surface Stay

The heliocentric transfer trajectory was designed to allow ample time to manufacture the propellant for the return trip and to conduct planetary explorations and experiments. The mission allows for a range of stay times of 547 to 574 days.

4.4.5 Mars Escape

As discussed in the previous section on mission windows, the launch window from Mars was specified by defining a maximum C_3 value of 14 km^2/s^2 and an Earth arrival date of March 31, 2006. For the calculations of the return trip velocity increments, a circular orbit altitude of 300 km prior to injection was assumed. The calculations for the velocity increment for injection into the Mars-Earth transfer trajectory, ΔV_{im}, are similar to the Earth departure calculations, as shown in the following:

$$V_{im(max)} = \sqrt{C_3 + 2\frac{\mu_m}{r_{im}}} = 6.097 \text{ km/s} \tag{4.6}$$

where: V_{im} = injection velocity

r_{im} = injection radius, $R_m + h_i$ = 3680 km

h_i = 300 km

It follows that, for $C_3 = 14 km^2/s^2$:

$$\Delta V_{im} = V_{im} - V_{cs} = 2.693 \text{ km/s} \tag{4.7}$$

The minimum ΔV_{im} can be found by using the minimum value of C_3 for the launch window; 13.197 km^2/s^2.

$\Delta V_{im(min)}$= 2.626 km/s

4.4.6 Mars-Earth Heliocentric Transfer

The Mars-Earth heliocentric transfer trajectory is determined in a manner similar to that of the Earth-Mars heliocentric transfer. The transfer variables are summarized below in Table 4.4.

4.4.7 Earth Capture

Earth capture will also be achieved through aerobraking. This will save a significant amount of propellant, which is of critical importance, as this propellant would need to be manufactured on Mars, requiring more raw materials to be transported to Mars.

Table 4.4 Mars to Earth transfer trajectory variables.

Launch Date	C_3 (km^2/s^2)	δ_∞ (deg)	α_∞ (deg)	Time of Flight (days)	ΔV_{im} (km/s)
June 25, 2005	14.00	-5.0	248.0	280	2.693
July 8, 2005	13.20	-12.0	240.0	260	2.627
July 21, 2005	14.00	-12.5	236.0	253	2.693

4.5 CONCLUSIONS

The process for designing a transfer trajectory for an interplanetary mission is one of optimization. For Project Hyreus, the most important factor is the energy requirement. When the transfer trajectory energy requirements are minimized, the velocity increments needed are also minimized. Thus, less propellant must be carried and expended by the vehicle. The weight savings can be applied towards carrying more payload.

For this reason, departure energy requirements were minimized for Project Hyreus. A Type I trajectory was chosen for the Earth-Mars heliocentric transfer while a Type II was chosen for the Mars-Earth heliocentric transfer. The launch from Earth will occur on June 7, 2003. The Mars sample will return to an Earth orbit on March 31, 2006. The energy requirements for Project Hyreus will be further reduced through aerobraking of the Mars landing vehicle at Mars and aerobraking of the sample container at Earth.

The total trip time of Project Hyreus is approximately 2.8 years. The Martian stay time is approximately 1.5 years. If the project goes as planned, this will be plenty of time to carry out Mars planetary science experiments and produce the required amount of propellant for the return trip. However, if the propellant plant operates at an unexpectedly lower rate of production, the launch from the Mars surface could be delayed until 2007. In this case, the Mars launch would occur on July 21, 2007 and the sample container would return to an Earth orbit on April 29, 2008. This alternate launch date could also be used in case of a failure of the propellant production plant before enough propellant has been produced for the 2005 launch. The later launch date has a lower departure energy requirement, thus it requires less propellant to return to Earth.

NOMENCLATURE

C_3	Departure energy of transfer trajectory
δ_∞	Declination; latitude of departure asymptote (vs. mean Earth equator and equinox of 1950.0)
JPL	Jet Propulsion Laboratory
r_a	Radius of apoapsis
r_e	Radius of Earth, 6378 km
R_e	Radius of earth's orbit around the Sun
r_{en}	Atmospheric entrance radius at Mars, 3522 km
r_{ie}	Injection radius at Earth, 6678 km
α_∞	Right ascension; equatorial east longitudeof departure asymptote from vernal equinox (vs. mean Earth equator and equinox of 1950.0)
r_m	Radius of Mars, 3380 km
R_m	Radius of Mars' orbit around the Sun
r	Radius of Earth , 6678 km
r_p	Radius of periapsis
r_∞	Radius of Earth's sphere of influence
TOF	Time of flight
V_{cs}	Circular orbital velocity of vehicle; at 300 km, V_{cs} = 7.726 km/s
V_e	Orbital velocity of Earth around the Sun, 29.78 km/s

V_m Orbital velocity of Mars around the Sun, 24.14 km/s

V_{en} Velocity upon entering the Martian atmosphere

VHP_e hyperbolic excess velocity at Earth

VHP_m hyperbolic excess velocity at Mars

V_{ie} Heliocentric speed at Earth departure point

V_∞ Hyperbolic excess velocity at Earth departure

ΔV_{ce} Change in velocity required for capture at Earth

ΔV_{cm} Change in velocity required for capture at Mars

ΔV_{ie} Change in velocity required for insertion into transfer orbit at Earth

μ_e Gravitational parameter of Earth, 3.986×10^5 km^3/s^2

μ_m Gravitational parameter of Mars, 4.2828×10^4 km^3/s^2

μ_s Gravitational parameter of Sun, 1.3271×10^{11} km^3/s^2

REFERENCES

1. Sergeryevsky, A. B., Snyder, G. C., and Cunnif, R. A., *Earth to Mars Ballistic Mission Opportunities, 1990-2007*, Publication 82-43, Jet Propulsion Laboratory, Pasadena, CA, 1983.

2. Bate, R. R., Mueller, D. D., and White, J. E., *Fundamentals of Astrodynamics*, Dover Publications Inc., New York, 1971, pp. 321-380.

3. Brown, C. D. "Orb: Mission Design software," in *Spacecraft Mission Design*, American Institute of Aeronautics and Astronautics, Inc., Washington D. C., 1992.

4. Beerer, J. G. and Roncoli, R. B., "Mars Observer Trajectory and Orbit Design," *Journal of Spacecraft and Rockets*, Vol. 28, 1991, pp. 515-521.

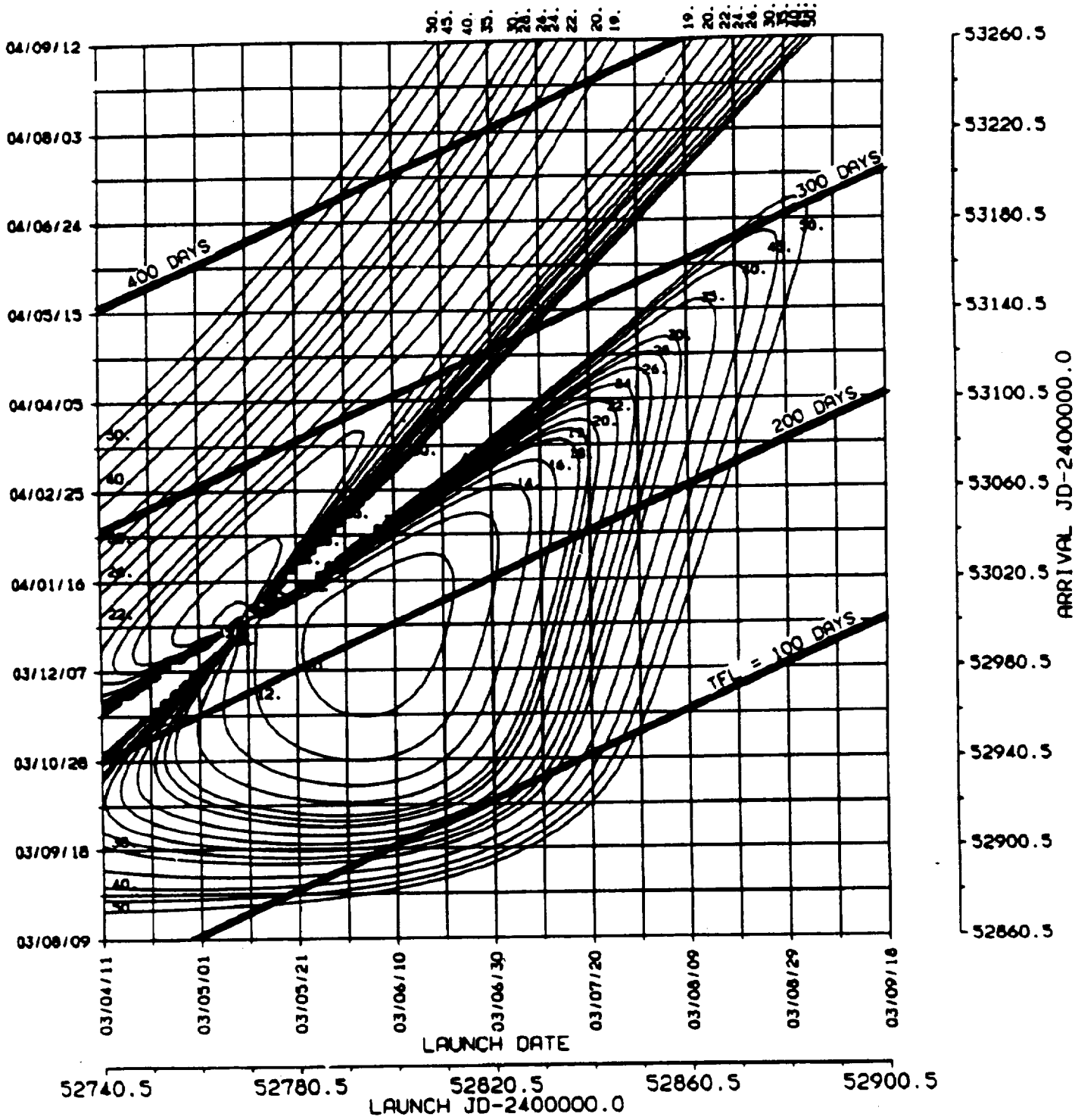

Fig. 4.1 "Pork-Chop" plot of C3 contours: Earth to Mars, 2003. Courtesy of Jet Propulsion Laboratory (JPL publication 82-43).

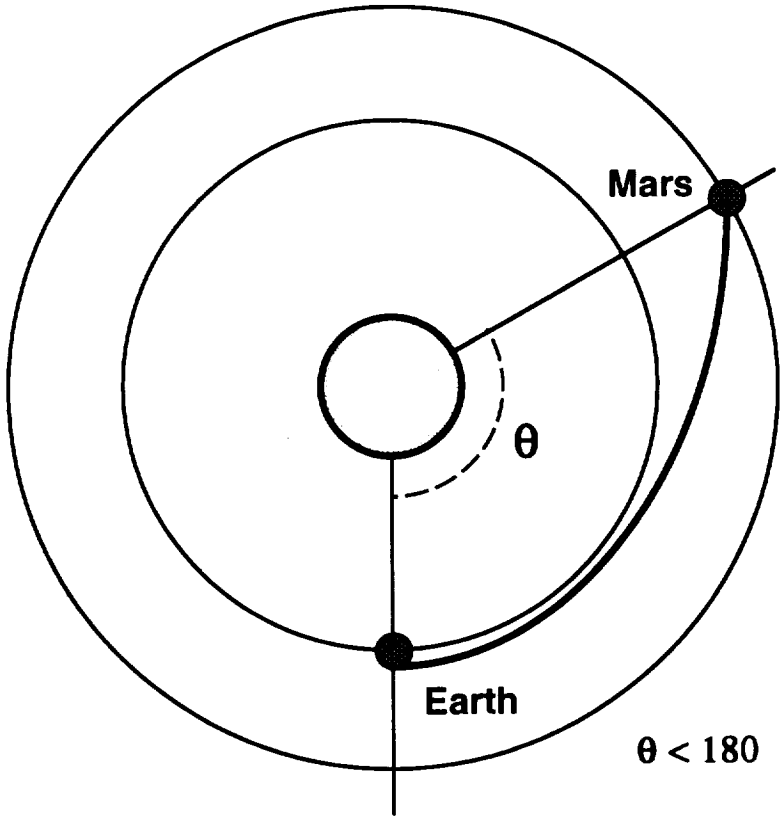

Fig. 4.2a Trajectory types (Type I).

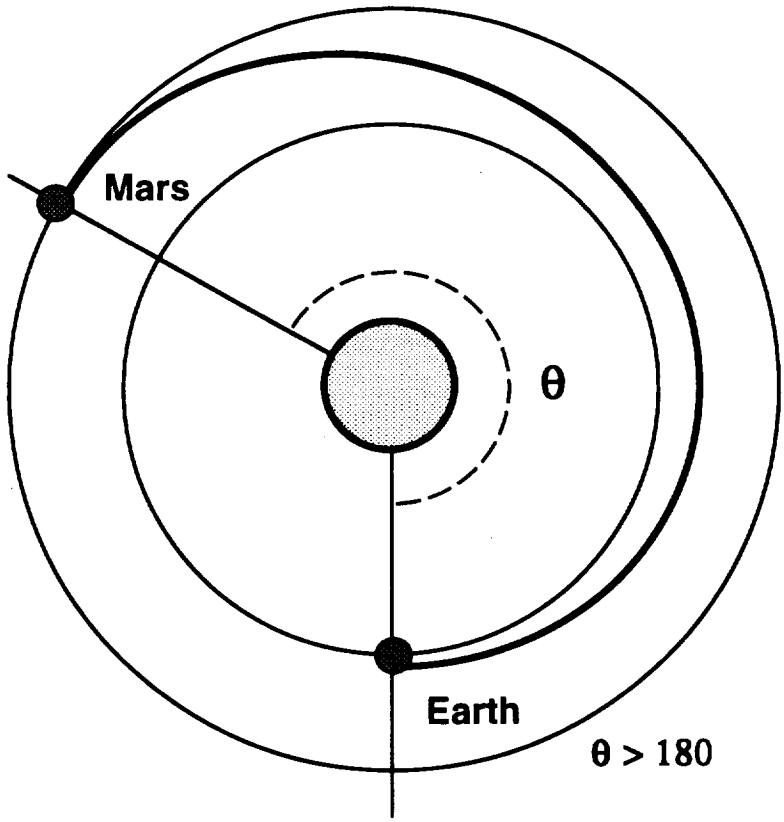

Fig. 4.2b Trajectory types (Type II).

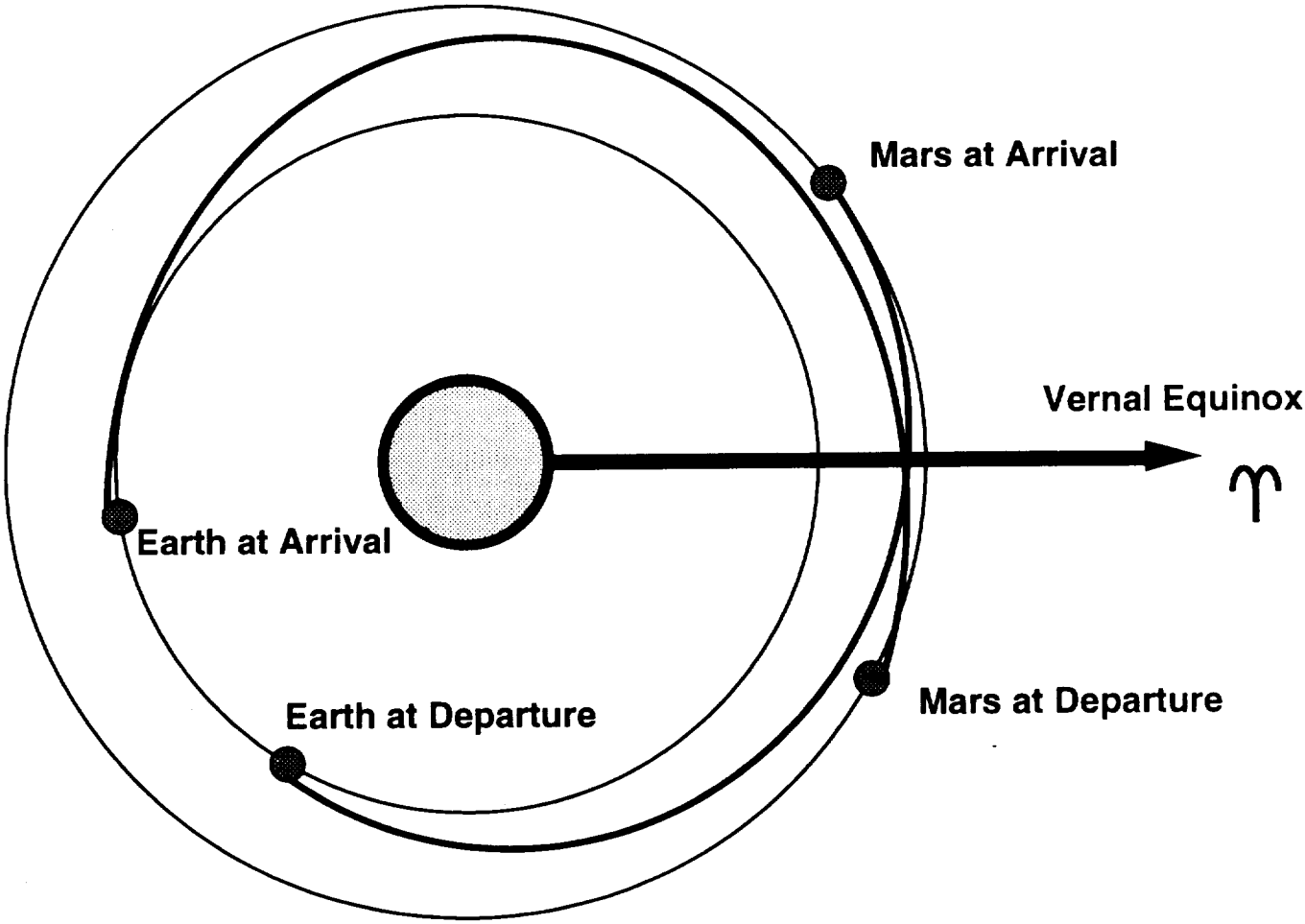

Fig. 4.3 Mission geometries.

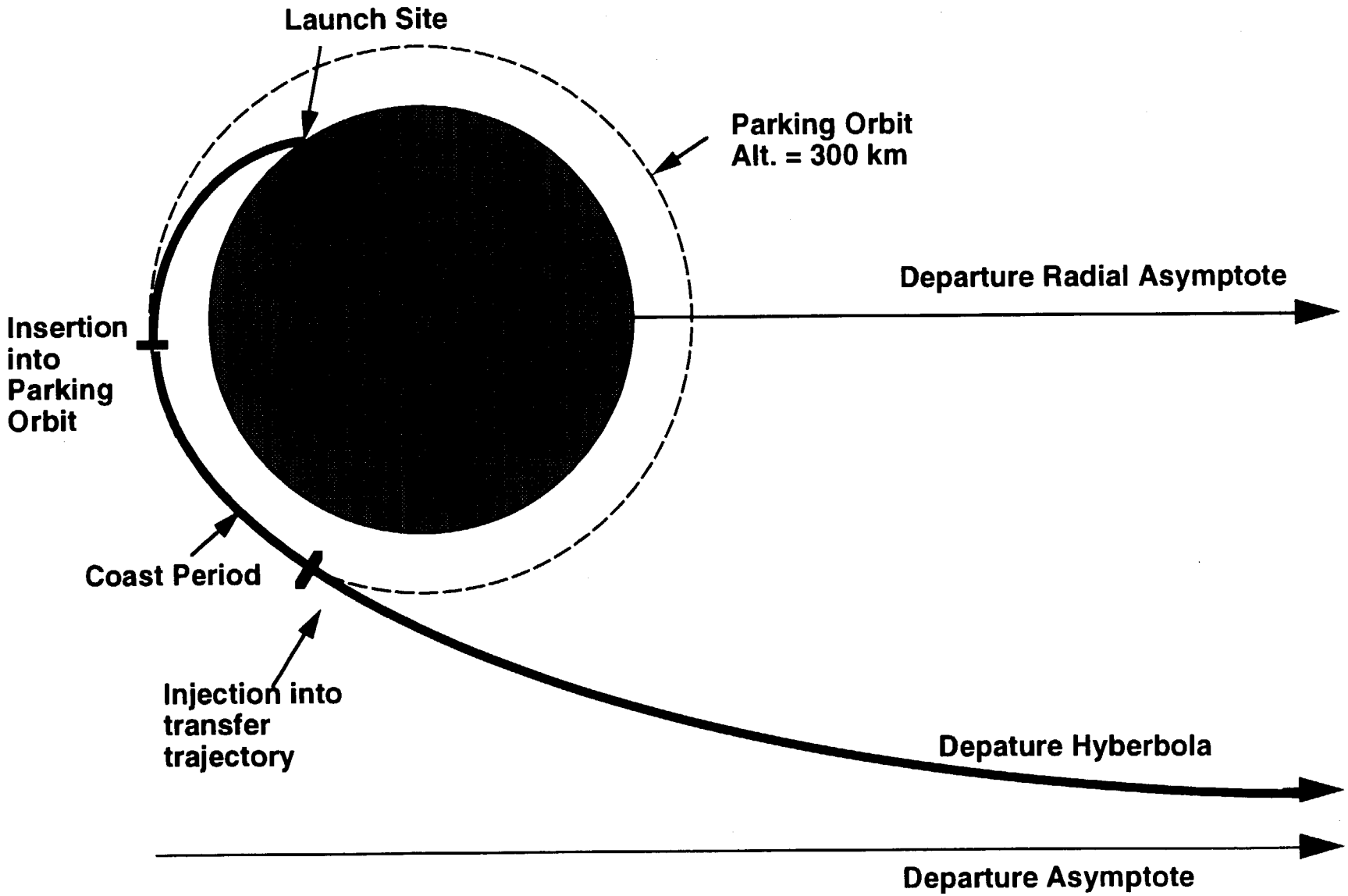

Fig. 4.4 Planetary escape velocity diagram.

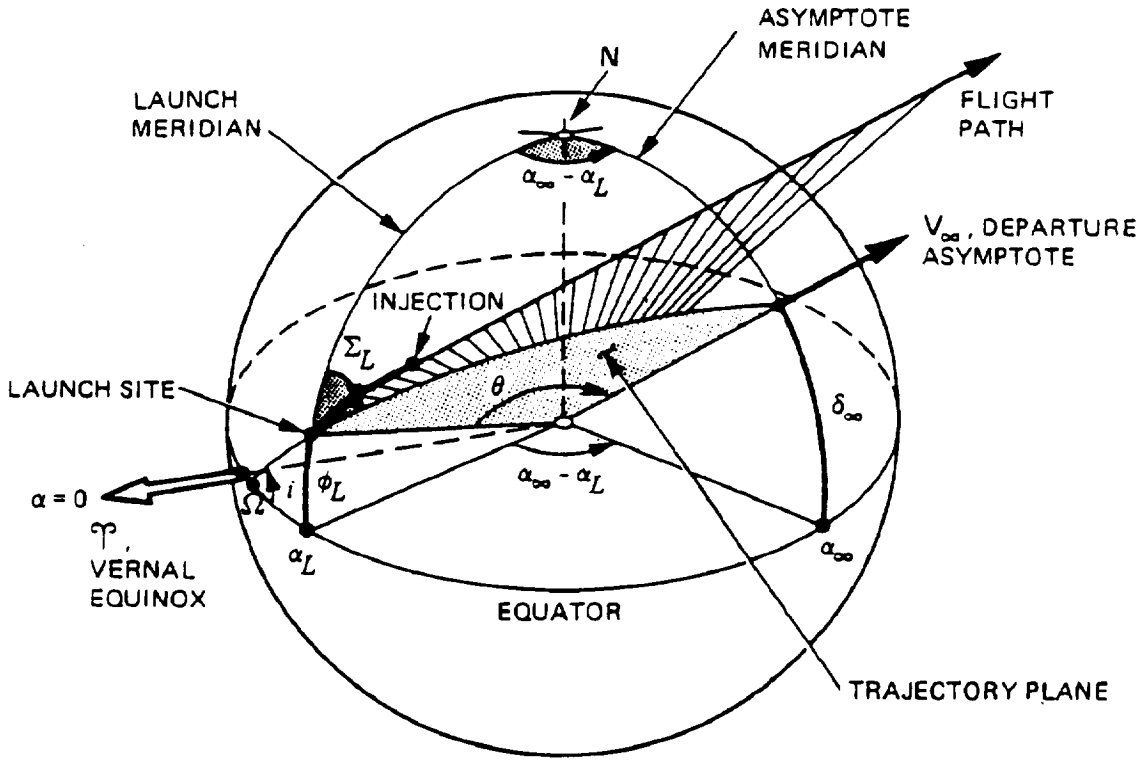

Fig. 4.5 Launch/Injection Geometry. Courtesy of The Jet Propulsion Laboratory. (JPL publication 82-43)

5.0 Atmospheric Entry and Aerobraking

Heather Nicholson

Laurie Nill

Eric Schug

Elsayed Talaat

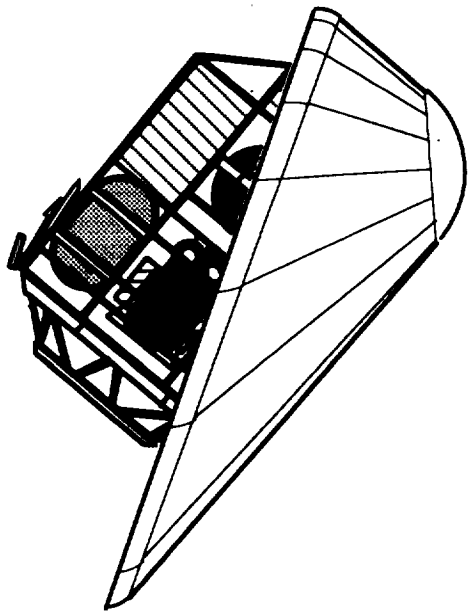

TABLE OF CONTENTS

5.1 INTRODUCTION 5.1

5.2 AEROBRAKING PASS AT MARS 5.2

5.2.1 Aerobraking Pass Scenario 5.2

5.2.2 Vehicle Trajectory Calculations 5.3

5.2.3 Heat Transfer and G-Loading 5.5

5.3 FINAL MARS ENTRY AND LANDING 5.7

5.3.1 Stage 1 ..... 5.7

5.3.2 Stage 2 ..... 5.7

5.3.3 Stage 3 ..... 5.8

5.4 MARS AEROBRAKE DESIGN 5.8

5.4.1 Mars Aerobrake Geometry 5.8

5.4.2 Mars Aerobrake Structure 5.10

5.4.3 Thermal Protection System for Mars Aerobrake 5.11

5.5 CONCLUSIONS 5.13

NOMENCLATURE 5.15

REFERENCES 5.16

FIGURES 5.18

5.1 INTRODUCTION

(Laurie Nill)

It is imperative on a Mars sample return mission to minimize the ΔV requirement, in order to reduce the amount of propellant required for the journey, and thus increase the payload, or in fact, make the desired payload a reasonable possibility. In an effort to decrease the ΔV requirement on both the outgoing and returning Mars trajectories, aerobraking is performed in both the Martian atmosphere and Earth's atmosphere [1]. It has been calculated that aerobraking decreases the launch mass to one-third the mass that would be required for an all-propulsive capture and descent at Mars. Aerobraking, or the use of atmospheric drag to reduce the velocity of a space vehicle, results in a change of orbit of that vehicle [2]. One aerobraking scenario that appears especially relevant for Mars aeroassist and entry for Project Hyreus is the multi-pass aerobraking scenario involving a highly elliptical orbital pattern [3,4]. The vehicle makes two passes through the Martian atmosphere before the final landing pass. Computer simulations were performed using the general equations of motion in order to calculate ΔV's for each atmospheric pass, as well as the maximum g-loading and maximum heat transfer at the stagnation point. The optimum aerobrake configuration, which is dictated by constraints such as lifting requirements to execute skip maneuvers out of the atmosphere and ease of satellite deployment, is a raked sphere-cone design. Specific materials have been chosen for the thermal protection system that can withstand the expected heating and loading. For the Earth return segment, similar computations were made and an ablative, Apollo style aerobraking shell was selected for re-entry [5] and are discussed in Section 11 with the entire Earth return segment of the mission.

5.2 AEROBRAKING PASS AT MARS

(Laurie Nill, Eric Schug)

For Project Hyreus, aeroassist at Mars consists of two aerobraking passes. The purpose of the first pass is aerocapture at Mars from the hyperbolic transfer trajectory into an elliptical parking orbit, and the purpose of the second pass is to lower the apoapsis in order to deploy the satellite and then do a final entry for landing in the Mangala Valles region on Mars [6,7].

5.2.1 Aerobraking Pass Scenario

(Laurie Nill)

When the Mars Landing Vehicle (MLV) approaches Mars in its hyperbolic transfer trajectory, it arrives in a polar plane of Mars. Capture into a polar orbit provides ready deployment of the satellite in a sun-synchronous orbit. The MLV enters the Martian atmosphere for an aerobraking pass at a velocity of 5.69 km/sec and decelerates enough to enter an elliptical orbit (See Fig. 5.1). The effective atmospheric altitude has been assumed to be 125 km. During this first aerobraking pass, the vehicle descends to an altitude of 55 km at which point the increased density of the atmosphere and the lift vector of the aerobrake cause it leave the atmosphere in a skip maneuver. A summary of the aerobraking pass characteristics is given in Table 5.1.

The vehicle exits the Martian atmosphere with a velocity of 3.901 km/sec, and a flight-path angle of 7.47°, which determines its elliptical orbit of r_p = 3361 km and r_a = 5852 km, where r_p and r_a are the periapsis and apoapsis radii of the ellipse. Because the exit flight path angle is large, the orbit obtained by aerobraking has a periapsis below the Martian surface, and a short burn of 56.5 m/sec at the apoapsis point is required to bring the periapsis back up to an altitude of 250 km (well outside the effective atmosphere). The

MLV remains in this elliptical parking orbit until the rotation of Mars brings the landing site into proper alignment for skip entry, deployment of the satellite, and finally, landing.

When the MLV is prepared for descent, another apoapsis burn of 36 m/sec brings the periapsis altitude back down to 72 km and the second aerobraking pass can begin. The MLV decelerates on this second pass to a velocity of 3.59 km/sec, which gives it an apoapsis altitude of 580 km. Once the MLV has reached the apoapsis point, the reconnaissance/ communications satellite is deployed, using its own ΔV capability to place it into a 580 km circular orbit around Mars (See Fig 5.2). The total ΔV capability needed for the MLV for apoapsis burns is 92.5 m/sec. Table 5.1 summarizes the elliptical orbit characteristics for aerobraking. It is necessary on the second pass to have a periapsis radius below the surface of Mars in order to re-enter at the proper angle. After deployment of the aerobrake, the MLV makes a final entry into the Martian atmosphere for landing at the selected landing site.

Table 5.1 Summary of Aerobraking Passes at Mars

	Entry Velocity (km/sec)	Exit Velocity (km/sec)	Exit Angle (γ)	Apoapsis Burn (m/sec)	Periapsis Radius, r_p (km)*	Apoapsis Radius, r_a (km)
First Pass	5.69	3.90	7.47°	-----	3361	5850
Parking Orbit	-----	-----	-----	56.5	3630	5850
Second Pass	3.91	3.59	5.13°	36	3283	3960

* Mars radius = 3380 km

5.2.2 Vehicle Trajectory Calculations

(Laurie Nill, Eric Schug)

In order to calculate the flight trajectory, the entry and exit flight-path angles, and the velocity change of the MLV as it performs aerobraking passes through the Martian

atmosphere, the equations of motion for the flight trajectory, which are listed below, were used in a computer simulation [8]. The assumptions that were made in using these equations are: the aerobraking pass is contained in a two-dimensional plane, the surface of Mars is not flat but spherical, the planet Mars is non-rotating, and the atmosphere can be approximated by using an exponential model. (These equations can be used for both Martian entry and Earth entry)

Atmospheric model:

$$\rho = \rho_0 \exp\left(-\frac{h}{H}\right) \tag{5.1}$$

Equations of motion:

$$\frac{dV}{dt} = -\left(\frac{\rho V^2}{2\beta}\right) + (g\sin\gamma) \tag{5.2}$$

$$V\left(\frac{d\gamma}{dt} + \frac{d\theta}{dt}\right) = g\cos\gamma - \frac{\rho V^2}{2\beta}\left(\frac{C_L}{C_D}\right) \tag{5.3}$$

Velocity components in the local frame:

$$(R+h)\frac{d\theta}{dt} = V\cos\gamma \tag{5.4}$$

$$\frac{dh}{dt} = -V\sin\gamma \tag{5.5}$$

where:

C_L/C_D = Lift to Drag Ratio = 0.4

g = variable gravity at Mars

h = Altitude of entry vehicle

H = Scale height for exponential atmosphere = 10 km

R = Radius of Mars = 3380 km

V = Velocity of vehicle in the atmosphere

V_E = Entry velocity of vehicle in the atmosphere = 5.69 km/sec (first pass)

β = Ballistic Coefficient = mass/C_d*Area = 66.5 kg/m^2

γ = Flight path angle to the local horizontal

γ_E = Flight path angle on entry to the atmosphere = -7.5° [9]

θ = Angle with respect to the inertial coordinate system of planet

ρ_0 = reference density ("sea level") = 0.012 kg/m^3

Figures 5.3a and 5.3b show graphical results obtained from the computer simulation. The ΔV which is obtained per pass can vary depending on the entry flight-path angle into the atmosphere. Therefore, it is necessary to interpolate flight-path angles for the two passes until an optimum parking orbit and second skipping pass are obtained which land the vehicle at the predetermined landing site at Mars [9]. Such an interpolation was performed to determined the characteristics of the aerobraking passes for Project Hyreus. One advantage of doing aerobraking passes before entering for landing on Mars is that the vehicle has an opportunity to take measurements of the atmosphere on the first pass, and thereby make any corrections that are deemed necessary to the attitude of the MLV in view of the new data.

5.2.3 Heat Transfer and G-Loading

(Laurie Nill, Eric Schug)

The maximum stagnation point heat transfer to the vehicle by aerodynamic heating is calculated for an aerobraking pass by using the same computer simulation that was used

to determine the trajectory of the MLV [8]. An additional equation required for the analysis is that for heat transfer at the stagnation point of the aerobrake, and is as follows:

$$\dot{q} = \frac{1}{4} C_F \rho V^3 \tag{5.6}$$

where:

C_F = average total friction coefficient = 0.5

q = heat transfer rate per unit area

According to the calculations performed using the above equation, the maximum stagnation point heat loading that will occur is approximately 75 W/cm^2. This maximum was determined to occur during the second pass through the Martian atmosphere. Although the heating rate is strongly dependent on the velocity of the MLV, the maximum heating rate occurs at approximately 0.72*V_E [8]. The variation of stagnation point heat flux with time is shown in Fig. 5.3b. Aerodynamic heating is not a determining factor, however, for aerobraking it will be an important factor as the materials chosen need to provide the required thermal insulation as well as be light weight [4,5,10]. The materials and structure of the aerobrake are discussed in more detail in Sections 5.4.1 and 5.4.2.

Aerodynamic loading is a second factor to consider. The transverse loading, or loading perpendicular to the central axis of the MLV structure, defines structural requirements for the landing vehicle. As with the calculations for heating, the g-loading calculations were done with the same computer simulation by finding the dynamic pressure, using the aerobrake surface area, and performing a force balance. The force on the vehicle is then normalized by the mass and Earth's gravity constant. Figure 5.3d shows the variation of the g-loading experienced by the aerobrake versus time on the first aerobraking pass. The amount of loading determines the characteristics of the support structure that is used for the aerobrake and the support structure of the MLV. By keeping

the aerodynamic loading down to minimal values, the structure of the system can be simplified and kept lighter, however, for a unpiloted mission to Mars, aerodynamic loading is also not a limiting factor.

5.3 FINAL MARS ENTRY AND LANDING

(Laurie Nill)

Mars entry and landing consists of three phases similar to that used by the Viking Lander [11]. Figure 5.4 is a diagram portraying the descent phases which are described in detail below.

5.3.1 Phase 1

The first phase is deceleration of the vehicle by aerobraking on entry into the atmosphere. The MLV decelerates to a velocity of 220 m/sec (M= 0.31) at an altitude of 10 km; at which point a small rocket pulls out the first parachute lines. As soon as the first parachute begins to open, the aerobrake is detached using explosive bolts. The aerobrake separates rapidly from the rest of the vehicle as the MLV and parachute system experience three times more drag than the aerobrake.

5.3.2 Phase 2

The second stage begins at an altitude of 8 km and involves deployment of the last two parachutes to further decelerate the MLV. The deceleration of the MLV upon parachute deployment was calculated to be only about 5 g if one parachute is deployed before the

other two. The parachutes are all of the conic ribbon style which has been shown to be reliable in operating conditions from subsonic flow regimes into transonic flow regimes [12,13]. Each parachute has a surface area of 980 m^2 and a drag coefficient of 0.5. (The cluster of parachutes has an effective drag coefficient of approximately 0.4) The parachutes are made of Kevlar 29 material because of its weight savings and superior heat load capacity over Nylon [14,15]. The total mass of the parachute system is 250 kg. The use of a cluster of parachutes instead of a single parachute acts to stabilize the parachute system in the lateral direction as well as to decrease the terminal velocity of the MLV. Once the terminal velocity of 40 m/sec is achieved at an altitude of 500 m, the parachutes are jettisoned to avoid entanglement with the MLV during the final phase of descent.

5.3.3 Phase 3

The last phase, which begins with the jettisoning of the parachutes, is firing of the retro-rockets. The landing rockets employed are bi-propellant hydrazine rockets which were described in detail in Section 2. Four throttleable Marquardt R40-B thrusters are located on the bottom of the MLV. Retro-firing slows the vehicle from 40 m/sec to a soft landing at the landing site in the Mangala Valles region on Mars.

5.4 MARS AEROBRAKE DESIGN

(Laurie Nill, Eric Schug, Elsayed Talaat)

5.4.1 Mars Aerobrake Geometry

(Eric Schug)

Initially, a multitude of aerobrake designs for use at Mars were investigated, but many were found to be inconsistent with the needs of this mission. Complex designs that

require large numbers of panels to be moved or that need complicated mechanisms for moving different sections were rejected. Preliminary investigation showed the biconic and the raked sphere-cone aerobrake shapes to be the most favorable to fulfill the requirements of Project Hyreus. Both are able to provide our need for moderate lifting design. Both are comparatively lightweight and have a simple design. The raked sphere-cone shape was chosen over the biconic shape, because of its lower mass, 20% less [5]. In addition, the biconic aerobrake causes problems with the placement of the satellite for deployment. The only open location inside the biconic is at the rear, next to the control and landing thrusters. The raked sphere-cone shape has also been extensively studied for various other missions, such as the Aeroassist Flight Experiment, which supplied information on its aerobraking characteristics.

The geometry of the Mars Aerobrake (MA), shown in Fig. 5.5, is set to provide a lift to drag ratio (L/D) of 0.4. This gives added controllability to make up for variances in atmospheric conditions or deviations from the predicted flight path. The MA is constructed of a 45° half-angle cone with a rounded spherical nose of 1.2 m radius. The rake angle is at 67° and sets the aerobrake dimensions at 11.3 m by 9.4 m. The trailing skirt has a radius of 0.4 m which provides added structural support and allows the flow to separate smoothly from the MA. The placement of the MLV within the MA sets the combined center of mass (c.m.) location at 5.1 m aft of the cone's apex and 1.4 m below the cone's axis , as shown in Fig. 5.6. This placement has been designed to place the MLV as far upward as possible while keeping it in the wake of the aerobrake, and allows for a nominal angle of attack of 0°. In order to decrease the size of the Earth launch vehicle fairing which must carry both the aerobrake and MLV, the aerobrake has hinged sections that fold around the MLV to provide a closer fit within the fairing, as shown in Fig. 5.7, and to enable the fairing diameter to be reduced from 9.5 m to 7.5 m. In addition, the hinged sections improve the c.m. location for the launch configuration by moving it closer to the center of the MLV.

5.4.2 Mars Aerobrake Structure

(Eric Schug, Elsayed Talaat)

The aerobrake structure is divided into three parts, the supporting framework, the shell structure, and the hinge configuration. The supporting framework transmits the loads from the shell to the MLV. The shell structure along with the thermal protection system is discussed in the next section. The hinges allow the aerobrake to fold tightly around the MLV for launching.

When the Centaur fires for the trans-Mars injection, the maximum g force is 6.5. The aerobrake must be able to hold its own weight at this loading, approximately 48 kN. During aerobraking maneuvers the forces on the shell can reach 33 kN. The supporting framework, outlined in Figs. 5.8, 5.9a, and 5.9b, is designed to direct the forces to the MLV structure. Attachment ribs, 1 cm thick, run along the inside of the aerobrake and connect the supporting members to the shell. The rods are 4 cm in diameter with a 0.4 cm wall thickness and are attached to the MLV structure with pyrotechnic bolts. The rods and ribs are constructed of aluminum-lithium 2090, the same material used for the MLV structure. The rods attach to the ribs by means of pin connections with aluminum-lithium 7075-T6 end fittings shown in Fig. 5.10. The tube end attachment uses two-piece fittings wound onto the support tube.

As noted above, the aerobrake has two folding panels whose purpose is to reduce the required fairing inside diameter from 9.5 m to 7.5 m. The 7.5 m aerobrake, however, is not yet narrow enough to fit inside the dynamic allowances needed for the fairing. Figure 5.7 shows the aerobrake in launch configuration with panels folded. Once in orbit, the panels are unfolded and the joints sealed tight. Figure 5.11 shows the hinging structure for these panels. Locking joint members are positioned on the inside of the aerobrake to

keep the panels sealed tightly and to provide structural rigidity across the seam. The shell is cut so that it is angled with the flow direction (Fig. 5.11). This angle provides two benefits. First, it allows the flow to move smoothly across the seam, preventing stagnation of the flow at the seam. Second, it provides high insulation as the heat must travel farther in the seam before it reaches the mechanical sealer. The mechanical sealer is a high-temperature flexible sealing mechanism that is used to prevent flow through the seam. The sealing mechanism is placed on the inner part of the shell where the temperature is lower. Figure 5.12 shows an example of one possible sealer which was designed by Boeing [16].

5.4.3 Thermal Protection System For Mars Aerobrake

(Laurie Nill)

The Thermal Protection System (TPS) of the aerobrake was specifically designed to meet maximum heating requirements based on the entry parameters and aerobrake geometry. Because the TPS contributes a significant portion of the total mass to the entry vehicle, the heating requirements must be thoroughly analyzed and a TPS designed to meet those requirements while minimizing mass. For Project Hyreus, the entry velocity of the MLV at Mars is 5.69 km/sec, so there will be maximum heating in the range of 50-75 W/cm^2 at the stagnation point. An existing material that is ideal for use in insulating the aerobrake is Fibrous Refractory Composite Insulation (FRCI-12) [5,17] which has a low density and thermal conductivity (See Table 5.2) and has recently been incorporated into the Shuttle TPS [18]. However, the heating rate found at Mars exceeds the maximum heating rate of 62 W/cm^2 for FRCI-12, so a layer of Advanced Carbon/Carbon Composite Material is added at the stagnation region (the entire stagnation region around the nose requires Carbon/Carbon insulation). Ablative materials are not needed for the Mars TPS, because at entry velocities below 8 km/sec, radiative heating is not significant compared to convective heating. The total heating stays low enough to use non-ablative materials for

most of the area of the aerobrake. Even with relatively low heat transfer rates, the majority of the heat transferred to the aerobrake must be absorbed or re-emitted by the TPS, the FRCI-12, because the support structural components which rigidify the aerobrake cannot withstand high heat loads and temperatures.

The other components of the thermal protection system are the protective coating on the surface of the FRCI-12, and the Nomex strain isolation pad (SIP) between the structural core and the TPS (A cross-section of the materials used in the Mars aerobrake is shown in Fig. 5.13). The coating used on this aerobrake is Refractory Cured Glass (RCG), which is a high emissivity material commonly used on the surface of thermal insulation systems such as the Shuttle tiles. With this coating, the maximum temperature of the surface is calculated to be 1900-2000 K. All of the layers are joined together with an adhesive. Table 2 below lists all of the materials used in the TPS and the structure of the aerobrake and gives the masses of the various components.

Carbon/ Carbon composite insulation is only used sparingly in the TPS because of its high density. The total mass of the aerobrake TPS system and honeycomb support is 705 kg. (This total does not include the structural supports that connect the aerobrake to the MLV.)

The thermal protection system of the Mars aerobrake is attached to an aluminum honeycomb core mounted between graphite epoxy face sheets [18]. The aluminum used for the core is Al 2024 which can withstand several MPa of loading in the transverse direction, yet has a low density [19]. The epoxy face sheets add stiffness to enable the aerobrake to withstand the g-forces on Earth launch and the g-forces from each aerobraking pass and the landing sequence. The maximum working temperature for the graphite epoxy is 650 K [19] which determines the thickness of the composite insulation. A safety factor

of two was incorporated into the thickness of the FRCI-12 in order to give it a large heating margin in the calculations.

Table 5.2 Thermal Protection System and Supporting Structure

	Density ρ (kg/m^3)	Mass (kg)	Max Heating (W/cm^2)	Thickness (mm)	Thermal Conductivity (W/m-k)
RCG ε = 0.85 emissive coating	2700	0.08	------	0.25	------
FRCI-12 composite insulation	193	193	62	10	3
Carbon/Carbon composite insulation	1650	83	88	5	24.2
Aluminum 2024 honeycomb Core	90	297	------	30	165
Graphite Epoxy core face sheets	1580	87	------	0.5	40
Nomex SIP	100	44	------	4	-----
Epoxy Resin adhesive(total)	0.01	0.001	------	1	-----

5.5 CONCLUSIONS

(Laurie Nill, Eric Schug)

The reduction in mass that results from using an aerobrake rather than using purely propulsive means increases the capability of Project Hyreus to accomplish its goals as a precursor to a manned mission to Mars, and as a scientific exploration mission by requiring only a single Titan IV launch vehicle. The use of the raked sphere-cone aerobrake design

permits significant improvements in the mission architecture, because of its ability to perform multiple skip maneuvers through the Martian atmosphere due to the L/D ratio of 0.4. In addition, because the entrance velocities into the atmosphere for the launch date chosen are lower than 8 km/sec, ablative heat shielding is not required and the aerobrake TPS is lightweight. The aerobrake structure can meet the diameter restrictions of the launch vehicle payload fairing, due to strategically placed hinges, therefore allowing fairing dimensions and Earth launch c.m. positioning to be improved. Aerobraking greatly simplifies the mission; decreasing the cost and increasing its feasibility because more payload mass can be used for scientific purposes, or for added redundancy, and for increased possibility of mission success.

NOMENCLATURE

A	Projected frontal area
C_D	Drag coefficient
C_F	Average total skin friction coefficient
C_L	Lift coefficient
c.g.	Center of gravity
g	Acceleration at surface due to gravity
h	Altitude of Entry Vehicle
H	Scale height for exponential atmosphere
r_p	radius of orbit at perigee
r_a	radius of orbit at apogee
R	Radius of Mars
V	Velocity of vehicle in the atmosphere
V_E	Entry velocity of vehicle in the atmosphere
β	Ballistic coefficient (m/C_DA)
γ	Path angle to the local horizontal
γ_E	Path angle on entry to the atmosphere
θ	Angle with respect to the inertial coordinate system of planet
ρ_0	reference density ("sea level")

REFERENCES

1. Walberg, G. D., "A survey of Aeroassisted Orbit Transfer," *Journal of Spacecraft and Rockets*, Vol. 22, 1985, pp. 1-5.

2. Woodcock, G. R. and Sherwood, B., "Engineering Aerobrakes for Exploration Missions," *Acta Astronautica*, Vol. 21, 1990, pp. 397-404.

3. Griffin, M. D. and French, J. R., *Space Vehicle Design*, American Institute of Aeronautics and Astronautics, Inc., Washington D. C., 1991, pp. 296-271.

4. Tauber, M., et al, "Aerobraking Design Studies for Manned Mars Missions," 91-1344, AIAA *26th Thermophysics Conference*, Honolulu, HI, June 24-26, 1991.

5. Williams, S. D., Gietzel, M. M., Rochelle, W. C., and Curry, D. M., "TPS Design for Aerobraking at Earth and Mars," NASA TM 104739 Lyndon B. Johnson Space Center, August 1991.

6. Arnold, J. O., Tauber, M. E., and Goldstein, H. E. "Aerobraking Technology for Manned Space Transportation Systems," 43rd Congress of the International Astronautical Federation, Washington, DC, August 28-September 5, 1992.

7. Eldred, C. H., "Aerobraking for Space Exploration," *Mars: Past, Present, and Future*, American Institute of Aeronautics and Astronautics, Inc., Washington, DC, 1991, pp. 307-322.

8. Regan, F. J., *Vehicle Re-Entry Dynamics*, American Institute of Aeronautics and Astronautics, New York, 1984, pp.100-101.

9. Lee, M. C. and Suit, W. T., "Preliminary Investigation of Parameter Sensitivities for Atmospheric Entry and Aerobraking at Mars," NASA TM 101607, September 1989.

10. Ishii, N., "Aerocapture Applied to Venus and Mars Mission," Proceedings of the Eighteenth International Symposium on Space Technology and Science, Kagoshima, Japan, Vol. II, 1992, pp. 1730-1734.

11. Corliss, W.R., "The Viking Mission to Mars," NASA SP-334, 1974, pp. 20-21

12. Peterson, C.W. and Johnson, D. W., "Advanced Parachute Design", Conference, *Parachute Systems Technology: Fundamentals, Concepts, and Applications*, June 22-26, 1987.

13. Cockrell, D.J., "The Aerodynamics of Parachutes," NATO Advisory Group for Aerospace Research and Development, AGARD-AG-295.

14. Peterson, C.W. and Johnson, D.W., "Parachute Materials," SAND-87-1396C, Sandia National Laboratories, 1987.

15. Peterson, C.W., "The Aerodynamics of Supersonic Parachutes", SAND-87-1395C, Sandia National Laboratories, 1987.

16. Woodcock, G.R., "Space Transfer Concepts and Analysis for Exploration Missions," Final Report, NASA Contract NAS8-37857, Boeing Space and Defense Group, Seattle, WA, Dec. 5,1991.

17. Kourtides, D. A., Chiu, S. A., Iverson, S. A., and Lowe, D. M., "Thermal Response of Rigid and Flexible Insulations and Reflective Coatings in an Aeroconvective Heating Environment," NASA TM 103925, Ames Research Center, 1992.

18 Lee, Stuart M., *International Encyclopedia of Composites,* VHC Publishers Inc. 1990, Vol. 1, pp. 254-265.

19. ASM International, *Engineered Materials Handbook*, Vol. 1, Metals Park, Ohio, 1987, pp. 399-400, 414, 724-725.

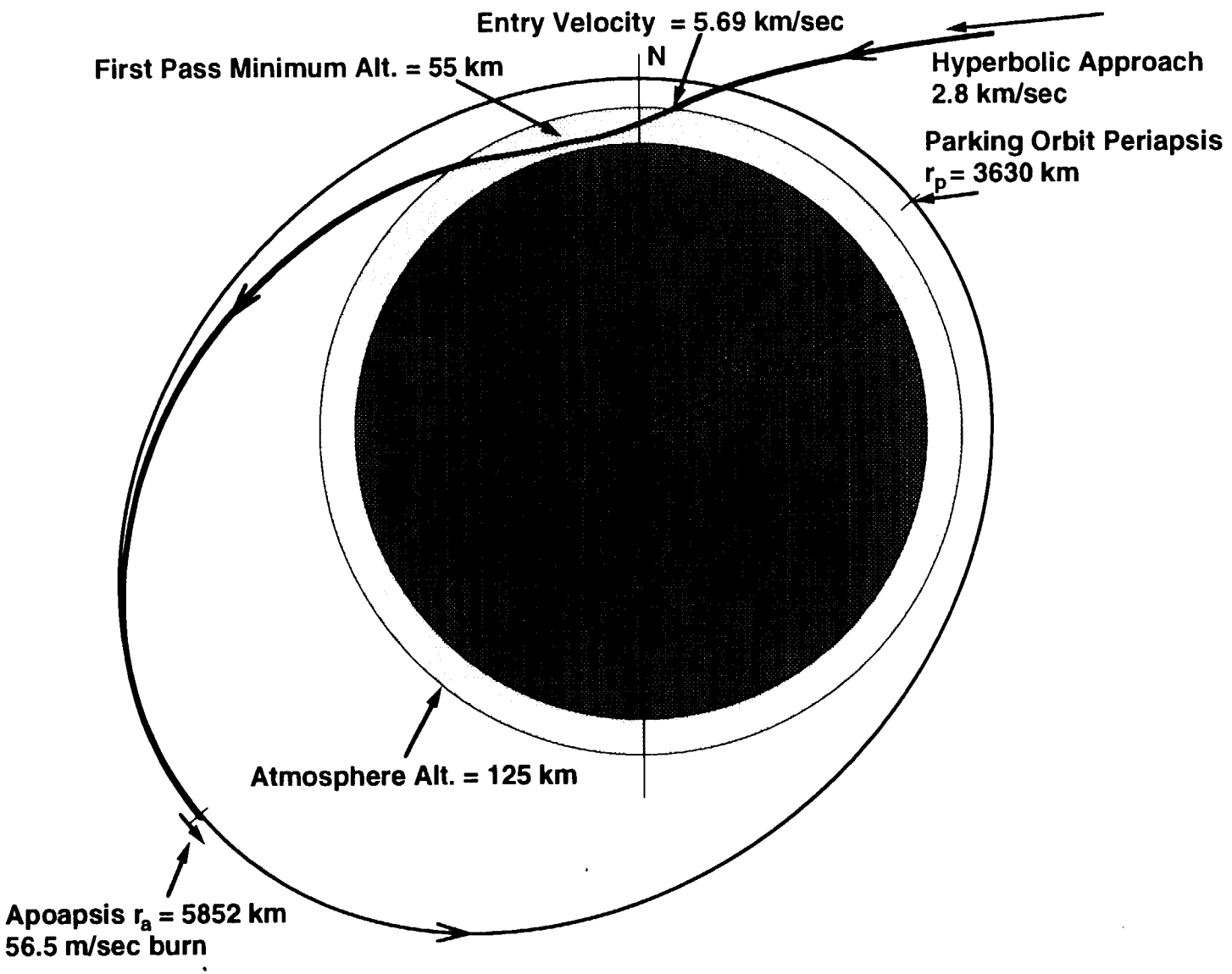

Fig. 5.1 Aerocapture at Mars into elliptical parking orbit.

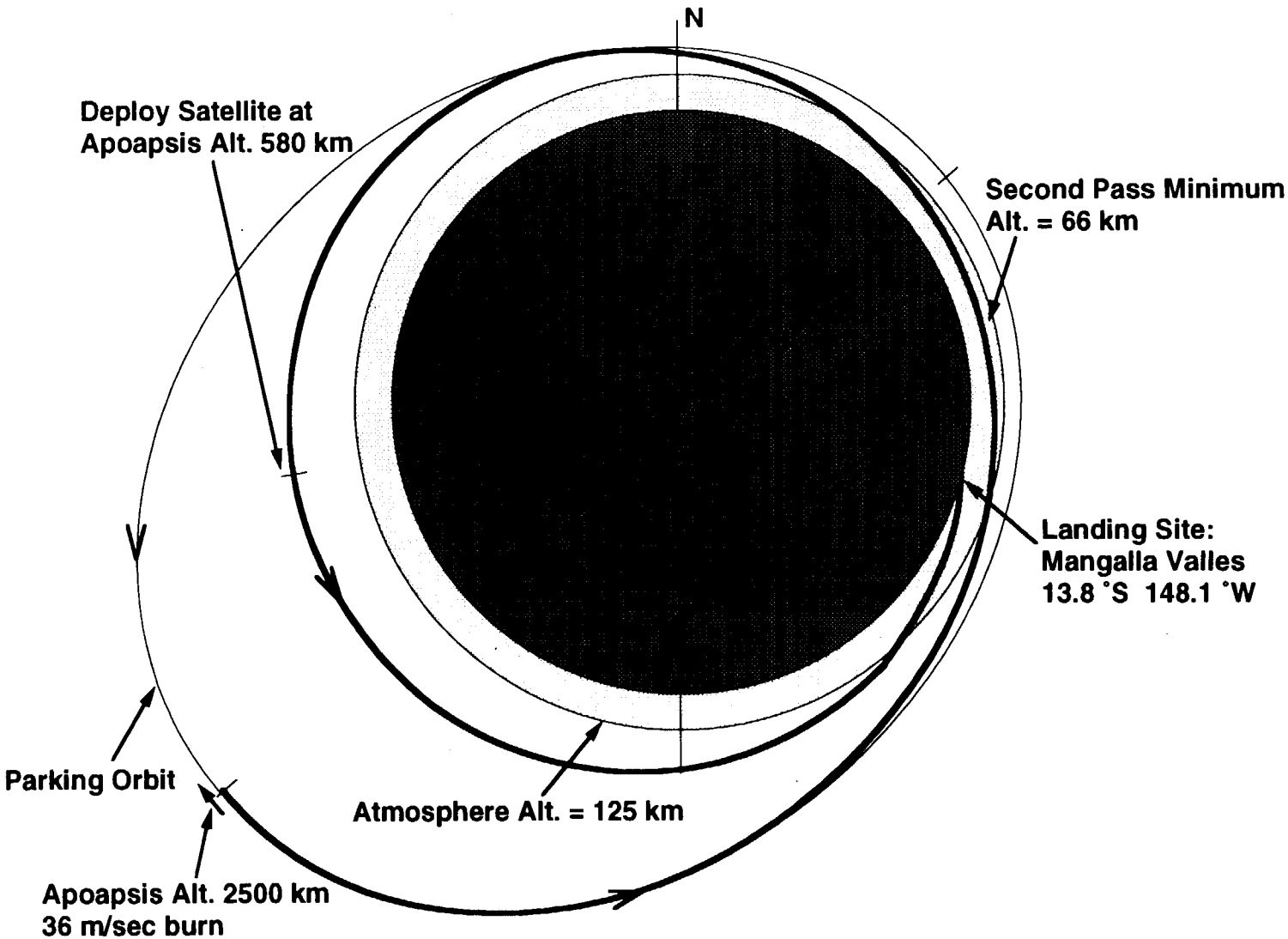

Fig. 5.2 Parking orbit to final entry at Mars.

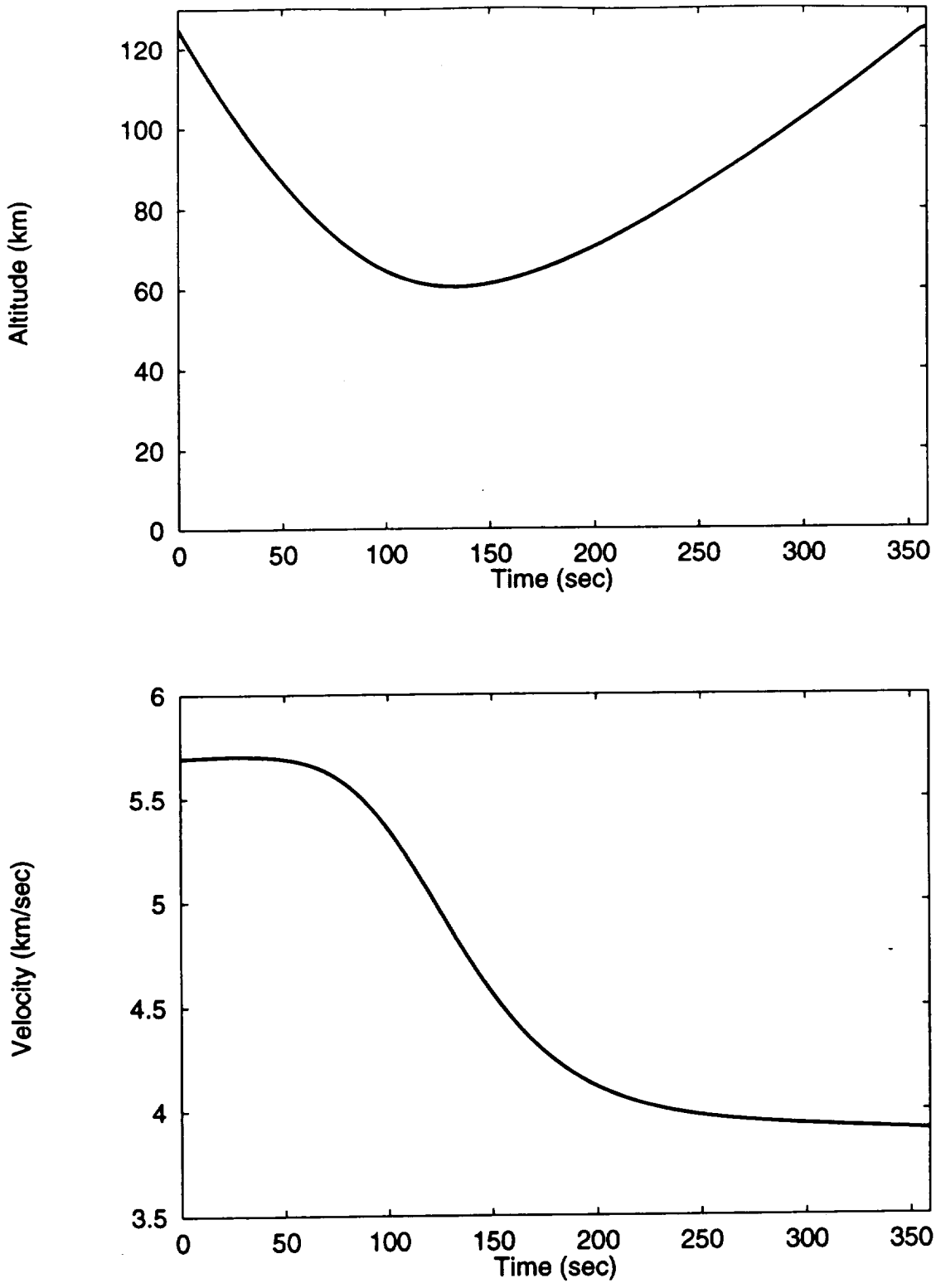

Fig. 5.3a Predicted flight trajectory and velocity for first pass.

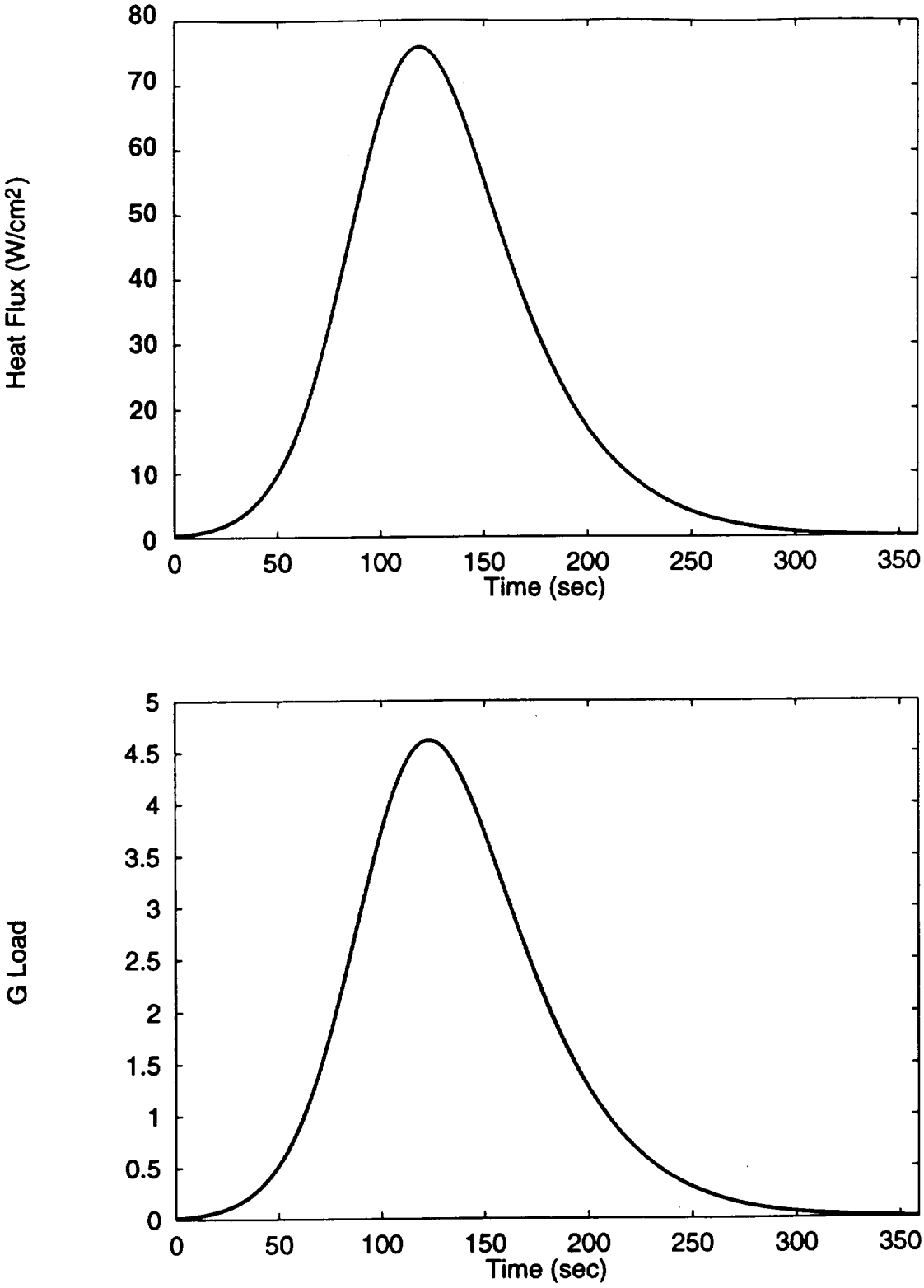

Fig. 5.3b Predicted heat load and deceleration for first pass.

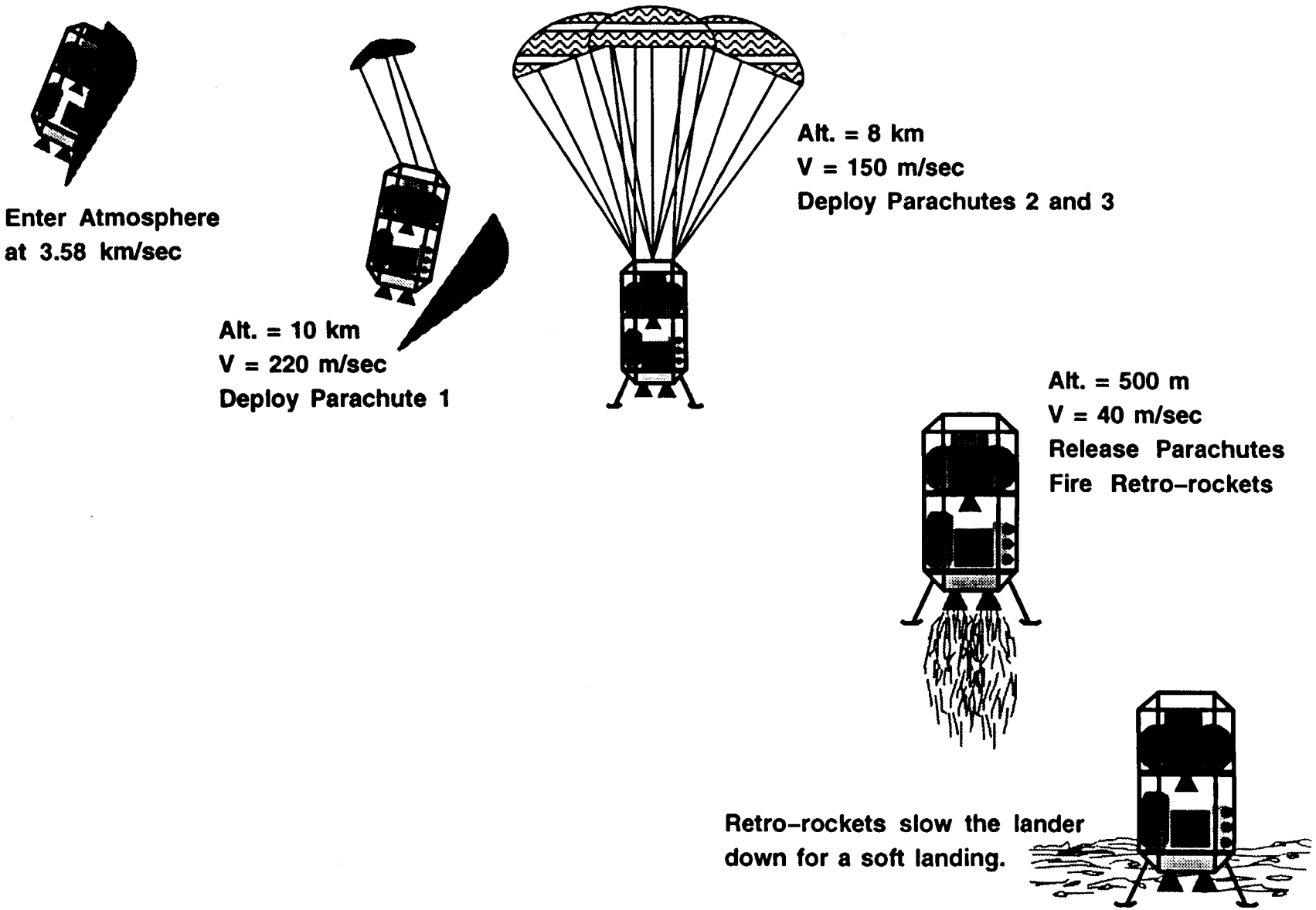

Fig. 5.4 Mars landing sequence.

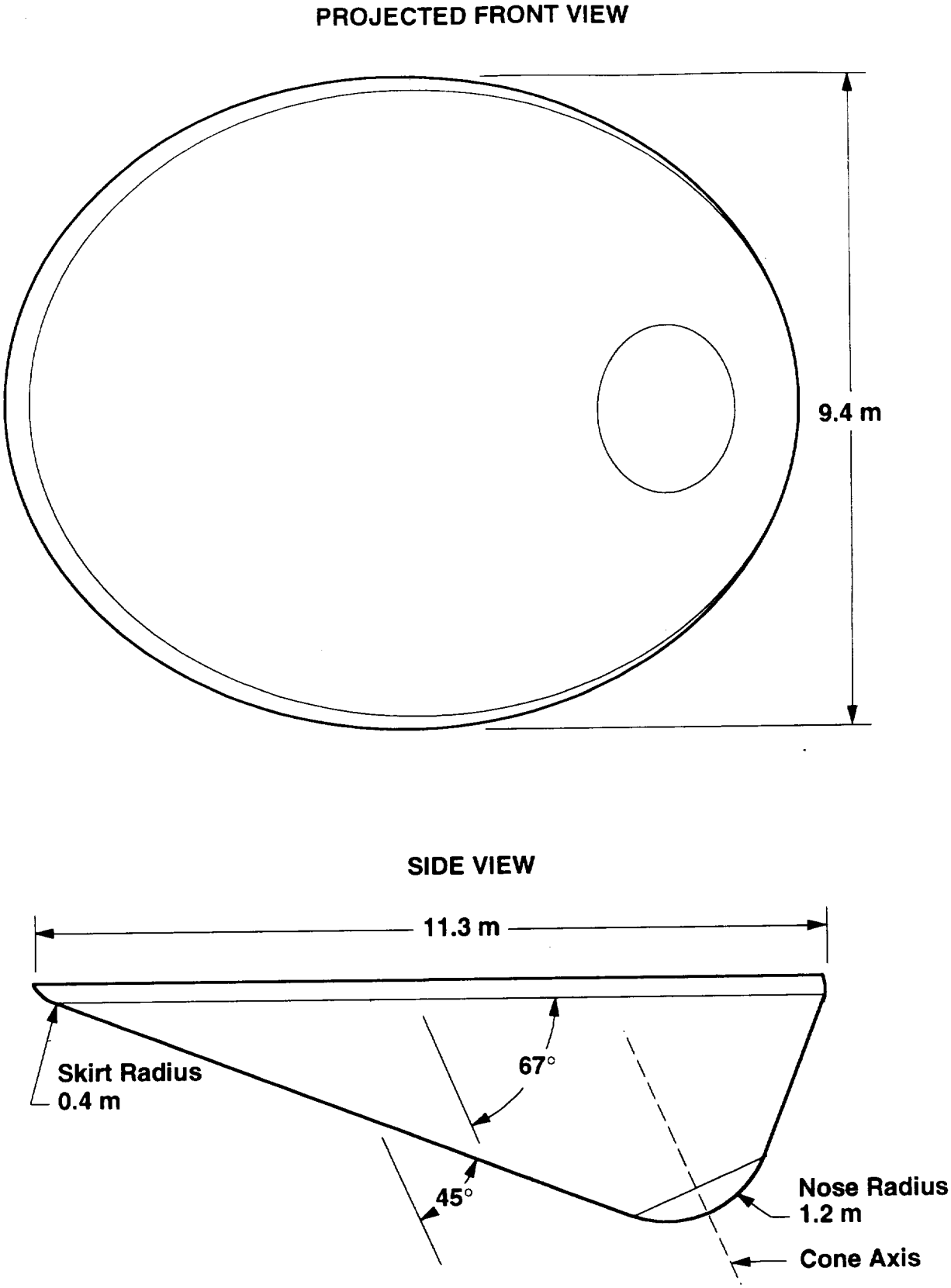

Fig. 5.5 Raked sphere-cone aerobrake configuration.

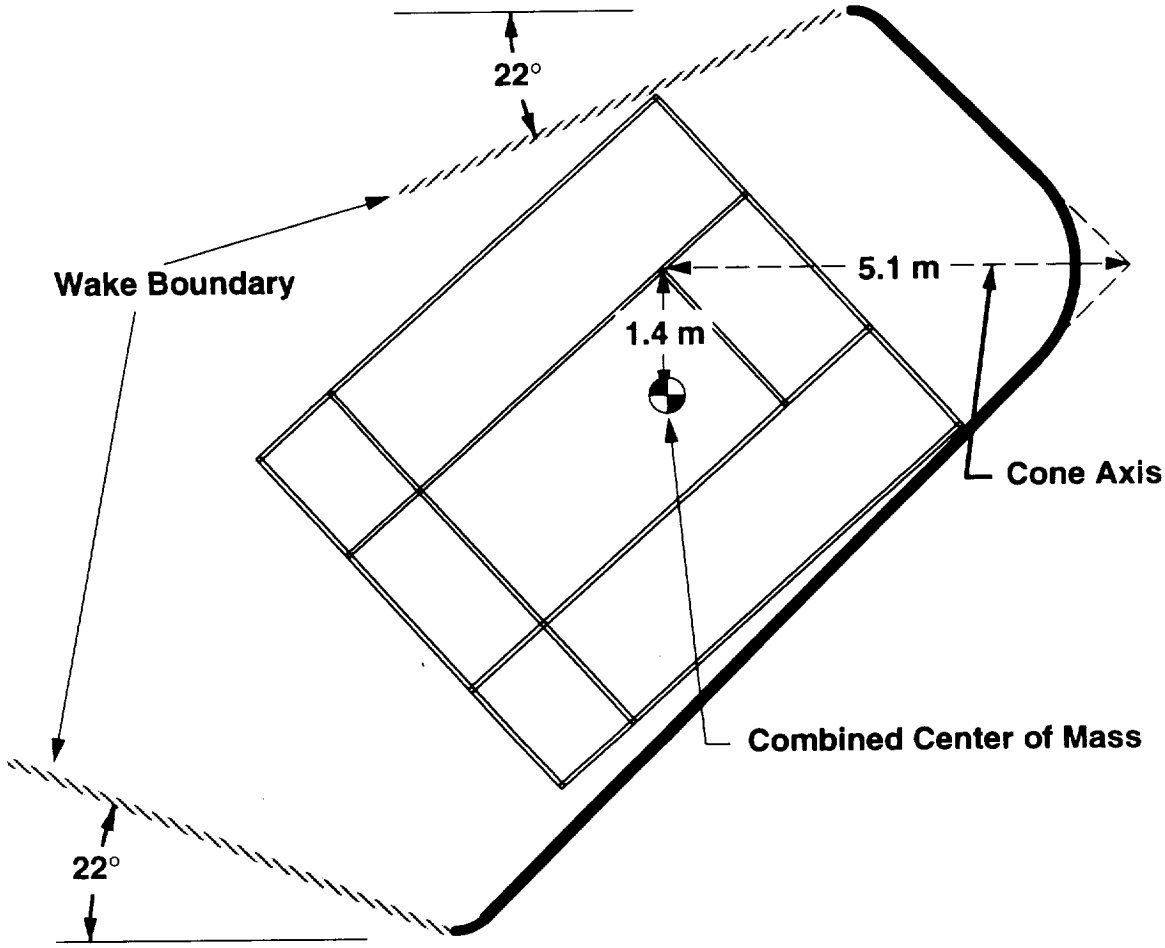

Fig. 5.6 Sizing aerobrake to shield Mars landing vehicle.

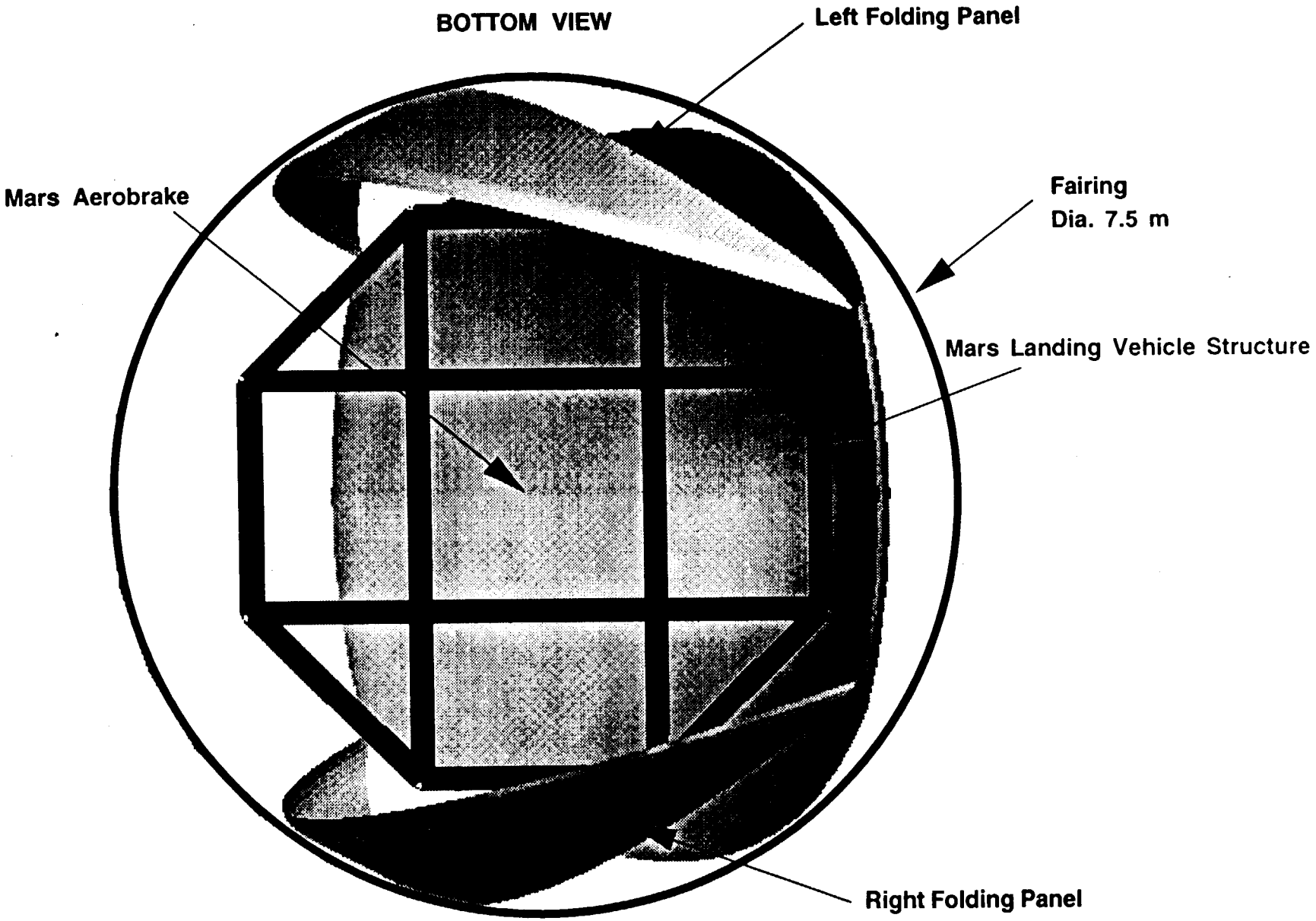

Fig. 5.7 Aerobrake in Launch Configuration.

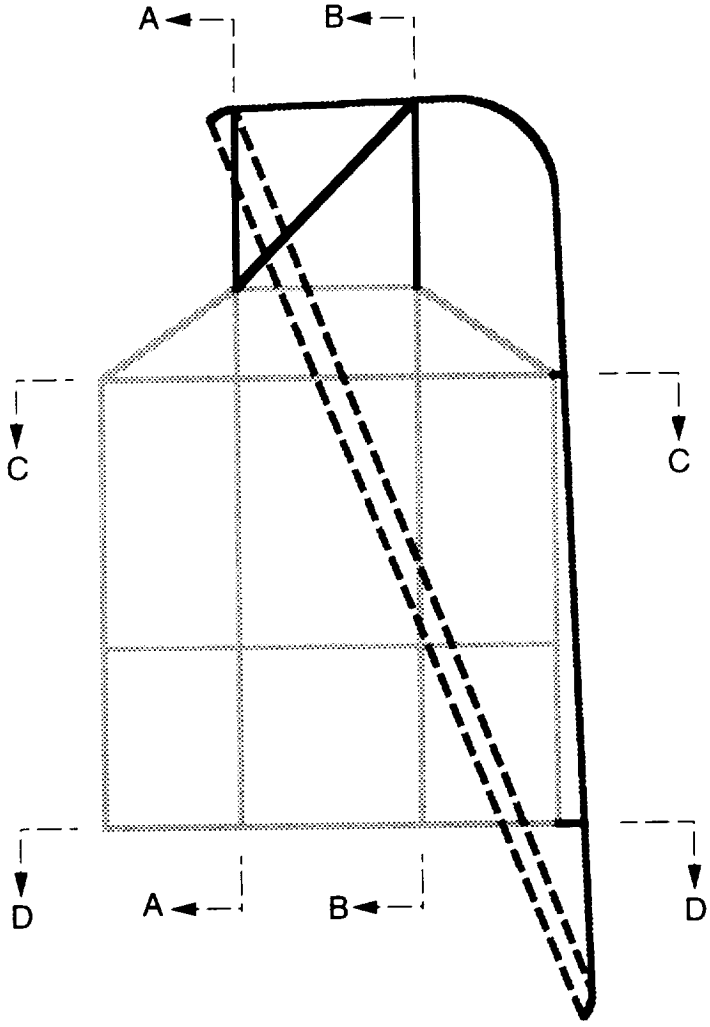

Fig. 5.8 Attachment of Mars landing vehicle to Mars aerobrake. Cross-sectional views are shown in Fig. 5.9.

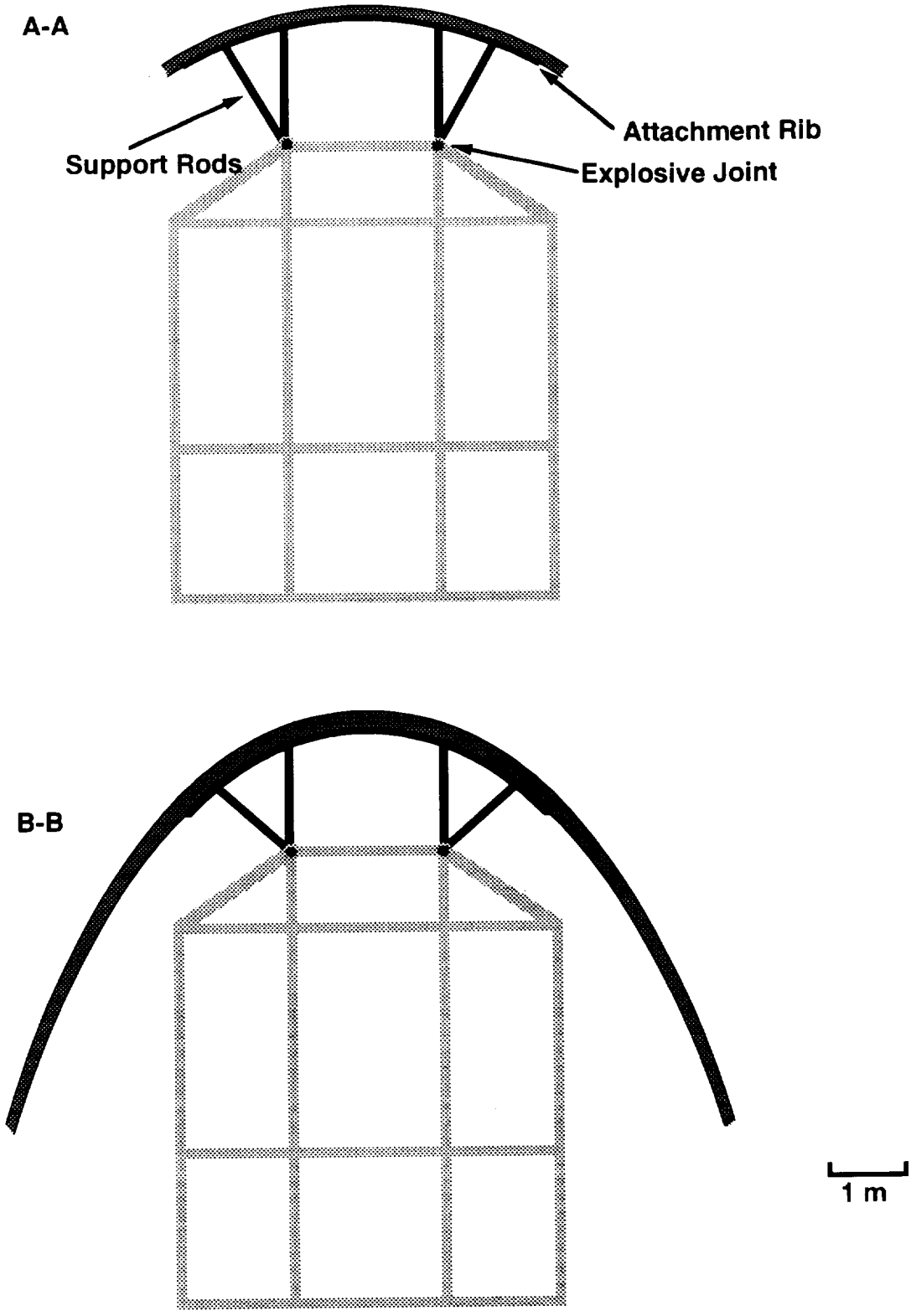

Fig. 5.9a Views A-A and B-B of aerobrake attachment points.

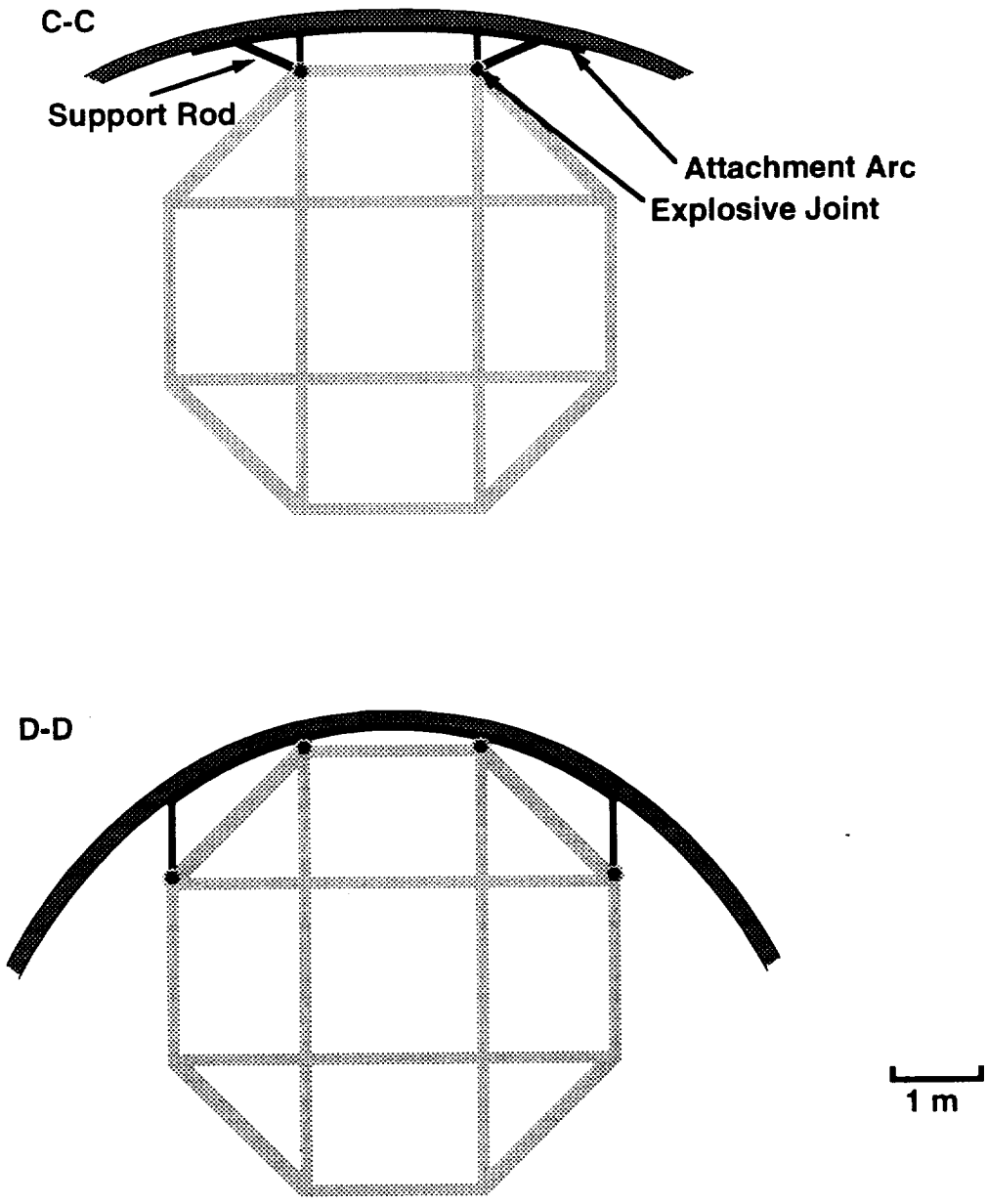

Fig. 5.9b Views C-C and D-D of aerobrake attachment points.

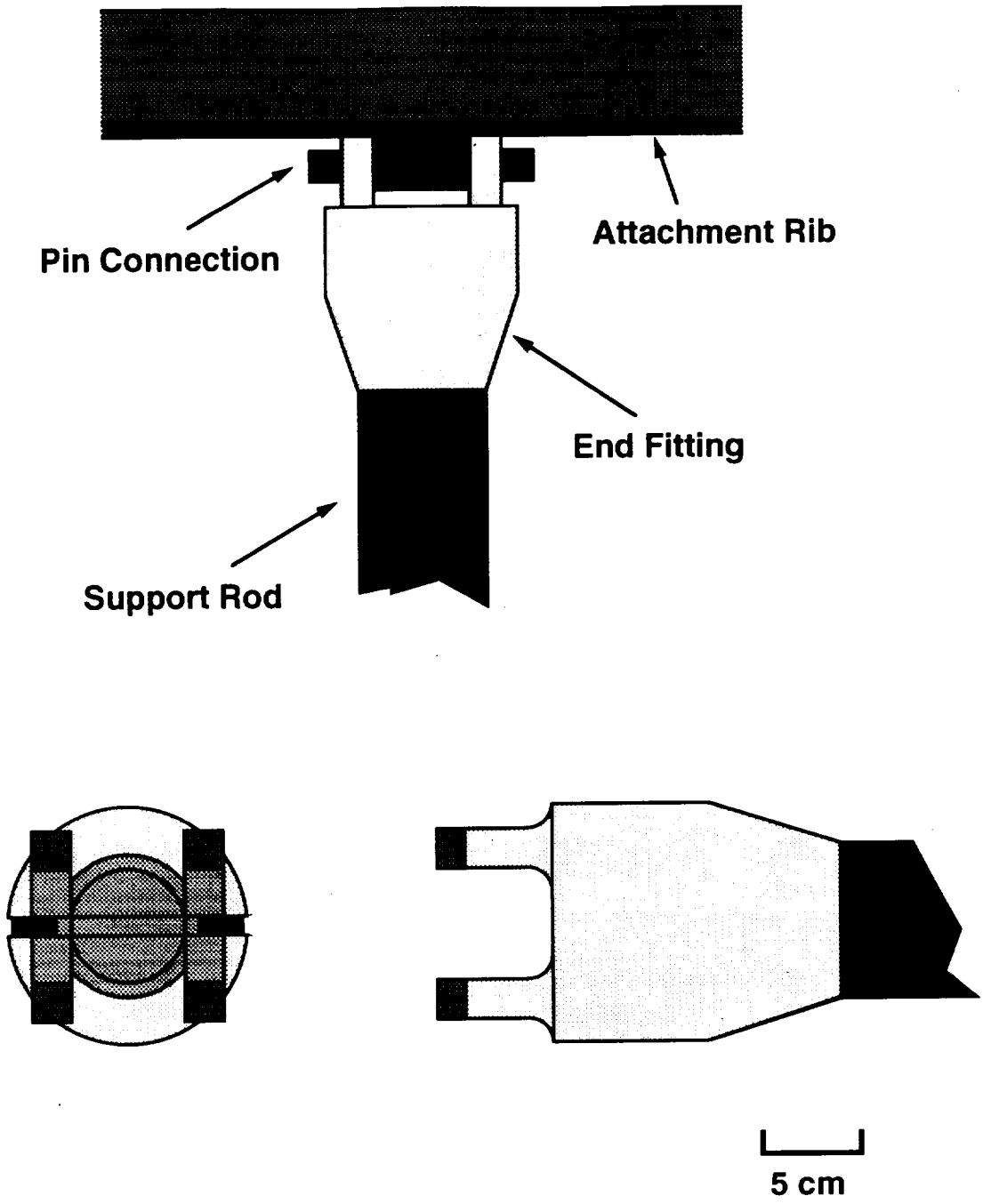

Fig. 5.10 Aerobrake support rods attachment joints.

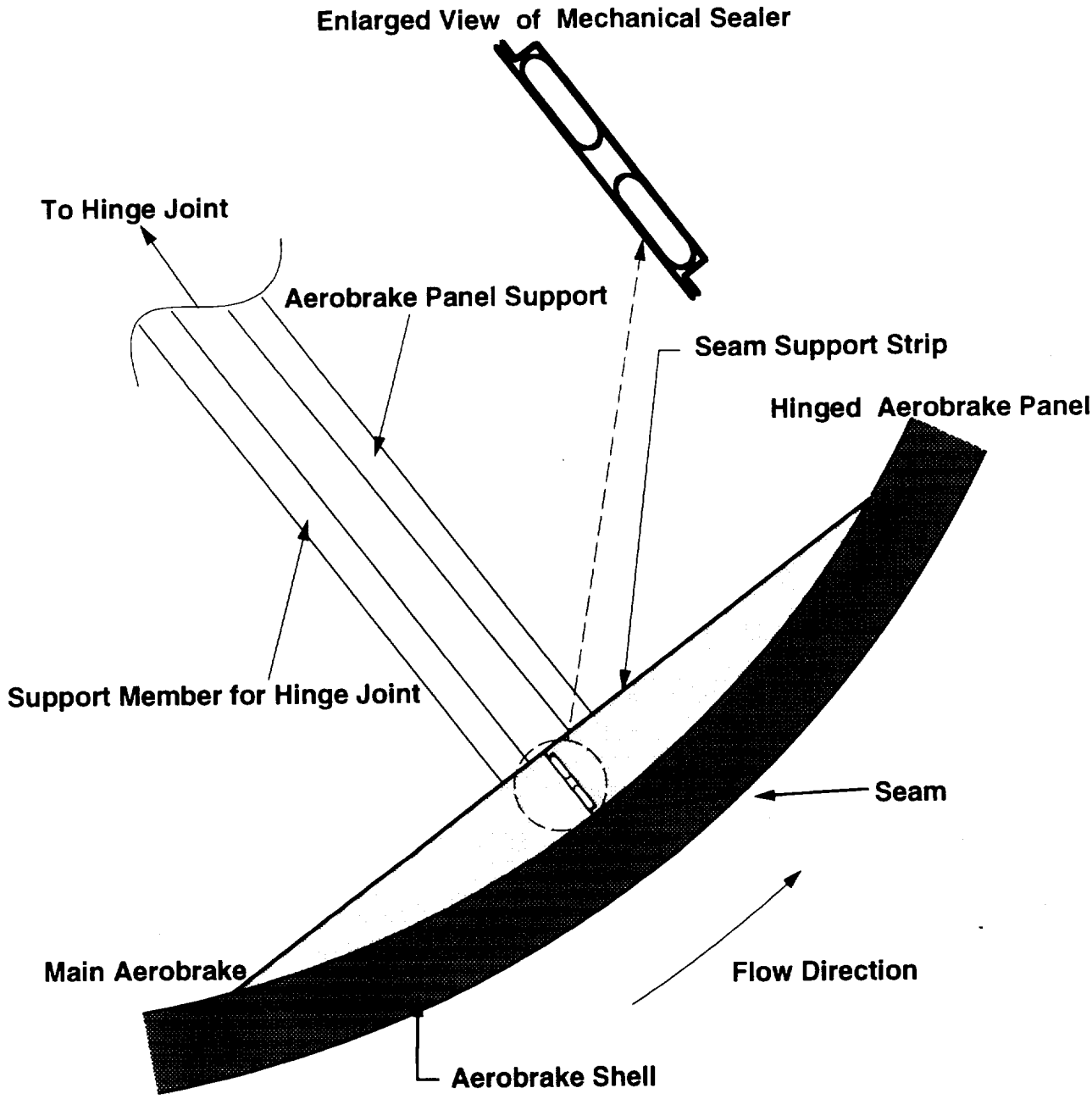

Fig. 5.11 Aerobrake seam with mechanical sealer.

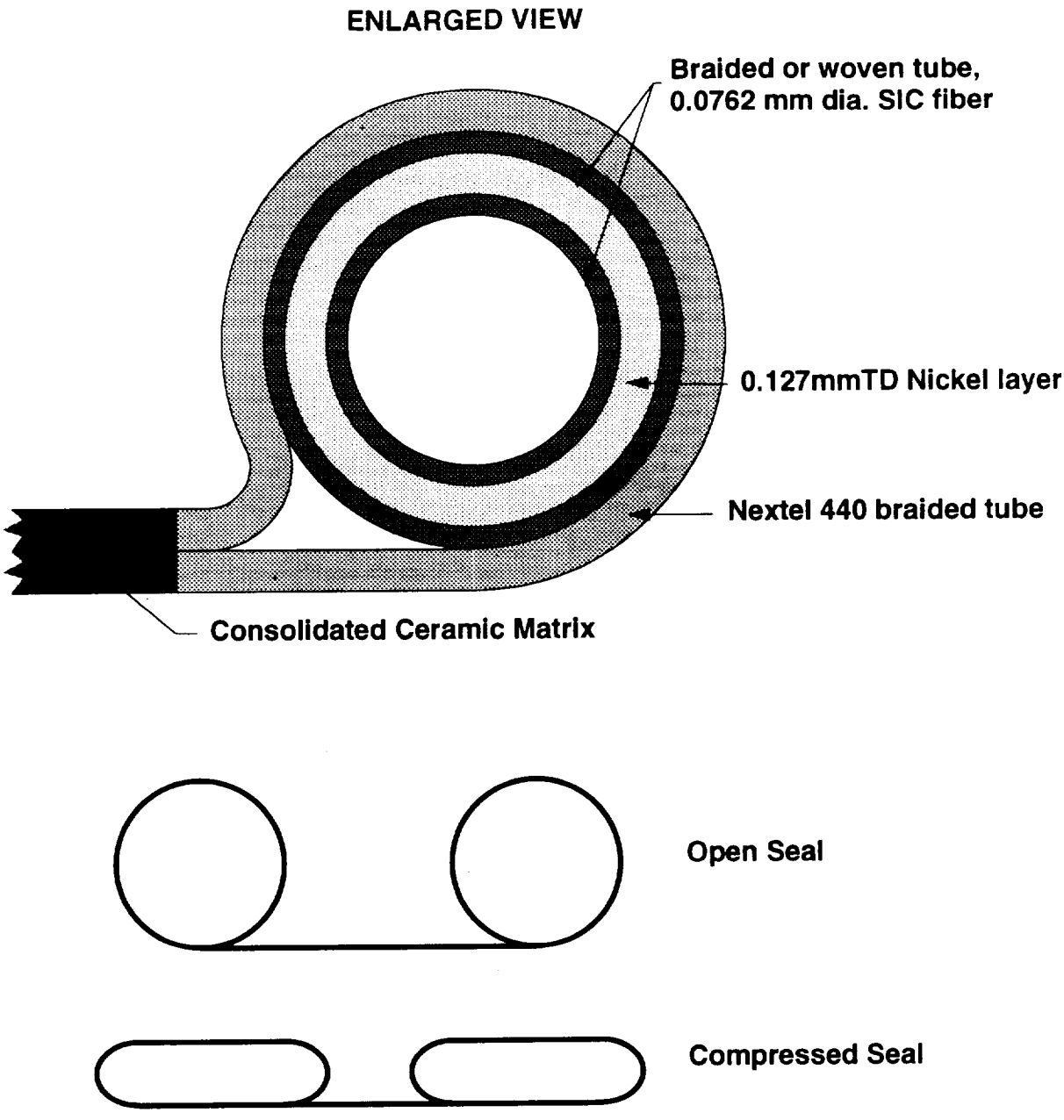

Fig. 5.12 Sealing mechanism for aerobrake panels [18].

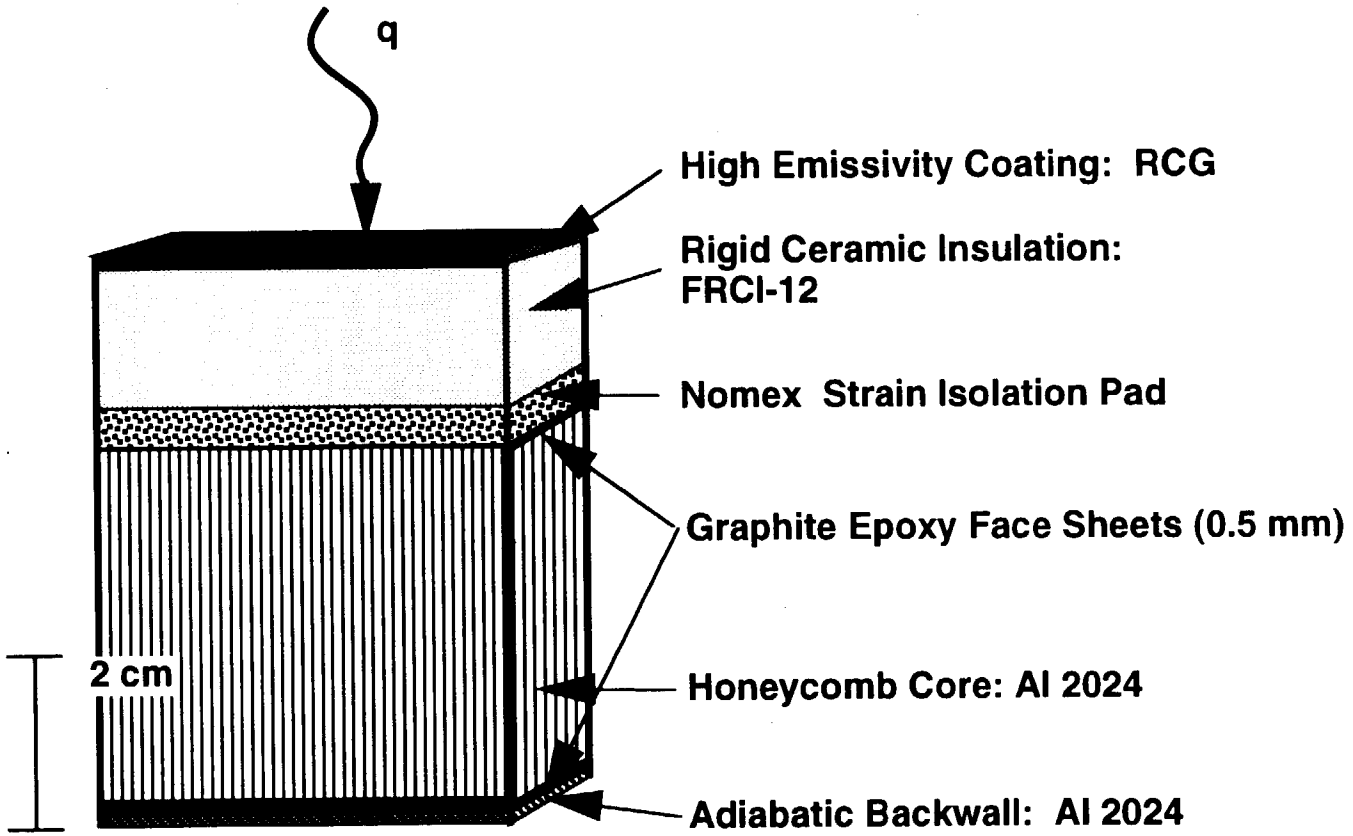

Fig. 5.13 Mars Aerobrake TPS Crossection

6.0 *IN SITU* PROPELLANT PRODUCTION

Anthony Hink
Craig Perras
Peter Sawyer
Brian Smith
Dave Van Noy
Leo Warmuth

TABLE OF CONTENTS

6.1 INTRODUCTION 6.1

6.2 BACKGROUND 6.1

6.3 PROPELLANT PLANT 6.3

6.3.1 Filter 6.5

6.3.2 Compressor 6.5

6.3.3 Sabatier Reactor 6.7

6.3.4 Reverse Water-Gas Shift Reactor 6.8

6.3.5 Condenser 6.9

6.3.6 Electrolyzer 6.10

6.3.7 Propellant Liquefaction 6.11

6.4 HEAT REJECTION 6.13

6.5 PROPELLANT STORAGE 6.13

6.5.1 Propellant Tank Insulation 6.13

6.5.2 Hydrogen Storage 6.17

6.5.3 Carbon Dioxide Storage 6.18

6.5.4 Refrigeration 6.18

6.6 CONTROL SYSTEM 6.19

6.7 POWER SYSTEMS AND THERMAL CONTROL 6.20

6.7.1 General-Purpose Heat Source (GPHS) 6.22

6.7.2 Radioisotope Thermoelectric Generators (RTG) 6.23

6.7.3 Dynamic Isotope Power System (DIPS) 6.25

6.7.4 Thermophotovoltaic Power Generators (TPVPG) 6.26

6.7.5 Thermionic and Nuclear Power Reactors 6.27

6.7.6 Solar Arrays and Batteries 6.27

6.7.7 Implementation 6.28

6.8 **CONCLUSION** 6.29

NOMENCLATURE 6.30

REFERENCES 6.32

FIGURES 6.34

6.1 INTRODUCTION

(Brian Smith, Peter Sawyer)

The purpose of this project is to demonstrate that a Mars sample return mission can be significantly enhanced by producing return-vehicle propellant from Martian resources. The overwhelming problem encountered in planning a round trip to Mars is the huge mass of propellant that must be taken along to fuel the return flight. If this mass penalty could be avoided, the Earth launch requirements would be greatly reduced. *In situ* propellant production is an inexpensive and reliable method of avoiding the penalty incurred by having to carry the return propellants to Mars. This chapter will focus on the propellant production plant's components, power requirements, mass, and propellant storage.

6.2 BACKGROUND

(Anthony Hink, Brian Smith, Peter Sawyer)

In designing a production plant for utilizing Martian resources, the foremost concern must be to determine which propellants will be used All feasible propellants require oxygen for combustion, but the Martian atmosphere is comprised of 95.3% carbon dioxide and contains virtually no oxygen [1]. Therefore, the main tasks are to choose an effective fuel, and to produce oxygen for use in the combustion process. There are several possible fuel/oxidizer combinations, ranging from methane/oxygen to carbon monoxide/oxygen to hydrogen/oxygen. When considering which propellant to use (and produce), consideration must be given to the available resources.

On Mars, the primary sources of raw materials are the atmosphere and the soil. Since little is known about the soil, and processing it would be cumbersome, the atmosphere is the logical manufacturing resource. Water is the only known source of hydrogen on Mars, but because it is only present in minute quantities in the atmosphere, it must be ruled out as a

potential resource. Although ice deposits are believed to exist in the soil, these underground reservoirs are too inaccessible for this mission. Therefore, using hydrogen/oxygen as a propellant combination is not a viable alternative.

A second possible fuel is carbon monoxide. It has a modest specific impulse of 290 sec [2], which means a large amount of it would be required to fuel the Earth Return Vehicle (ERV). However, there are two advantages to using carbon monoxide. First, carbon monoxide and its oxidizer can be produced using exclusively indigenous materials using the following reaction.

$$2CO_2 <=> 2CO + O_2 \qquad \Delta' = -280.7 \text{ kJ/kg} \tag{6.1}$$

Second, the carbon monoxide plant is simpler and smaller than the methane plant. However, carbon monoxide was not chosen because of its toxicity, an important consideration for following manned missions, and its low specific impulse. A description of the carbon monoxide plant is found in Appendix D.

Methane is a potentially effective rocket fuel. It has an I_{sp} of 370 sec when burned with oxygen at a 4 to 1 oxidizer to fuel (O/F) mass ratio [1]. This I_{sp} fulfills the thrust requirements of the mission, and because the propellant plant can be designed to produce the 4 to 1 O/F ratio, no additional manipulation of the propellants is needed A well-developed method of producing methane and water is to catalytically convert carbon dioxide and hydrogen in a Sabatier reactor [1]. The Sabatier reaction is defined by the stoichiometric reaction:

$$CO_2 + 4H_2 <=> CH_4 + 2H_2O \qquad \Delta H = -174 \text{ J/kg} \tag{6.2}$$

Reactors based on this equation have been proven reliable through years of testing and use in large production plants in the industrial world [1]. This reaction produces water, which can be converted into oxygen and hydrogen using an electrolyzing unit. The system is compact and reliable, but there are two drawbacks.

The first problem is that there is no accessible source of hydrogen at the chosen landing site on Mars. Hydrogen must be present for the reaction to take place, so seed hydrogen has to be imported to support production. The hydrogen occupies valuable space in the vehicle to Mars, thus lowering the allowable mass of scientific equipment that may be taken. However, this scenario is far better than importing the entire propellant supply [1].

The second problem with methane is that the standard Sabatier reactor produces oxygen and methane in a mass ratio of 2 to 1. When this fuel-rich mixture is burned, a heavy carbon build-up can form in the engine combustion chamber. Because the optimal oxidizer-to-fuel ratio is 3.5 to 1 [1], a water gas shift reactor must be included to supplement the oxygen supply. An alternative is to use an as-yet undesigned hybrid reactor. Such a reactor is currently under development at Hamilton Standard, and would combine the Sabatier reaction with a secondary reaction in a single unit to yield the proper mass ratio.

Though the use of carbon monoxide and oxygen as propellants has definite benefits, there are also several disadvantages. These disadvantages resulted in the initial choice of methane/oxygen for this mission. A comparison of mission parameters for each case is presented in Appendix E, together with the parameters for a mission what would import all the necessary H_2/O_2 propellant from Earth.

6.3 METHANE PROPELLANT PLANT
(Brian Smith)

This mission requires 480 kg of methane and 1,921 kg of oxygen to be produced during the 1.5 year stay on the surface of Mars. These are produced in a 1.4 year period, to allow for any delays in the landing sequence at Mars, and for any necessary plant shutdowns which may occur. Methane is produced at a rate of 0.94 kg/day and oxygen is produced at a rate of 3.76 kg/day. This requires 122 kg of seed hydrogen to be used at a rate of 0.24 kg/day and 4,016 kg of carbon dioxide to be processed at a rate of 7.86 kg/day.

A configuration and schematic of the propellant production plant are presented in Figs. 6.1 and 6.2. The Sabatier reactor uses carbon dioxide and hydrogen to produce methane and water; the reverse water-gas shift reactor (RWGS) uses carbon dioxide and hydrogen to produce carbon monoxide and water; the electrolyzer then dissociates the water into oxygen and hydrogen. The oxygen is stored and the hydrogen is recirculated back to the Sabatier reactor.

The propellant production plant consists of several components. First, a filtration system is needed to remove any small dust particles or other debris from the inlet gases. Such pollutants might damage the plant, and their presence could lead to impurities in the propellant. The Martian atmospheric pressure varies from 7 to 10 mbar [1] which is too low for the plant, which operates at a pressure of approximately 1 bar. Thus, a compressor is needed to raise the pressure of the carbon dioxide to the appropriate level for the two reactors.

The reverse water-gas shift reactor uses atmospheric carbon dioxide and seed hydrogen to produce water and carbon monoxide. The carbon monoxide is vented back to the atmosphere, and the water is sent to an electrolyzer, where it is dissociated into hydrogen and oxygen. The Sabatier reactor takes the hydrogen from the electrolyzer and atmospheric carbon dioxide to produce methane and water. This water is also sent to the electrolyzer unit for dissociation, and the methane is sent to the storage tanks. The oxygen produced in the electrolyzer is liquefied and stored for use in the ERV.

The output mixtures of both reactors are gaseous and include water vapor. A condenser is used to liquefy the water, and the other gases produced by the reactors are drawn off and processed for storage. The water is sent to an electrolysis unit for separation into hydrogen and oxygen.

Other components such as heat pipes, refrigerators, pumps, compressors, heaters, piping and valves are also needed, along with a power source to run the plant. A controls package is included, and a storage tank and refrigeration system are required to keep the methane and

oxygen at cryogenic temperatures for the entire duration of the vehicle's stay on the Martian surface.

6.3.1 Filter
(Leo Warmuth)

The Martian atmosphere contains wind-blown, particulate matter [1]. Thus, a filtration system is needed to remove the dust from the atmosphere. One approach is to use a hydrocyclone (Fig. 6.3) and membrane filter. The hydrocyclone, which acts like a centrifuge, can separate most of the particles over 5 μm in diameter [3] from the Martian air. These particles are accelerated outward to the sloped, conical wall by centrifugal force, which is caused by the swirling atmospheric gases. The particles lose their velocity near the wall and fall out of the bottom, where they are collected in a canister described in Section 7 of this report. The dust is returned to Earth as a sample of airborne particulates. The hydrocyclone forces the gases to flow into the vortex finder. The fine dust that remains in suspension is removed by the membrane filter. This is the best approach because of the system's simplicity, reliability and small size.

6.3.2 Compressor
(Leo Warmuth, Anthony Hink)

The Martian atmosphere consists of 95.3% carbon dioxide. The trace amounts of other gases in the Martian atmosphere include 2.7% nitrogen and 1.6% argon [1]. These gases will have little effect on either the Sabatier reaction or the RWGS [4]. However, after the reaction has taken place, the nitrogen and argon will be present in the methane supply. These impurities could cause a problem if they go through the rocket motor, because they would reduce its performance by interfering with the combustion process and raising the molecular weight of the exhaust. Therefore, the trace gases must be removed from the carbon dioxide supply.

The compressor is designed to take 8.25 kg/day of atmospheric gases from Mars ambient pressure and compress them to 13 bar. This flow rate will allow for the production of all the propellant required for the rover and ERV. The atmospheric pressure on Mars, as measured at the two Viking sites, varied over a Martian year between 7 and 10 mbar, with a year-round average of about 8 mbar observed at the higher altitude Viking I landing site on Chryse Planitia [3]. A pressure of 6 mbar, and a temperature of 300 K are used as the design conditions for the inlet. Since this pressure is lower than any experienced by Viking I, it serves as a design pressure for a worst case scenario. The same holds true for the temperature of 300 K, which is higher than anything Viking I experienced, and acts as a worst case scenario. A four-stage reciprocating compressor with interstage cooling and graphite lubrication will be used. The compressor is modeled as a polytropic process, assuming ideal gas modeling of carbon dioxide. Each stage has a compression ratio of 6.82 to 1, giving an overall compression ratio of 2,166 to 1. This system is cooled between compression stages to minimize the power requirement [3] and to ensure that cylinder temperatures do not exceed 450 K. The compressor rejects approximately 90 W of thermal energy at 435 K, some of which is used to heat the RWGS reactor in a regenerative thermodynamic cycle. The estimated mass of the compressor and intercooler is 100 kg. The compressor consumes approximately 100 W of electrical power.

Once the carbon dioxide and trace gases of the Martian atmosphere are compressed to 13 bar, the gases pass through a condenser. They are then allowed to equilibrate in a reservoir to ambient Martian temperature conditions (245 K average) [3] by rejecting 55 W of heat. The heat is rejected via the radiator system, and by performing preheating on the seed hydrogen before it enters the RWGS reactor. This condenses the carbon dioxide into a liquid state. The nitrogen, argon and other trace gases remain gaseous and are vented off to the atmosphere. The liquid carbon dioxide is then drawn from the reservoir at a rate of 7.86 kg/day and fed to the Sabatier and RWGS reactors.

6.3.3 Sabatier Reactor
(Leo Warmuth, Anthony Hink)

Once carbon dioxide has been acquired from the Martian atmosphere, it is reacted with the hydrogen produced in the water electrolyzer in the Sabatier methanation reaction:

$$CO_2 + 4H_2 <=> CH_4 + 2H_2O \quad \Delta H = -174 \text{ J/kg} \tag{6.2}$$

This reaction is exothermic and occurs spontaneously in the presence of a nickel-nickel oxide catalyst at 450 K and 1 bar [4]. The carbon dioxide enters the reactor at a temperature of 450 K, a pressure of 1 bar, and at a flow rate of 2.62 kg/day. The carbon dioxide is preheated by electric heaters to reach the inlet temperature. Hydrogen flows into the reactor at a temperature of 320 K, a pressure of 1 bar, and at a flow rate of 0.48 kg/day. The gaseous methane and water vapor mixture leaves the reactor at 373 K and 1 bar. The mixture is then sent to a condenser for separation.

A Sabatier reactor produced by the Hamilton Standard Division of United Technologies will be suitable for the propellant production plant. This reactor is available as a package which contains a condenser to liquefy the exiting water vapor, and a 33 W pump which passes water to the electrolyzer at 2 bar. The mass of this package is 43.1 kg. The Hamilton Standard Sabatier unit has been designed to meet NASA requirements for life support during manned flights. A schematic of this unit is shown in Fig. 6.4. Some of the factors which make this unit attractive are as follows:

- The reactor uses a 20% Ruthenium catalyst on alumina, which permits operation over a wide range of temperatures, molar ratios, and flow loadings with no active control.
- The reactor is lightweight (43 kg) and relatively small (0.18 m^3).
- The reactor "ignites" at approximately 450 K within five minutes of start-up.
- The reactor has no danger of overheating or failing under any load or molar flow ratio since the reverse Sabatier reaction is endothermic, and only takes place at

temperatures above 593 °C.

- The reactor is sized to convert more than 99% of the lean reactant in a carbon dioxide flow range of 0.91 kg/day to 3.6 kg/day, at cyclic or continuous operation over a H_2/CO_2 molar ratio range of 1.8 to 5.0.

6.3.4 Reverse Water-Gas Shift Reactor
(Leo Warmuth, Brian Smith)

The Sabatier reaction produces an oxygen to methane ratio of 2 to 1. This combustion ratio is far from ideal. To maximize thrust, increase efficiency and reduce cooling, the rocket engine requires a propellant ratio of 3.5 to 1. One way to achieve a higher oxygen to methane ratio is to employ a combination of two reactors. The first reactor carries out the Sabatier reaction (Eq. 1), and the second reactor uses the well-known water-gas shift reaction in reverse:

$$CO_2 + H_2 <=> CO + H_2O \quad \Delta H = 38.4 \text{ J/kg} \tag{6.3}$$

The reverse water-gas shift reaction is mildly endothermic, but occurs at 400 K in the presence of an iron-chrome catalyst [3]. The heat output from the Sabatier reactor can easily provide the thermal energy input requirement to sustain this reaction during steady state operation. During start-up, heating is performed by electric heaters, which require 400 W of power. Upon combination of these two reactors, an oxygen to methane mixture ratio of 4:1 can be achieved, providing an excess supply of oxygen which can possibly be used as back-up to life support during some future manned visit on Mars.

The RWGS reactor (Fig. 6.5) operates at 1 bar and 400 K. A power of 60 W is necessary for steady-state operating conditions, when the unit is properly insulated. The reactor receives 0.24 kg/day of hydrogen from the hydrogen storage tank and 5.24 kg/day of compressed liquid carbon dioxide obtained from the atmosphere. The reactor produces a mixture of 3.34 kg/day of

carbon monoxide and 2.15 kg/day of water. The mixture is sent to a condenser where the water is liquefied and the carbon monoxide is vented to the atmosphere.

The RWGS reactor has a forward equilibrium constant of only about 0.1, which implies that the left side of the RWGS equation must be overloaded with carbon dioxide, and that water must be condensed out and removed from the right side in order to drive the overall reaction to the right at an acceptable rate. This procedure will be used to ensure that the required mass flow of water is supplied to the electrolyzer.

It is worth mentioning that the Hamilton Standard Company is researching the development of a single reactor which employs the following chemical reaction that combines the Sabatier and RWGS reactions directly:

$$3CO_2 + 6H_2 <=> CH_4 + 4H_2O + 2CO \quad \Delta H = -94 \text{ J/kg} \tag{6.4}$$

This reaction is slightly exothermic, and if cycled together with electrolysis, would produce oxygen and methane in a mixture ratio of 4:1. This single reactor system would likely cut down on both the size and mass of the production plant compared to the two-reactor system, but it is as yet unavailable.

6.3.5 Condenser
(Brian Smith, Leo Warmuth)

Two condensers are required in the propellant plant. The first condenser immediately follows the Sabatier reactor. Water vapor and methane produced by the Sabatier reaction enter the condenser at a mass flow rate of 3.1 kg/day, a pressure of 1 bar and a temperature of 450 K. The second condenser immediately follows the RWGS reactor. Carbon monoxide and water enter this condenser at a mass flow rate of 5.48 kg/day, a pressure of 1 bar and a temperature of 400 K. Both condensers liquefy the water vapor and bring it to a temperature of 322 K, by rejecting approximately 57 W of heat each. The total heat rejection of 114 W is transferred to

the radiator system through heat exchangers. The condenser masses are estimated to be 5 kg each.

6.3.6 Electrolyzer
(Brian Smith, Peter Sawyer)

One of the important components of the plant is the electrolysis cell. In order for the plant to work, the water that is produced in the Sabatier and RWGS reactors must be dissociated into hydrogen and oxygen. The hydrogen supplements the seed hydrogen that is brought from Earth to be used in the Sabatier reactor. The electrolyzer must handle a water flow rate of 4.29 kg/day. This will produce 3.81 kg of oxygen and 0.48 kg of hydrogen per day, and will require approximately 55 W of power. Costly space is saved on the Mars Landing Vehicle (MLV) by using this recycled gas, as opposed to bringing the entire supply of hydrogen from Earth.

The electrolyzer consists of a stack of two cells, each with a mass of 0.73 kg. A single cell is a flat disk of 25 cm diameter and 0.3 cm thick. The cells operate at a temperature of 322 K and a pressure of 1 bar. These conditions require a current of 30 amps and 1.8 Volts. The two cells are held in place by two end plates, each with a mass of 6.8 kg and a diameter of 15.25 cm. The total electrolyzer mass is approximately 15 kg and the power usage is 55 W.

An electrolysis cell works on a simple and time-tested method. Water is brought into the central chamber, where it is exposed to a potential difference of 1.8 volts across a cathode/anode pair. The voltage difference causes the bonds in the water molecules to break. The hydrogen congregates at the negatively charged cathode, while the oxygen is attracted to the positively charged anode. The gases are then collected and piped to their respective destinations in the system. The governing reaction is

$$2H_2O <=> 2H_2 + O_2 \qquad (6.5)$$

The Hamilton Standard SPE™ water electrolysis unit is used in the propellant production plant. A schematic of this unit is shown in Fig. 6.6. This unit was originally designed for use on naval submarines to convert water into breathable oxygen for the crew. It has been in use since the 1970's in such applications, and one particular unit has been in constant use for over 110,000 hours (12.6 years) without developing any malfunctions or requiring any service.

The Hamilton Standard unit in Fig. 6.6 uses an ion exchange membrane with Teflon-bonded, finely divided metal electrodes to dissociate the water [5]. This system is more reliable than the old-fashioned post electrodes, because it has a far greater surface area to volume ratio. This allows for more efficient application of the voltage. The ion membrane works without "bubbling" the gases, meaning that the gases do not pass back through the water. Instead, they are drawn out immediately upon separation. This provides the advantage of unlimited range of operating pressures, for both the input water and the output gases. The pressures are limited only by the performance requirements and the structural limitations of the system.

6.3.7 Propellant Liquefaction
(Dave VanNoy)

When the methane and oxygen are produced, they must be liquefied for storage. The propellants enter the liquefaction cycle at approximately 1 bar of pressure and a temperature of 300 K. The minimum work to liquefy methane and oxygen from the initial conditions is 1,110 kJ/kg and 638.4 kJ/kg respectively [6]. The amount of propellant needing to be liquefied is 487 kg methane and 1948 kg oxygen. The liquefaction of the methane over a 1.4 year period requires a minimum of 12.2 W of power. The liquefaction of the oxygen over the same time period requires a minimum of 28.2 W. This adds up to a total minimum power of 40.4 W. Work requirements for real liquefaction cycles are typically 1.5 to 10 times greater than the minimum work [6], which means that the actual power requirements could range from 60 W to 400 W.

A typical liquefaction cycle used in industry is the throttle expansion cycle. In this process the gas is compressed, sent through heat rejection and partially liquefied by sending the gas through a throttling valve. Precooling can be used before throttling the gas, by sending it through heat exchangers. This increases the liquefied fraction and decrease the specific work requirement of the system. The heat exchangers utilize the fraction of the gas that was not liquefied in the throttling process. Multi-stage throttling can also be used to increase the liquefied fraction, but this is accompanied by a second compressor. To keep the system mass as low as possible, single stage throttling is used.

The chosen liquefaction cycle, with one throttling stage and precooling, is shown in Fig. 6.7. The cycle shown is capable of liquefying air at approximately 7 times its minimum power requirements [6]. To obtain an estimate of the system's power requirement , the minimum power to liquefy the propellants is multiplied by 7, which gives a power requirement of 283 W. The system mass of the liquefaction cycle comes mainly from the mass of the compressors. The masses of the two compressors for this system are estimated to be 10 kg each. A total system mass of 30 kg is estimated to account for the piping, throttling valves, reservoirs and insulation. This system uses a radiator to reject the heat of compression (~283 W), to the atmosphere.

6.4 HEAT REJECTION
(Dave VanNoy)

Heat is rejected from each plant component, using a radiator similar to the DIPS radiator (see Section 6.7). It is made of the same material and structure, but it is smaller. The size is determined by assuming radiative heat transfer only. The temperature of heat rejection is assumed to be 300 K, which is a worst case scenario. Using the blackbody radiation law, the heat flux from the radiator is calculated to be 370 W/m^2. The radiator rejects 450 W, thus the surface area is 1.2 m^2 and the mass is 10 kg.

6.5 PROPELLANT STORAGE
(Dave VanNoy)

Once the propellant has been manufactured, storage will be required for the duration of the stay on Mars. The propellants must be preserved at temperatures much lower than the surrounding Martian atmosphere. Insulation and refrigeration are used to maintain the necessary storage conditions.

6.5.1 Propellant Tank Insulation

A problem that occurs when propellant is liquefied and stored is boiloff. Because the propellant must be stored at temperatures much lower than the normal ambient temperatures of the surroundings, there is a heat flux into the tanks which causes the propellant to boil. Boiloff is a problem because of the pressure buildup in the storage tanks. The gaseous propellant must be vented to relieve the excessive pressures, resulting in a loss of propellant. Thermal protection in the form of insulation is used to reduce the heat load into the tanks.

The insulation used on this mission will be Multilayer insulation (MLI). MLI is used in most cryogenic systems built for use in space, because of its very effective thermal conductivity. There are two main types of MLI. The first type is composed of alternating layers of metal foil (shields) and a woven padding material. The second type is composed of shields of Mylar with metal coatings, alternating with optional layers of padding. The first type requires the padding, because its low thermal conductivity is lost when contact is made between shields. The second type requires no padding, but the Mylar is crimped to reduce the contact area between shields [14].

Aluminum is the most common metal used in MLI for operation at temperatures below 400 °C (673 K), because it is highly reflective, lightweight, and fairly inexpensive [14]. Other metals, such as copper or tin, are used for higher operating temperatures, but aluminum is

specified for this mission because the propellant tanks will not experience temperatures greater than 673 K.

The methane tanks are insulated by a 1 cm thick pack of aluminized Mylar without padding (25 shields/cm). Aluminized Mylar with no padding is the lightest insulation, with a density of 38 kg/m^3. It has an effective thermal conductivity of 32 μW/m K [14]. The oxygen tank uses a 1 cm thick pack of aluminized Mylar like the methane tanks, but it needs a glass fabric padding material (30 shields/cm), in order to eliminate any fire hazard [14]. MLI of aluminum foil and Mylar film ignites spontaneously in an oxygen atmosphere. In the event of a leak in the oxygen tank, MLI without glass fabric padding would ignite and possibly explode. The glass fabric padding reduces the flammability of the MLI, because the glass fibers do not burn in oxygen and the fabric contains very little organic material that could lead to a fire. The MLI used for the oxygen tank has a density of 75 kg/m^3 and a thermal conductivity of 55 μW/mK [14].

The methane and oxygen are stored at 10 bar at 135 K and 108.2 K, respectively. The average temperature on the surface of Mars is 245 K, but it ranges from 200 K to 300 K [15]. The heat transfer to cylindrical and spherical containers resulting from this temperature difference can be approximated using the following equations [16]:

$$q_{cylindrical} = \frac{T_1 - T_3}{\frac{\ln(r_2/r_1)}{2\pi k_A L} + \frac{\ln(r_3/r_2)}{2\pi k_B L}} \tag{6.5}$$

$$q_{spherical} = \frac{T_1 - T_3}{1/2\pi k_A(1/r_1 - 1/r_2) + 1/2\pi k_B(1/r_2 - 1/r_3)} \tag{6.6}$$

where,

T_1 = Cold wall temperature

T_2 = Warm wall temperature

k_A = Thermal conductivity of tank wall material

k_B = Thermal conductivity of insulating material

L = Cylinder length of tank (zero if spherical)

r_1 = Inner radius of tank wall

r_2 = Outer radius of tank wall

r_3 = Radius to outer surface of insulation

These equations only calculate the heat transfer due to one heat transfer mechanism, which is conduction. The tanks will actually be subjected to conduction, convection and radiation, but conduction is assumed to be the dominating heat transfer mechanism. The solar radiation is neglected, because of the low solar flux at Mars (590 W/m^2). The outer layer of insulation will be painted with white enamel paint which has a solar absorptivity of 0.252 and an emissivity of 0.853. This will be done to keep the warm wall temperature (T_2) below the design T_2 of 245 K. The warm wall temperature due to the solar flux can be calculated using the following equation [22]:

$$T_2 = \left(\frac{A_p G_s \alpha}{A_s \varepsilon \sigma} \right)^{\frac{1}{4}} \tag{6.7}$$

where,

A_p = Projected area of object (m^2)

A_S = Emitting surface area (m^2)

G_S = solar flux (W/m^2)

α = Solar absorptivity of surface

ε = infrared emissivity of surface

σ = Stefan-Boltzmann constant (5.67×10^{-8} W/m^2K^4)

The methane and oxygen tanks have a projected area to emitting surface area ratio of 0.5 if the tanks only emit from one side. The tanks have a T_2 of about 198K (from Eq. 7) due to the solar flux at the Martian surface, thus the radiative heat transfer is neglected. It is assumed that the T_2 of the tanks is the average Martian atmospheric temperature (245 K). This assumption compensates for the convection of the Martian atmosphere. The average heat load experienced by each of the two methane tanks and the oxygen tank aboard the ERV is 1 W and 2 W, respectively (calculated from Eqs. 5 and 6). This adds up to a total heat load of 4 W.

6.5.2 Hydrogen Storage

The imported seed hydrogen must be protected during Earth launch, transfer to Mars, entry into Mars' atmosphere and throughout the propellant production process on the surface of Mars. Earth launch and Mars entry are short duration events and boiloff occurring during these phases will be remedied by bringing extra hydrogen. The extra mass of hydrogen is only 28.5 kg, therefore the mass penalty associated with this remedy is small.

The transfer to Mars and the propellant production process are both long in duration. The heat load into the hydrogen tank during the transfer to Mars is minimized by the thermal

radiation shielding present in the insulation and by painting the outer surface of the insulation with white enamel paint, like the methane and oxygen tanks. When the hydrogen tank is exposed to direct sunlight, it will have a projected area to emitting surface area ratio of 0.57 and the T_2 will reach a maximum of 252 K at Earth, and a minimum of 204 K at Mars (from Eq. 6.7). By orienting the MLV in such a way as to keep the hydrogen tank in its shadow, the T_2 should stay below the design T_2 of 245 K. Boiloff during the propellant production process is prevented through insulation and refrigeration. The hydrogen tank is covered with aluminized Mylar MLI without padding (25 shields/cm), like the methane tanks. The insulation is 5 cm thick. From the same analysis of the hydrogen tank as was performed on the methane and oxygen tanks (Eqs. 6.5 and 6.6), the heat load is found to be 4 W when the storage temperature is 30 K at 10 bar.

6.5.3 Carbon Dioxide Storage

Carbon dioxide is required by the rover to dilute its fuel mixture. Without this supply of inflammable gas, the rover's thermophotovoltaic power generator will run too hot. The rover requires 10 kg of carbon dioxide per excursion, so this will be the capacity of the tank. Any additional gas produced in the plant between refuelings is vented to the atmosphere. The tank is a spherical container constructed of Weldalite, with a diameter of 30 cm, a volume of 0.014 m^3 and a mass of 10 kg. The gas is stored at a temperature of 240 K and a pressure of 13 bar.

6.5.4 Refrigeration

The insulation cannot completely eliminate the heat transfer to the tanks. Thus, to prevent boiloff, refrigeration must be used to remove heat from the propellant tanks and the

hydrogen tanks at the same rate as it is transferred to the tanks from the surroundings. The insulation reduces the total heat load into the tanks to 8 W.

Heat transfer and energy balance analysis is needed to determine the power requirements and system mass of the refrigeration system. A preliminary estimate has been made using several assumptions. The first assumption is that several refrigerators will be used, each performing a single cooling task. The second assumption is that each refrigerator will operate at a coefficient of performance (COP_R) which is 30% of the Carnot coefficient of performance ($COP_{R,\,Carnot}$). The third assumption is that heat will be rejected from the radiator coils at a temperature of 260 K. Similar assumptions were made in Reference 17.

The $COP_{R,\,Carnot}$ can be determined from the storage temperature of the refrigerated substance (T_L) and the temperature at which the heat is rejected (T_H) from the following equation:

$$COP_{R,Carnot} = \frac{1}{T_H/T_L - 1} \tag{6.8}$$

From the COP_R the power requirements can be determined, using the following equation:

$$\dot{W} = \dot{Q}/COP_R \tag{6.9}$$

where $\dot{W}$ is the required power and $\dot{Q}$ is the rate of heat removal from the refrigerated volume. From Eq. 5 and 6, an estimate of 125 W was obtained for the refrigeration of the *in-situ* propellants and hydrogen tanks. The following table shows the results from the calculations for each component.

Table 6.1 Refrigeration power requirements.

Component	T_L (K)	$COP_{R,\ Carnot}$	COP_R	$\dot{Q}$ (Watts)	$\dot{W}$ (Watts)
LH_2 Tank	30	0.13	0.04	4	109
LO_2 Tank	108.2	0.71	0.213	2	12
LCH_4 Tank	135	1.08	0.324	2	4
Total					**125**

6.6 CONTROL SYSTEM
(Brian Smith)

Since the plant is almost completely autonomous, with little help from mission control, an elaborate control system must be used (Fig. 6.8). Upon arrival at Mars, the system receives the order from Earth to begin operations. The plant performs a diagnostic check, and once it is determined that everything is in working order, the plant begins operation.

The valve that had been separating the inner workings of the plant from the vacuum of space on the trip from Earth opens, exposing the system to the Martian atmosphere. The Sabatier reactor, condensers, RWGS reactor, and refrigeration systems all turn on, and the hydrogen tank valve opens. Once the electrolyzer is full of water from the RWGS, it starts. When there is enough hydrogen going to the Sabatier reactor, it starts. If the electrolyzer ever dries out, it cracks and becomes useless, so the unit shuts down and ask mission control for help if it ever dries. Once the pressure in the hydrogen tank reaches ambient, a pump engages to utilize all of

the seed hydrogen. When all of the hydrogen is gone, the plant begins shutting down in stages, leaving only the refrigeration operating in a stand-by mode, ready to shut off upon launch back to Earth.

The only periodic interruption occurs when the rover returns to the MLV to refuel (see Section 8). The rover enters a docking bay, triggering the refuel sequence. The nozzle extends from the plant and engages the fuel coupling on the rover. This nozzle has three pipe leads in it. One carries the methane and another carries the oxygen, both from the ERV tanks. The third lead contains carbon dioxide, which is bled off the initial compressor that removes the trace gases (see Fig. 6.9). This inflammable gas is used in the rover power system to lower the combustion temperature.

6.7 POWER SYSTEMS AND THERMAL CONTROL
(Craig Perras)

Project Hyreus will require a total electrical power of approximately 2 kW to supply the methane/oxygen propellant plant and its subsystems, the Mars science experiments, and communications and control. A rough breakdown of the power requirements is given in Table 6.2.

A number of power systems were considered which could provide the power necessary on the sometimes hostile Martian surface, while meeting a number of design criteria, including: reliability, availability, survivability, specific power, cost, and safety. The following power systems were investigated and are described sequentially in the following sections:

Radioisotope Thermoelectric Generators (RTG)

Dynamic Isotope Power Systems (DIPS)

Thermophotovoltaic Power Generators (TPVPG)

Thermionic Nuclear Power Sources (TNPS)

Solar Arrays and Batteries

Table 6.2 Breakdown of Power Requirements for Mars Lander

Power Plant	Power Required (W)
Propellant Plant	
Compressor and Pumps	200
Electrolyzer	50
Reverse water-gas shift reactor	400
Liquefaction	300
Storage refrigerator	300
Sub total	**1,250**
Mars Science	
All experiments running simultaneously	1000
At any one time	500
Sub total	**500**
Miscellaneous	
Control, communications, etc.	250
Total	**2,000**

6.7.1 General-Purpose Heat Source (GPHS)

The GPHS incorporates a modular design, with each 250 W_{th} module completely autonomous, with its own passive safety provisions. These safety provisions center around immobilization of the plutonium fuel to the maximum extent possible during all phases of the mission, including ground transportation and handling, launch operations, launch, ascent and orbital insertion, on-orbit operations, and reentry, impact and post-impact environmental

behavior [7]. The modules are flight qualified, and they have been used successfully on a number of missions, including the two GPHS-RTG's on the Galileo mission.

Each GPHS module (Fig. 6.10) consists of an aeroshell containing two graphite impact shells. The graphite aeroshell serves as the structural element and as an ablator. Each impact shell has two fueled clads, each of which consists of a 0.6 kg pressed Pu-238 fuel pellet (PuO_2) encased in an iridium shell. The modules are constrained by locking members that minimize any relative lateral motion by individual modules, and are also packaged in a support system that provides axial compression to prevent separation of the modules [7].

Pu-238 is currently the fuel of choice because of its long half-life (87.7 yrs) and good power density (0.55 W_{th}/gm). It is very expensive and difficult to handle, however, and the cost is approximately \$3000/W_{th} [8]. Sr-90 appears to offer a much higher power density (0.93 W_{th}/gm) and is more than an order of magnitude cheaper [8]. However, Sr-90 has a half-life of 28.0 years and is a beta emitter (Pu-238 is primarily an alpha-particle emitter), which would require a much more massive radiation shield.

The GPHS reference design consists of 18 GPHS modules stacked in a column. This is the heat source used for both the GPHS-RTG and the MOD-RTG, both explained in detail in the next section. The results are summarized in Table 6.3.

Table 6.3 GPHS performance data

Fuel form	10.7 kg of pressed PuO_2
Specific power	172 W/kg
Fuel quantity	1.3×10^5 Curies
BOL fuel inventory*	4500 W_{th}
Cost of radioisotope	13.5 million dollars

*Beginning of life

6.7.2 Radioisotope Thermoelectric Generators (RTG)

The GPHS-RTG is the current state of the art in RTG power systems, and two were flown in the Galileo mission, with both exceeding expectations. The modular RTG (MOD-RTG) is currently under development and will produce a 45% increase over the GPHS-RTG in specific power. The number of GPHS modules can be selected to customize the power output required [9]. If properly funded, the MOD-RTG could be mission-ready before 1996. Table 6.4 lists performance data for both RTG's, using the standard reference design of 18 individual GPHS modules stacked in a column.

Table 6.4 RTG performance data

	GPHS-RTG [7]	Modular RTG[9]
BOL Output Power (W_e)	290	340
Specific power (W_e/kg)	5.2	7.9
Output voltage (volts)	29	30.8
Conversion Efficiency	6.8%	7.5%
Thermoelectric Couples	576 SiGe Unicouples	144 Multicouples
Avg. hot junction temp (K)	1275	1270
Cold side reject temp (K)	575	570
Mass (kg)	54.1	42.2
Envelope		
Diameter (cm)	42.2	33
Length (cm)	114	108

Another major difference between the two RTG's resides in their thermoelectric converters. The GPHS-RTG uses 576 SiGe unicouples, whereas the MOD-RTG uses 144 multicouples. Each multicouple employs a close-packed, glass-bonded thermopile array of 20

thermoelectric unicouples connected in a series circuit, giving the MOD-RTG a slightly higher efficiency [10]. The unicouples are the same type as the ones used in the GPHS-RTG, and are made of SiGe doped with phosphorous (for n-type material) and boron (p-type material). SiGe is used because it is the best material to use in the high temperature range necessary for greater efficiencies (around 1200K for both RTG's).

Thermoelectric unicouples convert heat directly into electricity by using a temperature gradient across the p-n junction, the temperature gradient provided in this case by the Pu decay. By connecting a series of unicouples in series and parallel, the desired dc output voltage is produced. These devices are completely passive, so there is no mechanical wear. However, as can be seen from Table 6.4, these devices are not very efficient, between 6 and 8 percent. The high cost and high concentration of Pu radioisotope fuel makes RTG's entirely inadequate when power requirements of much over 1.5 kW are required. They may be useful as an auxiliary power source, such as in the earth return vehicle, or for use in the satellite and/or the rover.

6.7.3 Dynamic Isotope Power System (DIPS)

Rockwell International is currently researching a DIPS module operating on a closed Brayton cycle (CBC) using a He-Xe working gas mixture for power conversion [11]. DIPS requires three heat source units (HSU's) very similar to the GPHS-RTG for thermal power, employing 17 rather than 18 GPHS modules, giving it a greater factor of safety (see Fig. 6.11 for a comparison). This system has a net efficiency of 21.6%, provides 2.5 kWe, and has an overall mass (including radiator and fuel) of 345 kg. DIPS would be much more efficient, cheaper (it uses less that 25% of the Pu) and lighter than a corresponding RTG configuration at this power level. Figure 6.12 shows the DIPS power conversion unit components, and Fig. 6.13 shows the state point diagram of the CBC loop. Funding for Rockwell's DIPS has been cut to zero as of March 1993, but it is hoped to be resumed in 1995, and, if so, a DIPS module could be mission ready by 2001.

The turboalternator compressor (TAC) rotor consists of a solid piece of metal spinning on a film of gas so it does not make contact with any surfaces, and is the only moving part in the whole system [11]. A gas tube-and-fin radiator assembly would probably be selected over a heat pipe radiator panel since most of the power requirements are on the Martian surface for the methane production plant, and this type of radiator uses only one side of the radiator panel to reject heat into space. The gas tubes are armored, and the radiating fins double as bumper armor for their gas tube[12]. Figure 6.14 depicts a typical gas tube-and-fin surface configuration.

6.7.4 Thermophotovoltaic Power Generators (TPVPG)

The Boeing Company is currently developing a TPVPG for the Pluto mission sponsored by NASA. Preliminary reports indicate that this system might be lighter and more reliable than DIPS, with an overall efficiency between 20 and 25 percent. The system would have an overall specific power (including radiator, etc.) between 9 and 10 W/kg, so a 2.5 kWe system would have an approximate mass of 275 kg, much less than Rockwell's DIPS mass of 345 kg.

A TPVPG operates by absorbing the infrared radiation emitted from a heat source; in this case the heat source consists of standard GPHS modules. The radiant energy is directly converted into electrical energy in the thermophotovoltaic cells, so it has no moving parts, giving it an edge in reliability over a DIPS.

These data are quite preliminary, and have not been validated. This system does appears to hold definite promise in providing moderate amounts of power much cheaper and lighter than any other system investigated in this report. Either DIPS or TPVPG are the next logical step to provide the larger amounts of power required for the next generation of space missions, including manned space exploration of Mars, the establishment of a lunar base, and for utilizing indigenous resources (to make oxygen, fuel, etc.).

6.7.5 Thermionic and Nuclear Power Reactors

These power sources were investigated in case the power requirements for this mission had been grossly underestimated. If a mission requires much over 15 kWe, a small nuclear reactor or thermionic reactor may be the only feasible alternative. Safety and cost would make RTG's impractical because of their large radioisotope payload required due to their low efficiency. Even DIPS or TPVPG may not have an efficiency high enough for the power system to be cost-effective (15 kWe would require 143 kg of Pu if the system had an efficiency of 25%). Fortunately, nuclear reactors are not required for the Hyreus mission.

6.7.6 Solar Arrays and Batteries

Solar cells may be useful as an auxiliary power supply on the surface of Mars, due to some recent improvements in their conversion efficiency. With 592 W/m^2 of solar radiation intensity on the surface, Ga-As cells with an efficiency of 22%, and a cell packing density of 90%, 117 W/m^2 can be generated. This would require a 17 m^2 solar array with an estimated mass of 80 kg. However, considering that the solar arrays must be perpendicular to the sun's rays for maximum efficiency, that they can only be operated during the day, and that the Martian dust storms will severely degrade their effectiveness over the 547 to 574 days they will be operating on the surface, it appears doubtful whether they should be used even as an auxiliary power source while on the Martian surface. However, solar array panels could be useful as a power source for the Earth Return Vehicle (ERV).

Batteries could be useful when used in conjunction with the solar arrays. Since solar arrays will not be used on the Martian surface, there will not be a need for a large set of batteries on the MLV. However, batteries may be useful on the rover and/or the ERV.

6.7.6 Implementation

Mars Landing Vehicle (MLV)

One DIPS module can provide over 2.5 kWe, which is more than enough power for the propellant production plant, refrigeration of the seed hydrogen fuel tank, any recharging which may be required by the rover, and the scientific instrumentation detailed in Section 7. A mass inventory of the DIPS is given in Table 6.5.

The three HSU's lie in a horizontal plane, and not have to be shielded since there is not any particularly sensitive equipment on the MLV. The radiator gas-tube-and-fin assembly is built vertically into the structure, facing outwards. This is illustrated in Section 2. The cycle working gas is pumped through an array of 100 parallel finned tubes using a pair of inlet/outlet gas headers in order to minimize the pressure drop. The radiating surface is covered with OSR tiles to reduce the effective sink temperature and improve the CBC system efficiency [7]. Rockwell optimized their radiator for use on the lunar surface, and it was to be a horizontal 7.5 m^2 one-sided radiator. The sizing of the radiator for use on the Martian surface was approximated to be 8.5 m^2 as a worst-case scenario. This calculation was based on a number of assumptions, including:

- Purely radiative transfer between gray surfaces, neglecting all convective effects
- Martian atmosphere was considered transparent to radiation transfer
- Martian surface temperature was taken to be 260 K at the maximum
- Radiator surface temperature was taken to be uniform, and was determined from a fourth-degree weighted average, since the radiation emits as T^4
- The working fluid was taken to be a He-Xe 0.28 mole fraction gas mixture with a molecular weight of 40

- The view factor from the radiator panel to the ground was estimated to be 0.2, and the area of the ground was taken to be a square 25 m on a side, past which the radiative transfer effects to the radiator panel were negligible

Table 6.5 Mass breakdown of DIPS

Component	Mass (kg)
Three fueled heat source units (HSU)	145
Turboalternator compressor (TAC)	16
Recuperator	47
Radiator assembly	70
Power conditioning and controls	72
Ducting and bellows	20
Total:	370

Earth Return Vehicle (ERV)

The ERV should not carry radioactive isotopes, as it could conceivably impact the Earth, since the return scenario calls for an aerobrake maneuver. Even if the ERV is planned to separate from the sample return module, there is a small but finite chance that separation might not be successful.

6.8 CONCLUSION
(Leo Warmuth)

A methane/oxygen propellant production plant is proposed for use on Mars to manufacture the propellant necessary for both the rover and the return trip to Earth. The plant

uses a dual reactor system, consisting of a Sabatier reactor and a reverse water-gas shift reactor. The plant operates over the 1.5 year stay on the Martian surface, utilizing the carbon dioxide in the Martian atmosphere and imported seed hydrogen from Earth. *In situ* propellant production is a key aspect of the Hyreus mission. Producing the propellant for the return trip to Earth greatly reduces the Earth launch mass requirement and allows for additional payload, such as a satellite, a large Mars science equipment package, and a large rover.

NOMENCLATURE

α	Solar absorptivity of surface
A_p	Projected area of object
A_S	Emitting surface area
COP_R	Coefficient of Performance for refrigerator
COPR CARNOT	Coefficient of Performance for Carnot Refrigerator
DIPS	Dynamic Isotope Power Systems
ε	Infrared emissivity of surface
ERV	Earth Return Vehicle
GPHS	General-Purpose Heat Sources
G_S	Solar flux
k_A	Thermal conductivity of tank wall material
k_B	Thermal conductivity of insulating material
L	Cylinder length of tank (zero if spherical)
MLI	Multilayer Insulation
MLV	Mars Landing Vehicle
O/F	Oxidizer to Fuel
r_1	Inner radius of tank wall
r_2	Outer radius of tank wall
r_3	Radius to outer surface of insulation
RTG	Radioisotope Thermoelectric Generators
RWGS	Reverse Water-Gas Shift
σ	Stefan-Boltzmann constant
T_1	Cold wall temperature
T_2	Warm wall temperature
TAC	Turboalternator Compressor

TPVPG	Thermophotovoltaic Power Generators
TNPS	Thermionic Nuclear Power Sources

REFERENCES

1. Zubrin, R. M., "In-Situ Propellant Production: The Key Technology Required for the Realization of a Coherent and Cost-Effective Space Exploration Initiative," paper AIAA 91-668, 42nd Congress of the International Astronautical Federation, Montreal, Canada, October 1991.

2. Kaloupis, P., Nolan, P. E., and Cutler, H., "Martian Resource Utilization," Space Power, in press.

3. *Project Minerva: A Low Cost Manned Mars Mission Based on Indigenous Propellant Production*, Final Report, AA420/421 Space Systems Design, NASA/USRA Advanced Design Program, University of Washington, Seattle, WA, June 1992, pp. 7.1-7.28.

4. Kleiner, G. N. and Cusick, R. J., "Development of an Advanced Sabatier CO_2 Reduction Subsystem," ASME publication 81-ENAs-11, 1981, pp. 1-7.

5. McElroy, J. F., "The Status of SPE Water Electrolyzers in Support of Space Energy Systems," Hamilton Standard Division, United Technologies Corporation, April 1992.

6. Arkhanov, A., Marfenina, I., and Mikulin, Ye., *Theory and design of Cryogenic Systems*, Mir Publishers, Moscow, 1981, pp. 163-231.

7. Angelo, J. A. and Buden, D., *Space Nuclear Power*, Orbit Book Co., Inc., 1985.

8. Griffin, M. D. and French J. R., *Space Vehicle Design*, American Institute of Aeronautics and Astronautics, 1991.

9. Hartman, R. F., "Modular RTG Technology Status," 25th Intersociety Energy Conversion Engineering Conference, August 12-17, 1990, Vol. 1, pp. 235-238.

10. Hartman, R. F. and Kelly, C. E., "MOD-RTG Multicouple Test Results and Mission Readiness," 10th Symposium on Space Nuclear Power Systems, Jan. 1993.

11. Johnson, R. A. and Stadnik, A. G., Intersociety Energy Conversion Engineering Conference-90, August 12-17, 1990, Vol. 1, pp. 216-221.

12. Dynamic Isotope Power Systems (DIPS) for Space Exploration - Technical Information Rockwell International, Rocketdyne Division, August 1992, Maribeth Hunt, Rocketdyne, Program Manager.

13. Houts, M., Buksa, J., and Howe, S., "Nuclear Power for Mars Surface," AIAA/AHS/ASEE Aerospace Design Conference, Irvine, CA., Feb. 16-19, 1993, AIAA931182.

14. Kaganer M.G., *Thermal insulation in cryogenic engineering*, Israel Program for Scientific Translations Ltd., Jerusalem, 1969, pp. 117-120.

15. Incropera, F. P. and Dewitt, D. P., *Fundamentals of Heat and Mass Transfer*, 3rd ed., Wiley, New York, 1990, pp. A.3.

16. Carr, M.H., *The Surface of Mars*, Yale University Press, 1981, pp 190-195.

17. Ash, R.L., Dowler, W.L., and Varsi, G. "Feasibility of rocket propellant production on Mars," *Acta Astronautica*, 1978, Vol. 5, pp. 705-724.

18. Strauss, W., *Industrial Gas Cleaning*, 2nd ed., Pergamon Press, 1993, pp. 229-245.

19. Cengel, Y.A. and Boles, M.A., *Thermodynamics*, McGraw-Hill, Inc., 1989, pp. 46-58.

20. Keiski, R.L., *The Water-Gas Shift Reaction in Nonisothermal Conditions Over an Iron Oxide/Chromium Oxide Catalyst,* University of Oulu Printing Center, Oulu, Finland, 1991, pp. 2-13.

21. Larson,W.J. and Wertz, J.R., Space Mission Analysis and Design, Microcosm, Inc., Torrence, CA, 1992, p. 420.

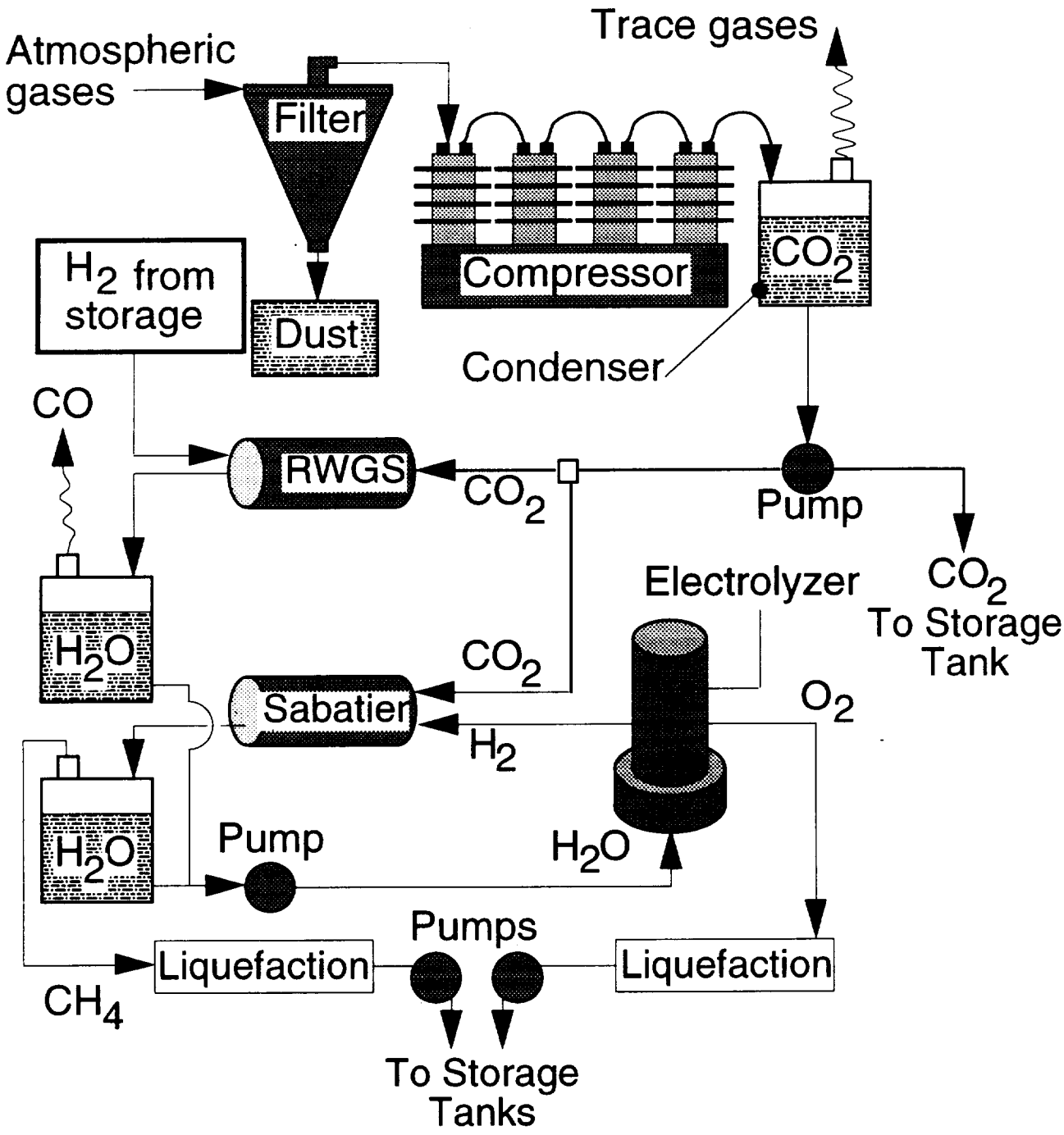

Fig 6.1 Schematic of methane production plant.

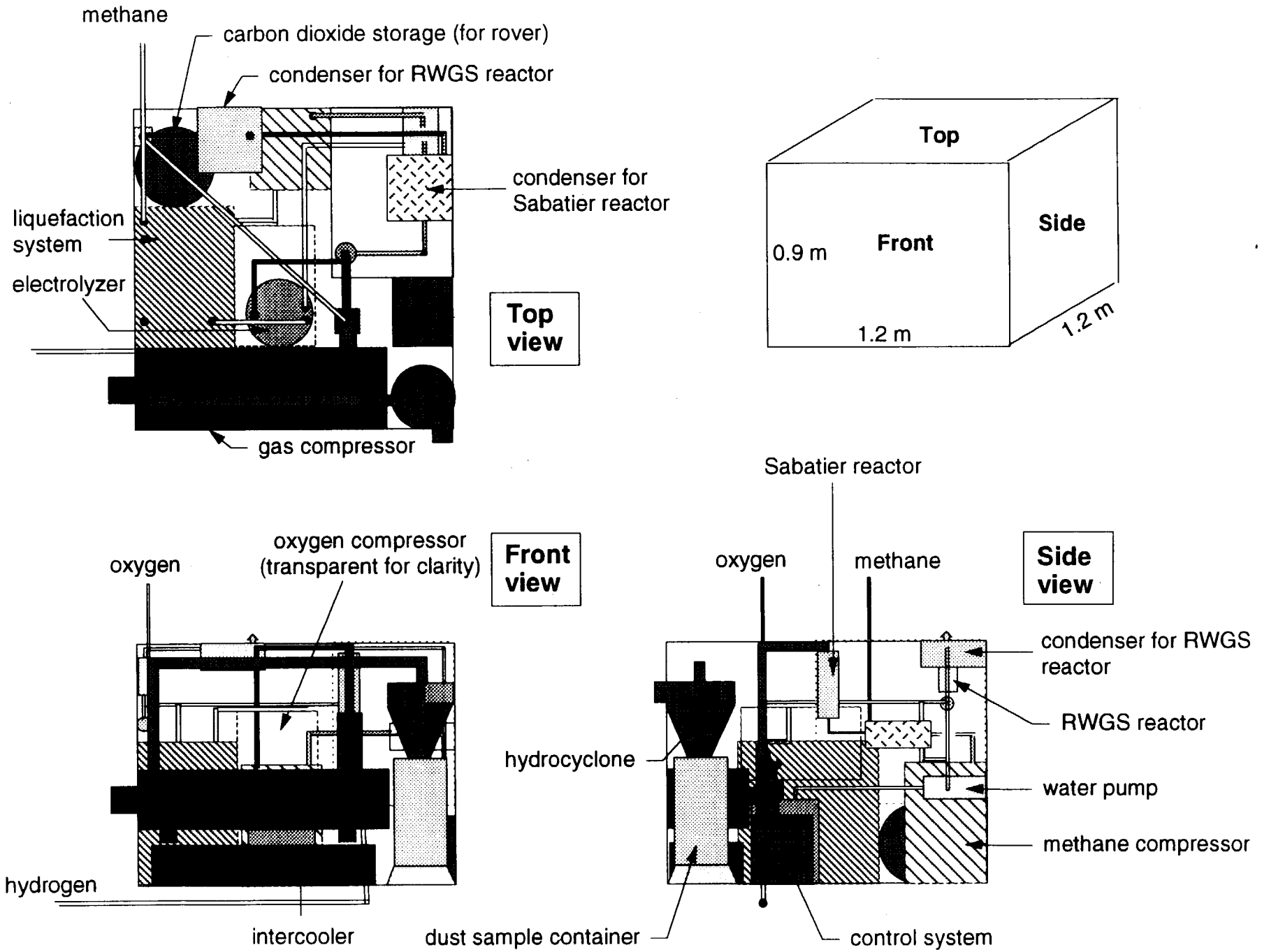

Fig. 6.2 Methane production plant configuration.

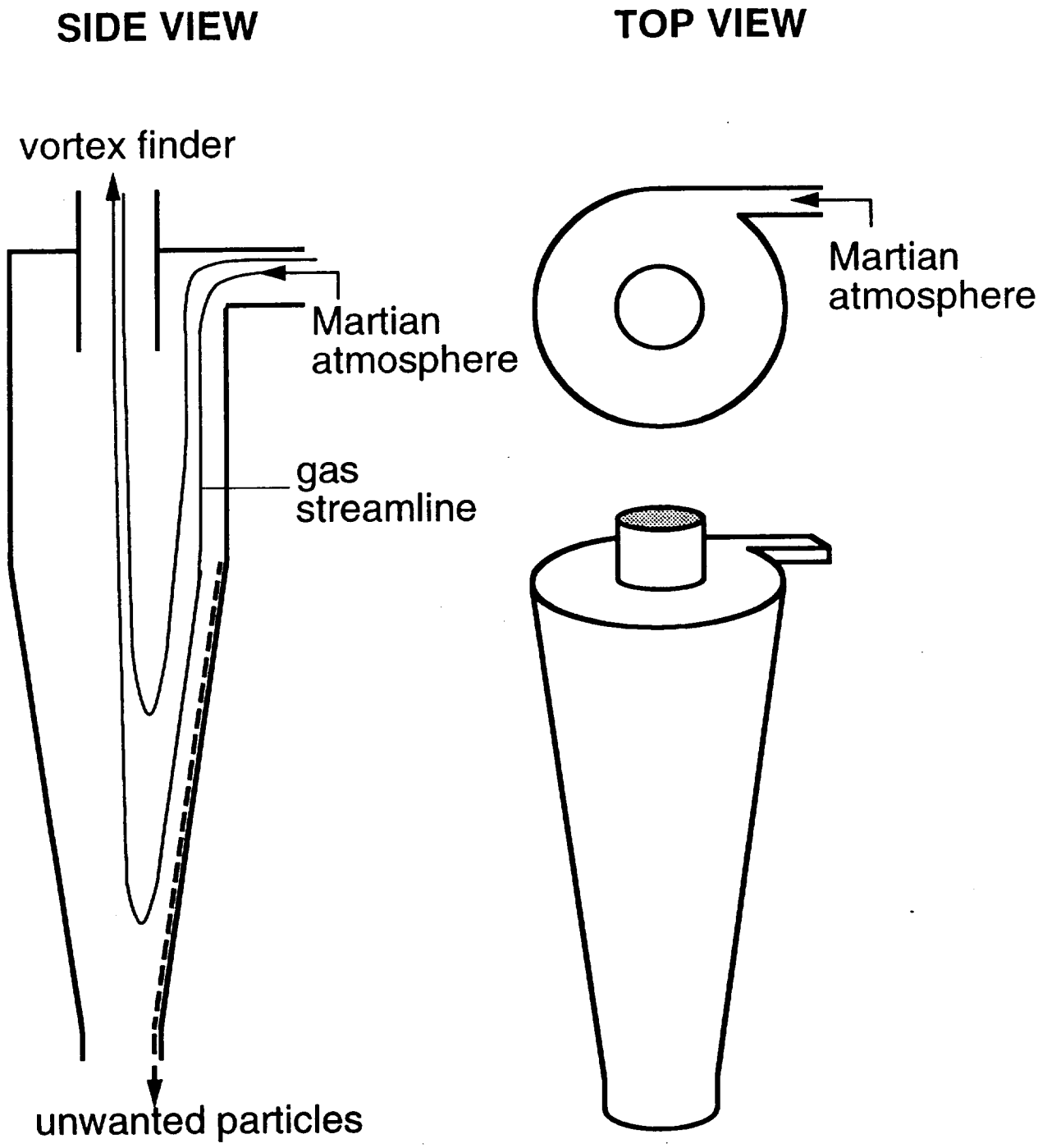

Fig. 6.3 Schematic of hydrocyclone.

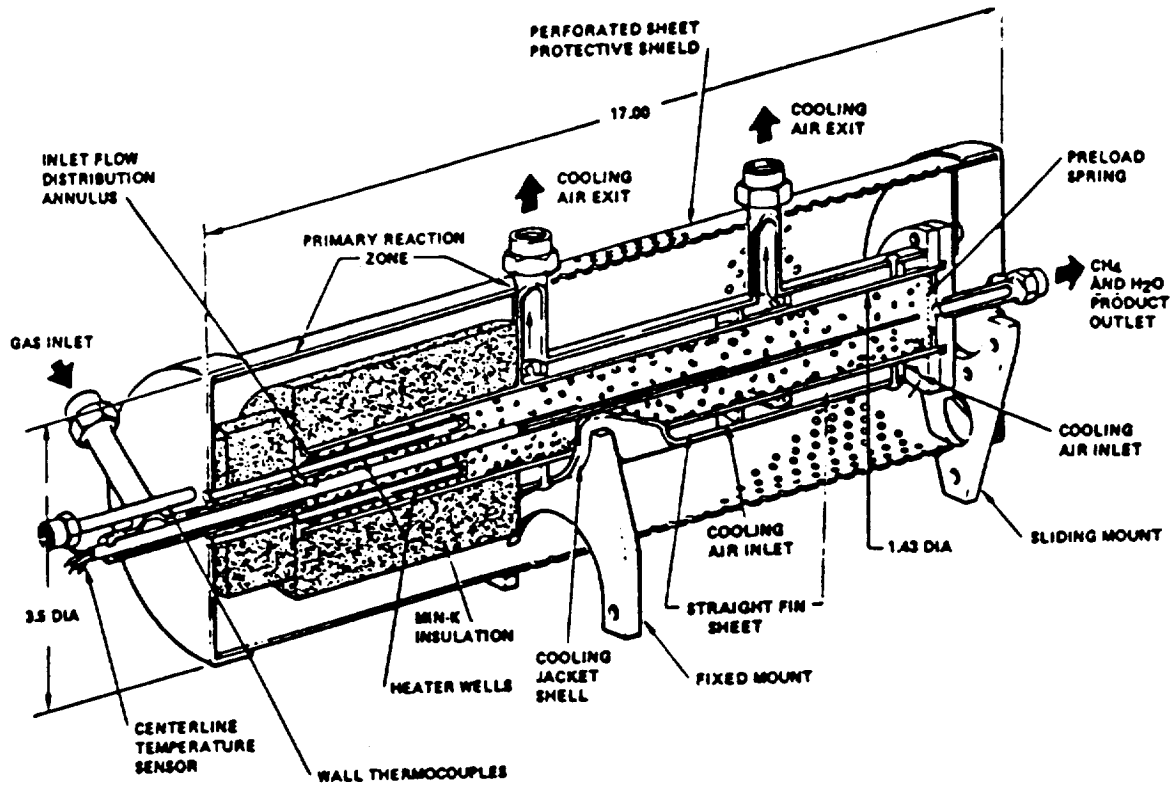

Fig. 6.4 Hamilton standard Sabatier reactor cross section [3].

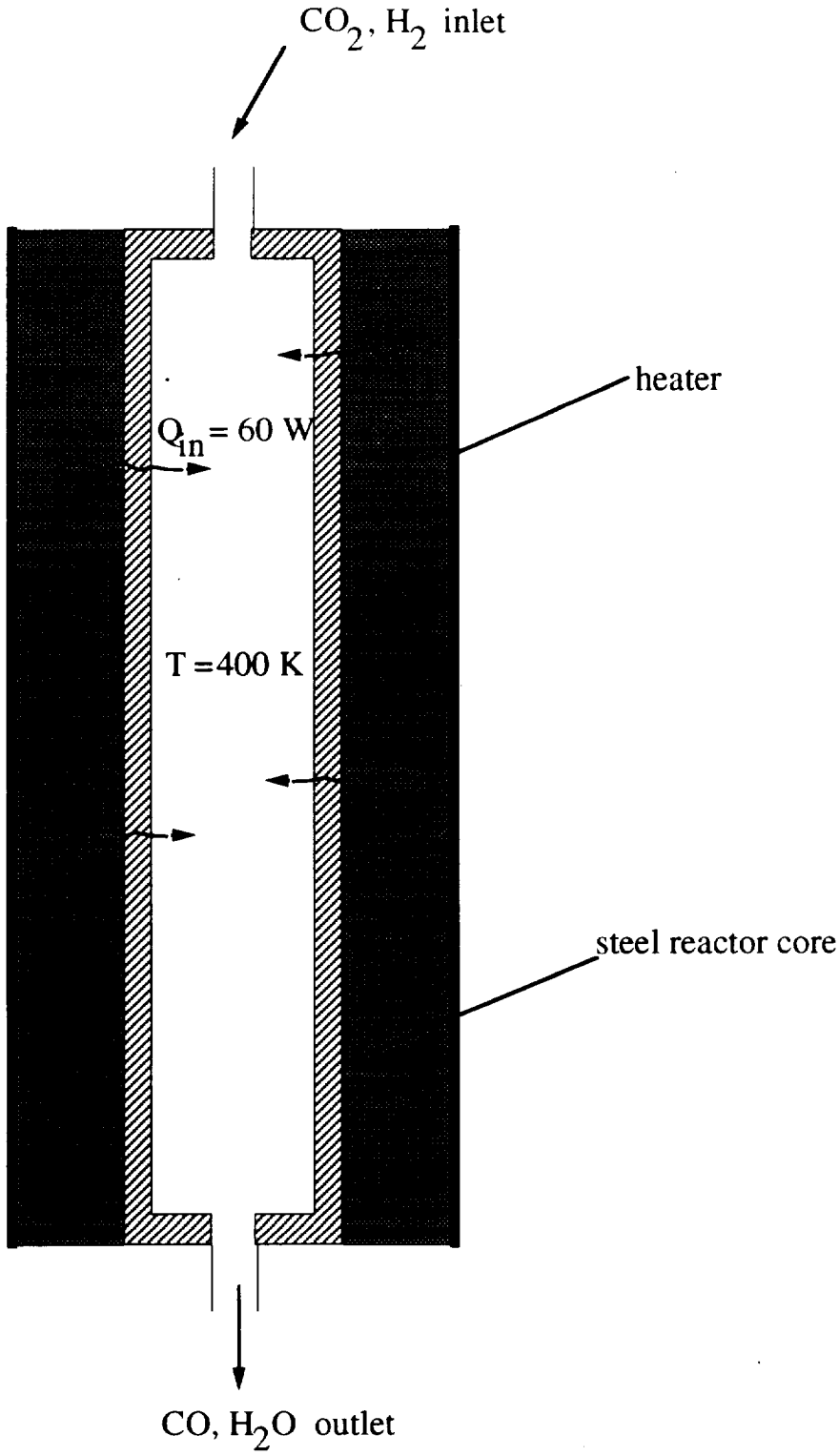

Fig. 6.5 Reverse Water-Gas Shift Reactor.

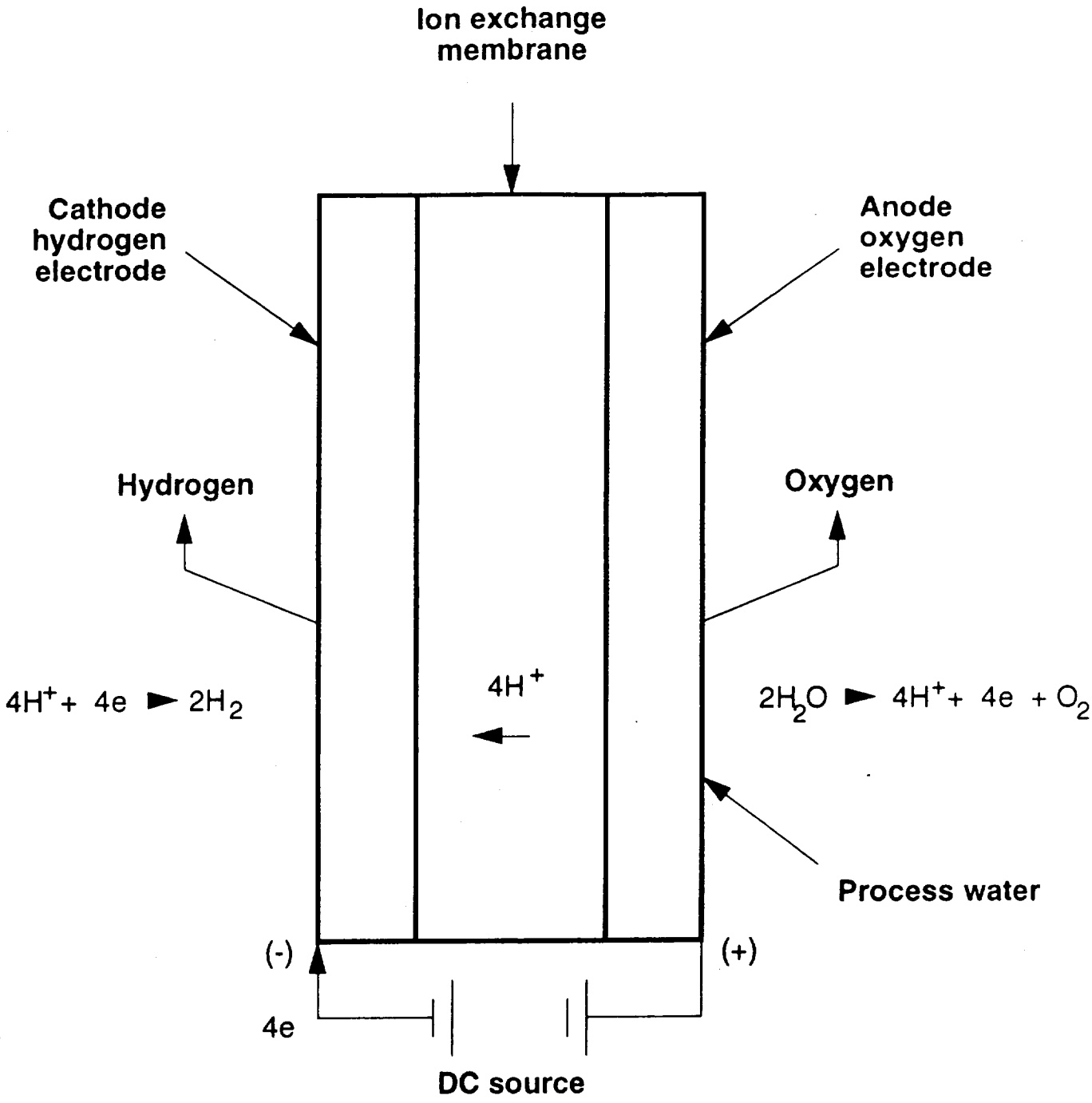

Fig. 6.6 Schematic of Hamilton Standard water electrolyzer [5].

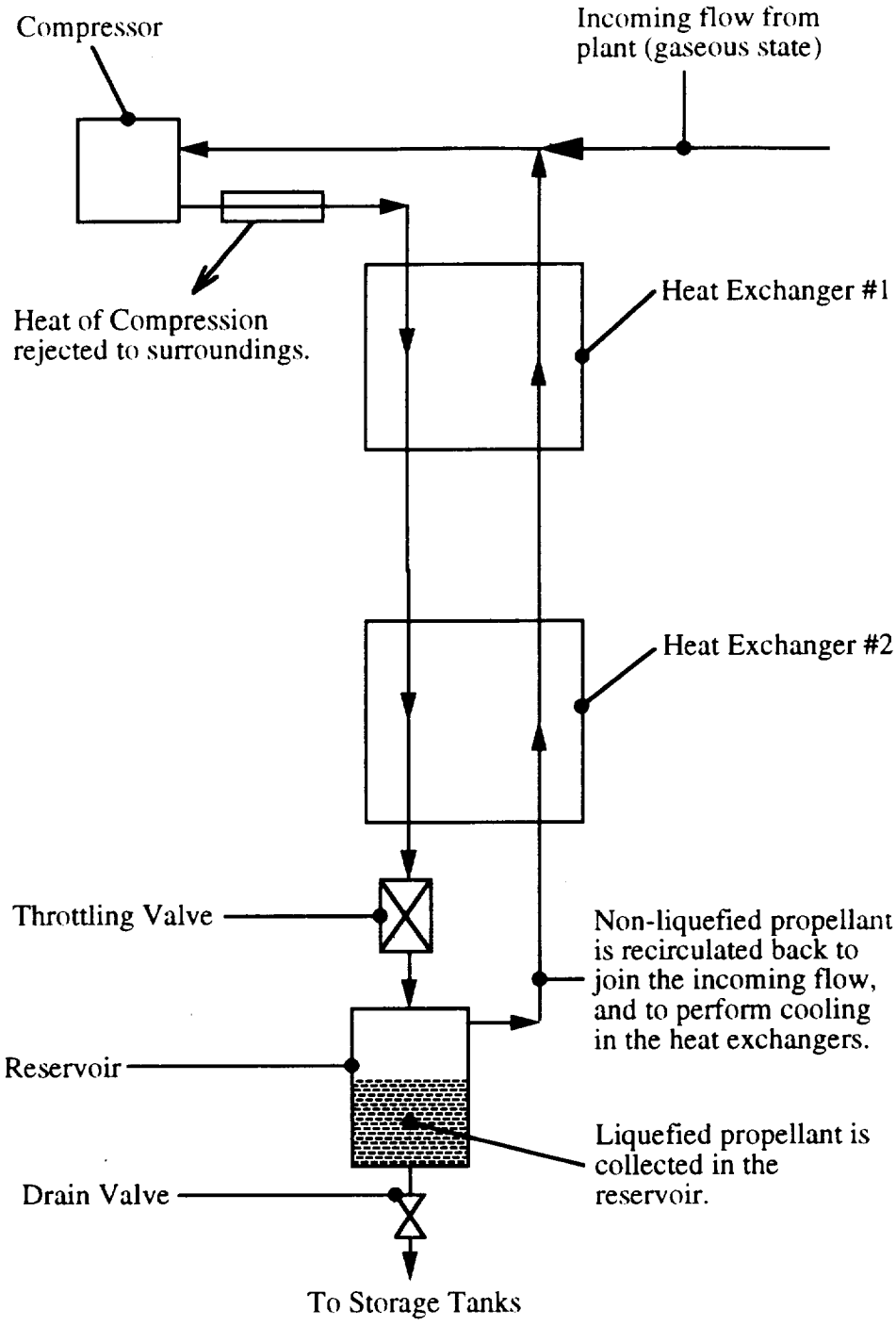

Fig. 6.7 Liquefaction cycle.

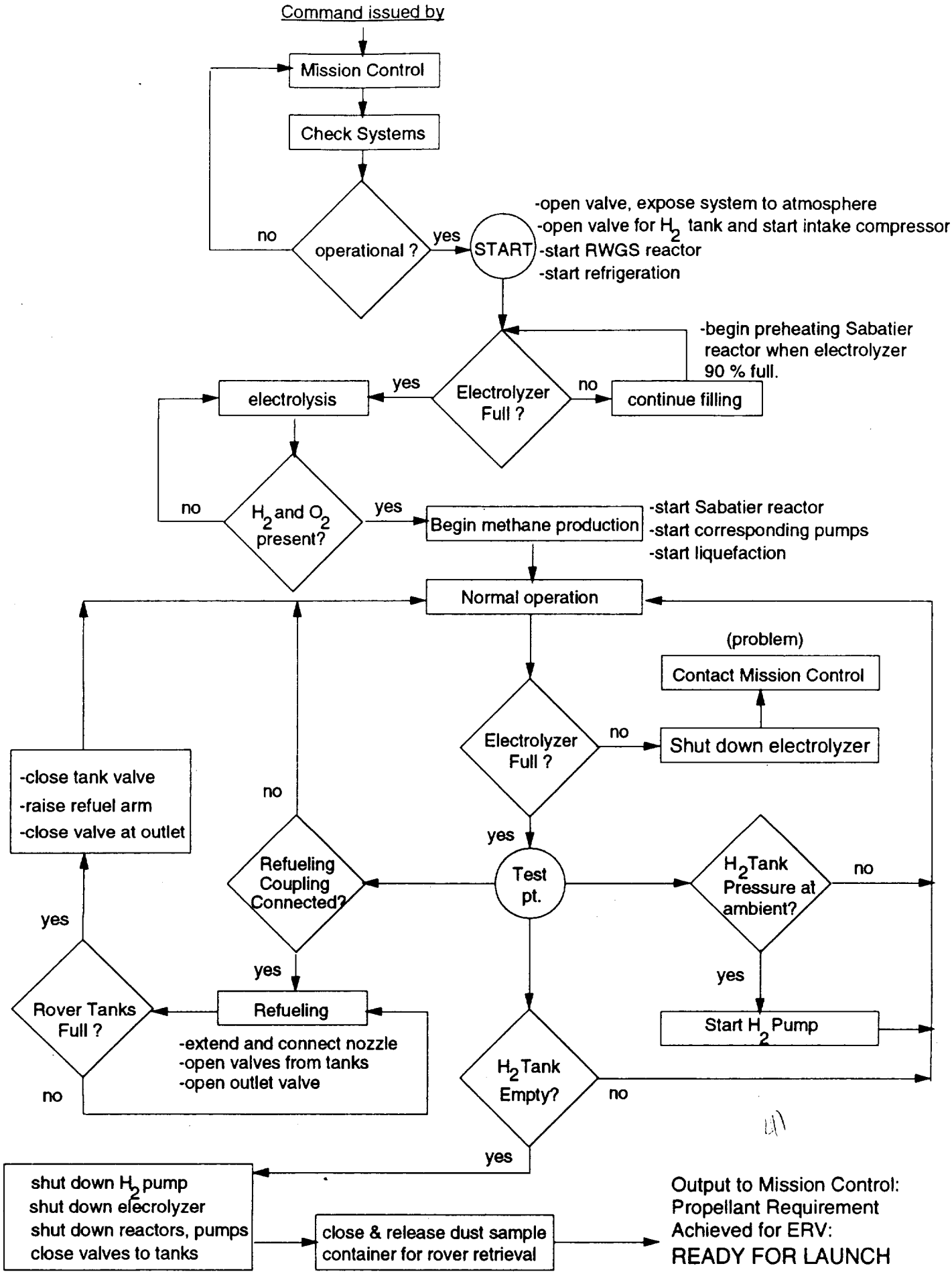

Fig. 6.8 Controls logic tree.

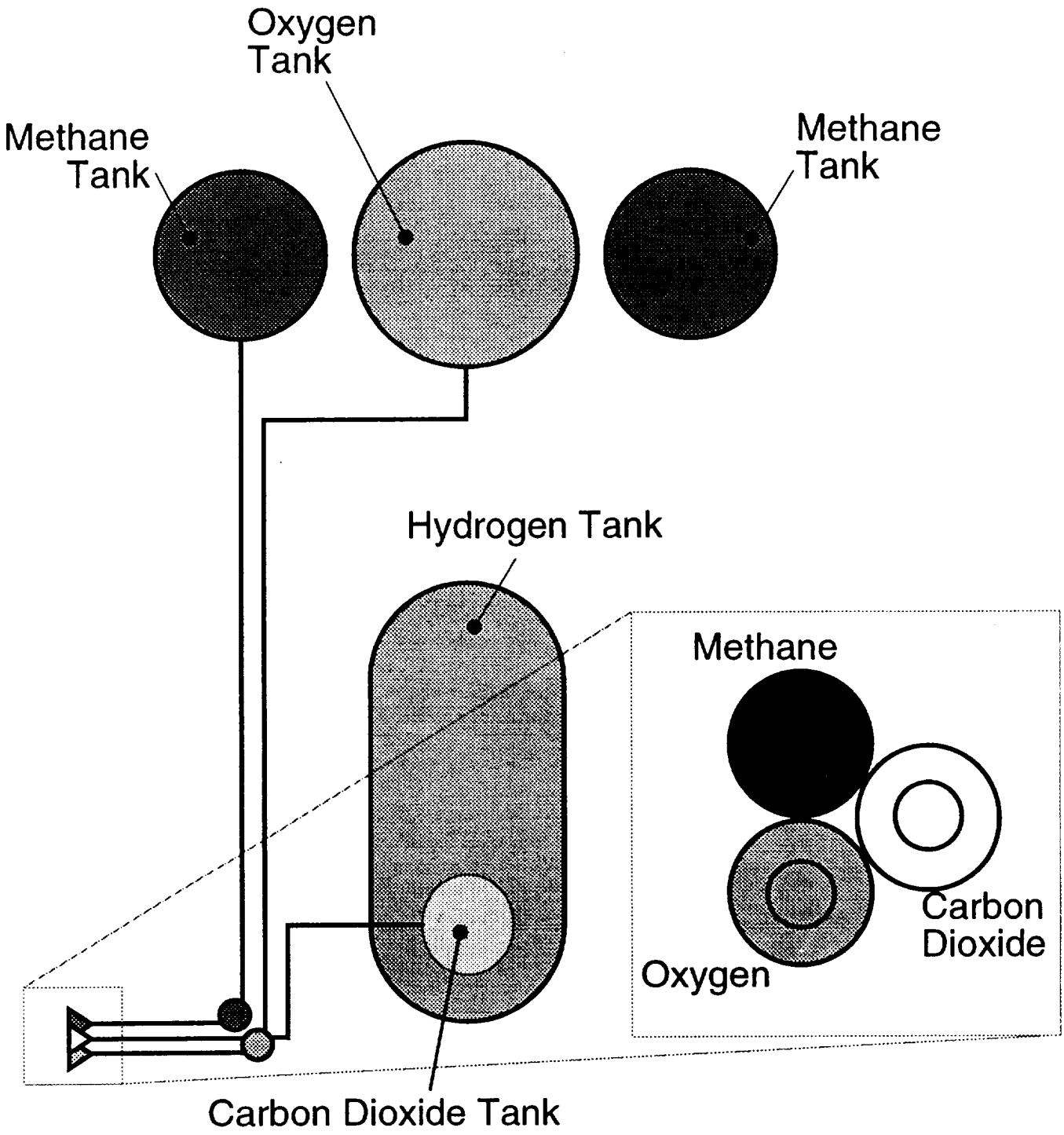

Fig. 6.9 Rover refueling schematic.

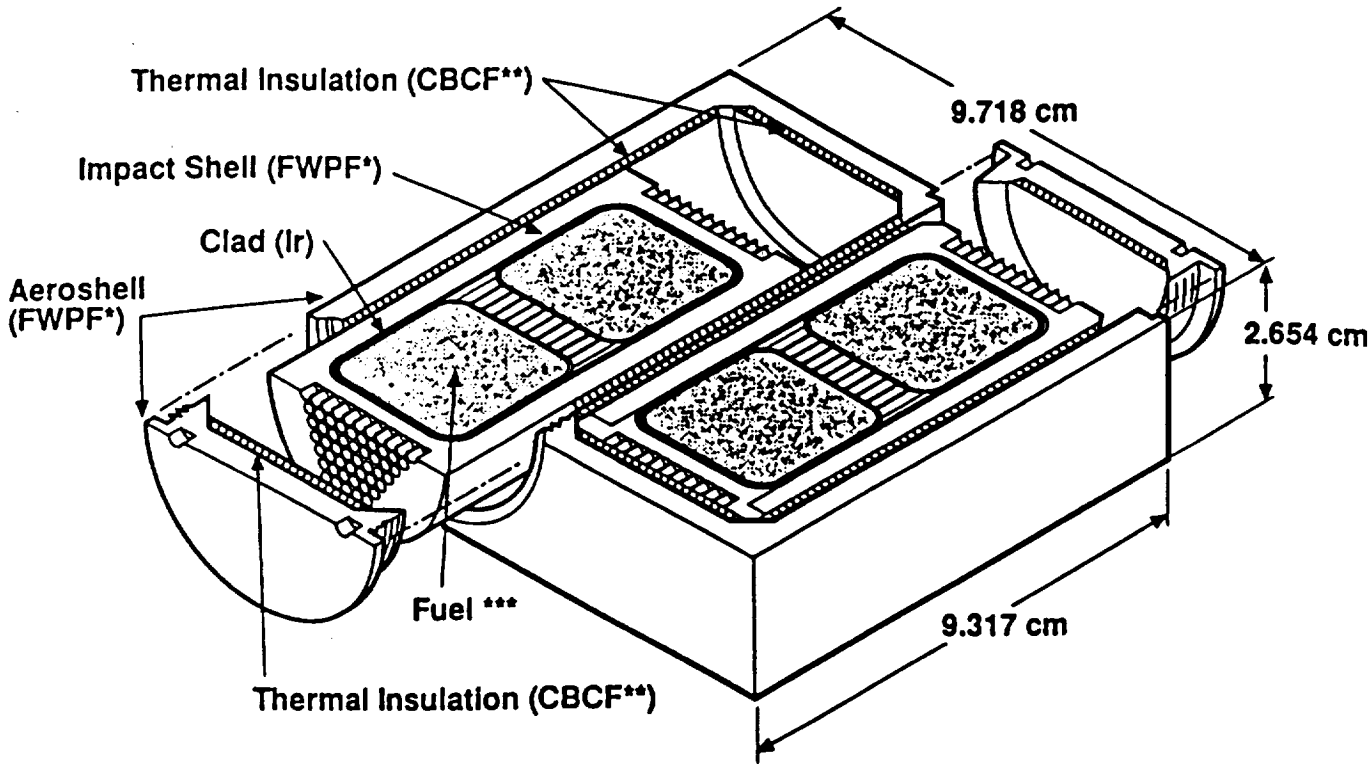

Fig. 6.10 GPHS module sectioned at mid plane.

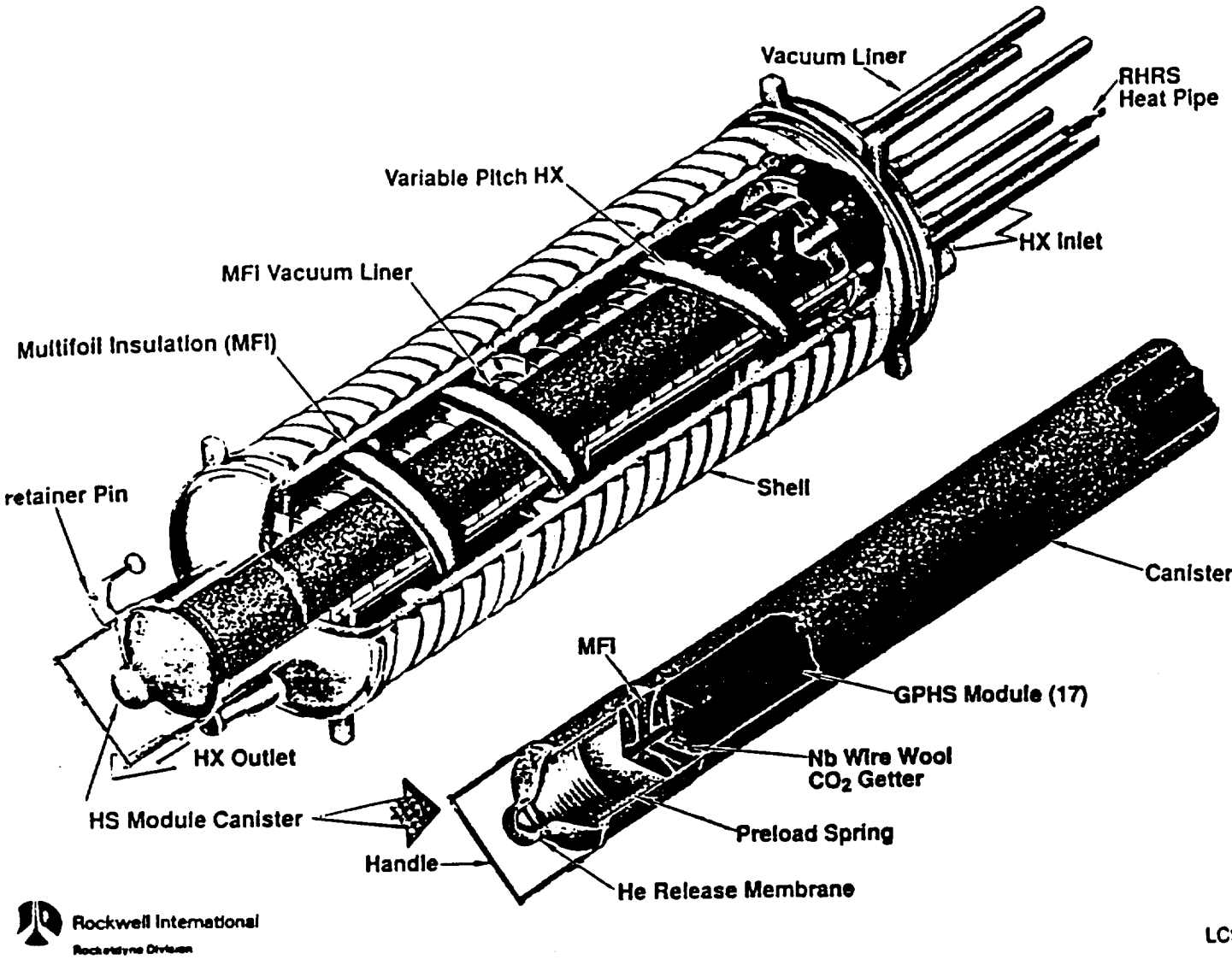

Fig. 6.11 DIPS heat source module.

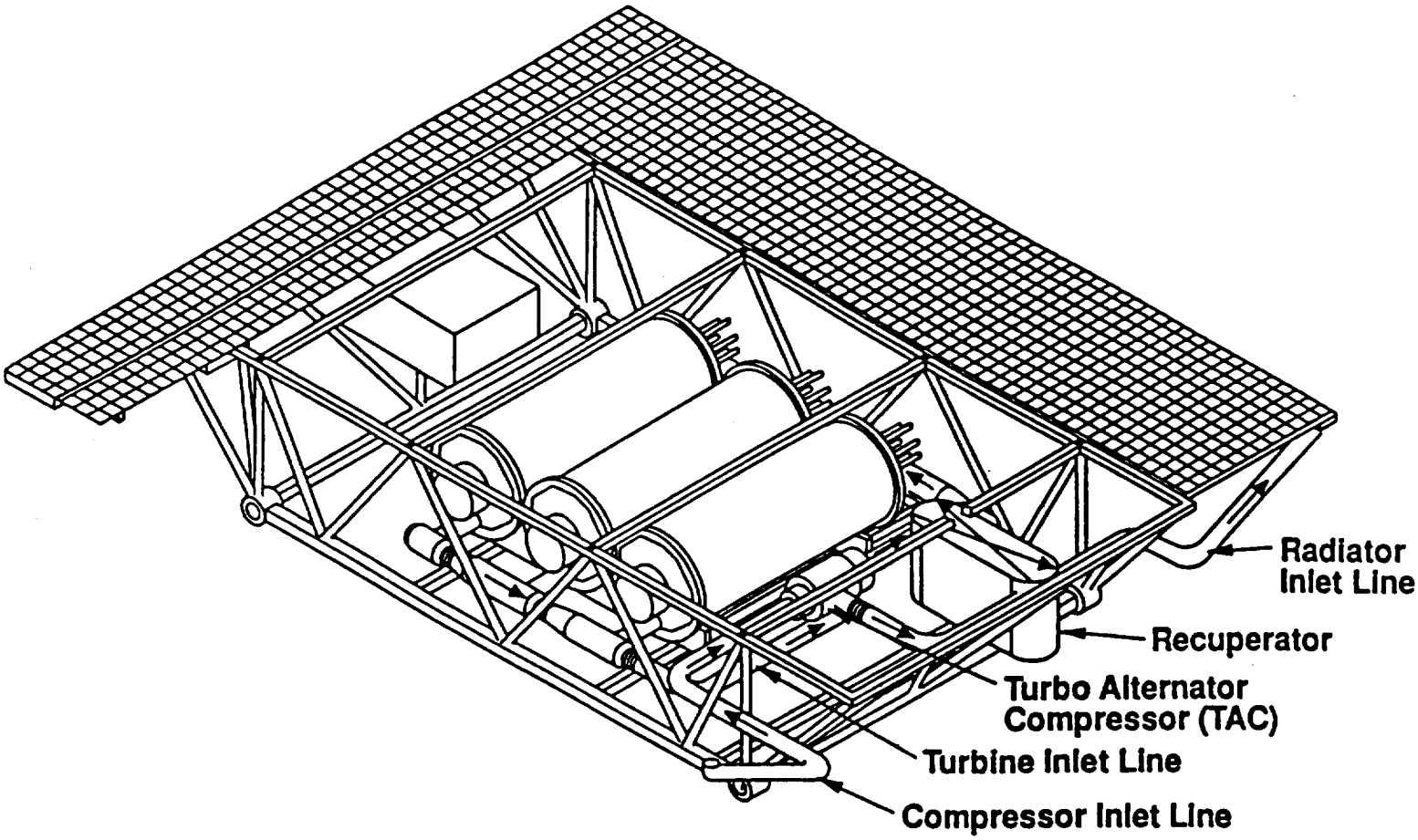

Rockwell International
Rocketdyne Division

92c-29-80
M662

Fig. 6.12 DIPS power conversion unit components.

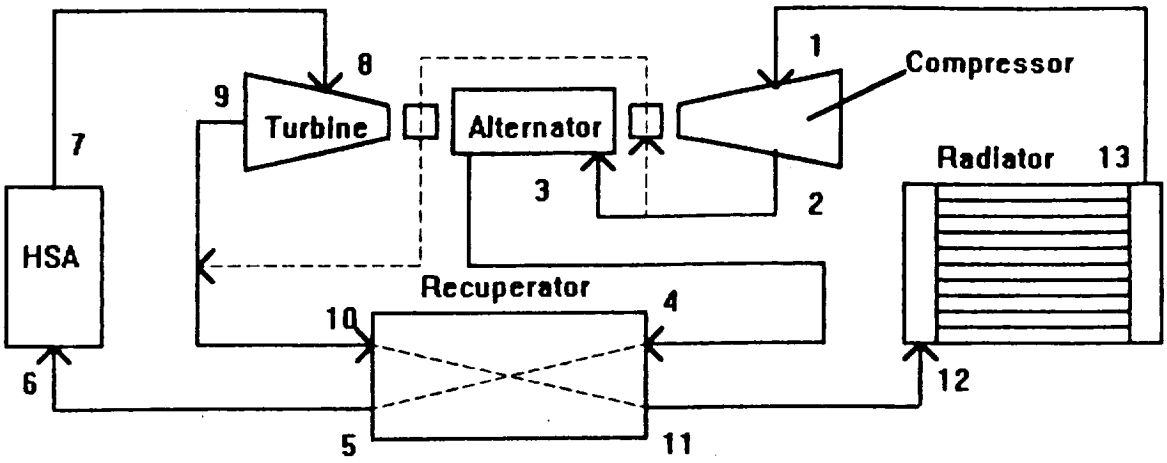

No.	Stream	Temperature (K)	Pressure (kPa)	Flow (Kg/s)
1	Compressor inlet	360.83	321.50	0.2007
2	Compressor discharge	469.23	538.55	0.2007
3	Alternator discharge	475.39	538.55	0.1987
4	HP recuperator inlet	475.39	536.69	0.1987
5	HP recuperator outlet	929.87	534.97	0.1987
6	HSA inlet	926.52	533.86	0.1987
7	HSA outlet	1136.67	531.59	0.1987
8	Turbine inlet	1133.31	530.49	0.1987
9	Turbine outlet	960.97	327.78	0.1987
10	LP recuperator inlet	953.79	327.16	0.2008
11	LP recuperator outlet	503.90	325.57	0.2008
12	Radiator inlet	503.90	324.88	0.2008
13	Radiator outlet	360.83	322.81	0.2008

Fig. 6.13 DIPS state point diagram.

Typical Surface Configuration - One Side Rejects Heat

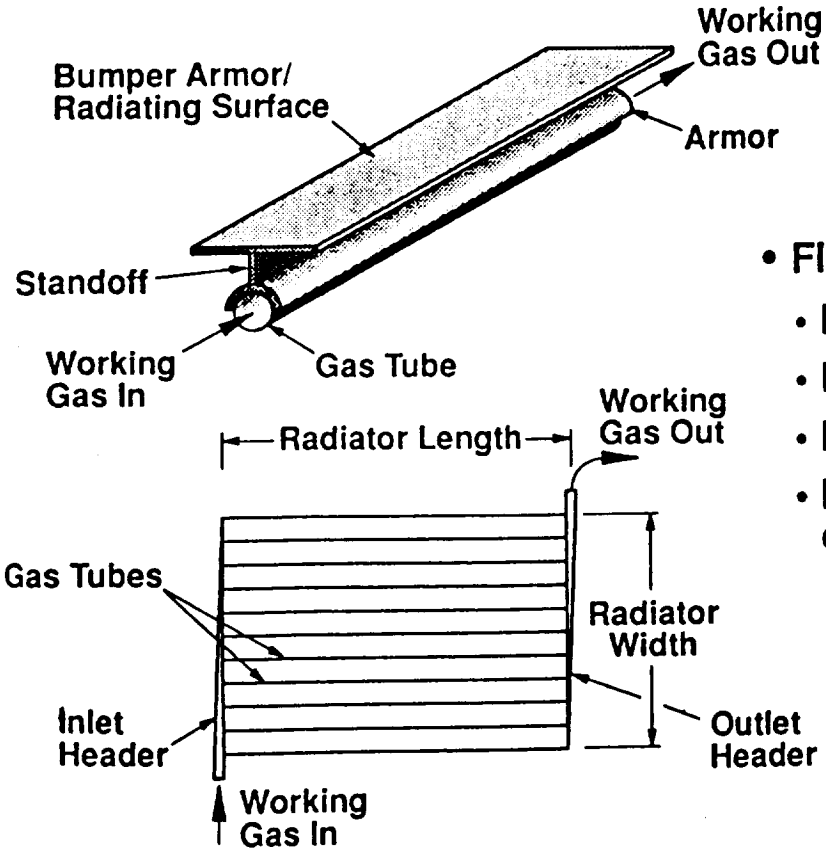

- Flat horizontal facing space
  - Minimum heat sink temperature
  - Low temperature alternator cooling
  - Minimizes "g" impact on heat pipes
  - Minimizes astronaut thermal exposure

Rockwell International
Rocketdyne Division

92c-29-90
M662

Fig. 6.14 Gas tube-and-fin radiator assembly.

7.0 MARS SCIENCE

Jae Kim

Andre Williams

Dung Ngo

TABLE OF CONTENTS

7.1 INTRODUCTION 7.1

7.2 SCIENTIFIC GOALS OF HYREUS 7.2

7.2.1 Scientific Objectives Suggested by Complex 7.2

7.2.2 Scientific Gain in Mariner and Viking Missions 7.3

7.2.3 Goals to be Achieved by Mars Observer 7.4

7.2.4 Scientific Goals in Hyreus 7.5

7.3 SELECTION OF LANDING SITES 7.5

7.3.1 Landing Sites 7.6

7.3.2 Mangala Valles 7.6

7.3.3 Vallis Marineris 7.8

7.3.4 Chryse Planitia 7.8

7.4 SCIENTIFIC INSTRUMENTS 7.8

7.4.1 Lander 7.9

Remote Manipulator Arm (RMA) 7.9

Exobiology 7.10

Seismometer 7.11

Meteorology Package 7.12

7.4.2 Rover 7.12

Camera 7.12

Infrared Spectrometer 7.13

Scoop and Grabber 7.13

7.5 SAMPLE COLLECTION AND RETURN 7.14

7.5.1 Sample Return Module 7.14

7.5.2 Sample Return to Earth 7.14

7.5.3 Heat Transfer Analysis of the Samples 7.15

7.6 PAYLOAD MANIFEST 7.17
7.7 CONCLUSION 7.18
NOMENCLATURE 7.20
REFERENCES 7.21
FIGURES 7.22

7.1 INTRODUCTION

(Andre Williams)

Past missions, including the Mariner flybys and Viking Landers, have generated much data about Mars. The Mars Observer mission with its ability to obtain high resolution photographs (1.4 m/pixel) for detailed coverage of selected areas, will attain a number of important objectives. However, without the return of samples from the Martian surface, some of the highest priority objectives, as outlined by the U.S. National Academy of Sciences Committee on Planetary Exploration (COMPLEX), will not be fulfilled.

The Hyreus mission proposed here will afford the opportunity to utilize current rover and sample return technologies to return a variety of both surface and sub-surface samples. The most accurate landing techniques will be used to place the lander near geologically interesting features [1]. A capable rover will be an essential element of the sample return strategy to maximize the diversity of samples. The sample collection and return systems will keep the samples at conditions as close to Mars ambient as possible, in order to preserve the abundance and distribution of volatile components for analysis on Earth [1].

Hyreus is an essential element in the overall rationale of planetary exploration. The sample return objective, along with several exobiological and meteorological experiments will be major elements in the strategy to obtain a detailed understanding of Mars. In particular, this mission will focus on the search for accessible water/ice reservoirs and for the possible existence of present or past life. This information will be essential in helping to formulate the strategy for future manned missions and colonization, and will help in determining whether or not ideas such as terraforming are feasible.

7.2 SCIENTIFIC GOALS OF HYREUS

(Andre Williams, Jae Kim, Dung Ngo)

In order to establish the scientific goals of Project Hyreus, the scientific objectives as stated by COMPLEX have been referenced. In addition, past missions to Mars have been reviewed for their scientific achievements.

7.2.1 SCIENTIFIC OBJECTIVES SUGGESTED BY COMPLEX

(Andre Williams)

After the Viking landings in 1976, the U.S. National Academy of Sciences' COMPLEX made the following recommendations on the primary objectives for the continued exploration of Mars by unmanned missions [2]:

1. The intensive study of local areas
    a) To establish the chemical, mineralogical and petrologic character of different components of the surface material, representative of the known diversity of the planet;
    b) To establish the nature and chronology of the major surface forming processes;
    c) To determine the distribution, abundance, and sources and sinks of volatile materials, including an assessment of the biological potential of the Martian environment, now and during past epochs;
    d) To establish the interaction of the surface material with the atmosphere and its radiation environment;
2. To explore the structure and general circulation of the Martian atmosphere;
3. To explore the structure and dynamics of Mars' interior;
4. To establish the nature of the Martian magnetic field and the character of the upper atmosphere and its interaction with the solar wind;
5. To establish the global, chemical, and physical characteristics of the Martian surface.

7.2.2 SCIENTIFIC GAIN IN MARINER AND VIKING MISSIONS

(Jae Kim, Andre Williams, Dung Ngo)

Preliminary reconnaissance efforts of the exploration of Mars were accomplished with the Mariner 4, 6, and 7 flyby missions, and the Mariner 9 Orbiter. The photographs taken by Mariner 4 in 1965, which covered only 1% of the total surface, gave the impression that Mars was much like Earth's Moon. However, the pictures of Mars from Mariners 6 and 7 in 1969, which covered about 20% of the surface, revealed a different and more interesting Mars than did Mariner 4 [3]. From the pictures, Mars appears to have very distinctive features, such as areas of broad featureless terrain, volcanic mountains, flood channels, and great chasms never seen on Earth's Moon.

Mariner 9 in 1971, the only orbiter in the series, mapped Mars completely, and yielded the most discoveries. It revealed very large volcanoes and chasms, and, notably, river valleys which have shapes that emerge full-size from the chaotic terrain, have no tributaries, and maintain their size downstream. These features strongly suggest that they are vestiges of large scale flooding rather than typical river valleys. The possible evidence of floods on Mars leads to the speculation of the existence of water as permafrost [4].

The Viking I and II lander missions in 1976 provided meteorological measurements, as well as more detailed photography of the Martian surface. In addition, the Viking missions included scientific equipment to detect certain kinds of life processes. These tests were based on the assumption that living organisms are reasonably well adapted to their environments, and that they are composed of chemicals that are available to them [5]. The results of the experiments were ambiguous, and in assessing the probabilities of life on Mars, each experiment was "conducted under conditions that deviated to varying extents from ambient Martian conditions," and may not be directly relevant to the issue of life on that planet [5].

7.2.3 GOALS TO BE ACHIEVED BY MARS OBSERVER
(Dung Ngo)

Mars Observer (MO), launched in September 1992, is a deep space planetary mission that will provide a major increase in available scientific data about Mars. Its mission objectives include geo-science measurements of the gravity and magnetic fields and climatology measurements of the Martian atmosphere, in addition to very high resolution images of the surface [6].

The three most important sensing devices are the gamma-ray spectrometer (GRS), the pressure modulator infrared radiometer (PMIRR), and the thermal emission spectrometer (TES) [6]. The GRS will measure the basic elements of the Martian surface with a 360-km spatial resolution and a spectral resolution between 0.61 and 1.22 KeV. The PMIRR, a nine-channel infrared radiometer in the 0.3 to 46.5 μm region, will determine the temperature, pressure, dust, and aerosol concentrations in the atmosphere. The TES is to map variations in the surface mineralogy.

Using an onboard camera, MO is to map the surface of Mars with a resolution of 250 m/pixel at nadir and 2 km/pixel at limb. Another camera will acquire very high resolution images at 1.4 m/pixel. This improved mapping will assist in determining the final landing sites for the Hyreus mission.

A magnetometer will be onboard to determine the extent of Mars' magnetic field and to search for any magnetic anomalies on the surface. Surface altimetry will also be an important part of the MO mission and will help to calculate the gravity field. Vertical resolution is expected to be about 10 m.

Man's knowledge of Mars is substantial, but it is trivial when compared to our knowledge of Earth. The MO instruments were selected to record global measurements of Mars' atmosphere, surface, and interior over a full Martian year. MO's work on Mars will be continued by unmanned rover missions to Mars planned by the U.S. and other nations.

7.2.4 SCIENTIFIC GOALS IN HYREUS
(Jae Kim)

As noted above, the exploration of Mars is still in its infancy, even though numerous unmanned spacecraft have been sent to explore the planet, and considerable knowledge of Mars has been gained. In Project Hyreus, Martian volcanics and surface composition will be investigated. Also, experiments for the existence of life on Mars will be conducted. Finally, samples of Martian rocks and soil will be gathered to be brought back to Earth for extensive analysis. The primary scientific goals of Hyreus are listed below.

1) Bring selected samples back to Earth
2) Locate water deposits
3) Investigate top soil, underground soil, rock, and lava
4) Investigate the surface composition
5) Investigate the existence of life on Mars
6) Investigate the evidence of volcanic activity

7.3 SELECTION OF LANDING SITES
(Dung Ngo, Jae Kim, Andre Williams)

The landing site selection for Project Hyreus is the most important factor of the sampling strategy. There have been many previously proposed landing sites for Mars missions, however the uncertainty associated with placing the lander at a specific site, the location relative to interesting geological features, and the range of mobility afforded by the Mars rover are all factors in judging the relative merits of candidate sites [1]. The lander should not be exclusively pre-programmed to land on the primary site, but should have the flexibility to switch to a back-up landing site in case of problems. The landing site for Hyreus should meet the following criteria :

1) Smooth and firm plain which is large enough to allow a safe off-target landing.
2) The site must take into consideration the rover's mobility. It is of interest to have a one-way roving distance of about 20 km.
3) Proximity to the equator for minimizing the velocity requirement of the return trip.
4) Proximity to different types of surface features (craters, river-beds, volcanoes etc.), to allow for a variety of samples.

7.3.1 LANDING SITES
(Andre Williams)

Proposed landing sites within 15° of the equator, so as to minimize the velocity requirement for the return trip, are listed in Table 7.1. The scientific yields from Mars Observer will play an integral role in facilitating the choice of landing site. Sites outside of the proposed latitudes have not been completely ruled out. If it is shown that important scientific yields can be obtained somewhere else, it will be made a priority to go to that site, and attempts to integrate the sample return objectives with the orbital mechanics requirements will be made. Mangala Valles has been chosen as the primary site. Vallis Marineris and Chryse Planitia have be selected as the second and third choices, respectively. A global view is shown in Fig. 7.1.

7.3.2 MANGALA VALLES
(Jae Kim, Andre Williams)

From the investigation of the possible landing sites in the previous section, Mangala Valles has been chosen as the site that best fits the criteria stated above. This area is located in the vicinity of 155° W, 5° S. The landing site chosen, shown in Fig. 7.2, is about 350 km long and has a primary channel that reaches a width of 10 km. It broadens slightly as it extends toward the north, until it meets Amazonia Planitia where it pinches off.

The Mangala Valles region has several attractions as a landing site. This area is

Table 7.1 Candidates for landing sites [7].

Candidates	Location	Features
1. Tharsis Mons	8° S, 132.5° W	Young volcanic rocks
2. Schiaparelli Basin SE	8° S, 356° W	Oldest Martian crustal rocks
3. Olympus Mons	14° N, 131° W	Largest known volcano in solar system
4. Iapygia	9° S, 279° W	Intermediate age volcanics
5. Chryse Planitia	20° N, 45° W	Ridge plains, large flood plain
6. Capri Chasma	14° S, 46° W	Gully region (water flows)
7. Lunae Planum	10° N, 65° W	Ridge plains, intermediate volcanics
8. Mangala Valles	5° S, 155° W	Young volcanics and channels Young and old craters
9. Vallis Marineris	16° N, 63° W	Large river-beds and canyons Horizontal layering, volcanic vents, channel out-flow

comprised of a variety of geologically interesting features: lava from young volcanoes, dry river channels, crustal rock, and old and new craters a short distance from each other (see Figs. 7.3, and 7.4). The scientific rationale for choosing this site is based upon extensive plains which are intimately related to flooding events in this area, while still providing access to other major geologic materials along relatively short traverses. The suite of samples could span much of the geologic history of the planet. An extensive roving mission could traverse down Mangala Valles. The lander is designated to land at 148.1° W, 13.8° S latitude, which is a smooth plain, near which are the geological features to be explored by the rover (see Fig. 7.5). Targets 2 and 3 are Noachian age cratered plains which will yield an abundance of sediment. Target 4 appears to be fresh appearing crater ejecta, which may yield volatiles, and target 4' is a lunar-like crater [7].

7.3.3 VALLIS MARINERIS
(Dung Ngo)

The back-up site under consideration is Vallis Marineris, centered at approximately 63° W longitude and 16° N latitude. This area has been shown to have interesting, thick horizontally-layered rock strata. Also, the canyon walls are good areas to examine to gain a better understanding of the nature of what lies beneath the Martian surface down to ten kilometers.

7.3.4 CHRYSE PLANITIA
(Andre Williams)

The third site under consideration is Chryse Planitia centered at 45° W longitude, 20° N latitude. It is one of the current backup sites. This area is thought to be a large flood plain and would be a likely candidate to search for signs of former life. It has one of the lower elevations on the surface of Mars. The Viking I lander is located on the western edge of the plain at 22.3° N latitude and 47.4° W longitude and would offer the chance to get first hand analysis of the eolian and other weather effects on the lander over the 20 years it has been there. Another feature of the site are the channels near the eastern end of the Vallis Marineris, which open into this plain. These channels could also be a good source of carbonates and fossils from the sediment of the former river/lake [8].

7.4 SCIENTIFIC INSTRUMENTS
(Dung Ngo, Jae Kim)

The scientific instruments to be installed on the lander and the rover are selected to accomplish the scientific goals in Hyreus. Accomplishing these objectives will involve geological field work, exobiological studies, and sample acquisition.

7.4.1 LANDER
(Dung Ngo)

Scientific equipment on the lander will include a Remote Manipulator Arm (RMA) with tools, an exobiological package, a seismometer, a meteorological package, and a mass spectrometer, all of which are located in the Mars Science Container (see Fig. 7.6). All of this equipment is listed in Table 7.2.

Remote Manipulator Arm (RMA)

The Remote Manipulator Arm (RMA, see Fig. 8.14) consists of three 1-m sections which are connected in such a way as to allow the arm to rotate with a maximum degree of freedom. The RMA has multiple purposes, such as loading and unloading the cylindrical sample cells from the Sample Return Module (SRM) into the rover, providing the exobiological studies with test samples, accessing the meteorological package, and loading and unloading the infrared spectrometer on the rover. In addition, the Mars Science Container (MSC) houses all of the RMA tools to be used by both the rover and lander (see Fig. 7.7). The various tools are listed in Table 7.3. There will be 18 different RMA attachments with a backup for each, totaling 36.

Table 7.2 Scientific instruments on lander [5,9].

Item	Volume (m^3)	Mass (kg)	Power (W)
Mars Science Container (MSC)	2	10	--
Exobiology experiments	--	30	50
Seismometer	--	2	10
Meteorology package	--	3	15
Remote Manipulator Arm (RMA)	--	4.1	300
Mass spectrometer	--	8	20
Scientific package controls	--	10	25
Total	**2**	**57.1**	**420**

Table 7.3 Remote manipulator arm tools [9].

Tool	Unit Mass (kg)	Unit Vol. (m^3)	Quantity	Mass (kg)	Volume (m^3)	Power (W)
Rock pick	0.5	0.001	2	1	0.002	300
Rake	0.4	0.001	2	0.8	0.002	300
Broom	0.4	0.001	2	0.8	0.002	300
Hoe/Scraper	0.4	0.001	2	0.8	0.002	300
Grabber	0.6	0.001	2	1.2	0.002	300
Rock crusher	1.2	0.001	2	2.4	0.002	300
Positionable chipper	0.7	0.001	2	1.4	0.002	300
Camera	0.9	0.001	2	1.8	0.002	15
Scoop/Sieve	0.8	0.002	2	1.6	0.004	300
Analyzer	0.3	0.001	2	0.6	0.002	300
Penetrometer	0.5	0.001	2	1	0.002	300
Vibrating pick	0.6	0.001	2	1.2	0.002	300
Claw	0.7	0.001	2	1.4	0.002	430
Rotary saw	1.2	0.001	2	2.4	0.002	430
Linear saw	1.2	0.001	2	2.4	0.002	430
Mini-coring drill	0.73	0.001	2	1.46	0.002	430
Drill	2	0.003	2	4	0.002	430
Drill bits	0.22	0.00016	40	8.6	0.0064	--
Scoobber	1	0.002	2	2	0.004	50
Total			**76**	**36.86**	**0.0504**	**430 (max.)**

Exobiology

Exobiology experiments, as listed in Table 7.4, were conducted on the Viking missions, but the results were ambiguous, because the soil used for the experiments was highly oxidized, and thus reactive to the testing fluid of the Vikings [5]. In Project Hyreus, the exobiology experiments, are based on those done on the Viking missions, but this time a wider variety of samples can be tested (see Fig. 7.8). Not only will samples obtained with the lander RMA be tested, but samples acquired with the rover will be as well. The exobiology experiments are designed to allow for the insertion of samples from the Cylindrical Sample Collection Cells (CSCC) which are collected by the rover. Unlike the Viking experiments, which were designed to test only one sample, Hyreus exobiological studies will make several test runs on a diverse cross-section of material.

The biological investigation is predicated on searching for evidence of metabolism, on the basis that

Table 7.3 Exobiological experiments [5]

Experiment	Measurement	Metabolic Process
Pyrolytic Release (PR)	Incorporation of CO/CO_2 into organic compounds	Photosynthesis and/or chemosynthesis
Gas Exchange (GEX)	Uptake or release of various gases	Decomposition of indigenous compounds
Labeled Release (LR)	Release of radioactive gas from simple organic compounds	Decomposition of labeled compounds

metabolic processes are sufficiently improbable to distinguish them from ordinary chemical reactions.

In the Pyrolytic Release (PR) experiment, soil is incubated under a light in the presence of "labeled" CO and CO_2 (see Fig. 7.9). After incubation, the gases are flushed out, and the soil is heated to see if any of the labeled carbon was metabolized to form complex molecules. In the Labeled Release (LR) experiment, labeled nutrient is added to the soil, then the gases are monitored to see if breakdown of the nutrient components occurs (see Fig. 7.10). In the Gas Exchange (GEX) experiment, changes in the composition of gases in contact with the soil and nutrients are examined (see Fig. 7.11) [5].

Seismometer

The seismometer measures ground oscillations on Mars due to marsquakes, volcanic activity and meteorite impacts. To avoid the constant vibration of the reciprocating pumps from the propellant production unit on the lander, the seismometer will be located

on the Martian surface by the rover and its RMA at a distance of at least 200 m away from the lander.

Meteorology Package

The meteorology package, containing the temperature, pressure, and wind sensors, will be accessed by the lander RMA, which will then serve as a meteorological boom, capable of being deployed up to an elevation of 5 m above the ground, well within the boundary layer, which undergoes large diurnal oscillations in temperature [5]. The meteorology package will include equipment to monitor and record temperature, pressure, humidity, wind speed, and atmospheric opacity.

7.4.2 ROVER
(Jae Kim)

The samplings of Martian soil and rocks are the main task of the rover. The samples are collected by using attachments from the RMA tools cache, located in the Mars Science Container. In addition to the traditional attachments, a "scoobber" can also be used during sample acquisition. Equipment to be used on the rover is listed in Table 7.5.

Camera

The camera is an attachment included in the RMA tools. When in use, it can be attached to the end of the rover RMA, and can be extended 3 m above the height of the rover. The pictures taken by the camera consist of an array of points, each of which has a numerical value from zero to 255, representing the brightness of that point. Zero represents black, 255 indicates white, and the 254 intermediate numbers correspond to the intermediate shades of gray. Each picture is composed of 704 lines with 945 points, or pixels per line [3]. By using the camera attached to the end of the rover RMA, panoramic views of the Martian surface can be acquired, in areas up to 20 km from the landing site.

Infrared Spectrometer

The infrared spectrometer [3] detects a wide variety of possible atmospheric species, including oxides and other compounds of hydrogen, carbon, nitrogen, and sulfur. In addition, the instrument can measure the surface temperature and identify surface constituents by obtaining reflection spectra.

The instrument uses two semiconductor detectors, one cooled to 165°K by radiation, the other to 22°K by a two-stage Joule-Thompson cryostat using N_2 and H_2. Rotating filters provide a spectral scan from 1.9 to 6.0 microns on the first channel and from 4.0 to 14.3 microns on the cryogenic channel.

Scoop and Grabber (Scoobber)

A reliable scoop and grabber are needed to gather the samples. In Hyreus, the scoop and grabber are designed into a single device, called a "scoobber", in an effort to save payload mass (see Figs. 7.12, and 7.13). The size of the scoobber is 24x12x8 cm, and it is made out of aluminum 2024-T6. Its exterior shape is similar to a scoop, except that it has grabbing surfaces and stiffening ribs. The grabbing surfaces are contoured to best fit an object that it grabs. The stiffening ribs keep the grabbing surfaces from bending. Without stiffening ribs, the grabbing surfaces could fail and fall apart in an extreme case. The scoobber scoops about 1,000 cm^3 of soil at a time and can grab a rock sized up to 15 cm across and having a mass of 4 kg.

Table 7.5 Scientific instruments on rover [3].

Item	Volume (m^3)	Mass (kg)	Power (W)
Cameras	0.002	1.6	15
Infrared spectrometer	0.04	8	20
Up to 4 RMA tools	0.006	4	300
Total	**0.048**	**13.6**	**335**

7.5 SAMPLE COLLECTION AND RETURN
(Andre Williams, Jae Kim)

The Martian samples returned to Earth are extremely valuable because they can be extensively analyzed with sophisticated instruments that cannot be flown to Mars. For maximum scientific gain, a variety of samples of the Martian landscape should be obtained. The proposed samples include lava, sediments from river-beds, underground soil, crustal rocks, and top soil, all of which are available near the proposed landing site, Mangala Valles. Finally, samples are to be brought back to Earth in the storage containers in a pristine condition ready to be analyzed. The proposed list of samples desired and their mass and volume is given in Table 7.6 below.

7.5.1 SAMPLE RETURN MODULE
(Jae Kim, Andre Williams)

The Sample Return Module (SRM), which will house Martian soil samples and rocks on the return to Earth, consists of a 0.534 m^3 module which contains twelve individual Cylindrical Sample Collection Cells (CSCC) (See Fig. 7.14). Each cell can house a variety of samples or may be configured as desired. It is made mainly of aluminum 2024-T6 and is heavily insulated and sealed. CSCC has an independent lid that is designed to seal tightly. Each lid is closed after the desired amount of sample is gathered (see Fig. 7.15) [9]. The interior of the SRM is heavily insulated with rigid urethane foam, and the outer skin of the rectangular module is covered with multi-layered aluminum foils sandwiched with glass fabric padding to minimize any conductive and radiative heat transfer. (see Fig. 7.16)

7.5.2 SAMPLE RETURN TO EARTH

After a sample has been gathered, the rover will return to the landing site and the CSCC will be transferred onto the SRM via the lander RMA. This will be repeated until

each CSCC is filled or it is deemed that an adequate amount of samples have been collected.

Upon arrival at Earth, the SRM will not be brought down to the Earth's surface due to the possibility of contamination by potentially fatal micro-organisms from Mars. The returned vehicle will remain in LEO, where it will rendezvous with the Space Shuttle or the space station (if it exists), where the samples will undergo the preliminary analysis under quarantine. After the samples are proven to be safe, they will be brought down to the surface by the Space Shuttle for further, extensive analysis.

Table 7.6 List of samples [9].

Kind	Explanation	Method of Collection	Volume (m^3)	Mass (kg)
Top soil	Exposed soil on Mars	Scooped	0.016	4
Sub-surface soil	Soil from 1.5 - 2 meters underground	Drilled	0.016	5
Lava	Volcanic rock	Grabbed	0.016	5
Rock	Typical rock on Martian Surface	Grabbed	0.016	5
Rock cores	Cores of large rocks	Cored	0.016	4
River sediment	Sediment on ancient river-beds	Scooped	0.016	4
Total			**0.096**	**27**

7.5.3 HEAT TRANSFER ANALYSIS OF THE SAMPLE

The samples need to be kept at 245 K, which is the average Martian surface temperature, for preservation during the trip back to Earth. Any heat transfer to or from the

SRM with outer space and the Sun needs to be balanced to keep the samples at the desired temperature.

The heat transfer within the SRM is calculated from the equation of conduction.

$$Q = \Delta T / (\Sigma R) \tag{7.1}$$

where :

$\Delta T = 97.6°K$ ($250°K - 152°K$ (temperature of outer foil))

$R = L/(k\ A)$, equivalent resistance (see Fig. 7.16)

The heat transfer between the SRM and outer space and the Sun is calculated from the equations of radiative heat transfer.

$$Q = \varepsilon\ A\ \sigma\ (T_f^4 - 3°K^4) \tag{7.2}$$

$$Q = \alpha\ S\ G \tag{7.3}$$

where :

ε = 0.05, for aluminum foil.

α = 0.15, for aluminum foil.

σ = 5.67×10^{-8} $W/(K^4\ m^2)$.

solar flux = 590 W/m^2 in the vicinity of Mars.

= 1405 W/m^2 in the vicinity of Earth.

A = 3.41 m^2, surface area of the SRM.

S = 0.713 m^2 or 0.563 m^2, depending on which side of the SRM is exposed to the Sun's radiation.

With the above equations, Q can be calculated. Values for different situations are given below.

If the SRM is not exposed to the Sun.

$$Q = -10.7 \text{ W}$$

If the SRM is in the vicinity of Mars and exposed to the Sun's radiation.

$$Q = 64.7 \text{ W, if the Sun shines on } 0.713 \text{ m}^2 \text{ side.}$$

$$Q = 51.1 \text{ W, if the Sun shines on } 0.563 \text{ m}^2 \text{ side.}$$

If the SRM is in the vicinity of Earth and exposed to the Sun's radiation.

$$Q = 150.3 \text{ W, if the Sun shines on } 0.713 \text{ m}^2 \text{ side.}$$

$$Q = 118.9 \text{ W, if the Sun shines on } 0.563 \text{ m}^2 \text{ side.}$$

7.6.1 PAYLOAD MANIFEST

(Dung Ngo, Jae Kim)

The following payload lists were put together for the scientific package of the mission. Tables 7.7 and 7.8 list payload manifests for the Mars trip and return to Earth, respectively.

Table 7.7 Volume, mass and power consumption of scientific instruments on Mars [3,5,9].

Item	Volume (m^3)	Mass (kg)	Power (W)
Lander			
Remote Manipulator Arm (RMA)	0.005	4.1	300
Mars Science Container (MSC)	2	10	–
Sample Return Module (SRM) (with 12 CSCC)	0.534	40	–
Exobiology package	--	30	50
Seismometer	–	2	10
Meteorology package	–	3	15
Infrared spectrometer	–	8	20
RMA tools	--	35.2	430 (max.)
Scientific package controls	–	10	25
Total	**2.539**	**142.3**	**850**

Table 7.8 Volume, mass and power consumption of scientific instruments for return to Earth [9].

Item	Quantity	Volume (m3)	Unit Mass (kg)	Mass (kg)	Power (W)
Sample Return Module (SRM)	1	0.534	28	28	150
Cylindrical Sample Collection Cell (CSCC)	12	–	1	12	–
Mars samples	12	–	2.25	27	–
Total		**0.534**		**67**	**150**

7.7 CONCLUSION

(Jae Kim, Andre Williams)

Our knowledge of Mars is the driving factor in future planning. Without a considerable understanding of atmospheric and structural activities, and the location and abundance of resources, sending humans to Mars will be both dangerous and expensive. In that respect, sending low-cost, scientifically oriented, unmanned missions to Mars, until we know enough about the planet, is the next step in the overall exploration strategy.

The Hyreus mission fits well within this strategy. The unmanned rover will be able to obtain a variety of geological samples for extensive analysis back on Earth. Also, further investigation of Mars' atmosphere, surface, interior, dust storms, indigenous resources and volcanics will be a step-forward towards a better understanding of Mars and will assist in planning for future human exploration.

Hyreus will bring a significant amount of Martian soil and rock back to Earth. This is made possible by the use of methane and oxygen processed from the indigenous resource, CO_2, and terrestrial H_2. It is known that CO_2 is abundant in Mars' atmosphere, but it is not known where and how much water there is on Mars. Indigenous water should

be utilized for manned missions if possible. Thus, it is in our best interest to find water deposits on Mars before beginning manned missions. Some believe that permafrost lies just beneath the surface of Mars; if they are right, it will be easily found. Even if permafrost is not found, it is likely that some sub-surface water in some form exists, which could be used in future manned exploration.

NOMENCLATURE

α	Absorptivity of the SRM.
A	Surface area of the SRM.
COMPLEX	U.S. National Academy of Sciences Committee on Planetary Exploration.
CSCC	Cylindrical Sample Collection Cell.
ΔT	Temperature difference between interior and exterior of the SRM.
ε	Emissivity of the SRM.
G	Solar flux.
GEX .	Gas Exchange Experiment.
GRS	Gamma-Ray Spectrometer.
LR	Labeled Release Experiment.
MO	Mars Observer.
MSC	Mars Science Container.
PMIRR	Pressure Modulator Infrared Radiometer.
PR	Pyrolytic Release Experiment.
R	Equivalent resistance of the SRM.
RMA	Remote Manipulator Arm.
σ	Boltzmann constant.
SRM	Sample Return Module.
TES	Thermal Emission Spectrometer.

REFERENCES

1. McKay, C.P., *The Case for Mars II*, Umvelt Incorporated, 1984, pp. 99-119

2. Bourke, R.D., Golombek, M.P., Spear, A.J., and Sturms, F.P., "Mesur and Its Role in an Evolutionary Mars Exploration Program," Paper No. IAF-92-0509, World Space Congress, Washington D.C., August, 1992

3. Collins, S.A., *The Mariner 6 and 7 Pictures of Mars*, NASA, Washington D.C., 1971, pp. 6-22.

4. Wilford, J.N., Mars Beckons, Alfred A. Knopf, Publisher, New York, 1990, pp. 178-179, pp. 219-222, pp. 86-105

5. Frosh, R.A., *Scientific Results of the Viking Project*, American Geophysical Society, Washington D.C., 1976 pp. 4277-4283.

6. Palocz, S., "Mars Observer Mission and Systems Overview," *Journal of Spacecraft and Rockets*, Vol. 28, 1991, pp. 491-500.

7. Greeley, Ronald, ed., *Mars Landing Site Catalog*, NASA Reference Publication 1238, 1990.

8. *Project Minerva: A Low Cost Manned Mission Based on Indigenous Propellant Production*, Final Report, AA420/421 Space Systems Design, NASA/USRA Advanced Design Program, Department of Aeronautics and Astronautics, University of Washington, Seattle, WA, June 1992

9. Reiber, D.B., *The NASA Mars Conference*, American Astronautical Society Publication, 1986, pp. 325-347.

10. Spitzer, C.R., *Viking Orbiter Views of Mars*, NASA, Washington D.C., 1980, pp.177-178.

11. Mutch, T.A., Arridson, R.A., Head III, R.E., Jones, K.L., and Saunders, R.S., *The Geology of Mars*, Princeton University Press, NJ 1976, pp. 299.

12. Baker, V.R., *The Channels of Mars*, University of Texas Press, Austin, 1982, pp. 46-47.

13. The Viking Lander Image Team, *The Martian Landscape*, NASA, Washington D.C., 1978, pp. 4-18.

14. Harmann, W.K. and Raper, O., *The New Mars*, The Discoveries of Mariner 9, NASA, Washington D.C., 1974, pp. 162-167.

15. O'Leary, B., *Mars 1999*, Stackpole Books, Harrisburg, PA, 1987.

16. Carr, M.H., *The Surface of Mars*, Yale University Press, 1981, pp. 190-195.

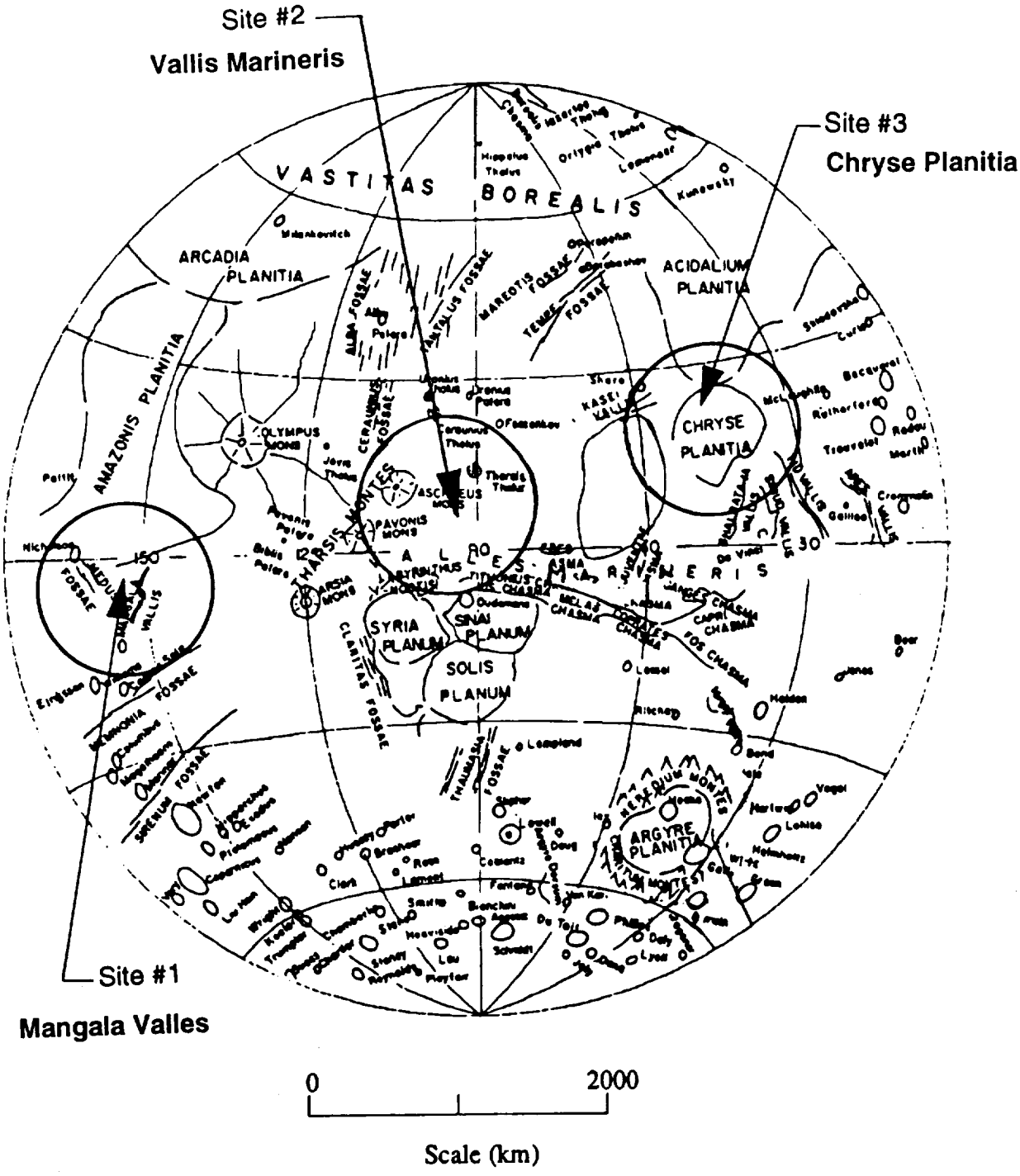

Fig. 7.1 Global view of Mars, showing potential landing sites.

Fig. 7.2 Mangala Valles closeup.

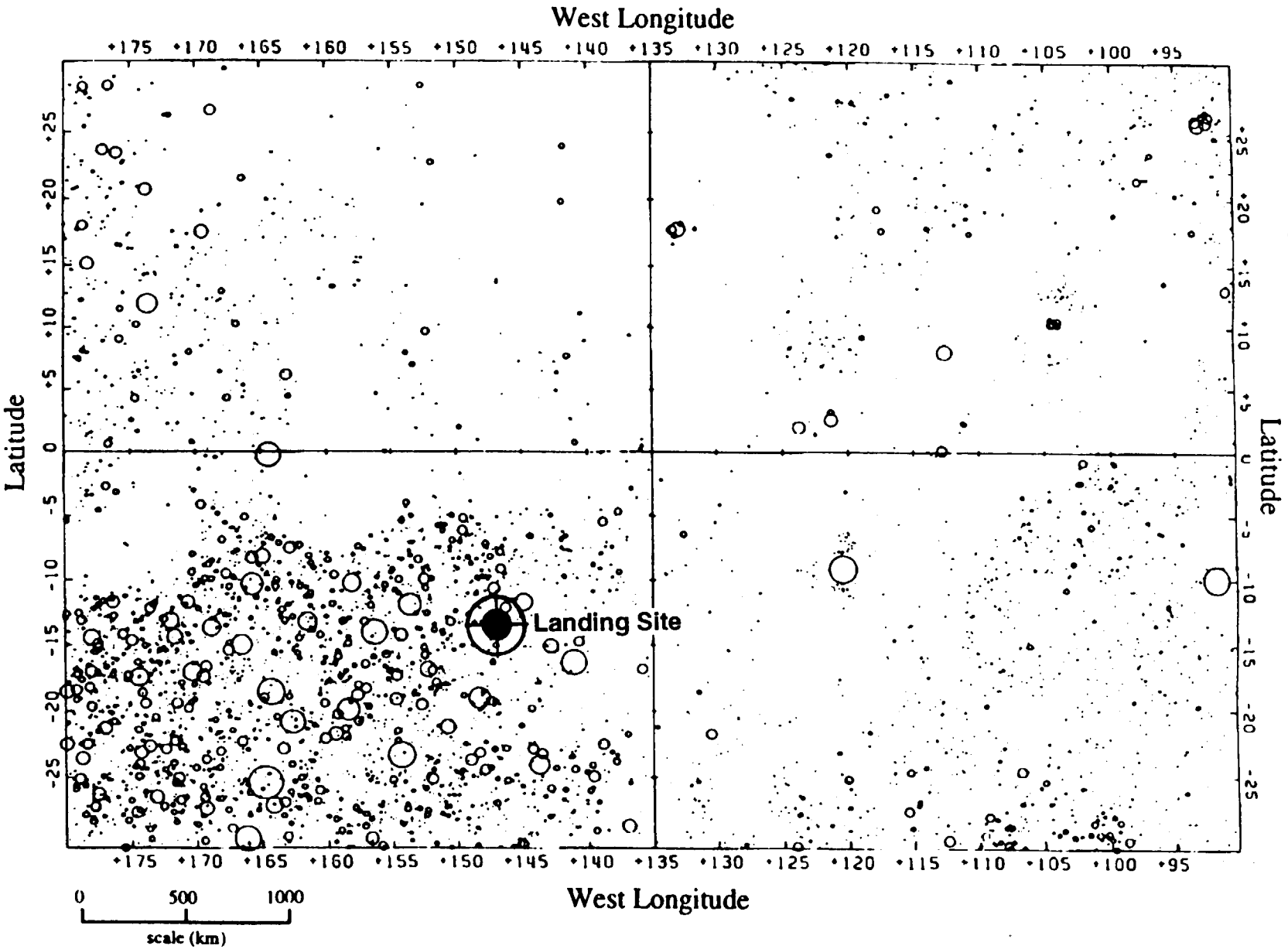

Fig. 7.3 Mangala Valles area crater map.

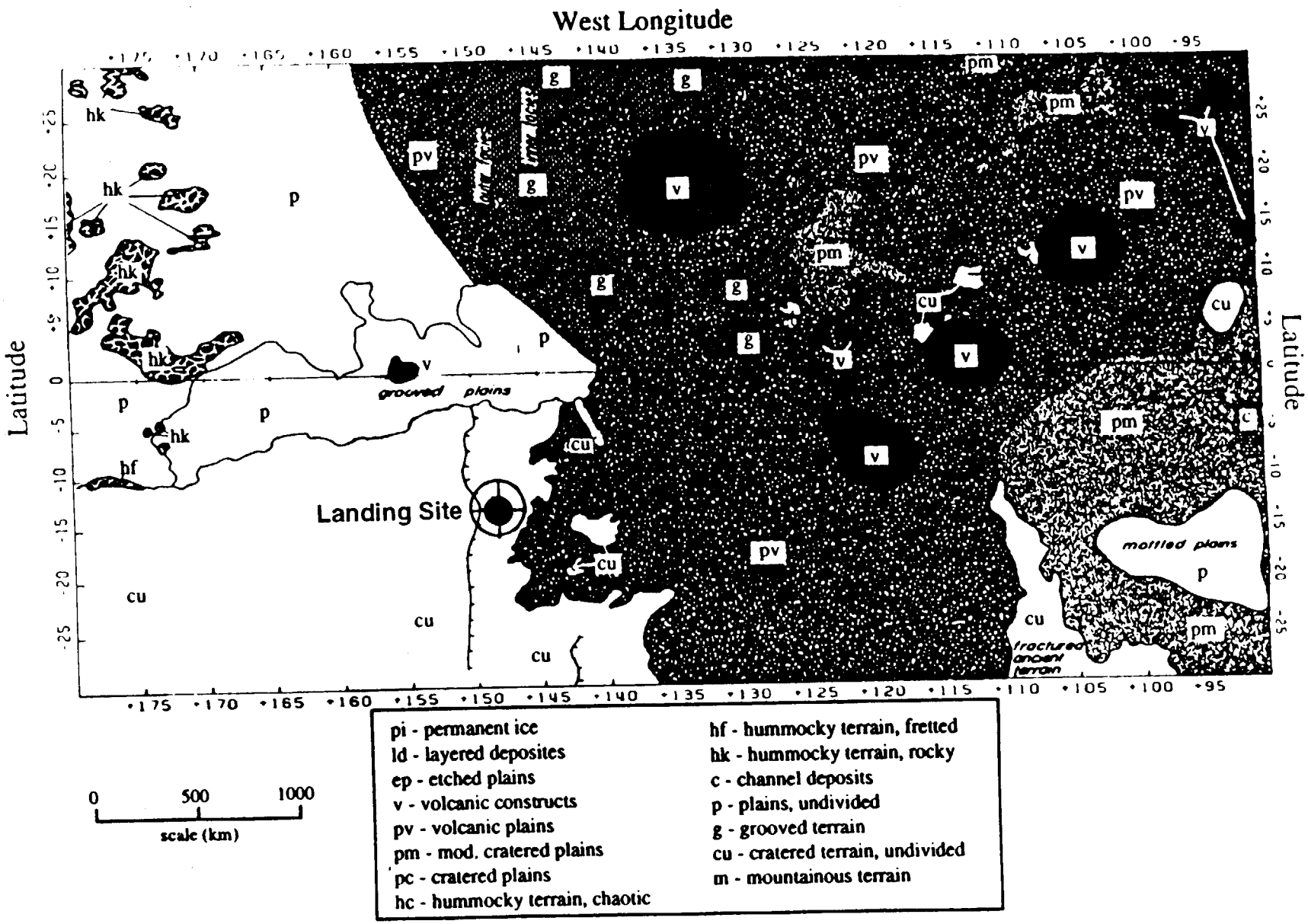

Fig. 7.4 Mangala Valles area geological map.

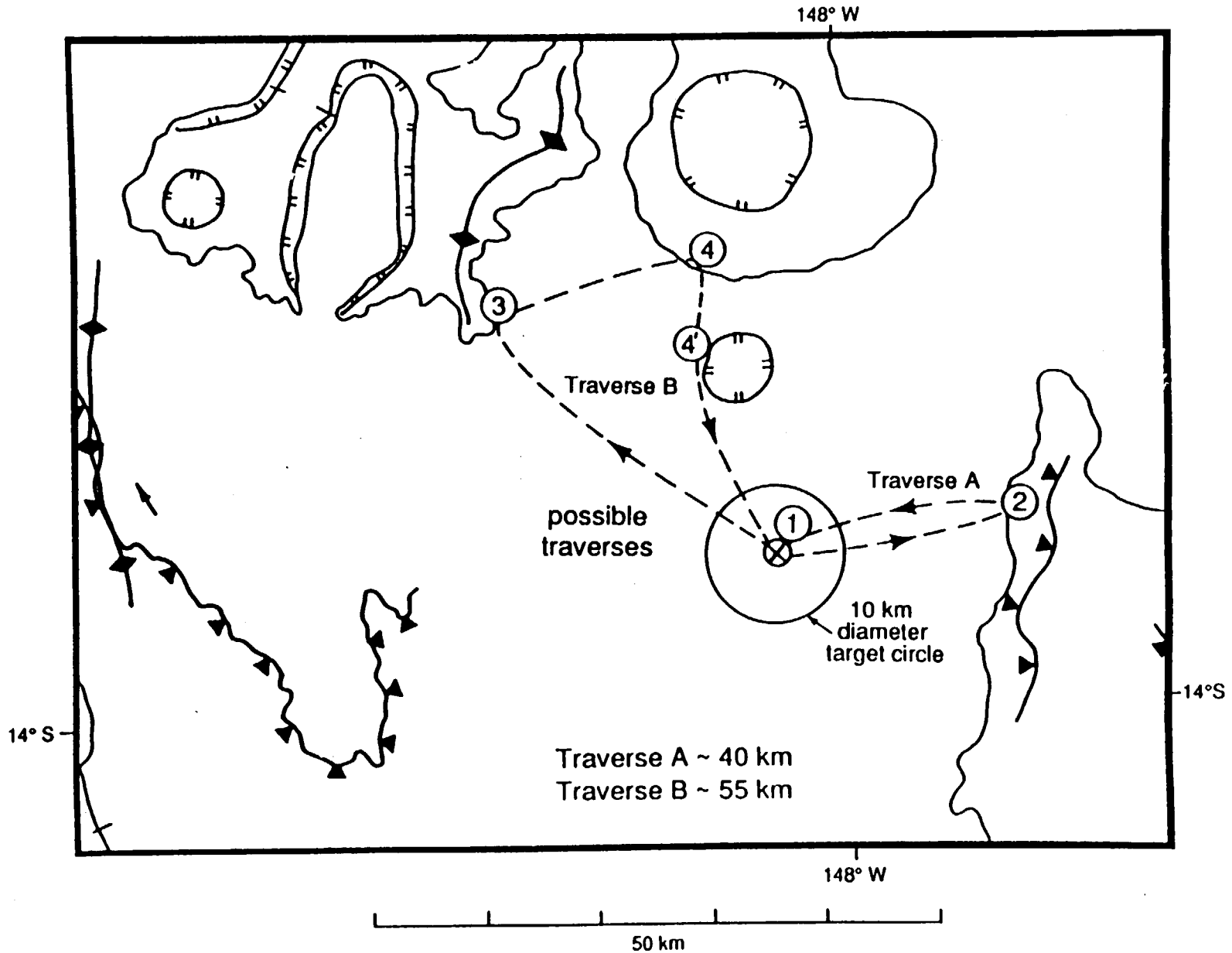

Fig. 7.5 Mangala Valles primary landing site.

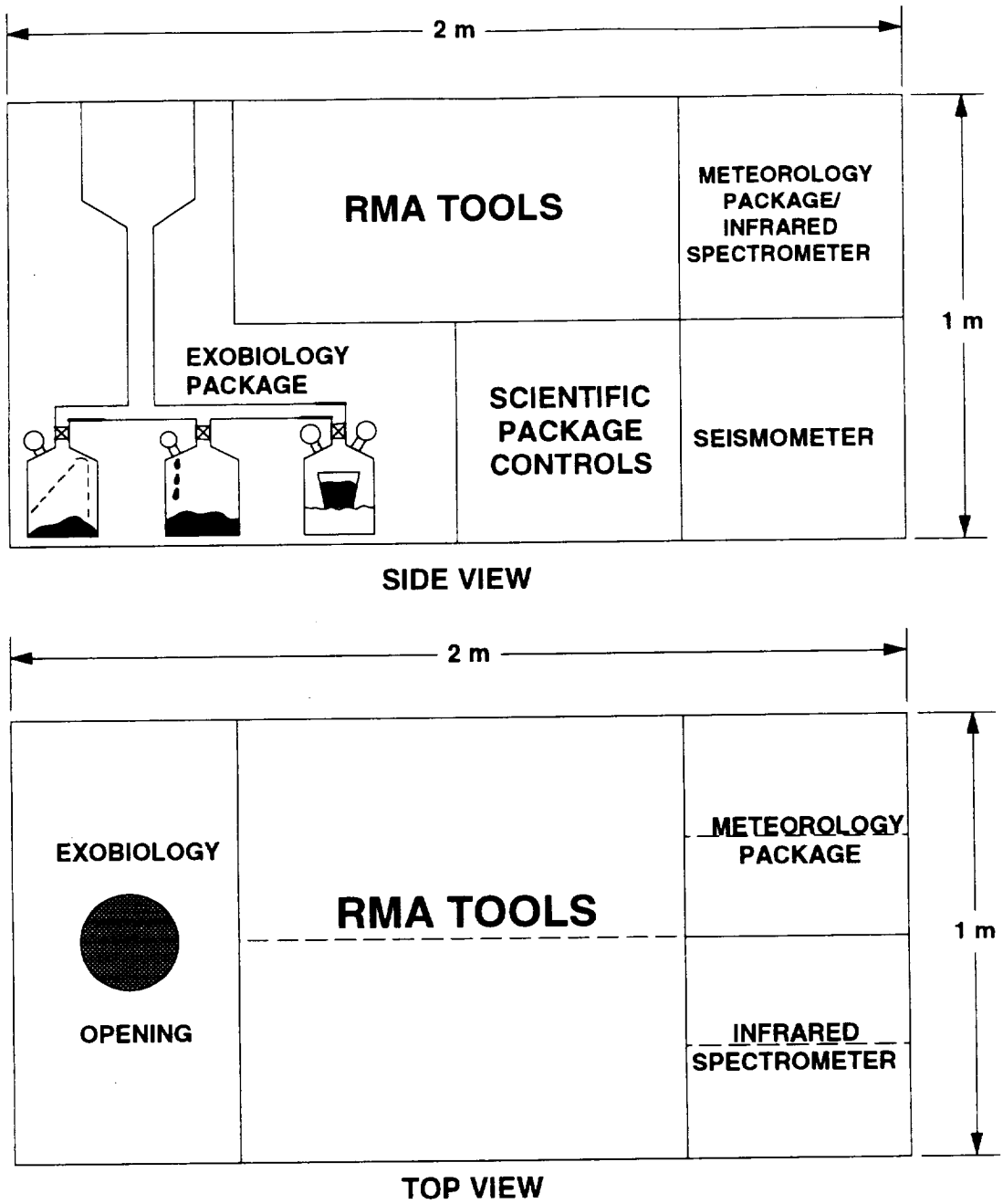

Fig. 7.6 Mars science box configuration.

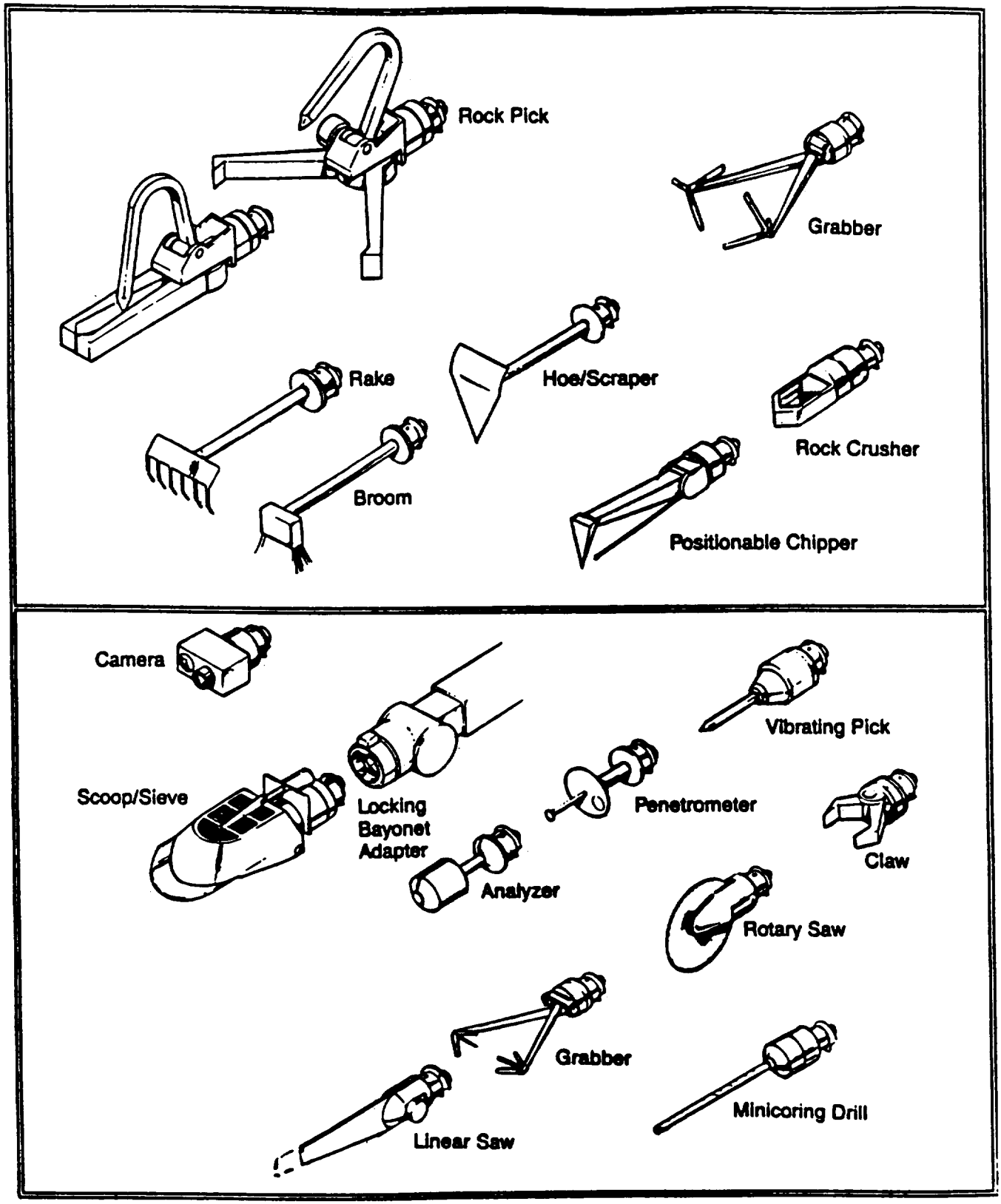

Fig. 7.7 Remote manipulator arm tools.[16]

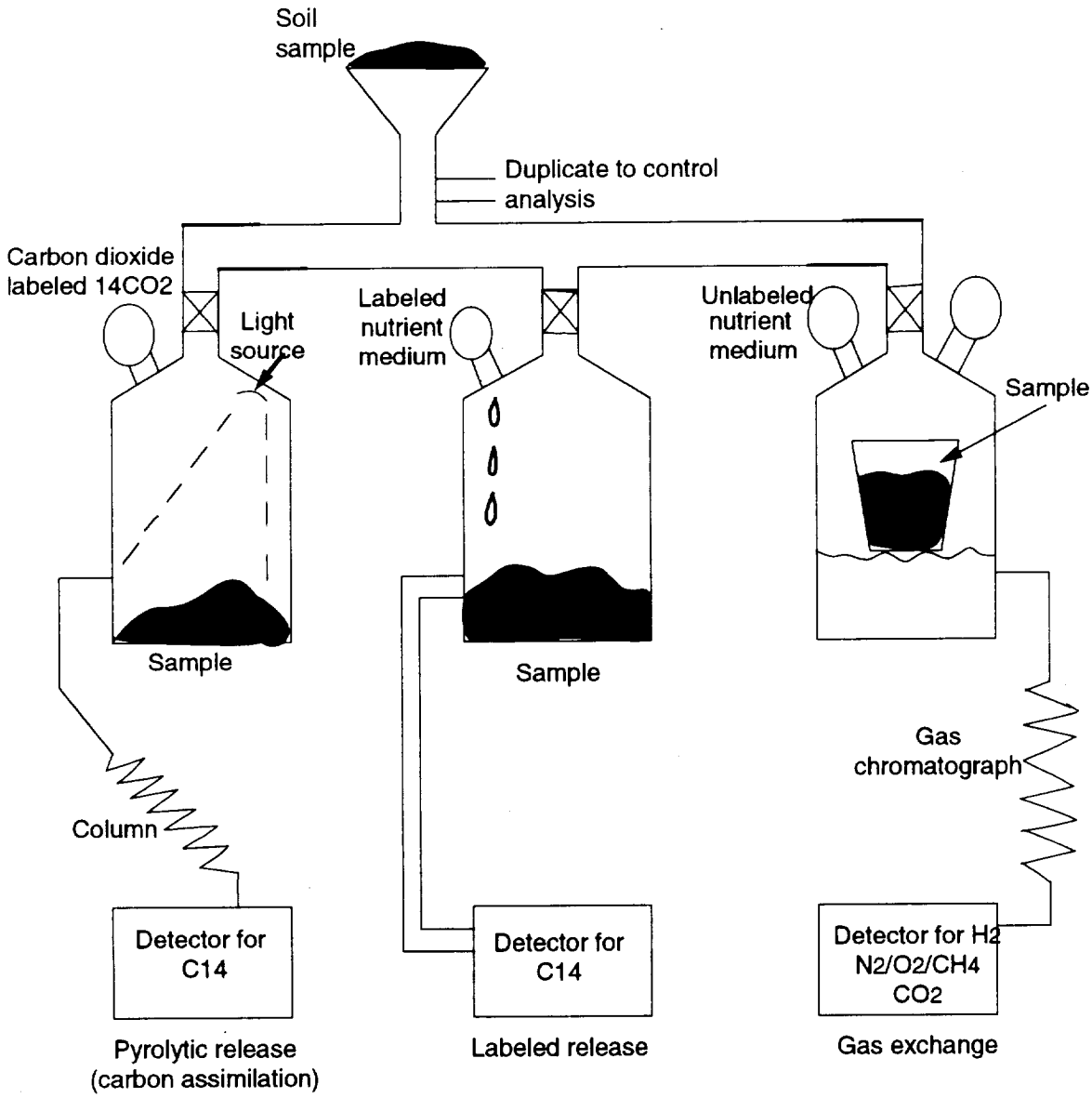

Fig. 7.8 Exobiology experiments.

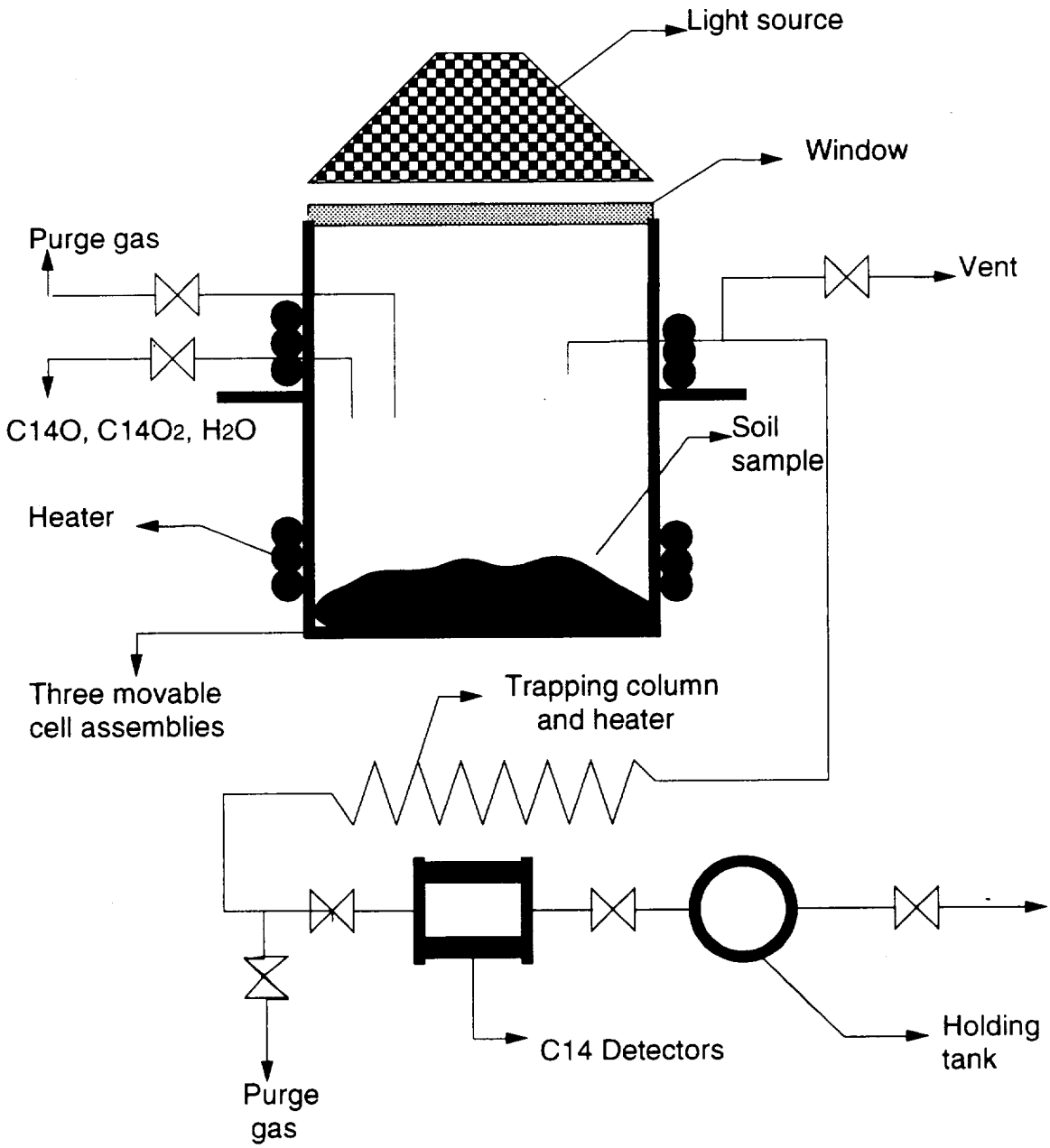

Fig. 7.9 Pyrolytic release experiment.

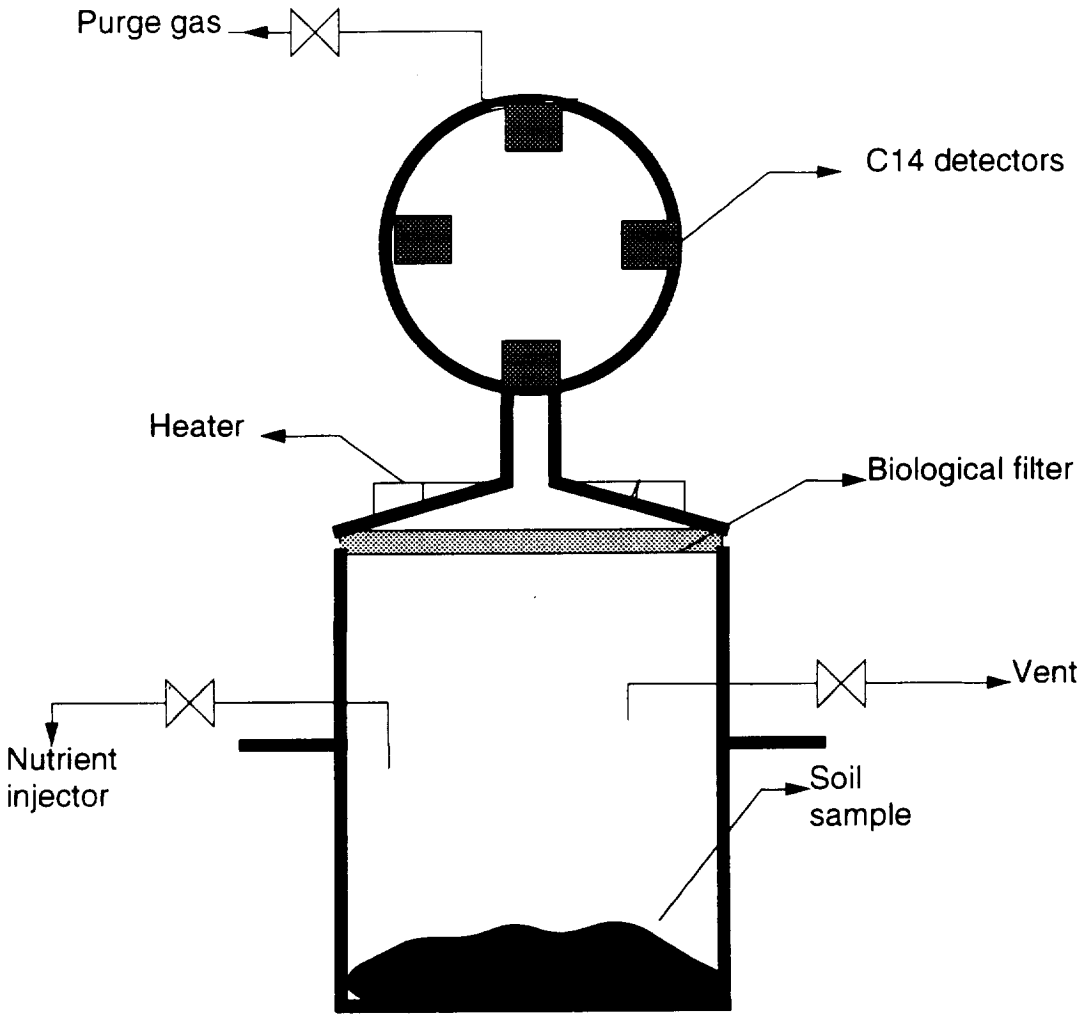

Fig. 7.10 Labeled release experiment.

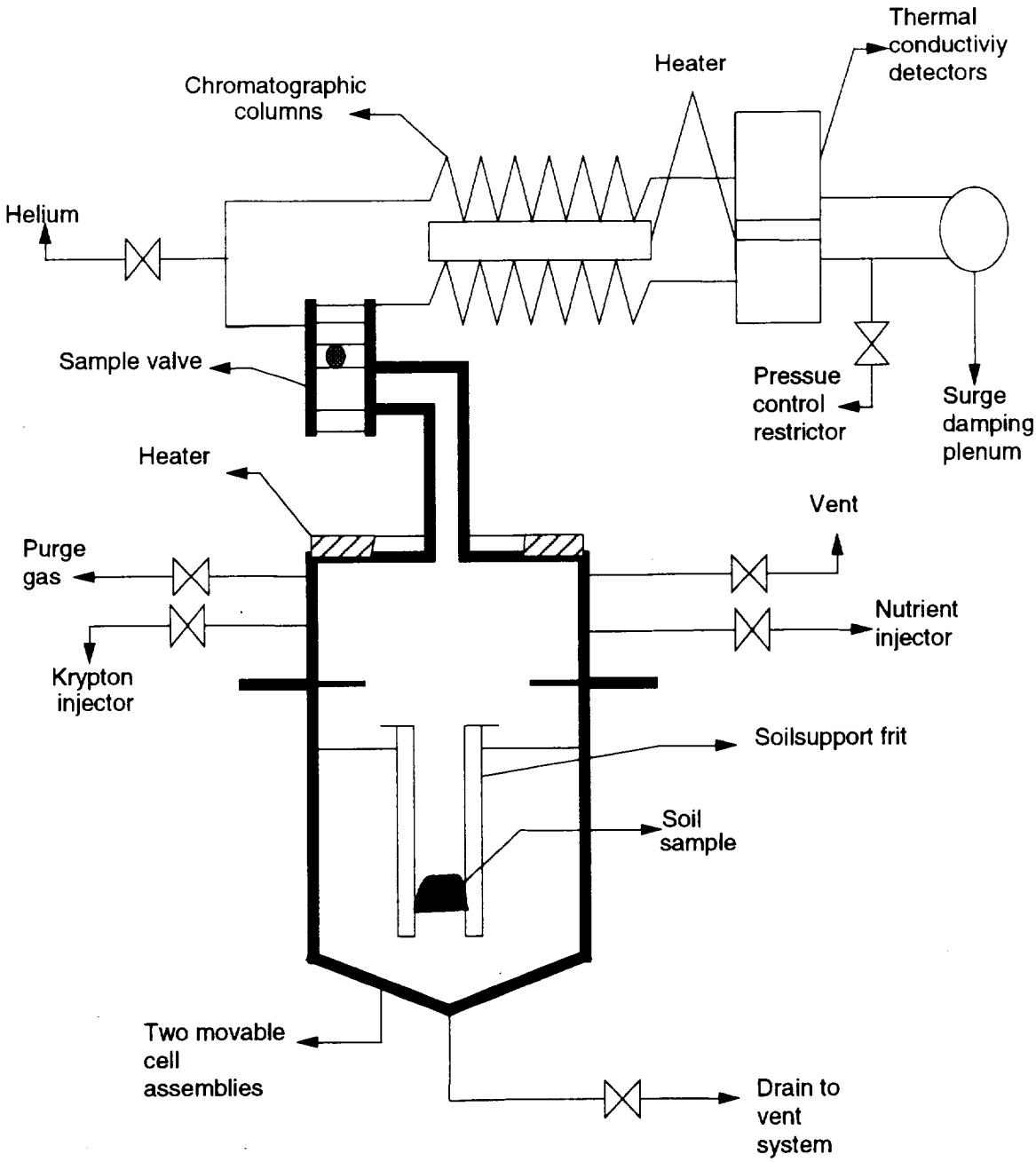

Fig. 7.11 Gas exchange experiment.

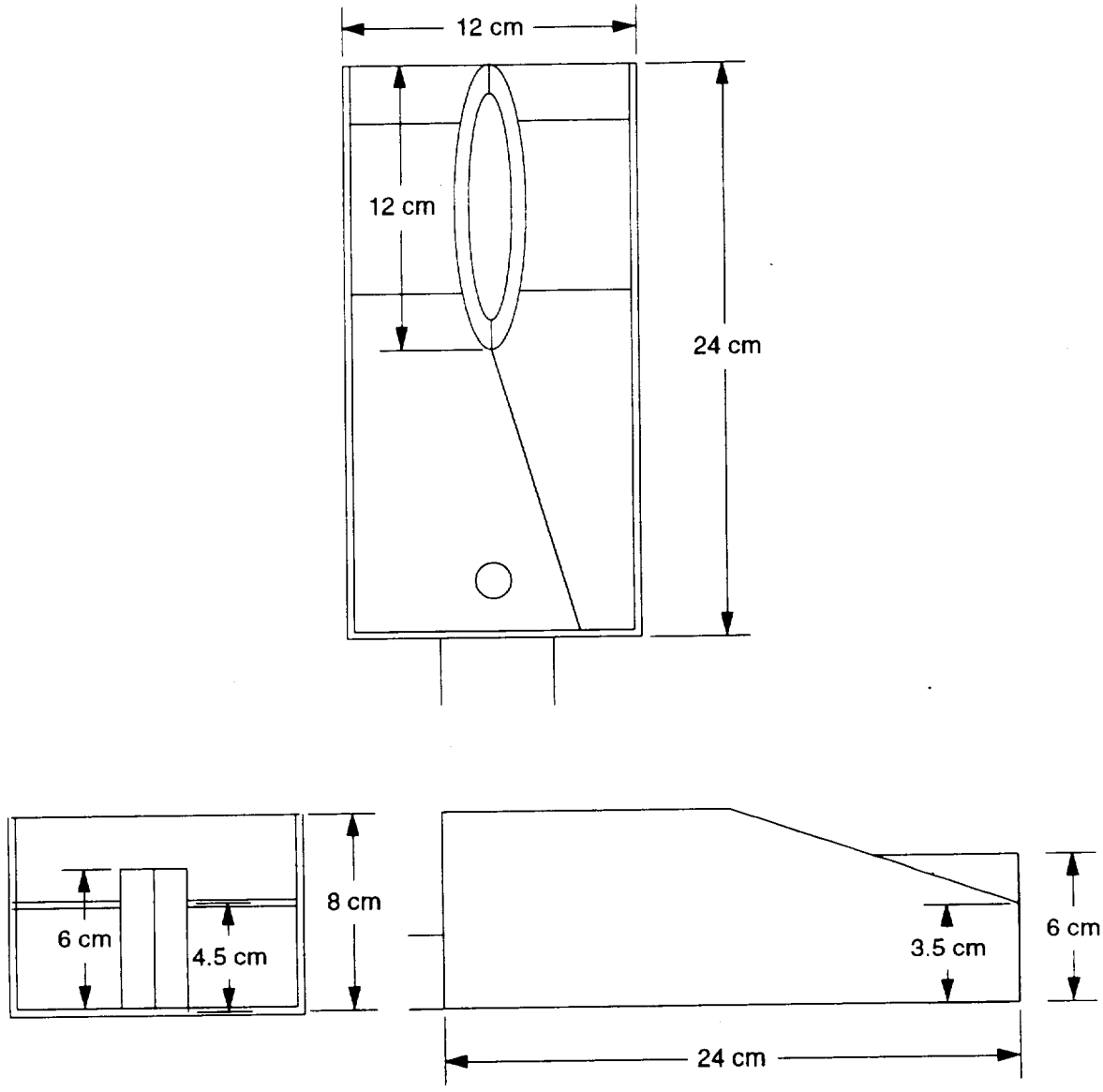

Fig. 7.12 Scoobber design.

Closed (Scoop)

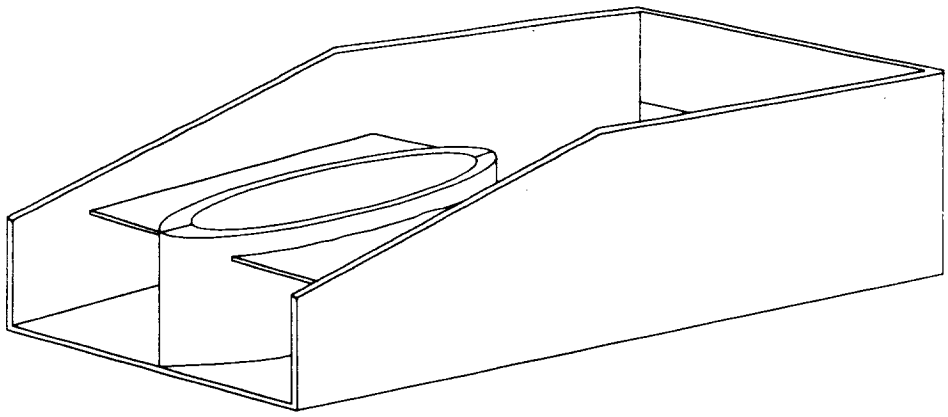

Opened (Grabber)

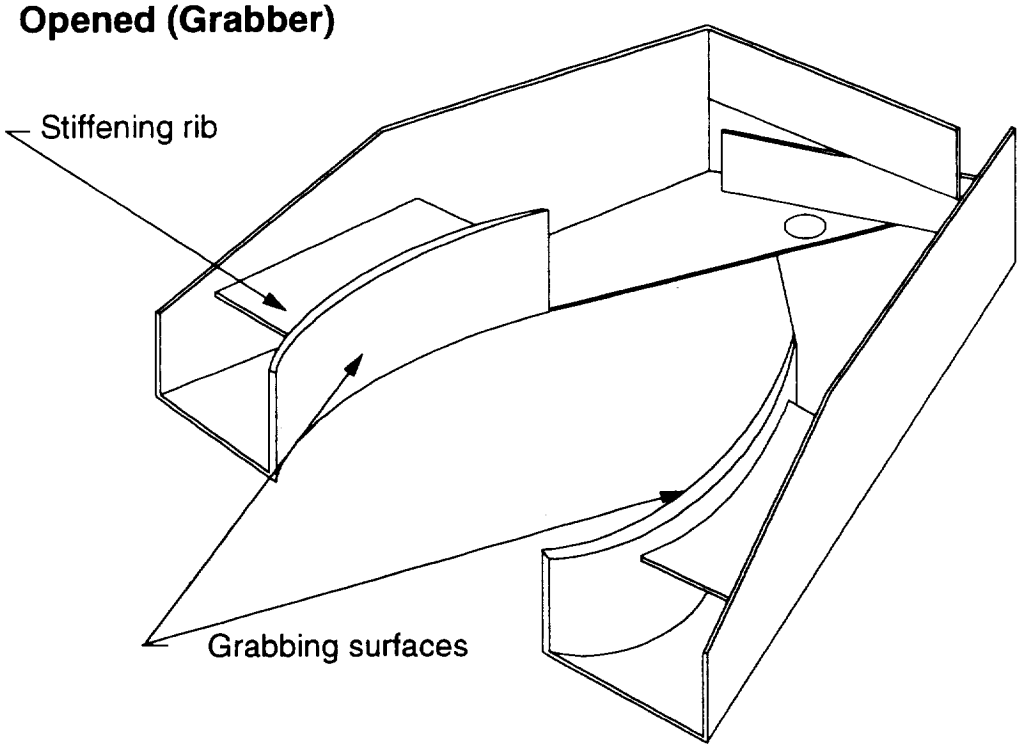

Fig. 7.13 3-D View of Scoobber.

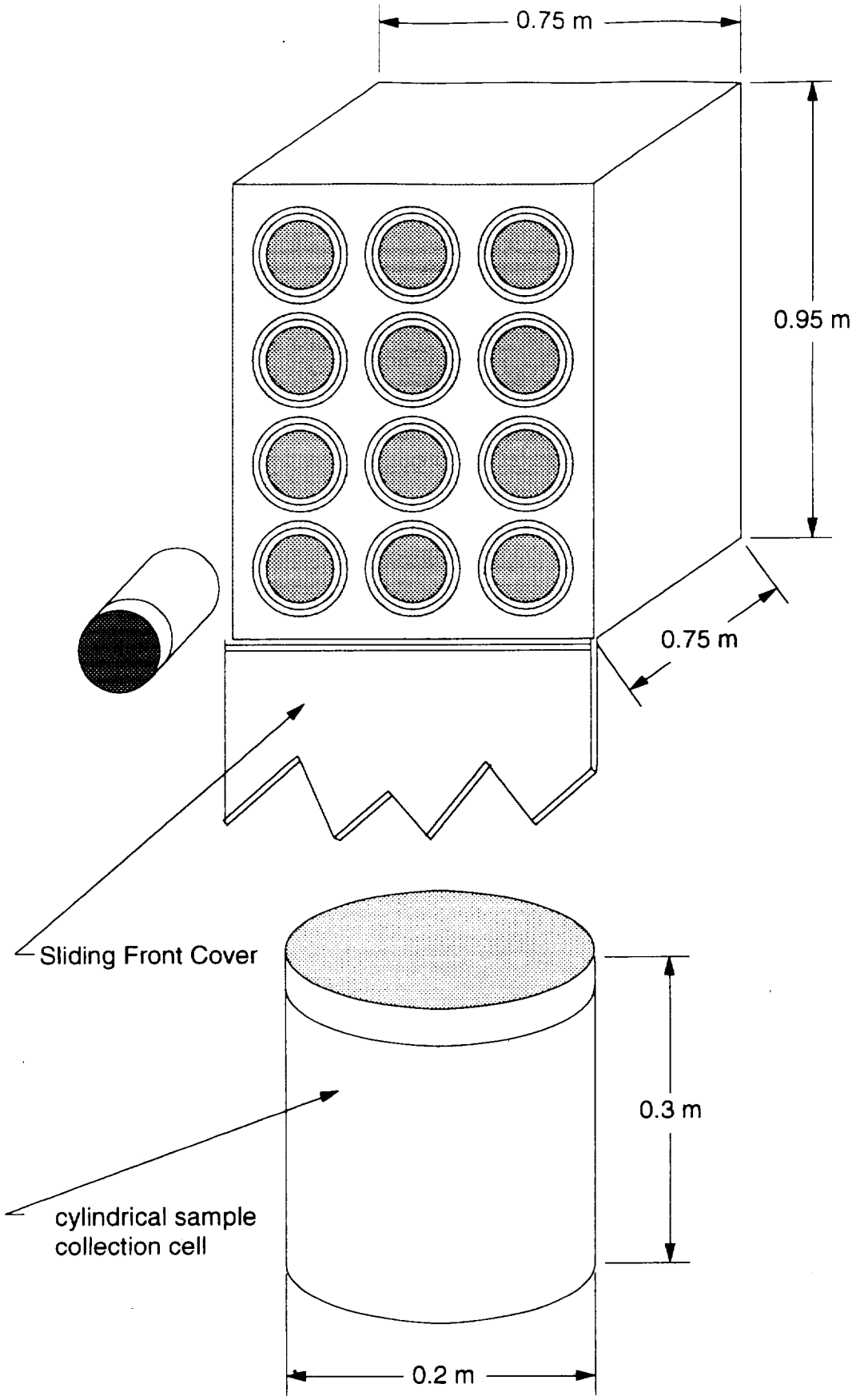

Fig 7.14 Sample Return Module (SRM).

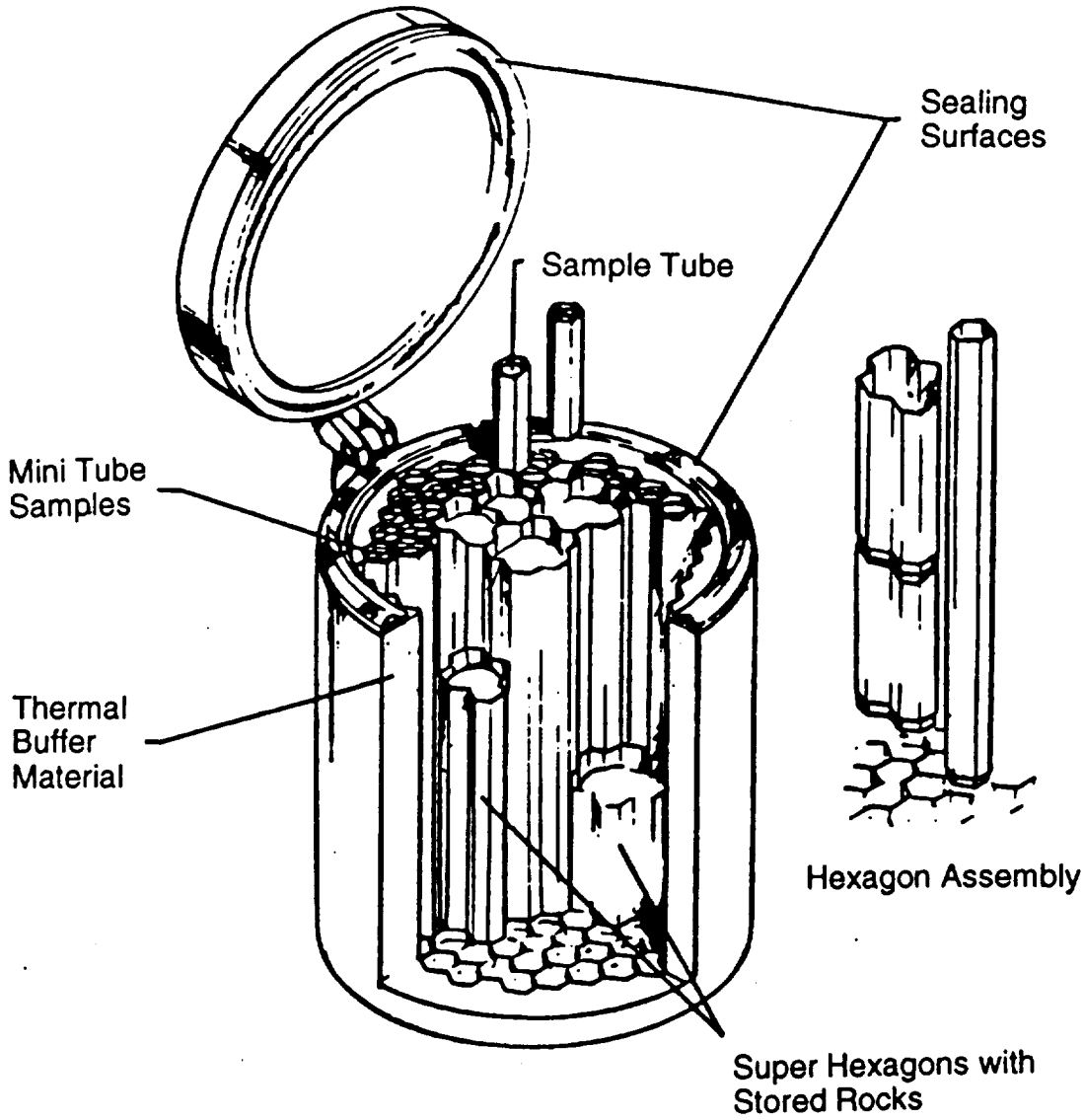

Fig. 7.15 Sample collection cylinder.[9]

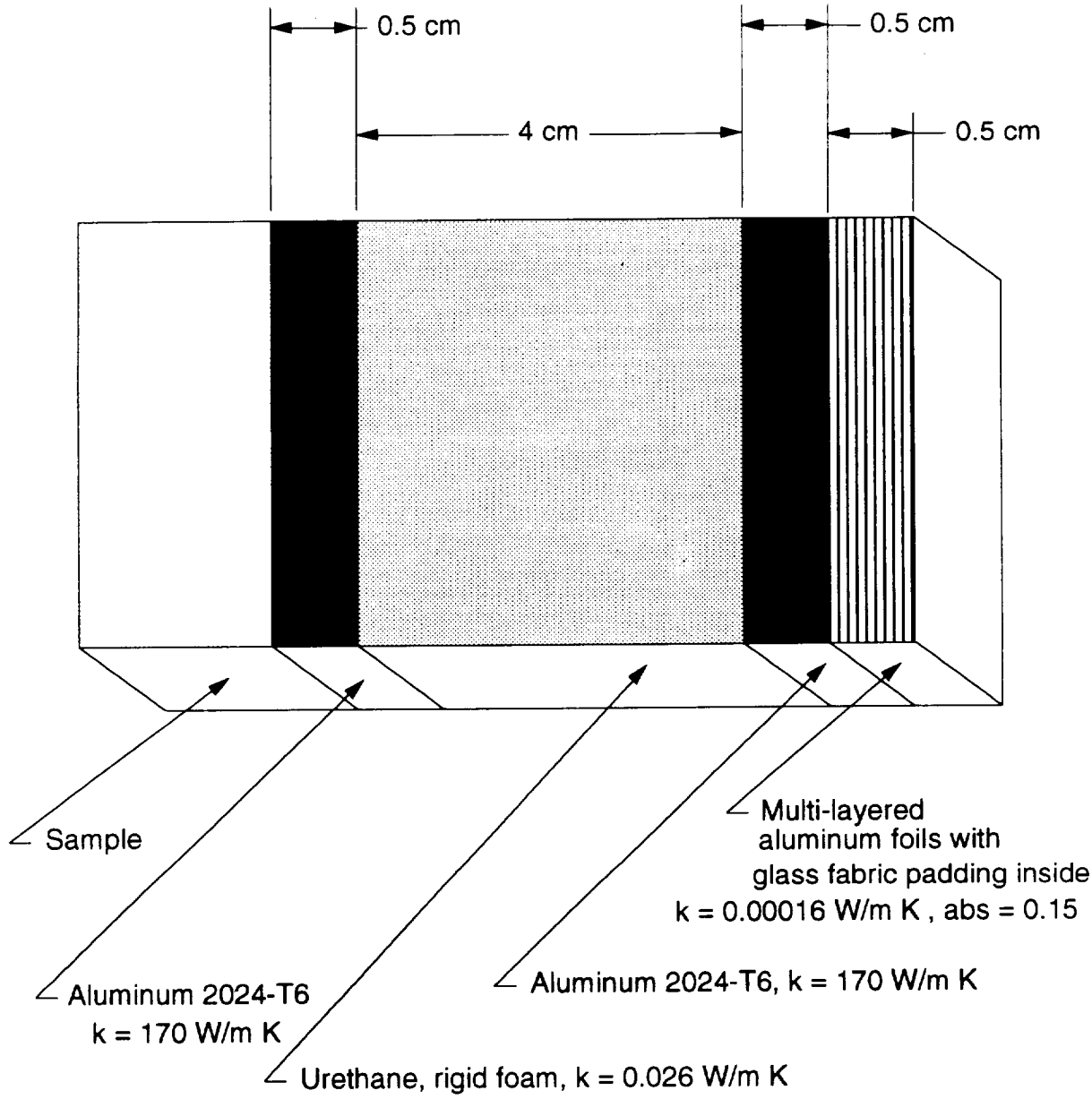

Fig. 7.16 Cross-section of Sample Return Module (SRM).

8.0 MARS ROVER

Anita Abrego
Kwong Shek
Gretchen Swanson
Patrick Sweeney
Thu Vu

TABLE OF CONTENTS

8.1 INTRODUCTION 8.1

8.2 BACKGROUND 8.1

8.3 Rover Design 8.2

8.3.1 Special Planetary Observation Transport 8.3

8.3.2 Rover Structure 8.5

8.3.3 Rover Suspension 8.7

8.3.4 Rover Wheel Design 8.7

8.3.5 Fuel Tanks and Refueling Systems 8.8

8.4 ROVER PROPULSION 8.9

8.4.1 Power Requirements 8.9

8.4.2 Rover Propulsion Options 8.10

8.4.3 Thermophotovoltaics 8.13

8.4.4 Rechargeable Batteries 8.17

8.4.5 Other Alternatives 8.18

8.5 ROVER EQUIPMENT 8.19

8.6 ROVER GUIDANCE AND CONTROL 8.20

8.6.1 Sensing Equipment 8.20

8.6.2 Teleoperation 8.22

8.6.3 Processor 8.24

8.7 POSSIBLE PROBLEMS AND SOLUTIONS FOR ROVER'S OPERATION 8.25

8.8 CONCLUSIONS 8.26

REFERENCES 8.27

NOMENCLATURE 8.29

FIGURES 8.31

8.1 INTRODUCTION
(Gretchen Swanson)

An important part of the Hyreus mission will be the sample collection itself, so the design of the sample collector, the rover, must take into account the mission objectives. The rover must be maneuverable, as light as possible, able to collect and carry any samples taken, and capable of avoiding obstacles. All of the objectives create unique problems in terms of controls, structures, and propulsion of the vehicle.

8.2 BACKGROUND
(Thu Vu, Gretchen Swanson)

While designing the Mars rover, research was done on rovers of the past and present. The design of the rover must satisfy mission requirements, such as surveying the terrain, loading and unloading components for base operations and collecting soil samples. One notable past rover is the Lunar Roving Vehicle (LRV), used by the United States in the Apollo missions. By today's standards, the LRV was very large, but it was also built to carry humans. The Mars rover designed for this mission takes advantage of some technology used on the LRV.

The Mars rover must traverse rugged terrain that includes large rocks and boulders, as well as craters and crevasses. Several designs have been suggested for walking rovers and wheeled rovers as the main source of transportation.

The simpler designs of wheeled rovers, as well as stability and control issues, make them preferable over walking rovers at this time. Jet Propulsion Laboratory's (JPL) Rocky IV is one of the rovers utilizing six electric powered wheels [1]. The Robotics Institute at Carnegie-Mellon University (CMU) built the Terregator, a six-wheeled vehicle with a speed of 2 cm/sec, powered by a gasoline generator [1]. This vehicle was designed to test autonomous mobility on the open road. Currently, it is exhibiting many problems and researchers at CMU are improving its capabilities. Martin Marietta designed and built the Autonomous Land Vehicle (ALV). The ALV utilized a computer vision system, including on-board processors and a microwave link to remote

processing systems. This system enables the vehicle to scan the terrain in order to avoid obstacles and to plan paths along relatively rock free regions.

Walking rovers, in comparison with wheeled rovers, have an increase in the complexity of locomotion and associated problems in stability and control issues. At Ohio State University (OSU), a terrain walking vehicle called the Adaptive Suspension Vehicle (ASV) was developed for experimental purposes [1]. The ASV requires a human operator sitting in the cockpit to command the vehicle by means of a joystick. The ASV contains six legs and is still in development. Other six-legged machines, which mimic insect locomotion, that have been developed are Hexapod at OSU, and MELWALK-III by Japanese researcher Kaneko [1]. The advantage of these walking rovers is their mobility over rough terrain. Their disadvantages include the complexity of control and stability systems and the difficulty in setting the center of mass to avoid tipping over.

Most rovers of today are being designed for unmanned missions, and are being downsized accordingly. A good example of this downsizing is JPL's mini-rover, named Rocky IV [2]. Rocky IV is a remote control Mars rover that has an estimated cost of $25 million. Rocky is powered by DC permanent magnet electric motors. Lithium-Iodide D cell batteries provide 2W of power to motors in each of Rocky's six wheels. In addition, Rocky uses solar panels capable of providing up to 100 W-hr/day to recharge the batteries. Rocky is small, weighing in at 7.5 kg, and has a length of 0.6 m and a height of 0.28 m. Rocky's maximum range is 23.3 m per day (due to communication delays with Earth), with a maximum speed of 1m/sec. The rover being designed for the Hyreus mission is substantially larger than Rocky, and has a longer daily range than Rocky, as well as a higher speed and greater sample collecting capabilities.

8.3 ROVER DESIGN
(Gretchen Swanson)

The rover concepts chosen for this mission are very different, but these concepts complement each other in Mars' hostile environment. The first design is a wheeled design, and the

second design utilizes Mars Balloon technology. The Mars Balloon is not discussed in this section, but information about the balloons can be found in Appendix E. With these designs, more in-depth exploration can be accomplished.

8.3.1 SPECIAL PLANETARY OBSERVATION TRANSPORT (SPOT)
(Gretchen Swanson)

The Special Planetary Observation Transport (SPOT), shown in Fig. 8.1 and Fig. 8.2, is a six-wheeled vehicle with three individual sections in tandem, joined together by swivel joints. Each section's frame is 1 m wide and 0.44 m long, and has a wheel attached to each side via a strut. SPOT's design includes a remote manipulator arm with tools, sample storage, controls, communications antenna, power source and a driller. SPOT has a maximum speed of 3 kph, and a maximum range of 45 km (round trip). Of the three sections, only the front two have powered wheels. The "trailer" section wheels are unpowered, but power must be supplied by the tractor to run the driller and its hydraulic stabilizing legs.

The wheel design for SPOT must be durable in order to have a useful lifetime, yet it must provide enough traction to allow SPOT to be mobile. Inflatable sector tires developed by the University of Arizona were considered for use on the rover [3]. This "Mars Ball" concept required the use of large tires made of several individually inflatable sectors. The sectors would be inflated and deflated as necessary through the use of on-board compressors. However, the complexities involved with this system made the tires unattractive for use on an unmanned rover.

The design of the wheels chosen for SPOT is similar to that of the Apollo Lunar Rover, but smaller [4]. The 0.5 m dia. wheels consist of a wire mesh attached to a titanium "bumper hub." A heavy-duty suspension system must be incorporated into this design, including shock absorbers and four-wheel independent suspension. Each tire on the two forward sections has its own electric motor, powered by the on-board power source. Steering is accomplished by reversing the wheel direction (with the motors) on the side the rover is turning.

In case of rover failures, contingencies have been planned. Rollovers must be avoided, as there is currently no clearance provided to protect the equipment carried on top of the rover. Hydraulic legs could be installed into the wheel hubs, so that they could deploy to prevent an impending rollover. In the event of an individual motor failure, the remaining motors have enough power to take over for the disabled motor.

Center of Mass Analysis
(Thu Vu)

To help prevent the rover from tipping over, the center of mass for the rover must be determined. The locations of Xcg (rover's center of gravity in the x direction, i.e. lengthwise), Ycg (rover's center of gravity in the y direction, i.e. widthwise) and Zcg (center of gravity in the z direction, i.e. vertically) are determined from the masses and the dimensions of individual components of the rover such as the frame, batteries, fuel tanks, etc. The procedures for determining the centers of gravity are as follows. First, the location of Xcg is determined by using the equation.

$$Xcg = \frac{(m1x1 + m2x2 + m3x3 + \ldots mnxn)}{M} \qquad (8.1)$$

The variables m1, m2, m3 and mn are each component's mass; x1, x2, x3 and xn are the distance from a reference point to the center of mass of each component. The variable M is the total mass of the rover itself. Similarly, the locations of Ycg and Zcg can be determined by using the same equation except the variables x1, x2, x3, and xn are changed to y1, y2, y3, yn, z1, z2, z3 and zn.

Using the formula given above, Xcg, Ycg and Zcg are found to be 0.754 m, 0.655 m and 0.301 m respectively. In Figure 8.3, the point of intersection between the center line of the rover and the vertical line of the rear wheel determines the highest point possible for the center of gravity for a given slope of terrain. At any point beyond this height, the rover is unstable. Once the location of the center of gravity is determined, the next step to consider is the elevation angle that

the rover can climb. The elevation angle ß is determined by the center of gravity height (Zcg) and half the length of the rover's wheel base.

$$\tan ß = \frac{\text{half length of wheel base}}{Zcg} \qquad (8.2)$$

Using the equation above, letting half the length of the wheel base to be 0.9 m and Zcg to be 0.301 m, the elevation angle that the rover can climb is 71.5°. This angle of elevation for SPOT does not take into account the coefficient of friction between the wheels and the Mars surface. Because the wheels will slip at high angles of elevation, the true maximum angle of elevation must be determined. From NASA data on the zinc coated piano wire wheels, the coefficient for friction for this type of surface is approximately 0.5. Therefore, the true maximum elevation angle that the rover can climb ranges from 25 to 35°.

8.3.2 STRUCTURE
(Gretchen Swanson)

Structural concerns are very important, since the rover must be kept as light as possible to keep the Earth launch mass low. However, SPOT must be strong so that structural failure does not occur while on Mars. A maximum launch mass of 185 kg is possible. This includes all necessary equipment that must be carried in order to perform sample collection and return.

The material being used for the rover's chassis is Aluminum 7079-T6. This metal was chosen because it is lightweight, and has the highest yield and ultimate stresses of the different types of aluminum considered. Another factor considered in the choice of aluminum was its ability to withstand radiation. This radiation resistance was determined through examination of aluminum parts of the Long Duration Exposure Facility (LDEF) [5].

Composites are used for secondary framework, such as fuel tank supports, and are incorporated into the chassis as well, through the suspension system. The chassis is not

constructed entirely of composites, because, while a mass savings would be realized, composites are much more sensitive to environmental effects than metal alloys [5].

The chassis and support structures are shown in Fig. 8.4. The chassis is made of circular tubing sections 4 cm in diameter, with a wall thickness of 0.4 cm. A total of 16 m of this tubing is necessary for the frame design, which yields a framework mass of 22 kg. A complete mass inventory is shown in Table 8.1.

Table 8.1 Mass inventory of rover components

Component	Mass (kg)
Frame	25
Cameras (2)	0.5
Lasers (2)	8
AHARS*	2.2
Controls	20
Electric motors (4)	4
TPV Generators (2)	8
Batteries	20
Wheels (6)	21
Antenna	1
Fuel tanks (3)	9.6
Hydraulic legs	20
Remote manipulator arm	4
Suspension	15
Cooling system	28
Total	**185**

*Attitude Heading and Reference System

As noted earlier, SPOT consists of three distinct sections that are connected by swivel joints. These swivel joints, shown in Fig. 8.5, are dumbbell shaped, with the spherical ends enclosed in a casing that contains a lubricant (MoS_2). These joints are very much like trailer hitches used on automobiles and are allowed to swivel in any direction. However, the sections are close to each other, and if significant rotations occur, the sections may bump into each other, which could damage the fuel tanks, as well as "jackknife" the rover. In order to prevent this from occurring, two small rubber bump stops (0.05 m long) are attached to the fronts of the middle and rear sections. These bump stops will prevent large rotations from happening, and jackknifing

hazards will be avoided. In addition, each section is able to rotate about a fore-aft axis in order to keep all six wheels in constant contact with the ground.

8.3.3 SUSPENSION
(Gretchen Swanson)

The suspension system will allow the rover's wheels to be completely independent of each other. First drafts of the design included the use of axles, but in the final design, the wheels are individually attached to the rover framework through a wishbone suspension, as shown in Fig. 8.6. A wishbone suspension system is usually used for the front wheels on automobiles, and was chosen for its simplicity [6]. The upper and lower wishbones are connected by an angled beam that is attached to SPOT's tubular chassis, and also are attached to a shock absorber and spring. A second angled member connects the lower corner of the strut to the chassis, which helps the strut absorb side loads. Each wishbone strut is rectangular in cross-section and is made of composite material, because composites allow for better damping of vibrations experienced by the rover. The rectangular cross-section (2.5 cm by 5 cm) is desirable because construction of the members is easier, and rectangular shapes hold up well under bending loads.

8.3.4 WHEEL DESIGN
(Gretchen Swanson)

The wheels, as stated earlier, are similar to those used on the Apollo LRV designed by Boeing [4]; however, SPOT's wheels will be 38% smaller in diameter, i.e., 50 cm. These wheels use wire mesh attached to a titanium bumper hub, and have a mass of 4 kg each (see Fig. 8.7). The mesh is made of zinc coated piano wire, which allows some tire inflection, so that the rover does not need to avoid every little rock it sees. Titanium treads are riveted to the mesh to assist in traction, and provide the wheels with a life span of 180 km which is more than required to fulfill the mission. Electric motors are installed in the hubs of each individual tire on the forward two pairs of wheels. In order to prevent the rover from tipping over, it may be necessary to install hydraulic or spring loaded arms into the hubs. SPOT does not have these arms included in its

design at this time, as incorporating both the motors and arms into the hubs causes installation problems and mass penalties.

8.3.5 FUEL TANKS AND REFUELING SYSTEM
(Gretchen Swanson)

Because the rover uses a power source that burns methane and oxygen, it must carry these propellants on sample collection missions. The propellants, along with a diluent (CO_2), are stored cryogenically on the rover. The tanks designed for the rover are constructed of Weldalite^{TM}-049, the same alloy as is used for storage tanks on the ERV. Using the same stress analysis procedure as was used in Section 2, the fuel tanks (cylindrical with spherical ends) were sized to accommodate 20 kg of methane at 10 atm pressure, 40 kg of oxygen at 7.1 atm, and 10 kg of CO_2 at 7.1 atm. However, since limited power resources and space limitations on SPOT do not allow for compressors and refrigeration units usually needed for cryogenic storage, the tanks were over-designed, so that the pressures generated within the vessels would not cause tank failure. To calculate the required tank thicknesses, the storage pressures given above were multiplied by a factor of five. The calculated dimensions are listed in Table 8.2, and shown in Fig. 8.8.

Table 8.2 Fuel Tank Dimensions

Propellant	Cylinder Length	Cylinder Thickness	Sphere Radius	Sphere Thickness	Mass
Methane	0.21 m	3.9 mm	0.2 m	1.8 mm	5.18 kg
Oxygen	0.14 m	2.8 mm	0.2 m	1.3 mm	3.06 kg
Diluent	0.24 m	1.8 mm	0.13 m	0.8 mm	1.32 kg

Refueling creates another problem for the rover, but this is easily solved. A refueling fitting, as shown in Fig. 8.9, is placed on the rover's rear section, with lines leading from it to the corresponding fuel tanks. The fuel tanks contain sensors that not only tell the rover when the tanks are nearly empty, but also when the tanks are full.

8.4 ROVER PROPULSION
(Gretchen Swanson)

Since another major function of the mission to Mars is the in-situ propellant production, it would be convenient to take advantage of the propellant being produced there to power the rover. As a result, the power systems considered thus far are focused on methane as a fuel. Using a methane powered system has the added benefit of extending SPOT's useful lifetime, because refueling is possible. If a radioisotope thermal generator (RTG) or batteries alone are used, chances for rover failure increase.

8.4.1 POWER REQUIREMENTS
(Kwong Shek)

SPOT has a mass of slightly under 200 kg. Rounding this figure up to an even 200 kg and given the fact that the rover will be driven by four wheels, it can be assumed that each wheel will be required to move a maximum of 50 kg of mass. This assumption is valid, because if the rover had to be raised vertically using four motors, each motor would be required to move a quarter of its share of the mass, 50 kg.

Assuming a worst case scenario that the largest rock the rover has to go over is 0.25 m in diameter, half the diameter of SPOT's wheels, the maximum power required from the motors can be calculated. From conservation of energy, the change in potential energy (ΔPE) of each wheel will be:

$$\Delta PE = m*g*(\Delta h) \tag{8.3}$$

where:

m = average mass that each wheel is moving

g = gravitational acceleration of Mars (3.73 m/sec^2)

Δh = change in height of the wheel

For the present example, a maximum of 46.6 J is required from each motor to ensure that the rover can go over rocks that are half the size of its wheels.

The rover's speed will be limited to a maximum of 3.6 kph. In rough terrain, this can be throttled back to any value necessary to ensure rover stability.

From the above two values and the fact that SPOT's wheels are 0.5 m in diameter, the actual maximum power required can be easily calculated from the equation below.

$$W = \Delta PE/\Delta t \tag{8.4}$$

where: Δt = time needed for a wheel to climb a rock

The work required is the 46.6 J calculated above. The time needed to go up a 0.25 m rock at 3.6 kph (1 m/s) for a 0.5 m diameter wheel is calculated to be 0.39 sec. Thus, a power output of 120 W is required from each motor.

Choosing drive motors that produce a maximum power of 240 W each is more than enough to satisfy the above requirement and also provides a redundancy factor in case one of the drive motors should fail. If one of the motors fails, the rover will still be fully functional with three powered wheels. The limits on how steep the rover can climb is not going to be determined by the power of the motors, but rather the angle at which the rover tips over. Utilizing new, high energy density traction motors and electrical controllers made by Unique Mobility, Inc. of Denver, CO, results in an average mass of only 1 kg for each motor [7].

8.4.2 ROVER PROPULSION OPTIONS
(Kwong Shek)

Four power systems were considered for the rover. One system involves the use of electric motors in each of the rover's wheels, with power coming from the rover's batteries, as well as from a self-sufficient charging system mounted on the rover. Another system involves the use of a direct-drive, methane-fueled, internal combustion engine. The third system involves the use of fuel cells to generate power to charge on-board batteries. The fourth is a thermophotovoltaic

generator. Each of the propulsion methods stated above has its advantages and disadvantages, so all were considered carefully before determining the best choice.

The primary advantage of using an electrical drive system is that it requires no transmission. This lowers the overall vehicle mass and eliminates the possibility of a transmission failure. Electric motors produce enough torque to accelerate the rover from a standstill to a reasonable speed on Mars (2-5 kph) without the need for different gears [7]. In addition, the power produced by these motors is more than enough to drive the rover over rocks, up hills, etc., without needing to shift. The lack of a transmission also means that there are fewer moving parts and thus, a lower likelihood of a power system failure.

The drawback of using such an electrical system alone is that numerous batteries are required to generate the power required to drive the motors and the on-board equipment, which adds to vehicle mass. Another disadvantage is the charging system that has to be used to keep these batteries charged. Solar cells and/or RTGs were considered for this purpose. Currently, the best solar cells available (GaAs type) give approximately 20% efficiency with a mass density of 5.3 g/cm^3 [8]. With the low solar constant on Mars (590 W/m^2), these solar cells would provide approximately 118 W/m^2 with a mass to area ratio of 53.2 kg/m^2 (assuming a typical solar cell thickness of 1 cm). This results in a power to mass ratio of roughly 2.2 W/kg, too low for practical use on the rover.

RTGs give better performance, but the power to mass ratios are still too low for use on the rover. The problem associated with RTGs is not the mass of the generators themselves, but rather the shielding of the RTG heat source that is required to keep high-energy radioactive particles from striking delicate electronic systems on the rover. Using an RTG composed of a $^{238}PuO_2$ heat source, a tungsten gamma ray shield, and a lithium hydride neutron shield coupled by heat pipes to a Stirling engine, produces 1 kW of power and has a total mass of 120 kg [9]. The power to mass ratio here of 8.3 W/kg is better than the 2.2 W/kg obtained by using solar cells, but as stated earlier, this is still too low for use on the rover.

Using a direct-drive, methane-fueled, internal combustion engine has the advantage of virtually eliminating the power to mass issue of the rover. The internal combustion engine would provide enough power to drive the vehicle directly as well as run an alternator to power the additional equipment on board. Methane produced by the manufacturing plant brought from Earth would give the rover a constant energy supply without dependence on time of day, weather conditions, etc.

One disadvantage of using a direct-drive system, however, is the added complexity and weight of a transmission. As with all internal combustion engines, power can only be taken from the engine when it is running at a high rpm [7]. Thus, a transmission is required when the rover requires excess power, as in starting from rest and climbing over rocks. The transmission adds more moving parts to the drive system, resulting in a heavier load on the rover and a greater likelihood of a drive system failure.

Another disadvantage of the direct-drive system is the range limitation. When the on-board fuel tanks are empty, the rover can go no further. With the solar cells and RTGs, the rover can simply stop and wait while its batteries recharge.

There is also the problem of cooling the internal combustion engine in a direct-drive system. The low density of the Martian atmosphere makes convection cooling almost non-existent. As a result, large radiator fins would have to be added to the engine to provide enough radiative cooling to keep the engine from overheating. This adds to the already large mass of the engine and transmission, thereby making the direct-drive method undesirable.

Fuel cells have the advantage of generating electrical power from the direct electrochemical oxidation of fuel. This process involves no combustion, thus, no moving parts are required in the system. In addition, some fuel cells can be operated at near room temperatures, thereby eliminating any cooling problems that occur. Presently, there are five main types of fuel cells available, based on the electrolytes present in the cells: alkaline potassium hydroxide, phosphoric acid, molten carbonates, solid oxides, and solid polymers [10]. Of these, only the alkaline

potassium hydroxide and phosphoric acid types are practical for use on the rover, because the others either involve high temperature operation (molten carbonates and solid oxides) or require further testing before they can be used for space operations (solid polymers).

The problem with fuel cells is that the direct electrochemical oxidation of methane is difficult. Currently, it can only be done using platinum electrodes and the power output is a mere 0.004 W/cm^2 of electrode area [11]. This means that it would require 25 m^2 of platinum area to generate 1 kW of power! This is much too large and expensive for practical use by the rover.

The most efficient fuel cells currently available run on hydrogen. Such systems do not require any precious metals for electrodes and provide 0.706 W/cm^2 of electrode area [11]. To generate 1 kW using this system requires only 0.142 m^2 of electrode area, which is practical for SPOT. The problem now is mass. A 1 kW hydrogen fuel cell has a mass of 109 Kg [10]. This is too high for use on the rover, so even with the most efficient of fuel cells, it appears that this option is not the best choice.

The remaining power system is the thermophotovoltaic generator. Its high efficiency, low mass, and lack of moving parts makes it a suitable power system for the rover. Details about this system are presented in the following section.

8.4.2 THERMOPHOTOVOLTAICS
(Patrick Sweeney)

The power generating system chosen for SPOT is a thermophotovoltaic (TPV) generator producing 1 kW of power. This unit utilizes mechanically stacked GaAs/GaSb tandem cells, in conjunction with an infrared emitter burning a mixture of methane, oxygen, and carbon dioxide. The configuration of this burner is shown in Figs. 8.10 and 8.11 [12,13]. The TPV unit is currently being developed by the Vehicle Research Institute (VRI) at Western Washington University in Bellingham, WA; for use in automobiles, but it is an ideal generator for use on the rover.

The methane burns with the oxidizer inside a tungsten tube having a diameter of 0.01 m and a height of 0.5 m, heating it to an average temperature of approximately 2,000 K. The combustion occurs at a constant pressure of 1 atm. which is accomplished by exhausting the combustion products through a sonic throat. The combustion chamber burns an O_2 to CH_4 mass ratio of 2:1. This is fuel-rich compared to the stoichiometric 4:1, but allows the rover to carry less oxidizer. The oxidizer consists of oxygen diluted with 0.1 moles of CO_2 per mole of O_2 to reduce the flame temperature to 2150 K, which is within acceptable limits for the tungsten tube.

The heat energy released by this reaction is approximately 10,000 kJ/kg. Assuming half the energy of combustion is lost in the exhaust gases, the necessary propellant mass flow rate to provide the required power is 8.36×10^{-4} kg/s. Assuming the tungsten has an emissivity of 0.3 at 2000 K, 4180 W of energy are emitted from the tube walls to the thermophotovoltaic cells. The reaction is sustained by means of a cyclonic injector nozzle[14]. This nozzle has been shown to produce steady flames in tubes up to 0.50 m in length by inducing rotational motion into the combustion gases for more complete combustion. Exhaust gases are directed toward the rear of the rover to help prevent contamination of the Martian samples to be taken. These gases will consist mainly of water vapor and carbon monoxide.

The combustion process is continuous rather than the batch firing of a typical internal combustion (IC) engine, resulting in a more complete combustion and a drastic reduction of exhaust emissions. In addition, this continuous combustion is more efficient than an IC engine because the power does not have to be put through a transmission before use. The result is a lighter, cleaner, and more efficient power source, as compared to an equivalent internal combustion engine.

The infrared radiation emitted by the hot tube peaks at a wavelength of 1.5 μm. Ga/Sb cells have a corresponding bandgap which makes them very efficient in this region of the spectrum. Because silicon and GaAs solar cells are mostly transparent to IR radiation, the GaSb cells are the key to the high efficiency (30%) of the TPV unit. However, when photons of greater

energy are absorbed, the extra energy beyond what is required to release a carrier is lost. This inefficiency can be quite large and is the driving force for two junction cells which collect photons at different band gaps. It is for this reason that the top GaAs cell is added to collect photons at lower energy states before reaching the higher band gap cell, GaSb. These tandem cell combinations show much higher efficiencies than conventional single junction cells. Another advantage of the GaSb/GaAs solar cells is their resistance to degradation from radiation. This resistance is due to the relative thinness of the photon gathering portion of the cell (this is a major consideration, as silicon cells degrade rapidly without heavy radiation shielding). One of the complications which arises from this combination is that electrical potential of these two cells is different. GaAs cells operate at about 1 V while GaSb cells operate at about 0.33 V. The solution chosen is to wire three GaAs cells in parallel with three GaSb cells which are wired in series, as is shown in Fig. 8.12 [15]. The photovoltaic surface area which must be used is determined by first finding the flux on the outer tube wall and then finding the needed cell area.

$$\Phi = \frac{E_{radiated}}{A_{outer}} \tag{8.5}$$

$$\Phi = \frac{4180\ W}{0.1842\ m^2} = 22.69 \frac{kW}{m^2}$$

The required photovoltaic surface area is found from:

$$A_{cells} = \frac{P_{req}}{\eta_{cells}\Phi} \tag{8.6}$$

$$A_{cells} = \frac{1\ kW}{0.3 \cdot 22.69 \frac{kW}{m^2}} = .044\ m^2$$

This analysis shows that approximately 25% of the inner surface of the TPV needs to be covered with photovoltaic cells. Because even the tandem cell cannot collect all photons at every wavelength, additions are made to the cells to reflect the unused portion of the spectrum back to the infrared emitter. This has the advantage of helping to maintain the inner tube temperature. Methods for accomplishing this reflection include a blue-red optical filter and increasing the back

surface reflectance (BSR). The tungsten infrared emitter, along with four panels of GaAs/GaSb solar cells, are put into the cylindrical container with reflectors mounted in such a way as to concentrate the radiant energy onto the GaSb cells, as shown in Fig. 8.10.

Of major concern in this design is the ability to reject waste heat. The emitted radiation is absorbed by the cells with an efficiency of 30%, therefore the heat rejection system must be capable of radiating nearly 3 kW of waste heat to the Martian environment. This is accomplished by using fins attached to the outside of the generator unit. These fins consist of heat pipes extending radially outward from the TPV unit, as is shown in Fig. 8.13. To find the area needed to keep the photovoltaic cells at an operating temperature of 373 K, an energy balance is set up between the inner radiating surface and the outside surface.

$$q_{radiated} = q_{thermal} + q_{electrical} \tag{8.7}$$

$$\varepsilon_{tungsten}\sigma A_{tube}T_{tube}^4 = \varepsilon_{fins}\sigma A_{fins}T_{fins}^4 + 0.3\varepsilon_{tungsten}\sigma A_{tube}T_{tube}^4 \tag{8.8}$$

$$A_{fins} = \frac{0.7\varepsilon_{tungsten}T_{tube}^4 A_{tube}}{\varepsilon_{fins}T_{fins}^4} \tag{8.9}$$

The fin area: $$A_{fins} = \frac{0.7(0.3)(2000\ \text{K})^4\left(0.01535\ \text{m}^2\right)}{(0.8)(373\ \text{K})^4} = 3.35\ \text{m}^2$$

where it has been assumed that the fins have an emissivity of 0.8. A cold plate attached to the back of the cells conducts the heat into the heat pipes. With this configuration, each of the four fins must be approximately 0.5 m by 0.7 m which is rather large. The mass for the fin radiators is approximately 14 kg per TPV unit.

The TPV is an effective generator for use on the rover, not only because of its high efficiency, but also because it has no moving parts to maintain. Because of the ability to refuel, the rover's supply of energy is limited only by the indigenous fuel production plant. Another reason the TPV is so attractive is that it continuously charges the on-board batteries. The rover is able to draw extra energy from the batteries if it needs to climb or overcome an inclined surface or

obstacle. Because the batteries remain charged as long as the methane and oxidizer last, the rover can use the batteries to attempt a return to the base camp for refueling in the event that the fuel is completely consumed in the field. The primary disadvantage of the TPV power system is the relatively large size of the radiator fins, which can act like sails in high winds.

8.4.4 RECHARGEABLE BATTERIES
(Kwong Shek)

SPOT's power system is highly dependent upon the battery it uses to store electrical energy from the TPV. Thus, SPOT's performance characteristics will be greatly affected by the type of battery used. A nickel metal hydride battery was chosen because it has a high energy density, high power, long life, great tolerance to abuse, a wide range of operating temperature, quick-charge capability, and totally sealed, maintenance-free operation [16].

The main feature that distinguishes a nickel metal hydride battery from other nickel-based battery systems (i.e. NiCd, NiZn, etc.) is that it uses a metal hydride for its second electrode rather than a pure elemental metal such as Cd or Zn. When a pure metal is used, oxidation-reduction reactions associated with battery charge and discharge constantly convert the electrode back and forth between a metal and a metal oxide. Since metal oxides are poor electrical conductors, a lot of battery inefficiency is introduced into the system. This, together with the changing physical properties of the electrode as a result of the dissolution and recrystallization processes occurring during charge and discharge, is what makes current batteries so inefficient.

The metal hydride electrode, on the other hand, uses a chemical reaction that reversibly incorporates hydrogen into a metal alloy [16]. Both chemical states are metallic in this oxidation-reduction reaction, so electrical conductivity is high in both the charged and discharged states. In addition, the small size of the hydrogen atom permits it to enter the metal during hydride formation with only a small volumetric expansion and no crystallization of the electrode at all. These differences are what gives the nickel hydride battery its many beneficial properties.

The most promising nickel metal hydride battery currently available is one made by Ovonic Battery Company, a subsidiary of Energy Conversion Devices [16]. Its performance characteristics are listed in Table 8.3 below.

Table 8.3 Characteristics of nickel metal hydride batteries

Specific Energy	80 Wh/kg
Energy Density	215 Wh/liter
Power Density	470 W/liter
Specific Power	175 W/kg
Cycle Life (number of cycles)	1000
Life	10 years
Environmental Operating Temperature	-30 to 60 °C
Recharge Time	15 min (60%) < 1 hr (100%)
Self Discharge	< 10% in 48 hrs

Since each of the rover's drive motors requires 240 W maximum, a total of 960 W is required to ensure that the rover has enough power to go at full throttle. Of course, the motors won't be driven at full power all the time, so the 1 kW provided by the TPV is more than adequate to power the motors and on-board systems without draining power from the batteries. A 1.4 kWh battery is chosen to power the drive motors along with all of the on-board control systems. This battery will weigh 17.2 kg. Because it is constantly kept charged by the TPV, the battery is more than enough to power the rover. The battery alone can provide 1 kW of power for 1.4 hours, so the rover can be fully operational for up to 1.4 hours without the TPV generator. This backup power will be useful for maneuvers near the landing site to prepare for refueling and/or other nearby work, and gives the rover approximately a 5 km emergency range.

8.4.5 OTHER ALTERNATIVES

(Gretchen Swanson, Patrick Sweeney)

If the use of other in-situ propellants, such as CO and O_2, for the return trip to Earth is desired, other forms of propulsion for SPOT may have to be considered. Up to this point, only systems involving the use of methane have been the subject of research; however, it may be possible to run the TPV generator if carbon monoxide is used for the primary fuel. With this fuel,

the flame temperature could be kept close to the same, but heat energy released would not be as great. This would require more mass of fuel with the same oxidizer to fuel mixture as currently used, 2:1.

8.5 ROVER EQUIPMENT

(Gretchen Swanson, Anita Abrego, Patrick Sweeney)

In order to carry out the sample collection mission, the rover will need to carry several pieces of equipment (See Sect. 7). One piece of equipment is the Remote Manipulator Arm (RMA), which in this case is a Martin Marietta design [17]. The objective for this RMA was to design a lightweight Mars sampling arm that satisfied all expected science goals and mission constraints . The arm length is 3 m with a 30 mm square cross-section, and can access a working volume of 45 m^3. The 4.1 kg arm has four degrees of freedom, four links operating in two planes, and a payload capability of 21.1 N, which is half its weight on Earth and almost twice its weight on Mars. The RMA design is shown in Fig. 8.14. It consists of tubular elements, chosen for greater stiffness and for their internal wire carrying ability. A square section was chosen since bending loads drive the cross-sectional requirements and to simplify fabrication. The baseline design of the structural cross-section is shown in Fig. 8.14.

The design requirements of the RMA include an arm reach of 2 m about the vehicle, a payload of less than 2.1 kg, a power requirement of less than 300 W, and a desired tip speed of 10-50 cm/sec. Power was not constrained because it was assumed that the arm would not operate while the vehicle is traversing from one test site to the next. It was also assumed that the power requirements for the rover are greater than for the arm. The computational needs of the arm are easily handled by the two onboard 80486 processors described in Section 8.6.3. The arm would have several different tools at its disposal, allowing it to choose the proper tool for the sample it is expected to collect. Tools to be carried include the scoobber being developed for this mission (Section 7). A drill is also necessary for the collection of core samples.

The rover will be carrying two CCD cameras to be used not only for guidance and control, but also to record the Martian terrain and to determine if a sample is to be collected. This would provide better resolution than could be achieved with a satellite. The cameras are attached to raised platforms at the front of the rover.

SPOT has no direct link to Earth but instead relays information through either the satellite or the ERV. This is accomplished by using a low-gain antenna (LGA) operating in the S band at frequencies between 2 and 3 GHz. This is a "T" shaped omni-directional antenna about 0.5 m tall with the top of the "T" about 0.5 m long. This antenna provides a data transfer rate of 6000 bits/s with a power requirement less than 5 W. This data transfer rate is enough for both the semi-autonomous navigation system to communicate with Earth and for transmission of pictures from the rover as long as some video compression is used. More information about the communication architecture for the mission can be found in Section 9.7.

8.6 ROVER GUIDANCE AND CONTROL
(Patrick Sweeney)

The remote distance of a Martian rover provides challenging problems for the control systems designer. Among these problems are those of navigation, obstacle avoidance, and sample collection. This section outlines proposed solutions utilizing existing hardware, combined with specially written software.

8.6.1 SENSING EQUIPMENT
(Patrick Sweeney)

For the rover to have an idea of its environment, an integrated sensing system must be included. Sensing equipment will include two CCD cameras, Attitude Heading and Reference System (AHARS), laser range finders, two inclinometers, four potentiometers in the four driven wheels, and a proximity sensor in front. A summary of this equipment is given in Table 8.4. Some equipment used will be modeled after a rover designed for the Stanford US-USSR Mars Exploration Initiative [18].

The CCD cameras are passive devices relying on outside light sources. They are lightweight at 0.25 kg each and have a 10 W power consumption. Gimbal mounted on rotating platforms, the cameras will have an unobstructed 360° view. Each camera has a 380 X 488 pixel resolution allowing detection of 25 cm objects at 100 m or 1.25 cm objects at 5 m. Space heaters are provided in the camera housings to keep operating temperatures between 0° and 50° C.

Two laser range finders are mounted underneath the CCD cameras. Although the CCD cameras will provide a stereo image, the range finders will provide information on exact range, and the intensity of the backscattered light will give an indication of rock porosity and reflectivity. Lasers used are the ERIM 3-D laser scanner currently under development by Daedalus and ERIM corporations [6]. The scanners operate by using a high frequency video camera (image dissector TV camera) coupled with an RF-modulated laser which measures range by modulating its beam and measuring the phase difference between the transmitted and received beam in each pixel of an image. While the system is still in development, it is set to be operable by 1994. Design goals include keeping the mass under 5 Kg and power consumption under 30 W. Its volume will be less than 0.015 m^3.

The AHARS developed by Honeywell is used to provide attitude and rate of climb information. Based on a GG1320 ring laser gyro, it is ideally suited for space applications and is radiation hardened. The AHARS has a mass of 2.27 kg, a volume of 0.001639 m^3, and uses 10 W of power.

On each body section, two inclinometers are mounted, one axially and one at 90° to the first. By monitoring both degrees of freedom, these devices will provide angular information for an emergency tip-over routine which monitors the rover's attitude and prevents it from exceeding its maximum stability range.

The rover will also have to deal with hazards which can only be detected at very close ranges. This is a result of not being able to completely determine the stability of rock and soil formations from visual data alone. Also, the path planning algorithm will need information about

rocks dislodged by the weight of the rover traversing over them. As these shifts could prove dangerous, a proximity sensor is installed on the rover. This sensor is a down-looking impulse radar which emits pulses of energy at a wide range of frequencies. By interpreting the returning information at various wavelengths, information can be gathered about the strength of soils before committing the rover to traversing unfamiliar terrain. This system is an important addition to the cameras and laser range finders, because these instruments fail to provide enough information to detect whether cavities in bedrock or soil have been filled in by drifting material [19].

Table 8.4 Rover sensory equipment

Component	Size (cm^3)	Mass (kg)	Power (W)
AHARS	1639	2.27	10
Inclinometers (4)	50	0.8	2
Proximity Sensor	850	2	25
ERIM laser (2)	1500	8	30
CCD cameras (2)	1200	0.5	10

8.6.2 TELEOPERATION

(Anita Abrego, Patrick Sweeney)

It has been decided that it is impractical to teleoperate the rover from Mission Control on Earth at all times, due to round trip communication time delays. Therefore, in order to navigate through its local environment, some autonomy on the rover is needed. Two teleoperation methods are being considered for the rover. The first is the Computer-Aided Remote Driving (CARD) method, and the second is a Semi-Autonomous Navigation (SAN) method [20,21].

The CARD method relies on stereo images acquired by the rover's camera system. The images are sent to Mission Control, where an operator analyzes them and designates a path for the rover. This plan is sent to the rover and is executed. A precautionary system the rover could possess is a maneuver level autonomous hazard detection and avoidance. For example, sensors that measure the angle at which the rover is inclined could aid in preventing the rover from overturning. The rover could also be aided by surface property determination sensing and expectation generation and monitoring, in which the rover senses its environment, associates it

with prior knowledge and then creates a map of the surroundings. The trajectory is simulated, containing run time expectations, and is monitored throughout the traverse. Once expectations are violated, a reflex stop is performed, a new set of pictures is taken and the process is repeated. The daily traverse capability of the rover using this navigation method depends on the imaging at each interval and the planet's surface. On Mars, the rover might travel about 5 to 30 m on each iteration [20].

The SAN method uses topographic maps which are produced from stereo photographs obtained from an orbiter. These images are sent to Mission Control where they are processed and larger global routes are planned in a manner similar to that of the CARD method. These global routes are approximate paths for the rover, and are designed to aid the rover in avoiding large obstacles, dangerous areas and dead-ends. The global route and the topographic map are sent to the rover. The rover, in turn, computes a local topographic map via its own stereo imagery and correlates it with that of the orbiter. After matching the local map of the rover to the global map of the orbiter, the rover analyzes the maps and autonomously determines a revised, high resolution map in the vicinity of the rover. This map and the global route is provided to the path planning system of the rover, where a new local path is computed and executed. This local path is also aided by the same systems as mentioned in the CARD method. The process is repeated as needed, possibly once a day or once between each site where experiments are to be done [22]. The SAN navigation system offers a much longer daily traverse of approximately 23 km on Mars [20].

The concept of visual terrain matching for the rover has been described elsewhere [23] and is briefly reviewed here. Since the imagery of the orbiter will be of lower resolution compared to that of the CCD cameras on the rover, a technique of matching the two sets of data was devised in order to make full use of the information that they contain. It uses uncertainty estimates in the form of covariance matrices of position and probabilities of correctness for the (arbitrary) points in each map. This matching process and means of extracting the necessary information from stereo vision are described in complete detail in Ref. 23.

Each method requires autonomous navigation through an unknown local environment that is assembled by the rover. One technique for this is called blooming. In this method, circles or polygons are set up around the scanned objects which have a greater radius than the width of the rover. By only navigating in the unoccupied regions, the rover is assured to not hit an obstacle [24]. One advantage of the blooming method is that it reduces the navigation algorithm to a simple geometric exercise. The disadvantage is that it does not take into account the true shape of the rover and thus may not allow certain paths because of its inherent inaccuracy. Another more promising method is constructing a "configuration space" which is a fairly accurate representation of the surrounding environment stored inside the computer's memory. The disadvantage of the configuration space method is the tremendous amount of processing power required.

A logic tree is essential to establish hierarchies for processor time involved in navigation, sample collection, and scientific experimentation. The design of the logic tree is shown in Fig. 8.15. This design shows the rover collecting sensory input for construction of a world map to navigate, as well as for experimentation. Because the rover will not navigate and move while collecting samples or experimenting, the processor alternates between a navigation and experimental algorithm. It is important to note the safeguards for detection and prevention of rollovers and collisions.

8.6.3 PROCESSOR

(Patrick Sweeney)

Three main parameters are used in determining the computational throughput needed in an onboard computing unit. The three parameters needed are the performance of the processor in millions of instructions per second (MIPS), power requirement for mobility, and the number of computer instructions needed per meter of safe travel. For a rover the size and speed of SPOT, these requirements can be estimated at 50 MIPS, 600 W, and 200 million instructions per meter of travel [25]. These requirements can be met by using two present technology 80486 processors running at 50 MHz. These processors have a capacity for 5 million floating point operations per second (FLOPS) when used in conjunction with Cyrex math coprocessors. In this setup, one

processor will perform path planning algorithms while the other processor constructs a world map based upon visual and other sensory data collected by the rover.

8.7 POSSIBLE PROBLEMS AND SOLUTIONS FOR ROVER'S OPERATION

(Thu Vu)

Due to the extreme environmental conditions on Mars, several factors have been considered in the design of the rover. Thermal fatigue, which degrades metal structures through expansion and contraction in response to extreme temperature changes, is being combated through the selection of materials with low coefficients of thermal expansion [26]. Micro cracking is caused by rough operation as well as thermal heating and cooling. The cracks degrade stiffness and strength in the metals, and are especially damaging in composite structures. Micro cracking effects are being reduced through the use of appropriate materials in the rover's structure [26]. Vibration damping is necessary to reduce structural vibration of the rover on rough terrain. Properly designed wheels and suspension help to reduce structural vibration of the rover. Composite structures are being emphasized in SPOT's suspension system since the damping characteristics of composites are superior to those of metals [26].

Adhesive wear occurs when two solid surfaces slide over one another under pressure. The surfaces between the two materials are plastically deformed and eventually welded together by the high local pressures. Abrasive wear is caused by particles of wear materials, external contamination such as dust particles, or abrasive grit. Contamination which is caused by inadequate quality of lubricant, a lack of control in fabrication, or handling impairs lubricant performance. Wear is avoided through the use of lubricants such as molybdenum disulfide (MoS_2), which is a dry lubricant used on the LRV [26]. Also, mechanisms with the most resistance to conditions of wear such as plastic bearings, magnets bearings, and brushless motors, are used to avoid failures due to wear [26].

Three types of radiation contributing to the degradation of polymers and the potential failure of the rover's mechanisms have been considered. Cosmic radiation, solar flares, and solar ultraviolet radiation are the main causes of polymer degradation. Solutions to these problems include shielding and thermal control coatings to reflect solar radiation. Problems caused by low operating temperatures on Mars can be minimized by using active solar powered thermal control devices. Particles on Mars have a mean diameter of 20 microns, and are capable of migrating onto every exposed surface of the rover. Ultrahard surface treatments and wear resistant materials are used on the outer surfaces of the rover to minimize the abrasion effects [26].

8.8 CONCLUSIONS
(Gretchen Swanson)

While most unmanned missions to Mars currently being planned include the use of mini-rovers, the Hyreus mission can support a relatively large rover, thus offering versatility in sample collection techniques. More equipment and samples can be carried, and a bigger power source can be used. The SPOT rover also has a longer lifetime than most mini-rovers because it has the ability to refuel , whereas RTG's shorter useful lifetimes. Since SPOT has wheels, the control and navigation system will not be as complex as it would be if a walking rover were used. In order to power SPOT, the use of the TPV generator is being advocated due to its simplicity and light weight, as well as the fact that the use of methane would be convenient

NOMENCLATURE

A_{cells}	Area of photovoltaic cells
A_{fins}	Total area of the fins
AHARS	Altitude Heading and Reference System
ALV	Autonomous Land Vehicle
A_{outer}	Outer area
ASV	Adaptive Suspension Vehicle
A_{tube}	Area of tungsten tube
BSR	Back surface reflectance
CARD	Computer-Aided Remote Driving
CCD	Charge-coupled device
CMU	Carnegie-Mellon University
$E_{radiated}$	Radiated energy
FLOPS	Floating point operations per second
IC	Internal combustion
IR	Infra-red
JPL	Jet Propulsion Laboratory
LDEF	Long Duration Exposure Facility
LGA	Low-gain antenna
LRV	Lunar Roving Vehicle
M	Total mass
m1, m2...mn	Component mass
MIPS	Millions of instructions per second
OSU	Ohio State University
P_{req}	Required power
$q_{electrical}$	Energy converted to electricity by thermovoltaic cells

$q_{radiated}$	Energy radiated to thermovoltaic cells
$q_{thermal}$	Waste energy radiated by fins
RMA	Remote Manipulator Arm
RTG	Radioisotope thermal generators
SAN	Semi-Autonomous Navigation
SPOT	Special Planetary Observation Transport
T_{fins}	Temperature of fins
TPV	Thermophotovoltaic generator
T_{tube}	Tungsten tube temperature
VRI	Vehicle Research Institute
x1, x2...xn	Component x distance from reference point
Xcg	Center of gravity in the x direction
y1, y2...yn	Component y distance from reference point
Ycg	Center of gravity in the y direction
z1, z2...zn	Component z distance from reference point
Zcg	Center of gravity in the z direction
ß	Elevation angle
ε_{fins}	Emissivity of the fins
$\varepsilon_{tungsten}$	Emissivity of the tungsten
Φ	Flux
η_{cells}	Photovoltaic conversion efficiency
σ	Boltzmann constant

REFERENCES

1. Lee, G. L., DeJarnette, F. R., and Walberg, G. D., "Design Issues For Mars Planetary Rovers," American Institute of Aeronautics and Astronautics, AIAA-93-0957, Mars Mission Research Center.

2. Reynolds, K., "JPL Rocky IV," *Road and Track*, April 1993, pp. 92-97.

3. Hilton, D. A., "Mars Ball Rover Mobility: Inflatable Sectored Tire Concept," *The NASA Mars Conference*, Vol. 71, American Astronautical Society, San Diego, 1988, pp. 351-365.

4. NASA News, Release No. 71-119K, Project: Apollo 15, July 15, 1971, pp. 77-85.

5. Rao, N.S., and Wallace, B.E., "Considerations for the Design of Lunar Rover Structures and Mechanisms for Prolonged Operation in the Lunar Environment," The Boeing Company, AIAA Paper No. 93-0993, Huntsville, AL.

6. Avallone, E.A. and Baumeister, T. (ed.), *Mark's Standard Handbook for Mechanical Engineers*, 9th Ed., McGraw-Hill, New York, 1978, pp. 11.11-11.12.

7. Nelson, T. T., "A Hybrid Natural Gas Vehicle," *SAE International Journal SP-832*, 1990, pp. 27-30.

8. Fahrenbruch, A. L., and Bube, R. H., "Fundamentals of Solar Cells,"*Photovoltaic Solar Energy Conversion,* Academic Press, NY, 1983, pp. 311-316.

9. Final Report, AA420/421 Space Systems Design, "Project Minerva: A Low Cost Manned Mars Mission Based on Indigenous Propellant Production,"NASA/USRA Advanced Design Program, June 1992.

10. Skerrett, P.J., "Fuel Cell Update," *Popular Science*, Vol. 242, Num. 6, June 1993, pp. 88-91, 120-121.

11. McDougall, A., *Fuel Cells*, 1st ed., John Wiley & Sons, New York, 1976,pp. 72-74.

12. Seal, M., Automotive Engineering Department, Western Washington University, Bellingham, WA, Personal Communication, March 11, 1993.

13. Fraas, L., Department of Material Science, University of Washington, Seattle, WA, Personal Communication, April 5, 1993.

14. Albright, L.F. and Alexander, L.G., "Stable Cyclonic Flames of Natural Gas and air," Jet Propulsion, October, 1956, pp. 867-872.

15. Fraas, L.M.,"Concentrator Modules Using Multiple-Junction Cells," JX Crystals, Issaquah, Wa., 1992.

16. Ovshinsky, S. R., Fetcenko, and M. A., Ross, J., "A Nickel Metal Hydride Battery for Electric Vehicles," *Science*, Vol. 260, April 9, 1993, pp.176-181.

17. Byler, E., "Design and Control of Ultralight Manipulators for Interplanetary Exploration," *Cooperative Intelligent Robotics in Space*, Vol. 1387, The International Society for Optical Engineering, Massachusetts, 1990, pp 313-327.

18. Stanford University, *The Stanford US-USSR Mars Exploration Initiative*, Stanford University Press, 1988.

19. Spiessbach, A.J., "Hazard Avoidance for a Martian Rover," *Mobile Robots III*, The International Society for Optical Engineering, Massachusetts, 1988, pp. 77-84

20. Lavery, D. and Bedard, B.D. Jr., "NASA Planetary Rover Program," National Aeronautics and Space Administration, NASA TN91-20651, Washington, DC, Jan. 1991.

21. Cooper, B. K., Cameron, J. M., Salo, R. A., Wilcox, B. H., "Planetary Rover Mobility Control," *Mobile Robots*, Vol. 727, 1986, pp 330-335.

22. Miller, D. P., Atkinson, D. J., Wilcox, B. H., and Mishkin, A. H., "Autonomous Navigation and Control of a Mars Rover," *Automatic Control in Aerospace*, Nov. 6, 1990, pp. 111-114.

23. Gennery, D. B., "Visual Terrain Matching for a Mars Rover," *Proceedings of IEEE Computer Society Conference on Computer Vision and Pattern Recognition*, Institute of Electrical and Electronics Engineers, Washington D.C., 1989, pp 483-491.

24. Kincaid, D.H., Autonomous Navigation of a Mobile Robot in an Unknown Environment , University of Washington, 1988, pp. 4-15.

25. Wilcox, B.H., Gennery, D.B., and Mishkin, A.H., "Mars Rover Local Navigation and Hazard Avoidance,"*Mobile Robots III*, 1988, pp. 72-76

26. Miller, D.P., "The Real-Time Control of Planetary Rovers Through Behavior Modifications," Jet Propulsion Laboratory, NASA TN91-20686, Pasadena, CA, Jan 1991.

27. The Mars Study Team, Solar System Exploration Division, "A Preliminary Study of Mars/Rover Sample Return Missions," National Aeronautics and Space Administration, NASA TN89-15141, Washington, DC, Jan 1987.

28. Askerland, D.R., *The Science and Engineering of Materials*, PWS-Kent Publishing Company, Boston, pp. 231-320.

29. Burke, J., Jet Propulsion Laboratory (retired), Personal Communication, April 2, 1993.

30. Ly, U., University of Washington, Seattle, WA, Personal Communication, May 19, 1993.

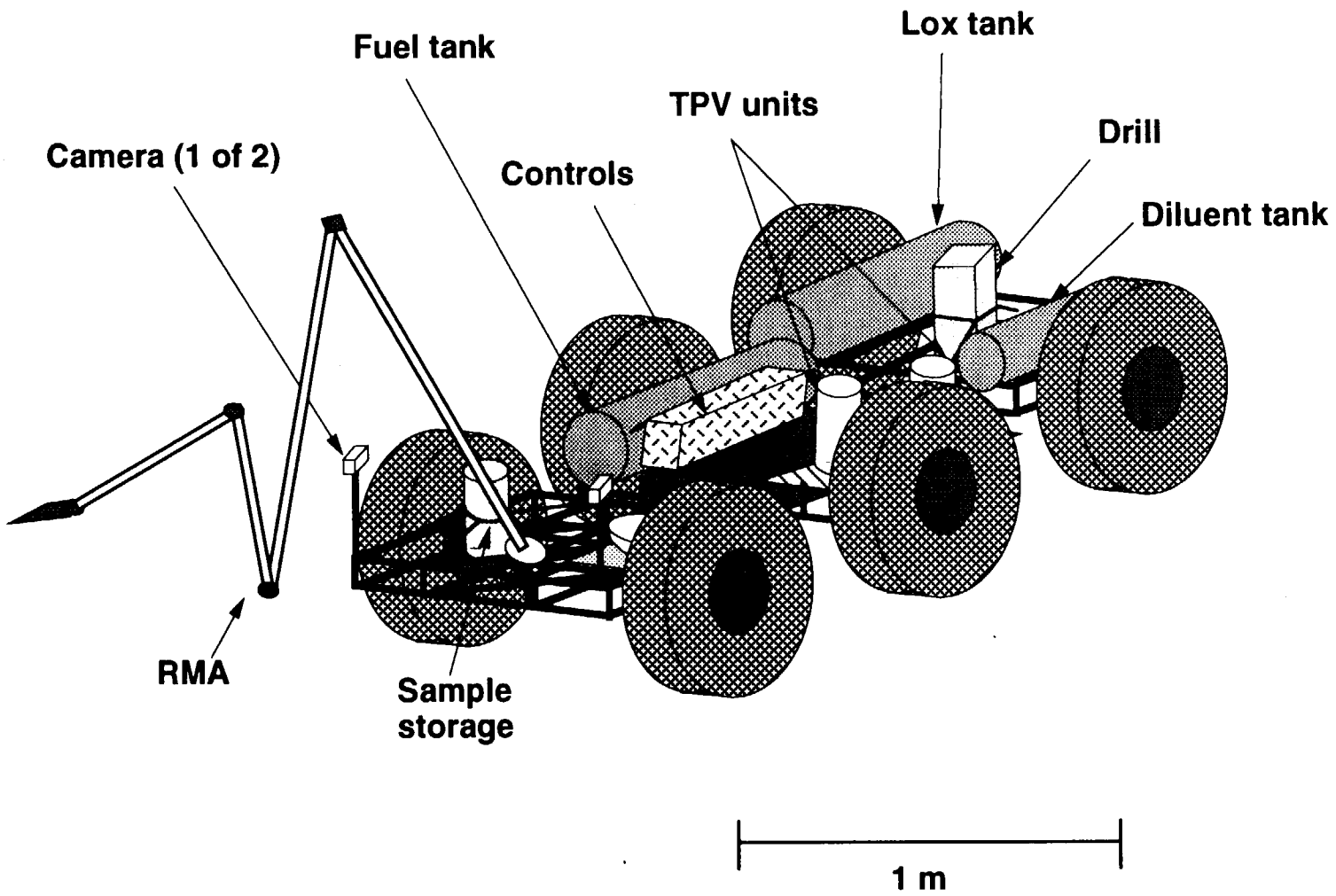

Fig. 8.1 Special Planetary Observation Transport (SPOT).

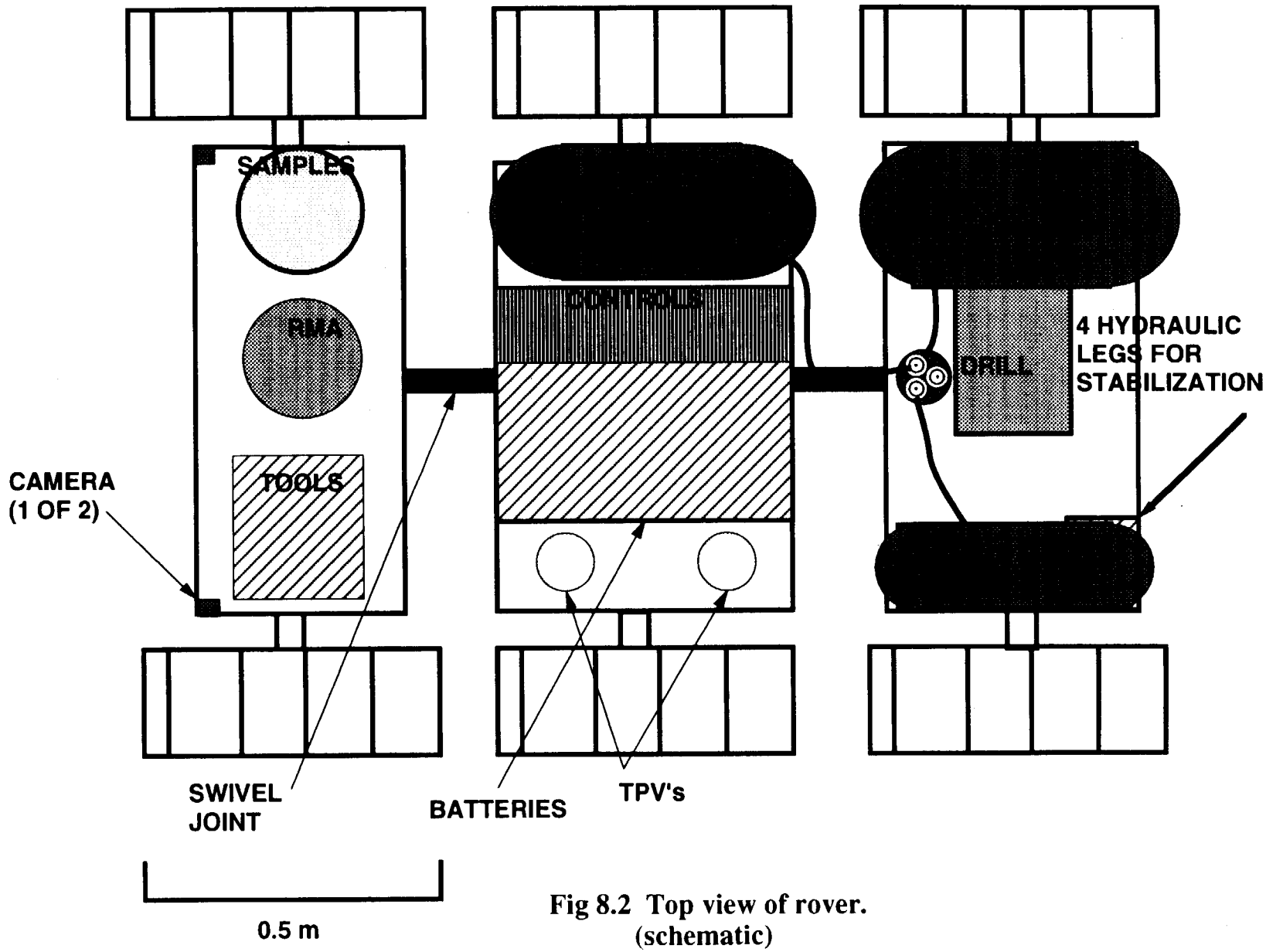

Fig 8.2 Top view of rover.
(schematic)

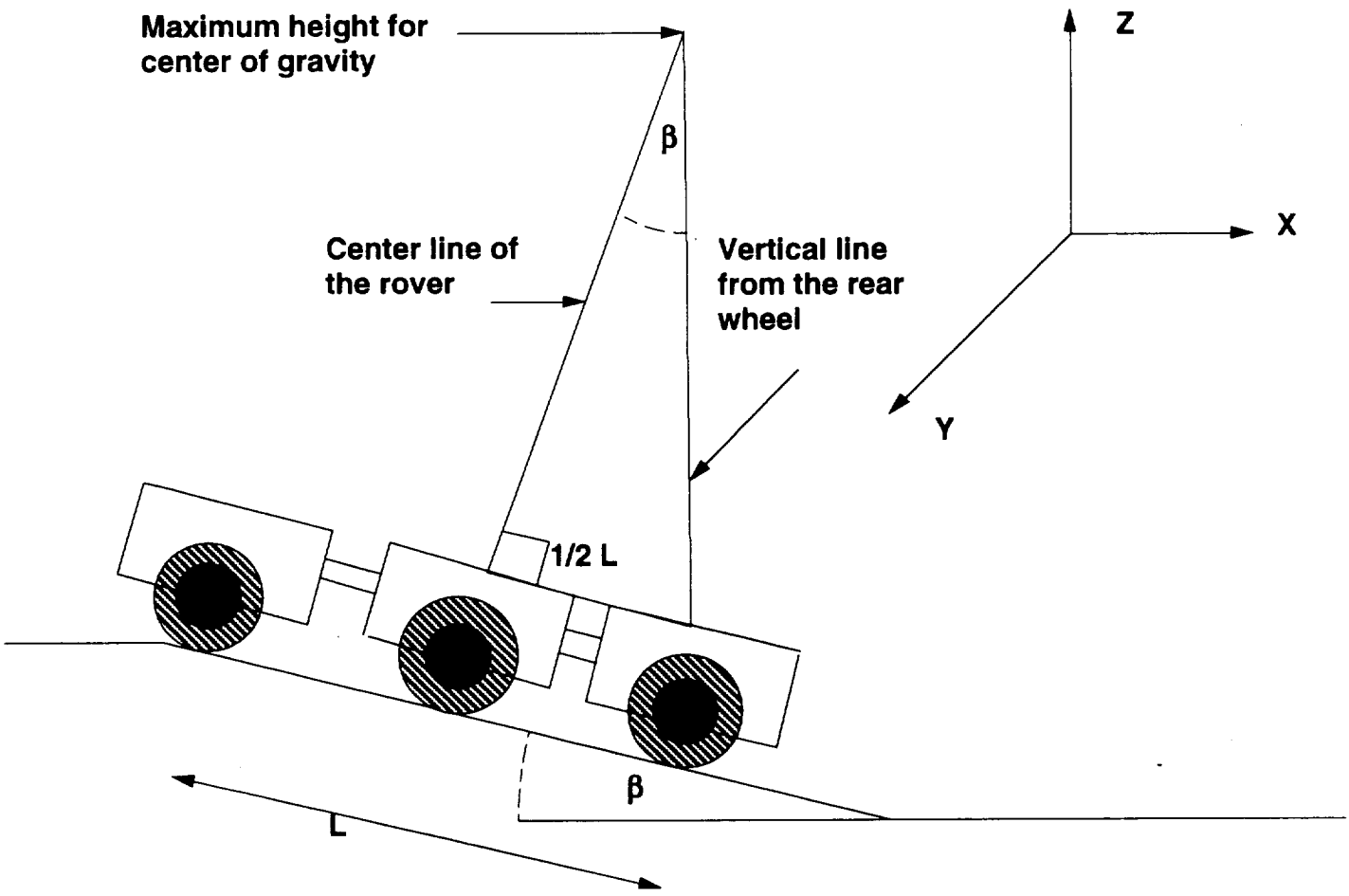

Fig. 8.3 Center of gravity analysis.

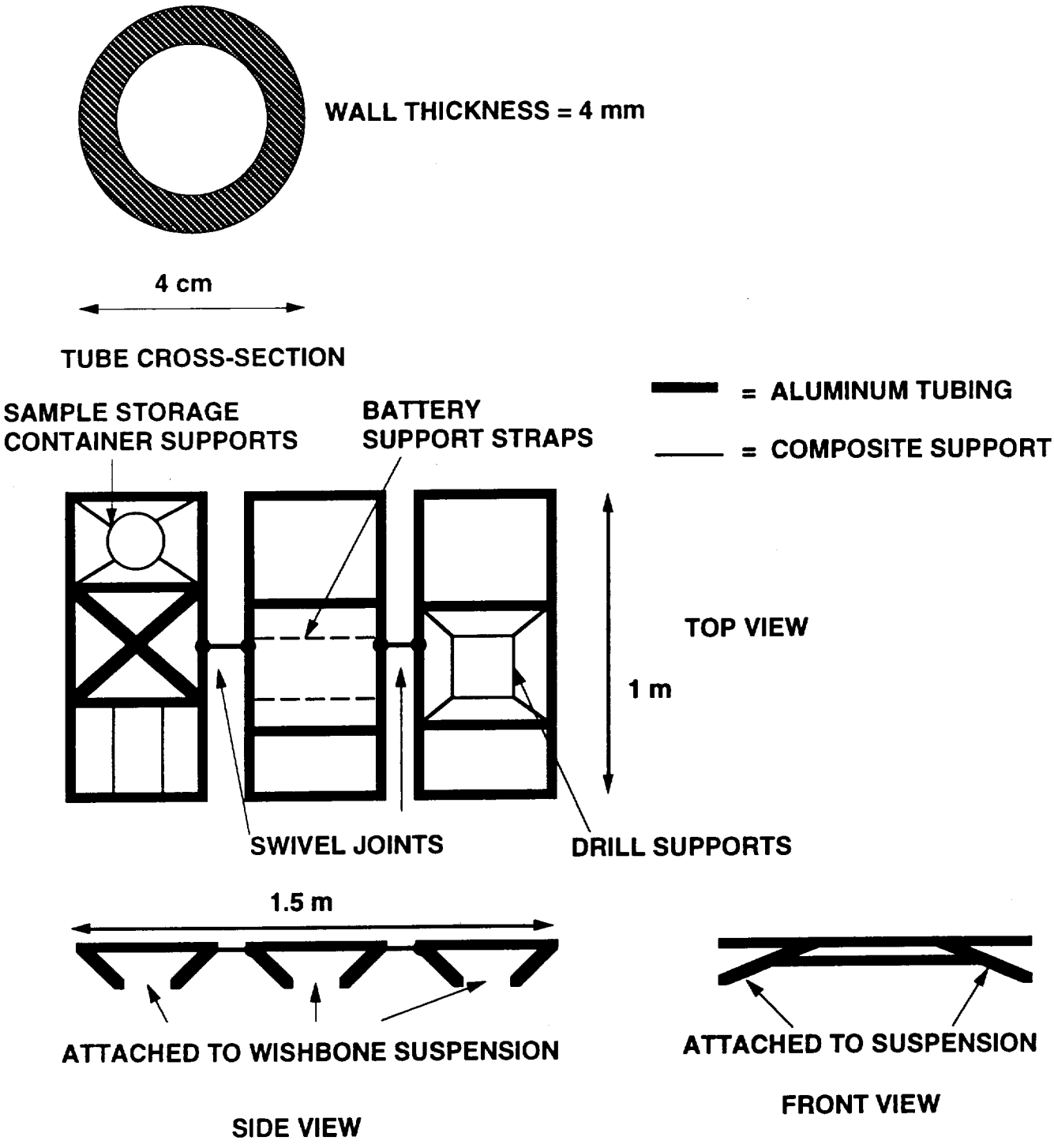

Fig. 8.4 Rover framework.

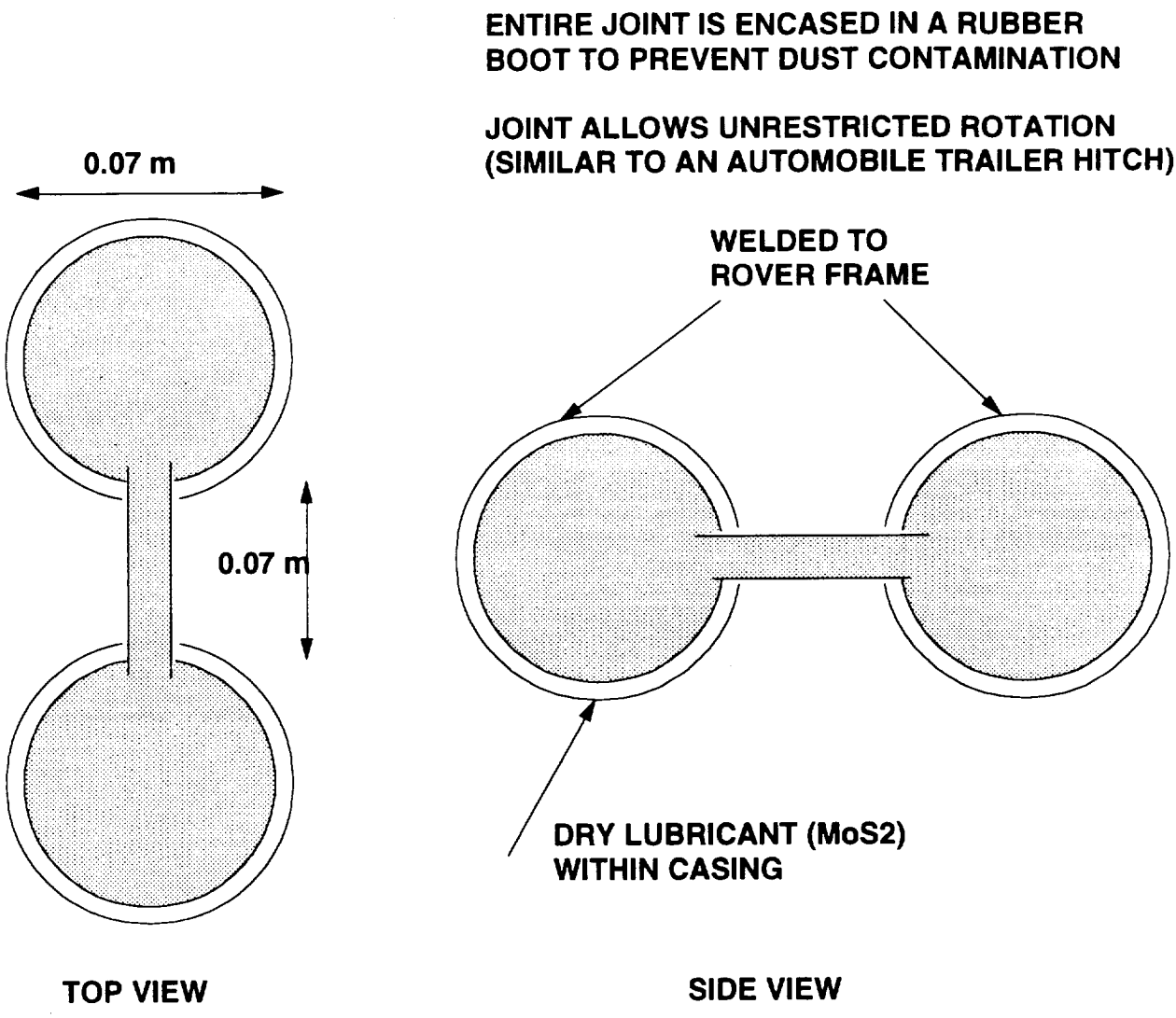

Fig. 8.5 Swivel joint.

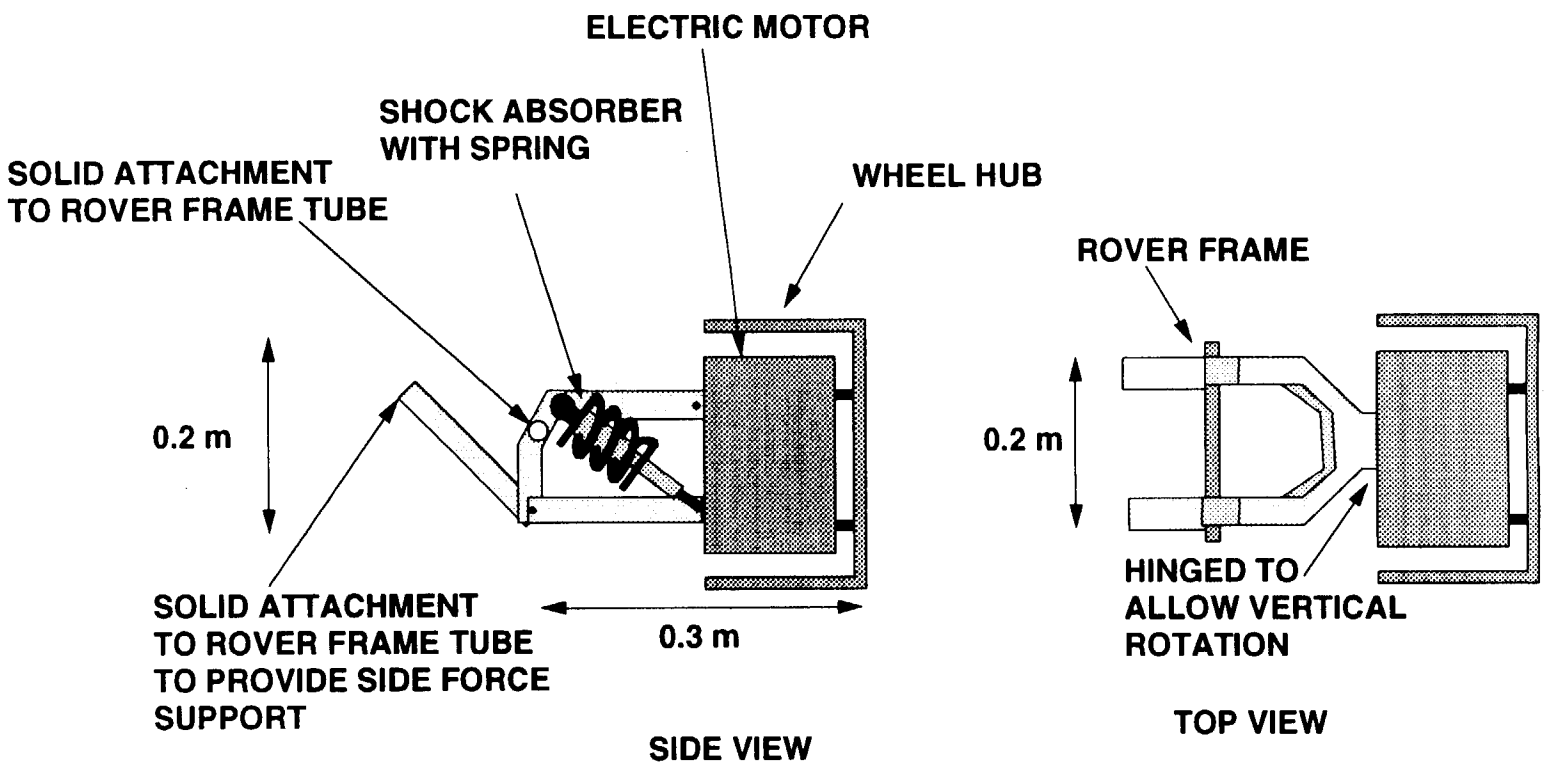

Fig. 8.6 Double wishbone suspension.

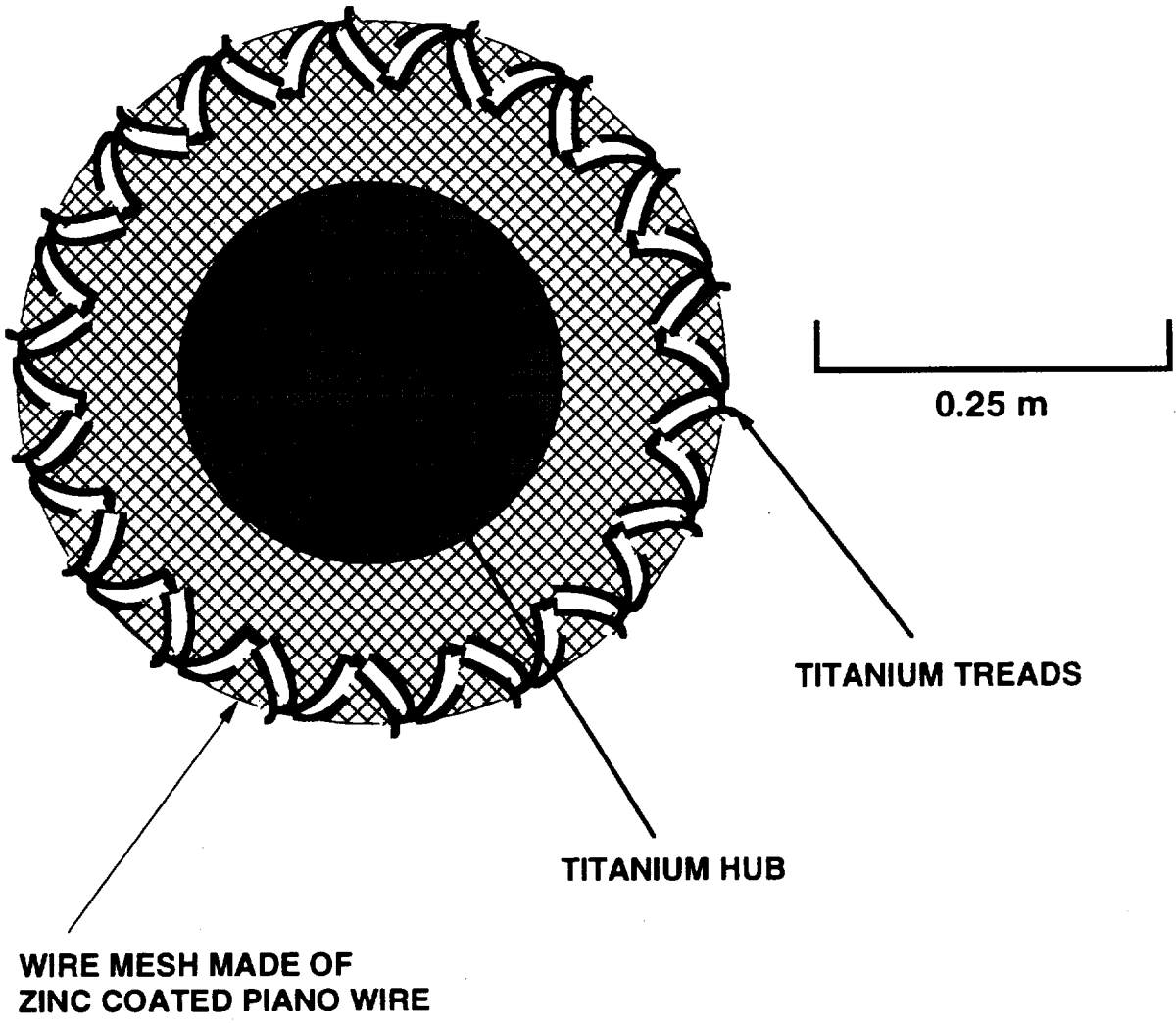

Fig. 8.7 Rover wheel design.

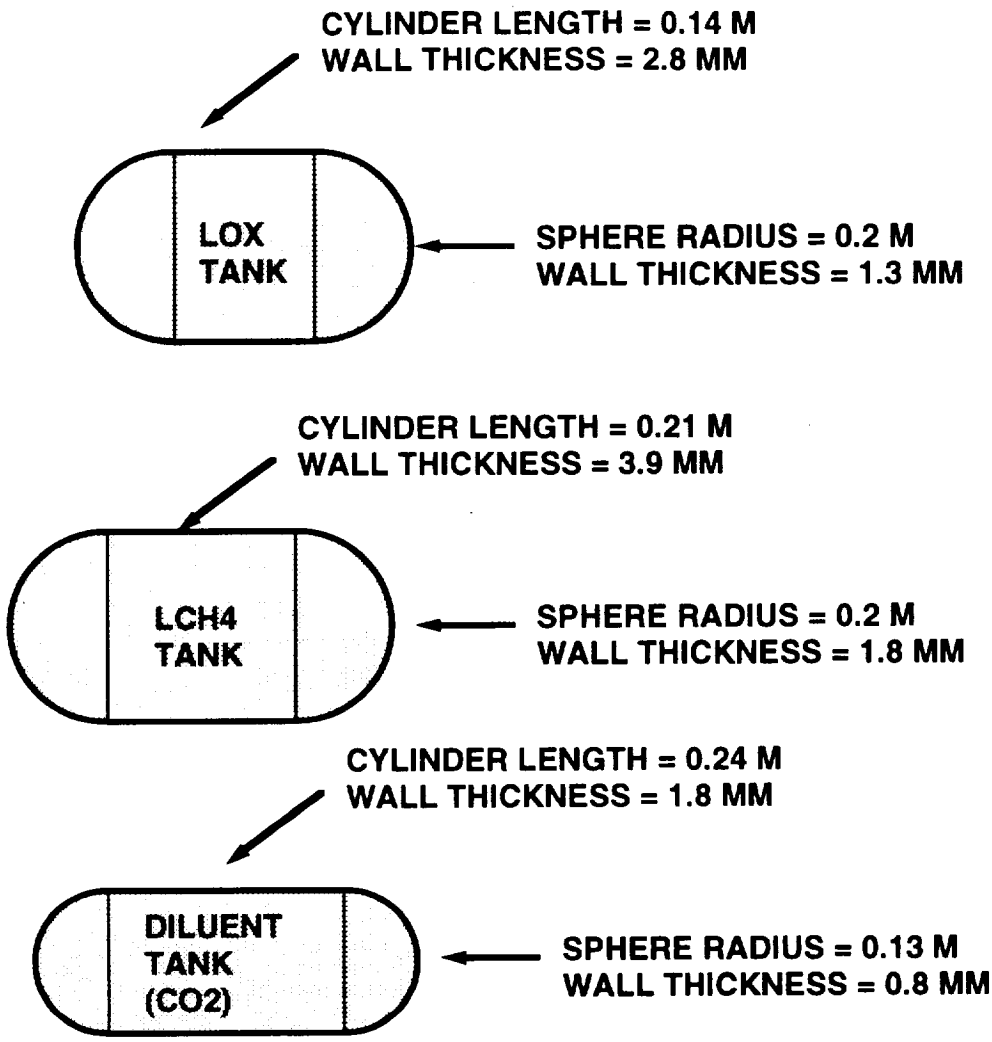

Fig. 8.8 Fuel tank dimensions.

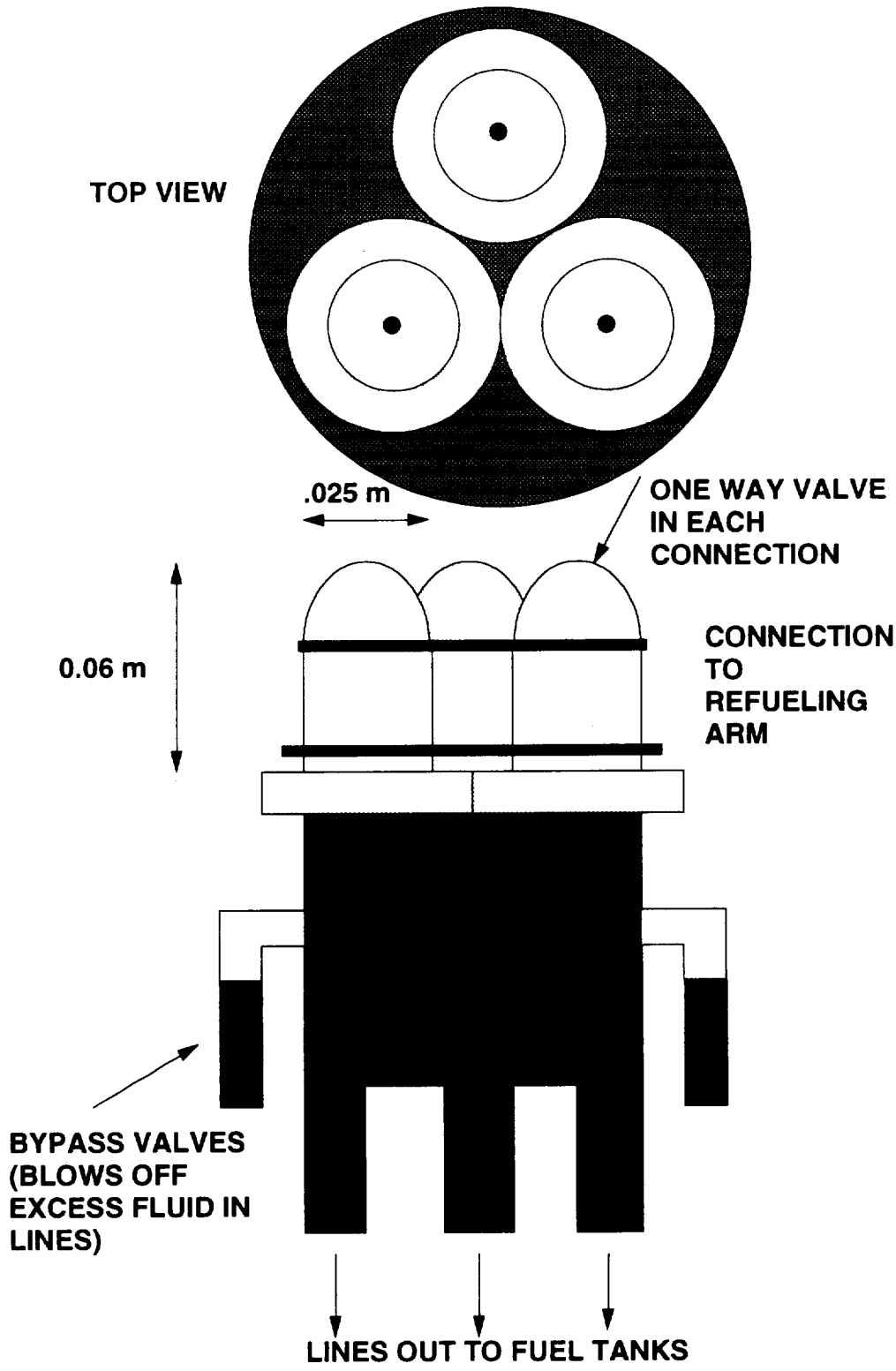

Fig. 8.9 Rover refueling connector.

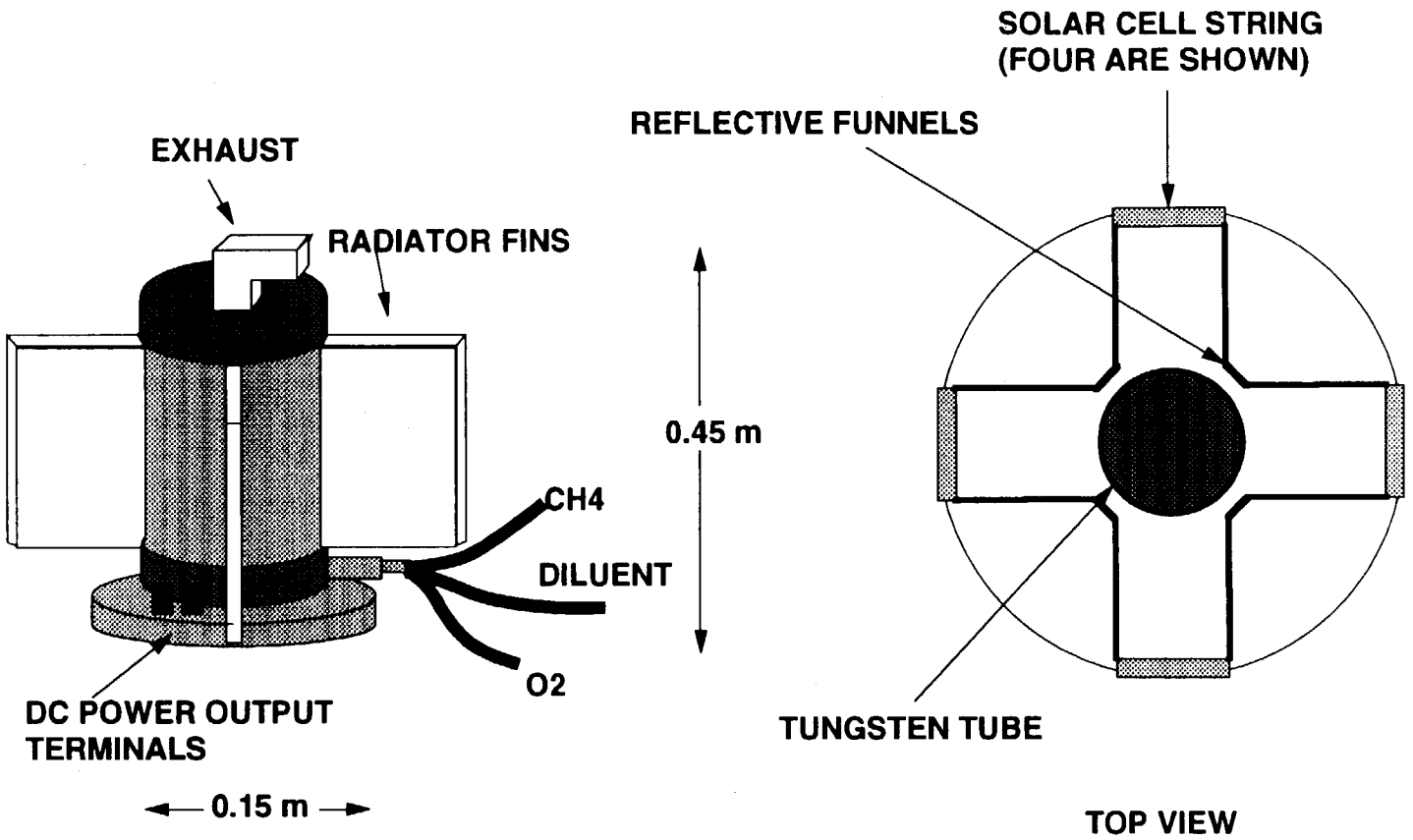

Fig. 8.10 Thermophotovoltaic generator.
(two are needed)

Fig. 8.11 Thermophotovoltaic Generator in Operation.

Figures shown on following page are as follows:
(clockwise from top left)

1. Dr. Lewis Fraas with TPV Generator [13]

2. Close up of infrared emitter

3. Exhaust Analysis of TPV Generator: shows that the TPV Generator emits 1 ppm of hydrocarbons

4. Dr. Michael Seal with TPV Generator [12]

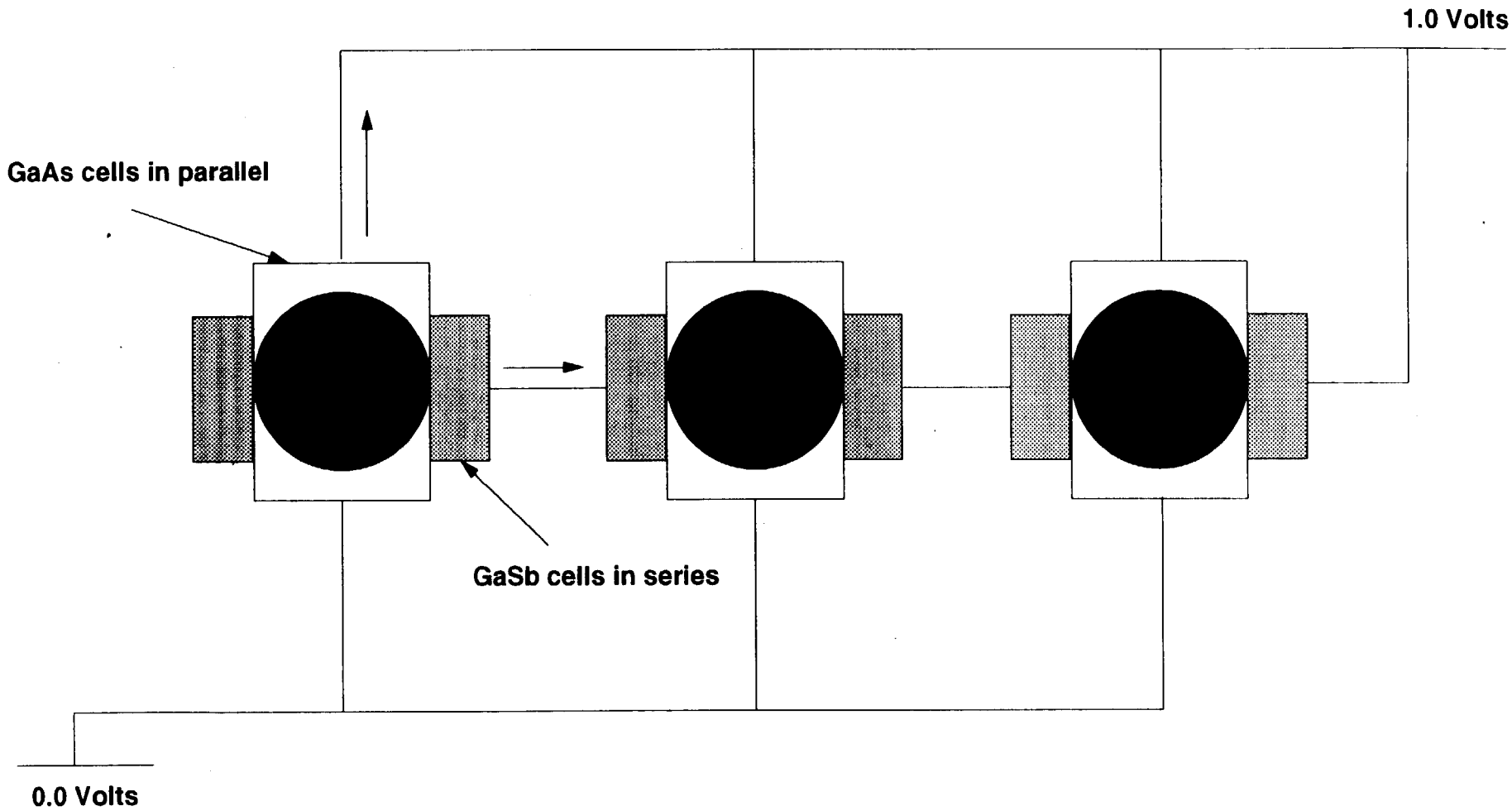

Fig. 8.12 Wiring diagram for GaAs and GaSb tandem cells.

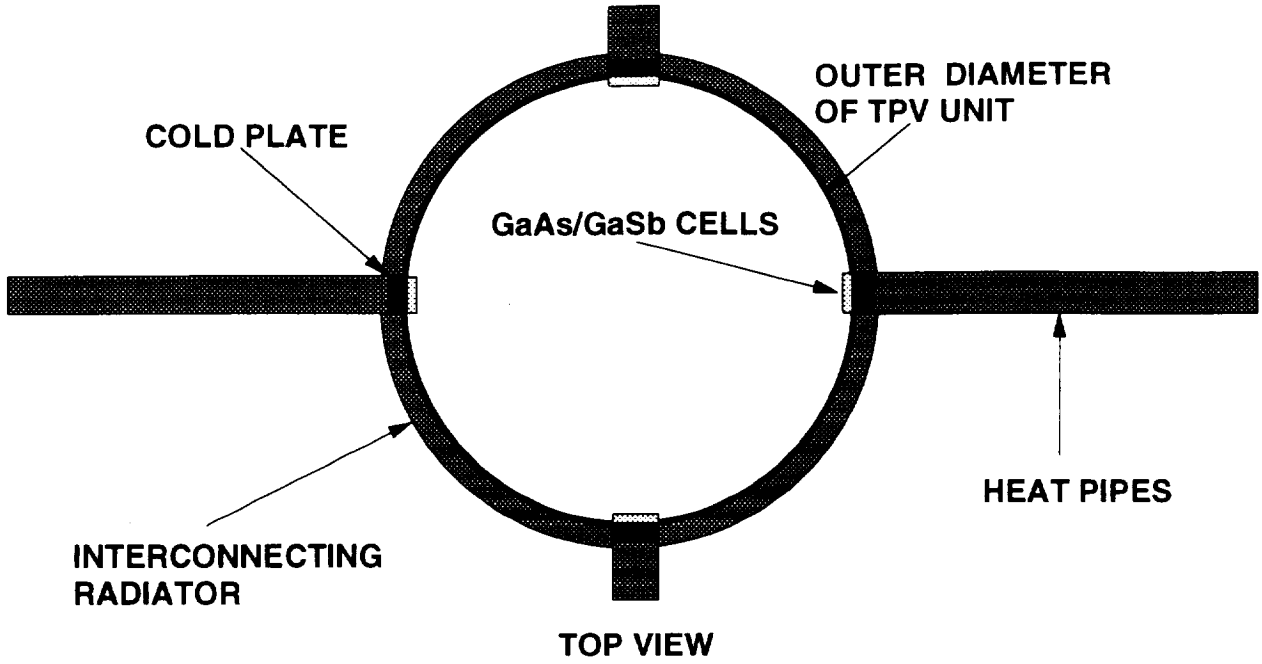

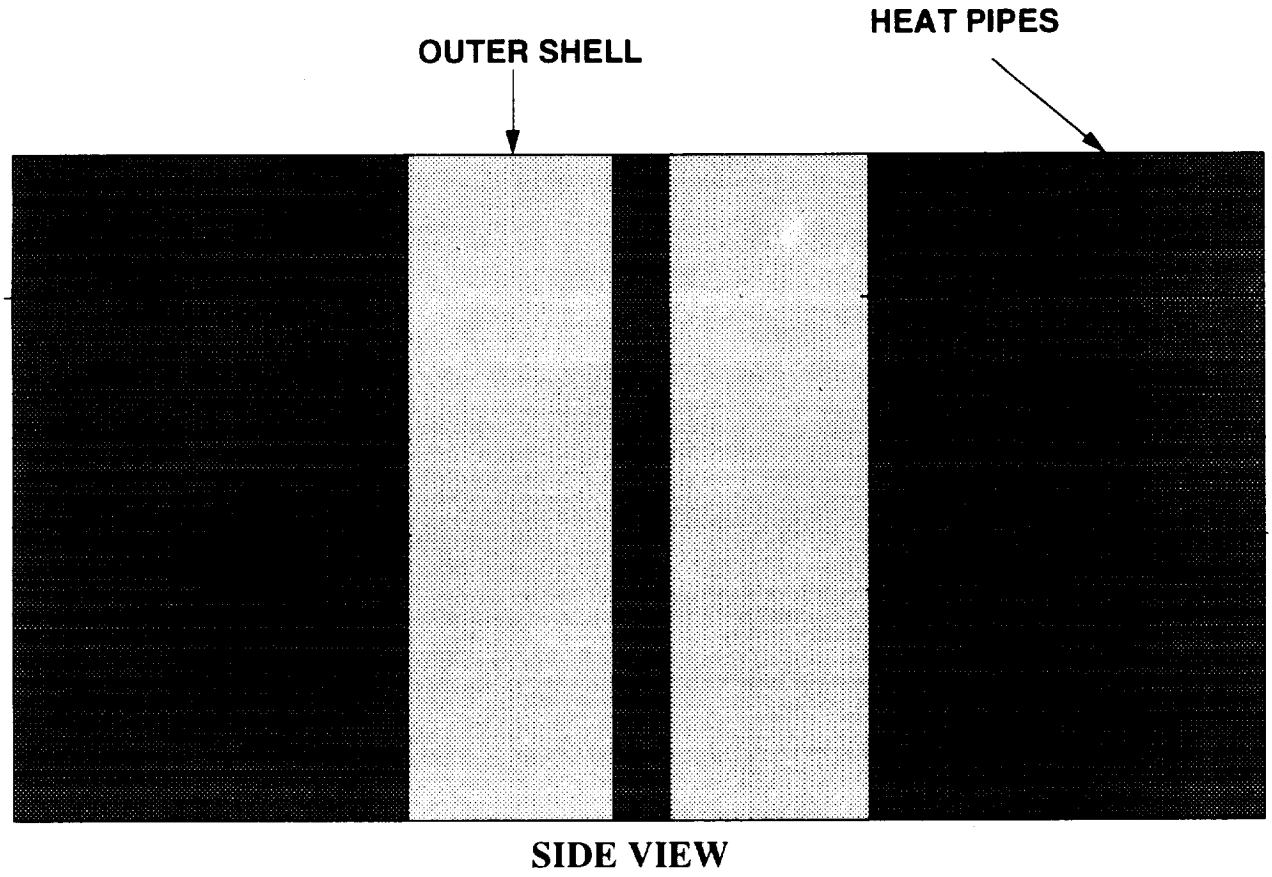

Fig. 8.13 Heat rejection system.

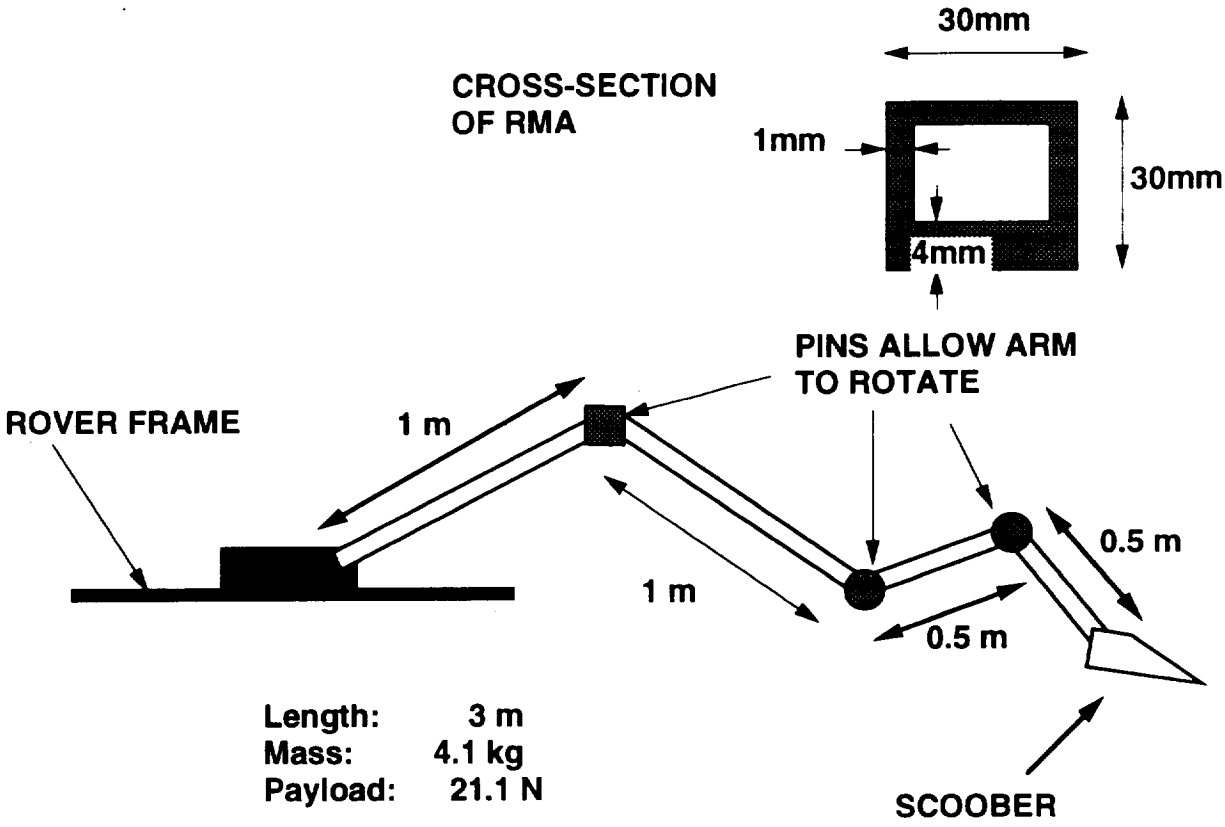

Fig. 8.14 Remote manipulator arm.

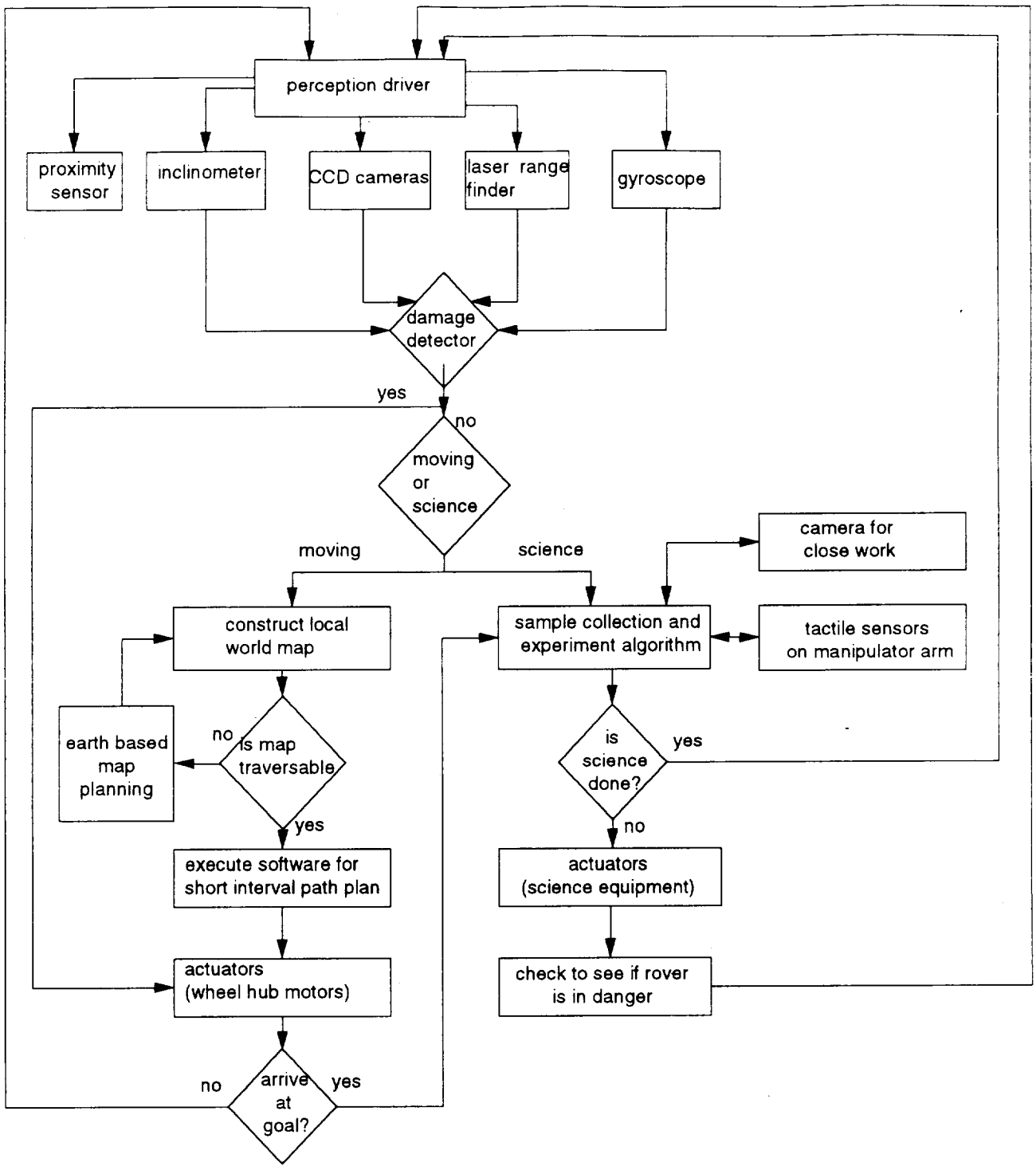

Fig. 8.15 Control logic tree.

9.0 SATELLITE OBSERVATION AND COMMUNICATION AT MARS (SOCM)

Christopher Bair
Amber Koch
Heidi Schubert
Michael Wu

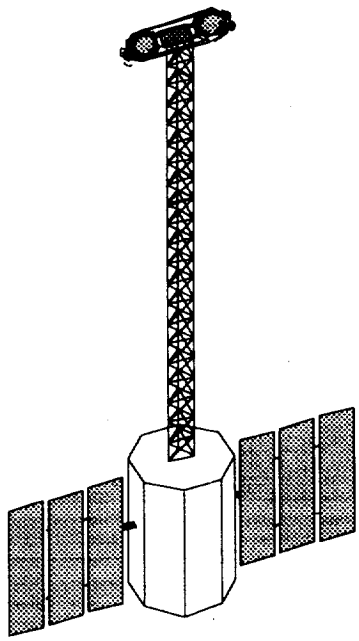

TABLE OF CONTENTS

9.1 INTRODUCTION 9.1

9.2 CONFIGURATIO 9.1

9.3 PAYLOAD 9.2

9.3.1 Camera 9.3

9.3.2 Ground Penetrating Radar 9.4

9.4 STRUCTURE 9.5

9.5 COMMUNICATIONS AND DATA HANDLING 9.6

9.5.1 In Transit to and from Mars 9.7

9.5.2 On Mars: Communication and Data Relay 9.7

9.6 POWER SYSTEMS 9.8

9.6.1 Power Source 9.9

9.6.2 Power Distribution 9.12

9.6.3 Power Regulation and Control 9.13

9.7 ENVIRONMENTAL CONTROL 9.13

9.7.1 Thermal Analysis 9.14

9.7.2 Thermal Control Subsystem 9.16

9.8 ORBITAL MECHANICS 9.17

9.8.1 Orbit Options 9.17

9.8.2 Orbit Calculations 9.18

9.9 ATTITUDE DETERMINATION AND CONTROL 9.21

9.10 CONCLUSION 9.24

NOMENCLATURE 9.25

REFERENCES 9.27

FIGURES 9.28

9.1 INTRODUCTION
(Amber Koch, Heidi Schubert)

A small satellite, SOCM (Satellite Observation and Communication at Mars), is placed in a sun synchronous orbit around Mars. The primary mission objective of SOCM is to look for subsurface water/ice deposits using a ground penetrating radar (GPR). Also, the satellite is equipped with a weather monitoring system (wide-angle camera) in order to warn the rover of impending Martian dust storms. In addition, the SOCM satellite provides a communication link between the rover and the Mars surface lander.

The design of the SOCM satellite is presented in the following format. The configuration and payload of the satellite are discussed first. Then the satellite subsystems are discussed: structure, communications and data handling, power systems, and environmental control. Next, the orbital mechanics of SOCM is given, followed by attitude determination and control.

9.2 CONFIGURATION
(Amber Koch, Heidi Schubert)

SOCM has two overall arrangements, the initial launch configuration and the final orbital configuration. In the initial launch configuration the satellite is compactly stored in the launch vehicle (Figs. 9.1 and 9.2.). The satellite is deployed from the MLV and performs an orbital circularization burn while in the folded launch configuration. After orbit insertion, solar panels are deployed, and an extendible boom separates the two sections of the satellite (Figs. 9.3 and 9.4.). The separation between these two sections is required for gravity gradient stabilization, which works by aligning the longitudinal axis of an elongated structure towards the center of Mars.

The design of SOCM is based on the need to accommodate the payload (Fig. 9.5). Also incorporated in the satellite configuration is the attitude control system, command and data

handling system, power system, and structure. The power consumption and mass of each component are given in Table 9.1.

Table 9.1 SOCM power and mass requirement breakdown.

Component	Power (W)	Mass (kg)
Wide angle camera	10	1
Ground penetrating radar	220	100
Thrusters (4)	10	8
Sun sensors (2)	2	3
Communications/control	30	20
Command and data handling	20	5
Solar arrays	5	30
Batteries	--	5
Structure	--	70
Cabling/thermal control	5	20
Total power	**300**	--
Dry Mass	--	262
Propellant Mass	--	20
Loaded Mass	--	**282**

The payload, consisting of a camera and a ground penetrating radar system, is located in the main body of the satellite. Also contained therein are a low gain antenna for Mars communications and a data handling subsystem. The solar panels fold out from the sides of the spacecraft bus. An extendible boom [1] separates two control thrusters and their propellant tanks from the main section of the body. This boom is a lattice mast type with a continuos longeron so it cannot recollapse after being deployed.

9.3 PAYLOAD

(Amber Koch, Heidi Schubert)

SOCM's payload consists of a wide-angle camera and a ground penetrating radar (GPR) system. The wide-angle camera provides a weather warning system for the rover and surface science experiments, while the GPR system conducts a survey of the Martian subsurface landscape. This survey serves as valuable insight into the characteristics of the Martian subsurface such as composition and ground water content. Discovery of water (ice) sources on Mars would be highly beneficial for future manned missions.

9.3.1 Camera

The wide-angle camera is a miniaturized and modularized UV/visible response charge coupled detector (CCD), which provides approximately 100 m resolution ground surveillance (Fig 9.6) [2]. The camera is configured as follows :

- Mass = 0.5 kg
- Size = 10.5 cm x 12 cm x 16 cm
- Power Requirement = 6 W
- Field of View = 4.2° x 5.6°
- Ground Coverage = 40 km x 50 km rectangle

This miniaturized camera is half the mass and size of traditional cameras. In addition, the power required to run the camera is extremely low (6W).

9.3.2 Ground Penetrating Radar

Ground penetrating radar systems for subsurface investigation have been under development for at least 30 years. For the last 15 years subsurface radar systems have been available commercially for shallow probing of rocks, soils, and other materials [3]. Ground probing techniques have been applied in a variety of technical fields including geophysics, civil engineering, and marine science. Although subsurface radar systems have been operated primarily from ground stations, limited testing of systems operating from helicopters, airplanes, and the Space Shuttle has been performed. Despite the limited testing of GPR systems in free-space, commercially available systems could be easily converted for satellite use [4].

The primary design constraints for GPR are physical limiting factors and operational requirements. The physical limiting factors of GPR include attenuation, clutter, and back-scattering of sent and received signals. Other design criteria are the electronic and mechanical system capabilities, speed, and reliability. Operational requirements vary according to whether the system is used from the ground, air, or space.

The system configuration for GPR is similar to that of conventional free-space radar. GPR is a technique which transmits short-pulse electromagnetic waves into the planetary surface [5]. Only subsurface features that are normal to some portion of the radiated signals are reflected back. The reflected signals are processed through the receiver and through an image processing system where an image of the subsurface is produced.

The main difference between the GPR system and conventional free-space radar is that the design of the GPR system is mainly constrained by the electromagnetic properties of the ground and the reflective characteristics of the target. In essence, the ground acts as a lowpass filter affecting the bandwidth of the received signal. In addition, the detection configuration and antenna must be designed for the target. Essentially, the attenuation of electromagnetic radiation rises with frequency. At a given frequency a wet material has a lower attenuation than a dry

material. Table 9.2 contains values for desired penetration depth and operation frequency for a variety of Earth materials.

Table 9.2 Ground-penetrating radar depth and frequency characteristics for various Earth materials.

Material	Typical Penetration Depth (m)	Maximum Frequency (MHZ)
Cold pure freshwater ice	10000	10
Freshwater	100	100
Sandy soil	3	500
Rocks	20	50

As Table 9.2 indicates, the wave properties of wet materials are different from those of dry materials [6]. In effect, moist materials have a larger permittivity and therefore a lower wave velocity. SOCM's GPR system conducts several sweeps of the Martian surface at various frequencies and depths. The data attained are analyzed and compared with known Earth data.

Because most existing ground penetrating radars are ground based or airborne, no suitable GPR for SOCM is currently available. Therefore, the mass, size, and power requirements for SOCM's GPR are estimated based on current space borne radar [7]. It is assumed that by the time the Hyreus mission is ready to be launched, a GPR can be developed for use on SOCM [8].

9.4 STRUCTURE

(Chris Bair, Heidi Schubert, Michael Wu)

The structure of SOCM is an octagonal design, chosen for rigidity and ease of fabrication. The structure is composed of two octagonal end frames and multiple hollow vertical and horizontal struts (Fig. 9.7). Extra struts are located in sections of the frame where extra strength and rigidity are required for larger loads and torques. Except for the eight vertical corner struts,

strut members have square 2 cm by 2 cm cross-sections. The eight vertical struts are constructed to accommodate their positioning. The material for the frame is Aluminum-Lithium 2090, which is lightweight (density = 2.59 g/cm^3), rigid, and readily available.

SOCM has support pads for its two solar arrays, two hydrazine thrusters, and the extendible boom incorporated into the structural frame. The support pads are used to attach the components to the main frame of the satellite. The support pads also provide added structural support against the loads which are applied at these points [8]. The structural components and their masses are listed in Table 9.3.

Table 9.3 SOCM structural mass

Structural Member	Number	Mass (kg)
Octagon	2	6
Vertical corner struts	8	8
Horizontal struts	6	5
Corner attach points	4	1
Mid horizontal struts	4	1
Thruster pads	2	1
Solar array supports	2	4
Extra support struts	4	1
Propellant tanks support structure	4	3
Boom attachment	1	3
Solar panel support	2	19
Outer shell and connectors	1	18
Boom	1	5
Total Structural Mass		75

9.5 COMMUNICATIONS AND DATA HANDLING
(Chris Bair)

The communication system for SOCM provides a link between the rover and the lander on the Martian surface and transmits satellite data to the lander. The lander provides a

communication link between Mars and Earth. In addition, the rover can communicate directly with the MLV.

9.5.1 In Transit to and from Mars

The MLV uses a conventional vehicle-to-Earth communication link while in transit to Mars. The spacecraft transmits data to the Deep Space Network (DSN) on Earth. The DSN performs four basic functions in support of the mission: tracking, data acquisition, command, and control. This system, operated by JPL, is the only network with assured capability of constantly receiving and transmitting data at interplanetary distances. For the portion of the mission between Earth and Mars, communication is between the DSN system and a low-gain omni-directional antenna (LGA) attached to the Earth Return Vehicle (ERV). The LGA is 0.75 m in length with a 0.05 m diameter circular aluminum wave guide near the end. The same LGA is used not only for the transfer orbit from Earth to Mars, but also for the return orbit from Mars to Earth. On the Earth to Mars and Mars to Earth trajectories, the LGA is adequate for telemetry and command [8,9].

9.5.2 On Mars: Communication and Data Relay

After the MLV has landed on the Martian surface, the lander is used for Mars-to-Earth communications (Fig. 9.8). Therefore, both a LGA and a high gain antenna (HGA) are provided on the Mars landing vehicle. Once the MLV is safely on the Martian surface the HGA is deployed. The HGA is a parabolic dish with a diameter of 1.10 m and depth of 0.15 m (See Fig. 2.2). The HGA provides a communications link between the landing vehicle and Earth; while the satellite relays information between the rover and the landing vehicle through the LGA. Furthermore, the satellite relays observation data obtained by the GPR and wide angle camera to the MLV, which in turn relays the information back to Earth.

C-4.

The satellite, rover, and MLV are all equipped with low-gain omni-directional antennas to transmit and receive radio waves back and forth between each other. The LGA on the satellite is identical to the one located on the MLV. The rover has a "T" style LGA to optimize transmissions when the satellite is not directly above the landing site. The "T" LGA has dimensions of 0.5 m by 0.5 m. The satellite is utilized when the rover ventures beyond line-of-sight radio contact with the MLV. However, the MLV-satellite-rover communications link is not operational when the satellite is out of range of the landing region. In addition, if the satellite's communication system fails, the rover cannot venture out of the line of site of the MLV.

The hardware size, power requirements, and data handling are listed in Table 9.4. The values listed in the table are projected from current communication systems of comparable size and load requirements [2,8,9].

Table 9.4 Communications hardware values.

	MLV LGA	MLV HGA	SOCM LGA	ROVER LGA
Size (m)	0.75 x .05	0.15 x 1.10	0.75 x 0.05	0.5 x 0.5
Power requirements (W)	5	20	5	5
Frequency (GHz)	2 -3	7 - 8	2 - 3	2 - 3
Wavelength (cm)	10 - 15	3.8 - 4.3	10 - 15	10 - 15
Band	S	X	S	S
Data rate (bits/sec)	7,000	11,000	7,000	6,000

9.6 POWER SYSTEM
(Chris Bair, Michael Wu)

The power system generates, conditions, regulates, and distributes the power throughout the satellite. The power system frequently regulates equipment such as the central processing unit (CPU), switching it on and off during data storage and data uplink from the Mars surface,

protecting against short circuits, and isolating faults. The power system components are: power source, power distribution, and power regulation and control.

The designing process for the power system includes the following steps: identifying requirements, selecting and sizing the power source, and identifying power regulation and control. The power requirement is the average power required by the satellite during the operational periods, i.e., the uplinking and downlinking of data to and from the Mars surface, the imaging of the CCD camera, and the imaging of the GPR. The selection and sizing of the power source is determined by the average power requirement. The power regulation and control subsystem is designed to maintain the amount of electrical power each subsystem receives, and to prevent each subsystem from overheating.

9.6.1 Power Source

Two power sources were considered for SOCM, a solar photovoltaic system and a radioisotope thermoelectric generator, RTG. Table 9.5 shows a comparison of RTG and solar photovoltaic power systems [8].

Table 9.5 Comparison of common spacecraft power sources .

Design Parameters	Radioisotope (RTG)	Solar Photovoltaic
Power range (kW)	0.2 - 10	0.2 - 25
Specific power (W/kg)	8 - 10	26 - 100
Specific cost ($/W)	16,000 - 18,000	2500 - 3000
Fuel availability	Very low	Unlimited

An RTG delivers various design power levels and has applications to low-power use in space. An RTG consists of a radioisotope heat source which can produce power by thermoelectric conversion (See Section 6.4). One concern in using an RTG is the disposal of excess heat during all mission phases, especially during launch preparation and boost. This

requires a radiator and its associated thermal management system, which can be massive. Solar arrays have an advantage over an RTG due to their higher specific power output and lower cost.

Gallium arsenide (GaAs) solar cells have been chosen for SOCM's solar array, as they have been proven to be reliable in past space applications [10]. Other, alternative solar cells which were examined were silicon (Si) cells and indium phosphide (InP) cells. Table 9.6 shows the efficiencies and radiation-degradation sensitivities of these three types of cells [8].

Table 9.6 Performance comparison of photovoltaic solar cells.

	Silicon	Gallium Arsenide	Indium Phosphide
Theoretical efficiency	18%	23%	22%
Achieved efficiency	14%	22%	19%
Time for 15% degradation			
-1 MeV electrons	10 yr	33 yr	155 yr
-10 MeV protons	2 yr	6 yr	89 yr

Gallium arsenide is the most efficient, while indium phosphide is the least sensitive to the degrading effects of radiation. The use of InP cells has never proven to be reliable in any mission. Also, they are very costly. Even though gallium arsenide cells cost more than silicon solar cells, the higher efficiency compensates for the added cost.

The solar arrays are planar panels pointed towards the Sun (Fig. 9.9). Their power output is proportional to the area facing the Sun. The SOCM satellite uses deployable arrays, which are folded in accordion style on two sides of the body for easy storage (Fig. 9.1). The orientation of the arrays is continuously controlled by two sun sensors so that the arrays remain pointing towards the sun as the spacecraft moves in its orbit. (Originally, the design of SOCM had body mounted arrays surrounding the entire satellite. However, only 25-35% of the total area of body

mounted arrays is actually exposed to the Sun, requiring three times the mass for the same amount of power).

The solar array for SOCM is sized to meet the power requirement at end-of-life, EOL, with the resulting solar array oversized for the power requirement at beginning-of-life, BOL. The longer the mission life, the larger the difference between power requirement at EOL and BOL because of natural degradation of the solar array. Because SOCM mission life is between 2-4 years, the difference between EOL and BOL is minimal.

To estimate the solar array area needed, the power required for operation of SOCM must be found. The required power the solar arrays must generate is [8]:

$$P_{sa} = \frac{P}{X} \tag{9.1}$$

P = power required for operation = 300 W

X = efficiency of paths from solar arrays to load = 0.85 [5]

Thus,

$$P_{sa} = 353$$

Given the solar constant at Mars (592 W/m^2), the relation of array area required, A_{sa}, to the spacecraft's power requirement, P_{sa}, with the GaAs solar cell efficiency of 22%, is

$$A_{sa} = \frac{P_{sa}}{(0.22 \times 592)} = 7.678 \times 10^{-3} P_{sa} \tag{9.2}$$

where A_{sa} is in m^2 and P_{sa} is in Watts.

Using the results from Eq. 9.1, the area of the solar arrays is 2.71 m^2. With a specific performance, SP, of 47 W/kg, the mass of the array, M_a, is related to the power required by

$$M_a = \frac{P_{sa}}{SP} \tag{9.3}$$

where M_a is in kg and P_{sa} is in Watts. From Eq. 9.3, the mass of the array is 7.51 kg.

Primary batteries provide power for initial deployment and computer operations of the satellite. The solar arrays' drive mechanism, used to align the solar panels toward the Sun, is also powered by the batteries initially. Once the array is aligned, the system switches to solar power.

The primary batteries are non-rechargeable. Two silver-zinc batteries are used in SOCM. With a specific energy density of 130 Whr/kg, for one-half hour, two such batteries have a sufficient capacity to provide an initial power of 260 W. Since the two solar array drive mechanisms require less than 15 W to operate, and the control unit requires about 70 W, the batteries still have more than enough power to run the thermal control unit. In addition, the mass of the batteries is only 2 kg without the cabling.

9.6.2 Power Distribution

A spacecraft's power distribution subsystem includes cabling, fault protection, and power switches. This subsystem depends on source characteristics, load requirements, and other subsystem functions. To select a power distribution subsystem, the mass and power losses must be minimized while taking into account the survivability, cost, reliability, and power quality.

Power distribution for SOCM consists of direct current (DC) converters, which control the power switches and provide on-off control to desired loads. Furthermore, these converters require less electronics than alternating current (AC) converters, which would add more mass to SOCM. The load profile of SOCM is the key in the design specification of the power distribution subsystem. The predominant loads of SOCM are the CPU, GPR, CCD camera and telecommunication, which range from 5-270 Vdc. With such range, a standard 28-Vdc power distribution system is chosen for SOCM.

9.6.3 Power Regulation and Control

Power regulation can be divided into two categories: controlling the power source and regulating bus voltage. Controlling electrical power generated by the solar array prevents undesired spacecraft heating. Two main types of power regulating subsystems are the peak-power tracker (PPT) and direct-energy transfer (DET). PPT is a converter that operates in series with the solar array and controls the peak power duration. Because SOCM is in constant exposure to the Sun, there is no peak power duration or low power duration. Thus, using a PPT regulating subsystem would be redundant. A DET converter operates in parallel to the array and shunts the array current away from the subsystem when the load does not need power. In addition, DET requires fewer parts, has lower mass, and provides higher total efficiency at EOL. Therefore, the DET was chosen as SOCM's power regulating subsystem [8].

9.7 ENVIRONMENTAL CONTROL SYSTEM
(Michael Wu)

The purpose of the environmental control system is to regulate and maintain an operating temperature for the electrical and hardware components of the spacecraft. The process of maintaining an operational temperature includes identifying the heat source and locating the radiating panel to dissipate the excess heat. Heat sources include solar radiation and electrical

energy dissipated in the electrical components. The components of the thermal control system are thermal control coatings, thermal insulation, thermostats, and space radiators. Selection of the proper thermal control components is determined by the thermal equilibrium of the SOCM satellite.

9.7.1 Thermal Analysis

The first step in the thermal design process is to determine the payloads' and subsystems' operational temperature limits. Table 9.7 shows the temperature ranges for selected spacecraft components [8].

Table 9.7 Temperature ranges for selected spacecraft components.

Components	Operating Temperatures (°C)
Electronics	–5 to +40
Batteries	5 to 20
Solar arrays	–100 to +100
Propellant (hydrazine)	7 to 35
Structures	-45 to +65

The average temperature, or the equilibrium temperature, is the operating temperature which the thermal control subsystem should maintain for successful operation. Thermal energy is emitted from the electronic components. Radiation energy is determined by the amount of solar flux absorbed by the solar arrays and body surfaces. Because the radiation from Mars is very small, it is neglected when finding the equilibrium temperature for SOCM. The equilibrium temperature for the SOCM satellite is estimated using an energy balance equation that results from the conservation of energy (Fig. 9.10):

$$E_{in} = E_{out} \tag{9.4}$$

$$q_{abs} + q_{gen} - q_{emm} = 0 \tag{9.5}$$

$$A_{so}\alpha_{so}G_s + Q_w - \sigma\varepsilon_{so}A_{so}T^4 = 0 \tag{9.6}$$

$$T = \left(\frac{A_{so}\alpha_{so}G_s + Q_w}{\sigma\varepsilon_{so}A_{so}} \right)^{\frac{1}{4}} = 170 \text{ K} \tag{9.7}$$

where,

A_{so} = area of SOCM body exposed to space = 3.471 m^2

α_{so} = absorbtivity of solar array = 0.04

G_s = solar constant = 592 W/m^2

Q_w = average electrical power dissipation = 30 W

σ = Stefan-Boltzmann constant = 5.67×10^{-8} $Wm^{-2}K^{-4}$

ε_{so} = emissivity of SOCM's outer shell = 0.66

T = equilibrium temperature of SOCM = 170 K

The equilibrium temperature acts as a guideline in selecting the protective material and the radiator size. The type of materials and coatings are discussed in the next section.

9.7.2 Thermal Control Subsystem

The thermal control subsystems are either passive or active (Fig. 9.11). A passive subsystem usually consists of a space radiator thermally coupled to heat dissipating equipment by conductive paths. Active subsystems include pumped-loop systems, heaters controlled by

thermostats, and mechanical refrigerators. A passive thermal control subsystem has been chosen for SOCM because of its simplicity, reliability and self sufficiency. A passive subsystem requires no moving parts, thus has lower mass. Components and devices which are used in SOCM's thermal control subsystem are thermal control coatings, thermal insulation, and a space radiator with controllable louvers.

Thermal control coatings are surfaces with special radiation properties that can provide necessary thermal dissipation. Examples are painted surfaces, high-quality mirrors, and silvered plastics. These coatings have different absorbtivities and emissivities, which can help prevent overheating from solar radiation. For SOCM's outer surfaces (shell), silver-coated teflon material is used to protect the payload and structure from solar radiation. Silver teflon has been used extensively on outer surfaces of spacecraft.

Thermal insulation used extensively to date is multilayer insulation (MLI), which is made up of numerous layers of aluminized mylar separated from each other by lightweight plastic knitting. To protect the inner components of SOCM from solar flux and UV radiation that might conduct through the outer shell, a layer of MLI is used. The MLI forms a layer between the outer satellite surface and the delicate electronic components.

A space radiator is a heat exchanger on the outer surface of a spacecraft that radiates waste heat, Q_W, to space. A space radiator is used on board of SOCM for its ability to modulate the heat dissipation rate to space, and keep the temperature about the equilibrium (152.2 K). This radiator consists of a cold plate and thermal louvers that are opened to space to control the amount of thermal radiation (Fig. 9.11). To maintain SOCM at the equilibrium temperature, the size of the space radiator is 625 cm^2. It is mounted on the side of the SOCM, close to the major heat sources such as the CPU and GPR.

9.8 ORBITAL MECHANICS
(Heidi Schubert)

Three types of orbits were considered for the SOCM satellite: a Halo orbit, a site synchronous orbit, and a Sun synchronous orbit. Parameters considered for choosing an orbit include the ΔV required for orbit insertion, communication with the rover, effectiveness of the gravity gradient stabilization, and effectiveness of the radar.

9.8.1 Orbit Options

A Halo orbit is an orbit around a Sun-Mars libration point [11]. In other words, the satellite is balanced between the gravity fields of the Sun and Mars. The orbit around this point would have a maximum amplitude of 493,000 km and a period of 370 days. The Halo orbit is ideal for Earth-Mars communication, however, it is too far away from Mars for effective surface observation. A Halo orbit is not suited for SOCM's mission, but would be a possibility for a future manned Mars mission to provide nearly constant communication between Earth and Mars.

A Mars site-synchronous orbit (radius = 20,463 km) would be good for communication because the satellite is constantly above the landing site. However, a site-synchronous orbit has other disadvantages. For example, gravity gradient stabilization does not work well at such a high altitude. In addition, the satellite could only survey a small portion of the Martian surface. Hence, the capabilities of the ground penetrating radar and camera would not be put to full use. Also, using a Hohmann transfer from the MLV's parking orbit (apoapsis = 5800 km and periapsis = 3600 km), the ΔV for orbital insertion would be 1500 km/s [8]. The mass of propellant needed for this ΔV is found using the rocket equation.

$$\frac{m_{dry} + m_{prop}}{m_{dry}} = \exp\left(\frac{\Delta V}{I_{sp} g}\right) \tag{9.8}$$

where m_{dry} = dry mass of the satellite = 260 kg

m_{prop} = propellant mass

I_{sp} = specific impulse = 300 s (for bipropellant hydrazine/ N_2O_4)

g = acceleration of gravity at Earth = 9.81 m/s^2

Thus a ΔV of 1500 m/s would require approximately 200 kg of propellant for orbital insertion. Because this would almost double the mass of SOCM, the mass penalty for a Mars synchronous orbit is too high.

A Sun-synchronous orbit is inclined to keep the orbital plane at a constant angle with respect to the Sun (Fig. 9.12). This orbital variation is accomplished by matching the variation in the right ascension of the ascending node of SOCM's orbit to Mars's motion around the sun (Fig. 9.13). Therefore, the satellite continuously sees the Sun, providing a constant power source. A Sun-synchronous orbit is almost polar, thus most of the planet's surface is covered by the satellite's camera and ground penetrating radar. Also, a Sun-synchronous orbit can be a low altitude circular orbit which is ideal for gravity gradient stabilization and the ground penetrating radar. For these reasons, a Sun-synchronous orbit was selected for this mission.

9.8.2 ORBIT CALCULATIONS

The gravity gradient stabilization requires a circular orbit. Also, gravity gradient stabilization works better for a low altitude orbit because the gravity field and its gradient are stronger at low altitude. Furthermore, in a low altitude orbit the ground penetrating radar and the camera have a closer view of the Martian surface. For these reasons, and to be consistent with the aerobraking scenario (Chapter 5), the altitude of the orbit was set at 580 km. The following equation calculates the period given the orbital radius [8].

$$TP = \sqrt{\frac{4\pi^2 r^3}{\mu_{Mars}}} \tag{9-9}$$

where: TP = orbital period

μ_{Mars} = gravitational constant of Mars = 42, 830 km^3 / sec^2

r = orbital radius

With r = 3960 km, the period is 126 minutes. At this altitude, SOCM makes 11.7 orbits per day.

For a sun-synchronous orbit, a nodal precession rate of 0.526°/day will match Mars' rotation rate about the Sun. The following equation is used to match the change in right ascension of the ascending node with the rotation rate of Mars about the Sun (Fig. 9.13) [8]:

$$\dot{\Omega} = -\frac{3}{2} J_2 \left(\frac{R_{mars}}{a}\right)^2 \left(\frac{\mu_{mars}}{a^3}\right)^{\frac{1}{2}} \cos i \left(1 - e^2\right)^{-2} \tag{9.10}$$

where: $\dot{\Omega}$ = rate of change in right ascension of ascending node

i = inclination of orbit

e = eccentricity of orbit

R_{Mars} = equatorial radius of Mars = 3380 km

J_2 = potential coefficient for Mars = 0.001964

a = semi-major axis

Solving for i,

$$i = \cos^{-1}\left[-\frac{2}{3}\frac{\dot{\Omega}}{J_2}\left(\frac{a}{R_{Mars}}\right)^2\left(\frac{a^3}{\mu_{Mars}}\right)^{\frac{1}{2}}\right]\left(1-e^2\right)^2 \tag{9.11}$$

With an altitude of 580 km, the inclination required for a sun-synchronous orbit is 86.6°. This orbit is nearly polar, which has the added advantage of giving SOCM coverage of almost all of the Martian surface. Thus the GPR and camera observe the largest possible surface area of Mars [12].

SOCM separates from the MLV after the second aerobrake pass through the Martian atmosphere (see Chapter 5). At apoapsis of the MLV orbit, the altitude of the spacecraft is 580 km and the velocity is 3.2 km/s. The satellite deploys from the MLV and burns to circularize its orbit (see Fig. 5.2) The following equations determine the necessary ΔV needed at apoapsis of the MLV orbit to circularize into SOCM's orbit.

$$V_{cs} = \sqrt{\frac{\mu_{Mars}}{r}} \tag{9.12}$$

$$\Delta V = V_{cs} - V_a \tag{9.13}$$

where: V_{cs} = circular velocity

V_a = velocity at apoapsis of MLV orbit

Therefore ΔV = 110 m/s.

To perform this ΔV, SOCM burns its four monopropellant hydrazine control thrusters simultaneously. Two of the thrusters are attached to the end of the extendible boom, and the other two thrusters are attached to the main body. To find the total propellant necessary for

SOCM's lifetime, an additional 50 m/s was added to the ΔV to account for attitude adjustment and orbital maintenance. Using an I_{sp} of 235 s, the propellant mass needed is 20 kg (Eq. 9.8).

9.9 ATTITUDE DETERMINATION AND CONTROL
(Amber Koch)

Attitude control is very important to the success of SOCM's mission. The purpose of SOCM's attitude control system is to not only place and maintain SOCM in the proper orbital configuration, but also to position the payload for optimal use. Therefore, the control system is designed to meet SOCM's mission requirements. In addition, the attitude control system must be designed as light and efficient as possible.

The attitude of a satellite (the spacecraft's orientation in space) changes as it experiences adverse torques. There are two types of torques: control torques and disturbance torques. While disturbance torques are unintentional environmental disturbances, control torques are intentional torques used for changing spacecraft attitude. Attitude and control systems consist of the following: attitude sensors which determine where the spacecraft is, computer implemented control laws which determine when and what control is needed, and control hardware or actuators which supply the needed control torques. Appropriate attitude sensors and control hardware were chosen for SOCM in both the undeployed and deployed configuration.

The first job of the attitude control system is to place SOCM in an operational orbit, the orbit from which the satellite operates for the duration of the mission. This requires active three-axis control using attitude sensing and control devices. Sun sensors provide attitude sensing by defining a single position vector in reference to the Sun. The accuracy of available Sun sensors varies from 0.005° to 3°, while their masses vary from 0.25 kg to 20 kg. The maximum power required to operate available Sun sensors is only 3 W. SOCM has two Sun sensors, one is located on the main satellite body, while another is located on the solar array system. Each sensor has a mass of 1.5 kg and a power requirement of approximately 1 W [8]. Sun sensors are

available off-the-shelf from the following companies: Adcole, TRW, and Ball Aerospace. Sun sensors provide satisfactory attitude determination for the mission while hydrazine thrusters provide three-axis control torques. Hydrazine thrusters with performance ranges from 0.5 N to 1,000 N are available off-the-shelf through Olin/Rocket Research and Hamilton Standard. SOCM's hydrazine thrusters have an I_{sp} of up to 230 s, a nominal thrust of 2.22 N, and a mass of 0.2 kg [8].

Once placed in operational orbit, SOCM's control method becomes quasi-passive. In essence, the primary control system is the passive gravity gradient method, however the three-axis thruster system is used intermittently for orbital maintenance. Three main advantages of using this type of control method are payload orientation towards surface, low power, and low propellant requirements for attitude control. This method results in a Mars-pointed orientation of the satellite (Fig. 9.14). The satellite utilizes the planet's gravity field to maintain a nearly fixed attitude directed to nadir and the orbit normal (Fig. 9.15) Thus the payload is always facing the planet's surface. Power is only required to position the low-gain antenna and solar arrays, operate the payload, and occasionally adjust the satellite attitude. In contrast, other control methods require power and propellant for attitude control at nearly all times. The typical range of performance for small satellites using this method of control is $\pm 5^{\circ}$ [8,13].

The success of the attitude control system for SOCM is highly dependent upon what type of environmental disturbances the craft might encounter. Three main environmental disturbances are aerodynamic, magnetic, and gravity gradient. The influence that each of these disturbances has on the satellite is highly dependent on the altitude of the satellite above the planet. For instance, SOCM uses the effects of gravity gradient for stability and control, which requires a lower orbit. SOCM feels the largest environmental torque from the gravity gradient, and the aerodynamic drag and magnetic torques are negligible in comparison.

In order for the gravity gradient control method to work effectively, several conditions must be met for satellite stability. The conditions for stability are based on the moments of

inertia of the satellite I_X, I_Y, and I_Z about the satellite's three axes [14] (See Fig. 15). I_X , I_Y, and I_Z for SOCM's final configuration are:

$$I_X = I_Y = 1270 \text{ kg-m}^2$$
$$I_Z = 35.5 \text{ kg-m}^2$$

One condition for stability of SOCM is that the gravity gradient torque must be the largest of the environmental torques experienced by the spacecraft. The minimum moment of inertia should be around the yaw axis (I_Z) to ensure that SOCM rotates properly (See Fig. 9.14), which SOCM satisfies. In addition, the following condition must be met for stability [13].

$$4\sqrt{\sigma_X \sigma_Z} \leq 3\sigma_X + 1 + \sigma_X \sigma_Z \tag{9.14}$$

where

$$\sigma_X = \frac{(I_Y - I_Z)}{I_X} \tag{9.15}$$

$$\sigma_Y = \frac{(I_X - I_Z)}{I_Y} \tag{9.16}$$

$$\sigma_Z = \frac{(I_Y - I_X)}{I_Z}. \tag{9.17}$$

The stability condition for SOCM results in RHS = 3.98 and LHS $\approx$ 0 in Eq. 9.14. This satisfies the stability condition for gravity gradient control.

9.10 CONCLUSION
(Heidi Schubert)

In conclusion, SOCM is another benefit of the use of *in situ* propellant production in Project Hyreus. Using indigenous propellant allows a medium-sized satellite to be included in the sample return mission. Thus, SOCM is not just a communications satellite but also a water/ice locator and weather station. Neither the Mars Observer or any other planned future Mars missions have a ground penetrating radar to locate ice deposits on the Martian surface. If SOCM's GPR is successful in finding subsurface ice on Mars, future piloted missions will be able to use such a resource for survival and perhaps for long term settlement.

SOCM is also necessary for support of Mars surface operations. The satellite's weather monitoring system is critical for warning the rover of impending dust storms, thus ensuring that the rover remains operational throughout the entire mission. The MLV-SOCM-SPOT communications link allows the rover to venture farther than would be possible without a satellite.

NOMENCLATURE

a	Semi major axis
AC	Alternating Current
A_{sa}	Area of solar arrays
A_{so}	Total surface area of satellite
BOL	Beginning of Life
CCD	Charge Couple Device
CPU	Central Processing Unit
DC	Direct Current
DET	Direct Energy Transfer
DSN	Deep Space Network
e	Eccentricity of orbit
EOL	End of Life
f	Effective fraction of array area
g	Acceleration of gravity
GPR	Ground Penetrating Radar
G_S	Solar constant
HGA	High Gain Antenna
i	Inclination of orbit
I_{sp}	Specific impulse
I_x	Moment of inertia about x-axis
I_y	Moment of inertia about y-axis
I_z	Moment of inertia about z-axis
J_2	Gravitational potential coefficient at Mars
LGA	Low Gain Antenna
M_a	Mass of solar arrays

MLI	Multi Layer Insulation
MLV	Mars Landing Vehicle
M_{prop}	Propellant mass
P	Power required for operation
PPT	Peak Power Tracker
P_{sa}	Power generated by solar arrays
Q_W	Electric power dissipation
r	Orbital radius
R_{Mars}	Equatorial radius at Mars
RTG	Radioisotope Thermal Generator
SOCM	Satellite for Observation and Communication at Mars
SP	Specific performance
SPOT	Surface Planetary Observation Transport
T	Equilibrium temperature of SOCM
TP	Orbital period
V_a	Velocity at apoapsis of MLV orbit
V_{cs}	Circular velocity
ΔV	Change in velocity
X	Efficiency of path from solar array
Esa	Emissivity of solar array
η	Solar array efficiency
μ_{Mars}	Gravitational constant of Mars
σ	Stefan-Boltzmann constant
θ	Inclination between solar panel and solar vector
$\dot{\Omega}$	Rate of change in right ascension of ascending node

REFERENCES

1. Cantafio, L. J., *Space-based radar handbook*, Artech House, Norwood, MA.,1989.

2. LtCol. P. R., *Executive Overview, Clementine*, Naval Research Laboratory, Washington D.C.

3. Oswald, G. K. A., "Geophysical Radar Design," *IEE Proceedings-F*, Vol. 135, 1988, p. 371.

4. Smith, S., Personal communication, Geophysical Survey System Incorporated, May 1993.

5. Waters, P. et al., "Applications of Remote Sensing to Ground water Hydrology," *Remote Sensing Reviews*, Vol. 4, Issue 2, 1990, p. 256.

6. Nicollin, F. et al., "An HF Bi-Phase Shift Keying Radar: Application to Ice Sounding in Western Alps and Spitsvergen Glaciers," *IEEE Transactions on Geoscience and Remote Sensing*, Vol. 30, 1992, pp. 1025-1032.

7. *Magellan, The Unveiling of Venus*, NASA -CR-185018, Jet Propulsion Laboratory, 1989.

8. Larson, W. and Wertz, J., *Space Mission Analysis and Design*, Kluwer Academic Publishers, Dordrecht, The Netherlands, 1991, p.141.

9. *Mariner-Venus 1967, Final Project Report*, NASA SP-190, U.S. Government printing office, Washington D.C., 1971.

10. Chetty, P.R.K., *Satellite Technology and Its Applications*, Tab Books Inc., Blue Ridge Summit, PA., 1988, p. 220-225.

11. Henry, D. and Jones, T., "Design of an Earth-Mars Communication Network Using Two Spacecraft in Halo Orbits Near Mars," AIAA paper No. 92-0136, 1992.

12. *The Astronomical Almanac*, U.S. Government Printing Office, 1992, p. E88.

13. Wertz, J. R., *Spacecraft Attitude Determination and Control*, D. Reidel Publishing Co., Dordrecht, Holland, 1978, Ch. 1, 5.

14. Beer, F. P. and Johnston E.R., *Vector Mechanics for Engineers-Statics*, 5th Ed., McGraw Hill Book Co., U.S.A. 1988, Ch. 3.

15. *Project Minerva: A Low Cost Manned Mars Mission Based on Indigenous Propellant Production*, Final Report, AA420/421 Space System Design, NASA/USRA Advanced Design Program, Department of Aeronautics and Astronautics, University of Washington, Seattle, WA, June 1992.

16. Redd, F. J. et al. *Copernicus Lunar Surface Mapper*, Utah State University, Logan, UT., 1991-1992

17. Randolph, J. E., "Mars Rover Sample Return Orbiter Design Concepts," AIAA paper No. 89-0421, 1989.

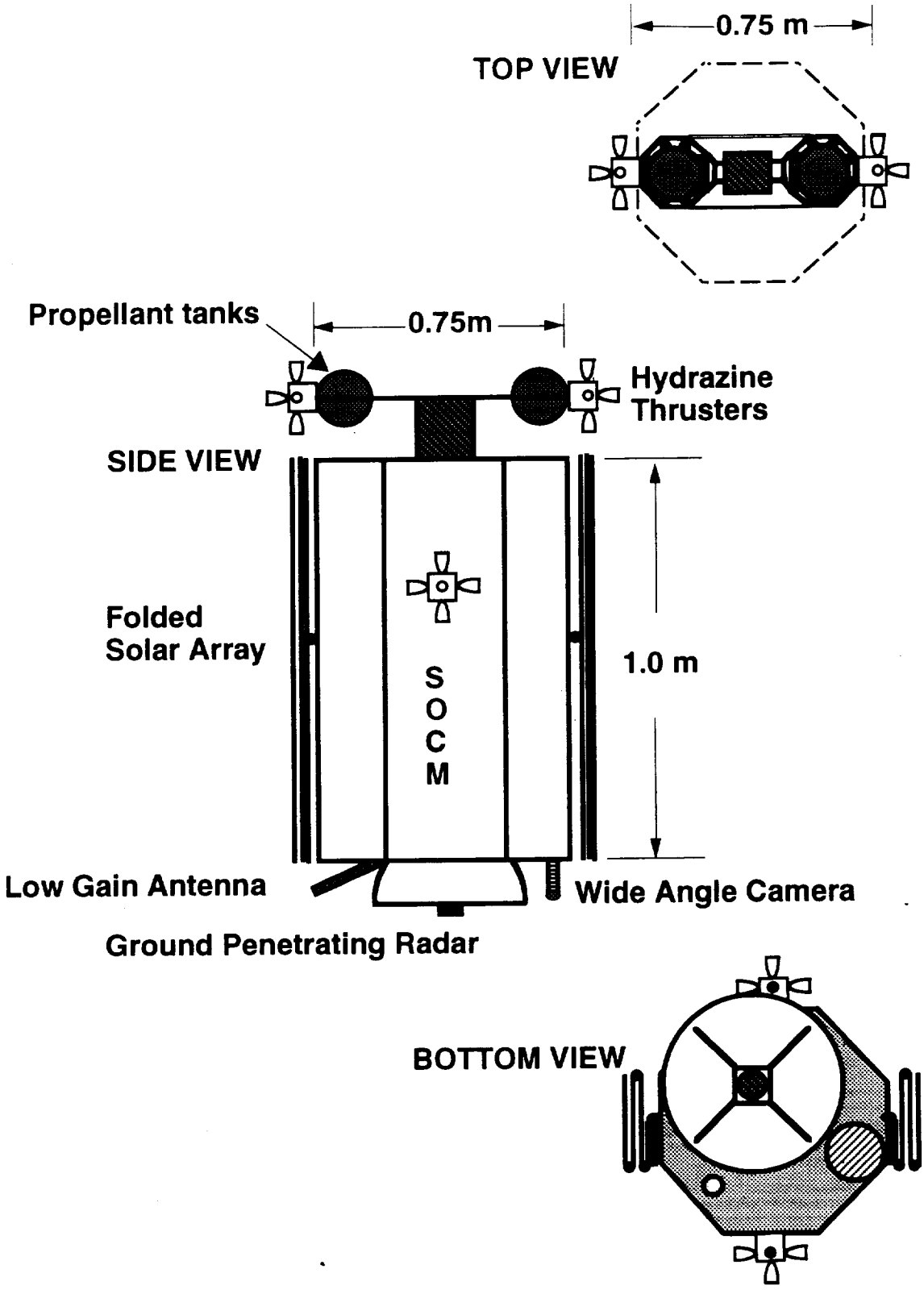

Fig. 9.1 Initial stored configuration of SOCM satellite.

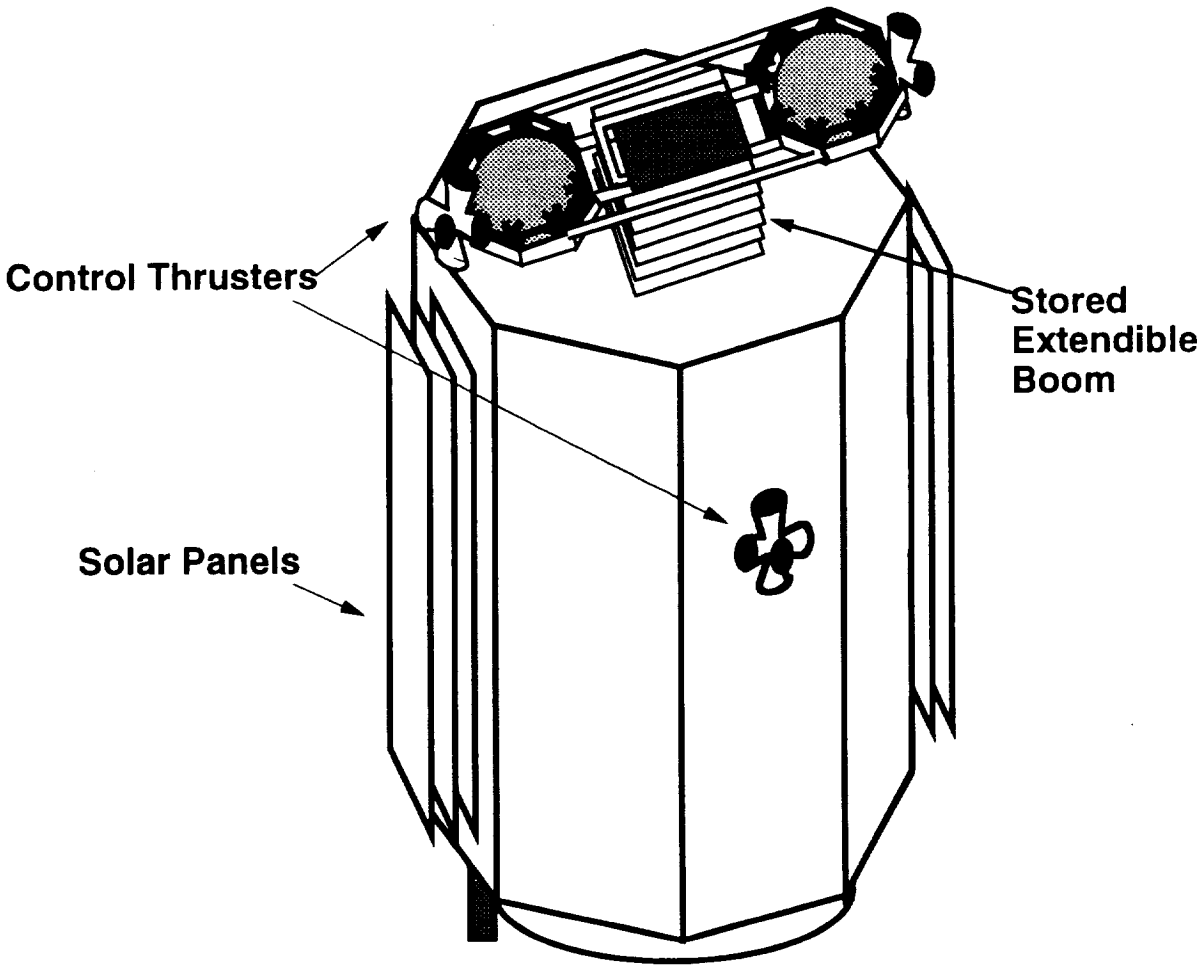

Fig. 9.2 Isometric view of initial configuration of SOCM, as stored in the MLV and during its orbital transfer.

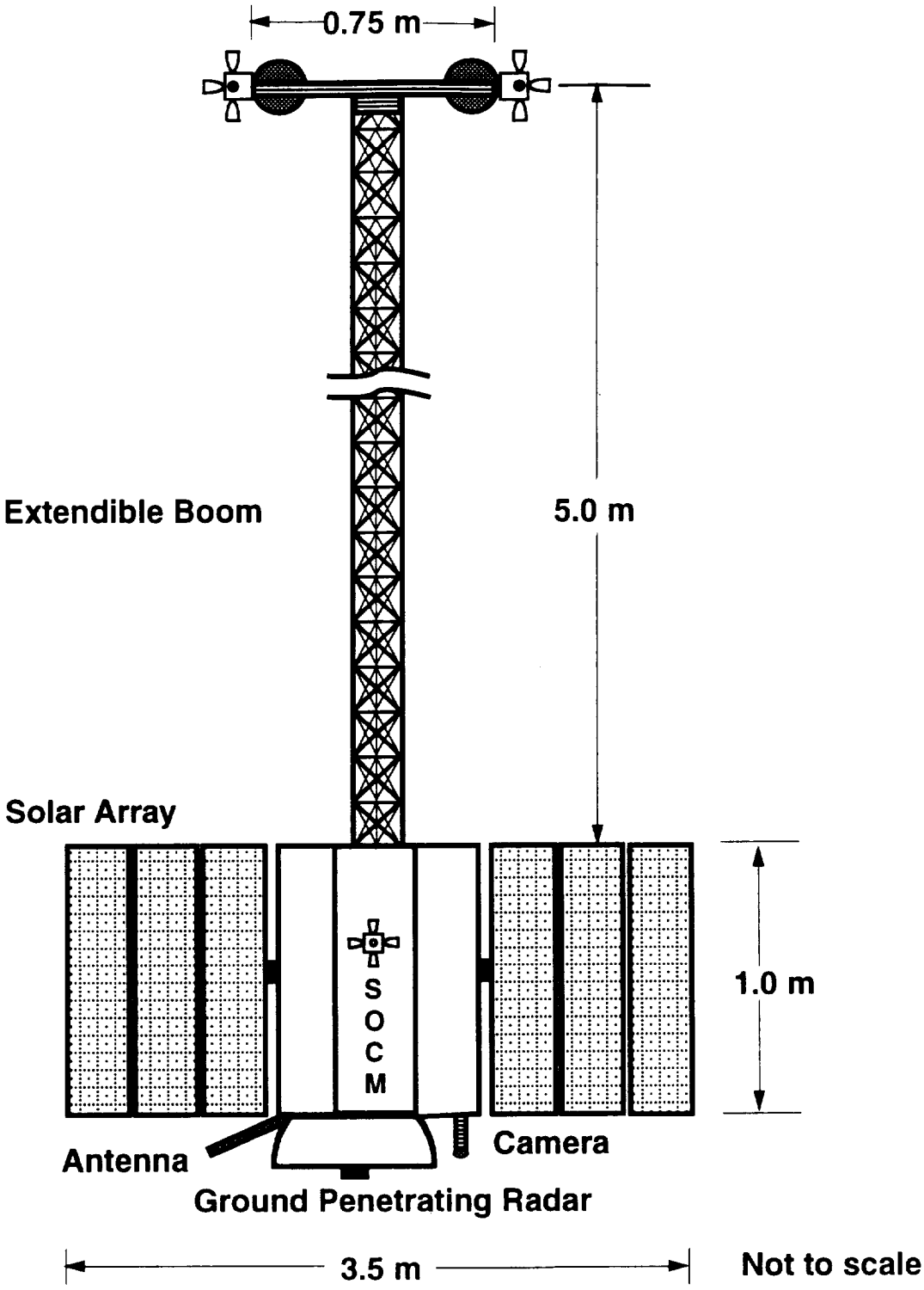

Fig. 9.3 Deployed configuration of SOCM satellite.

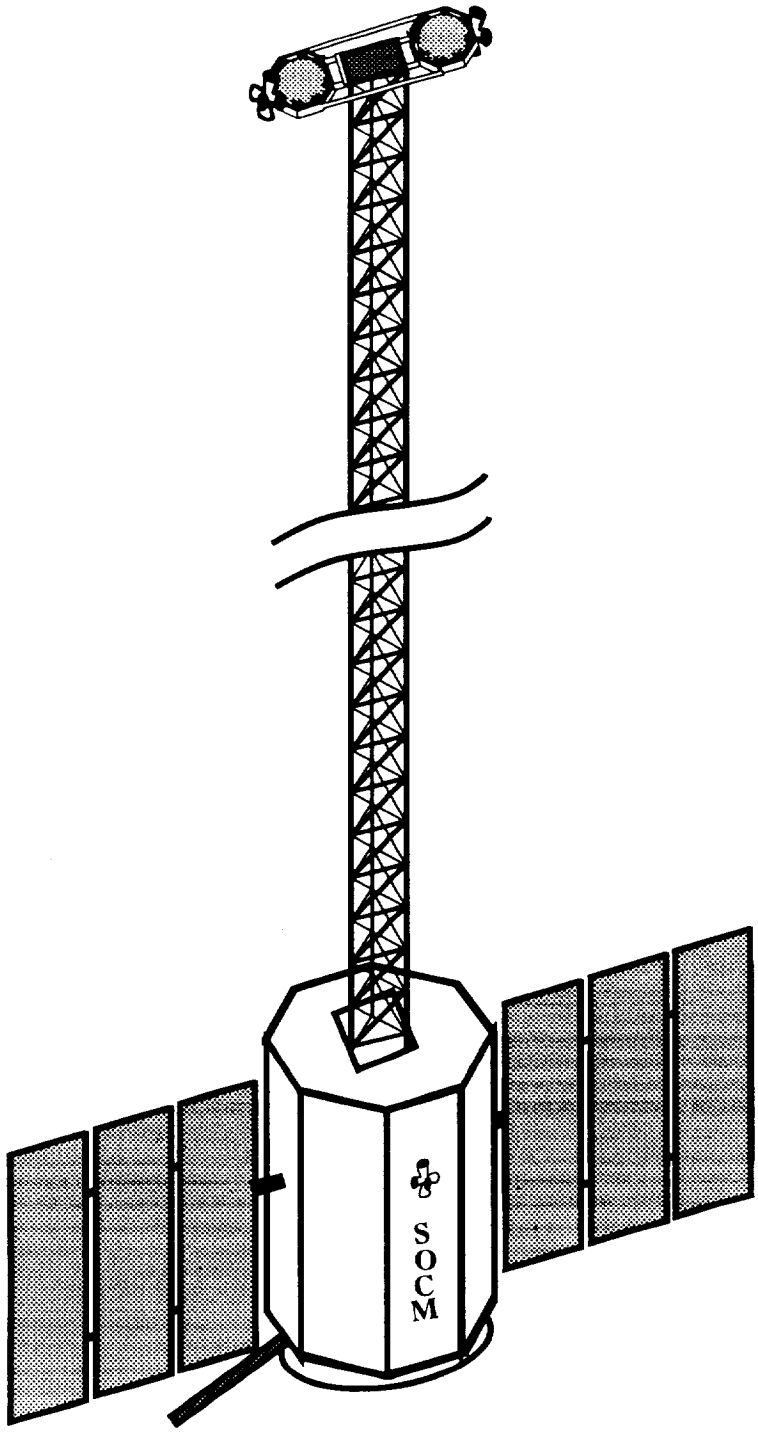

Fig. 9.4 Isometric view of deployed configuration of SOCM satellite.

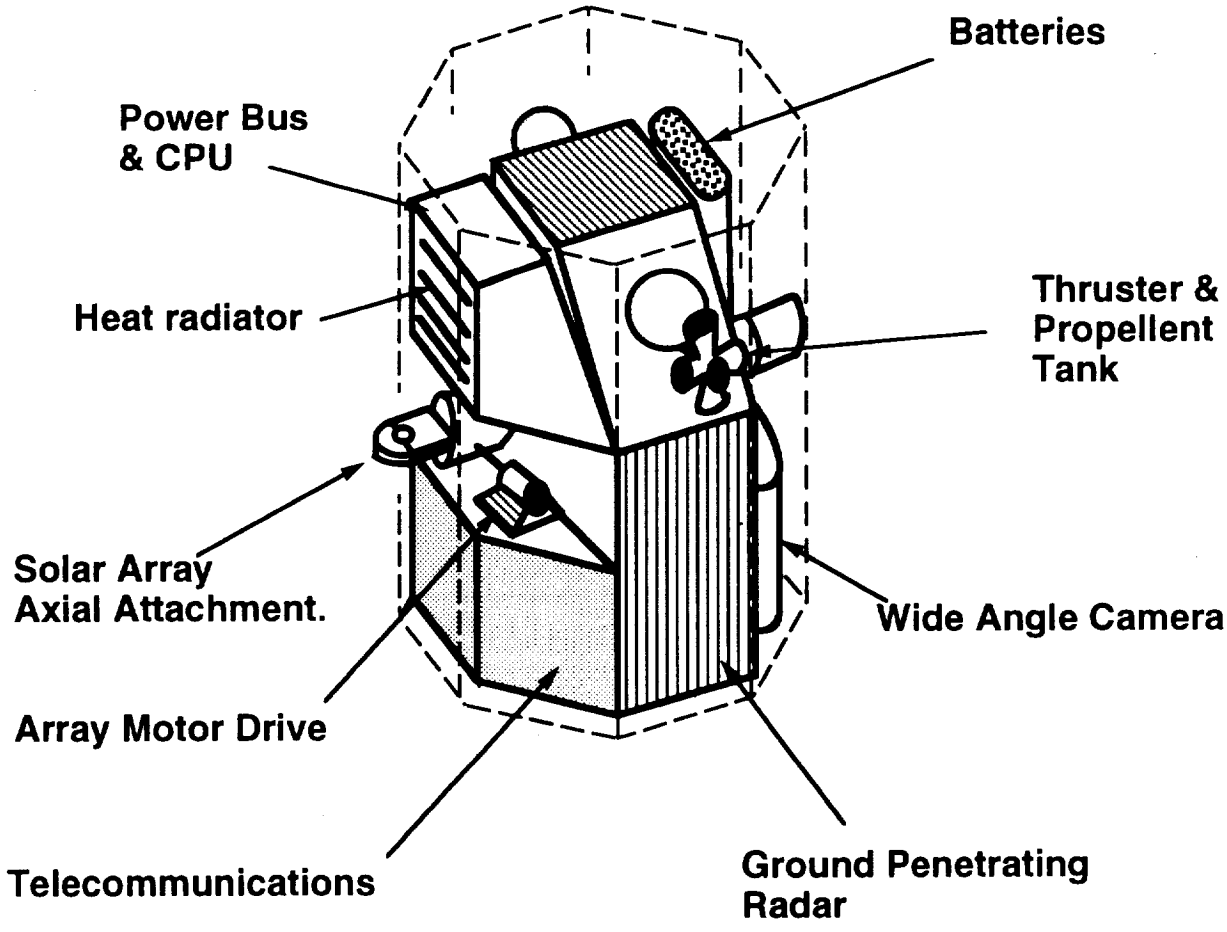

Fig. 9.5 Layout of payload inside SOCM.

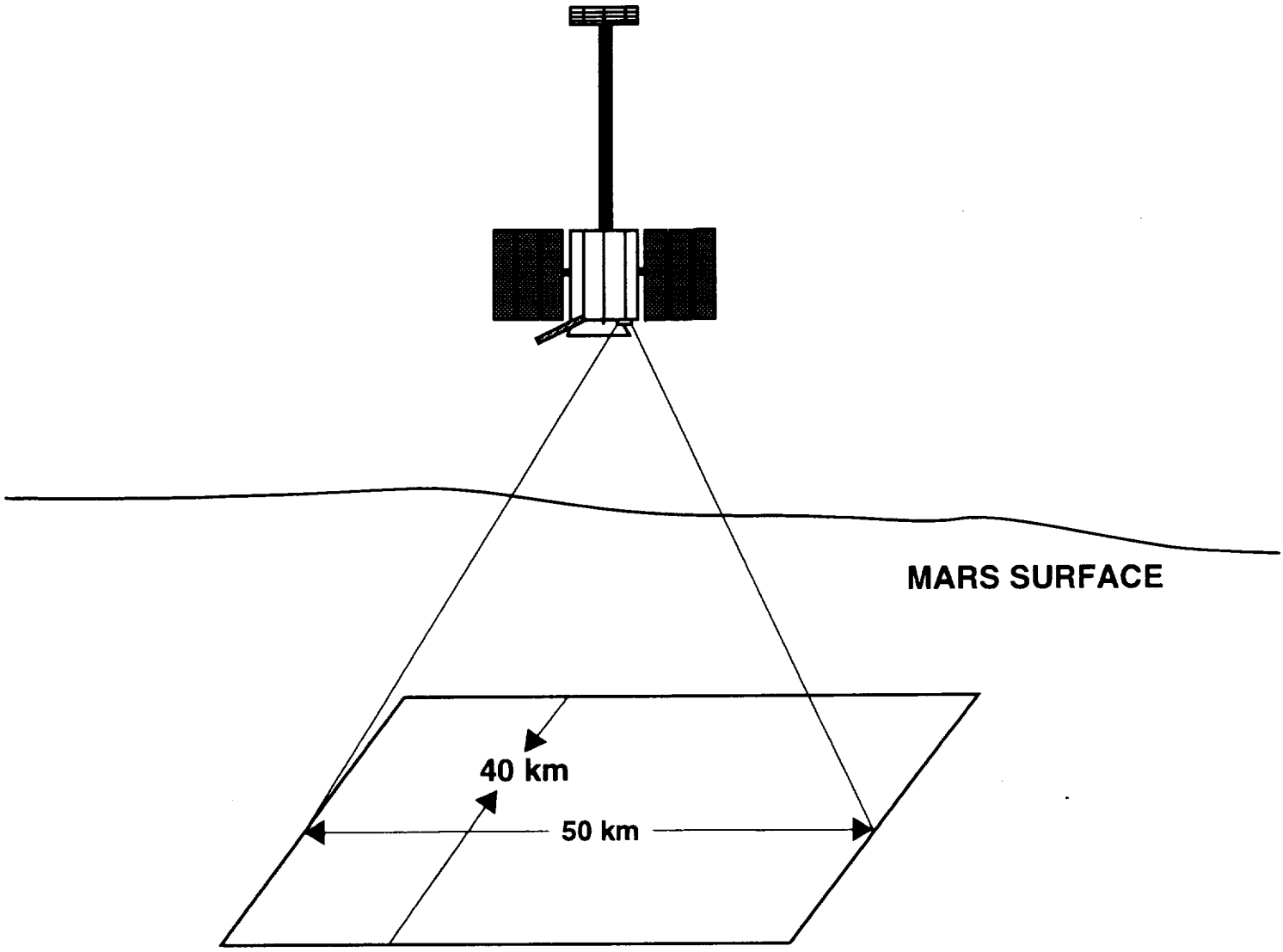

Fig. 9.6 Camera ground coverage.

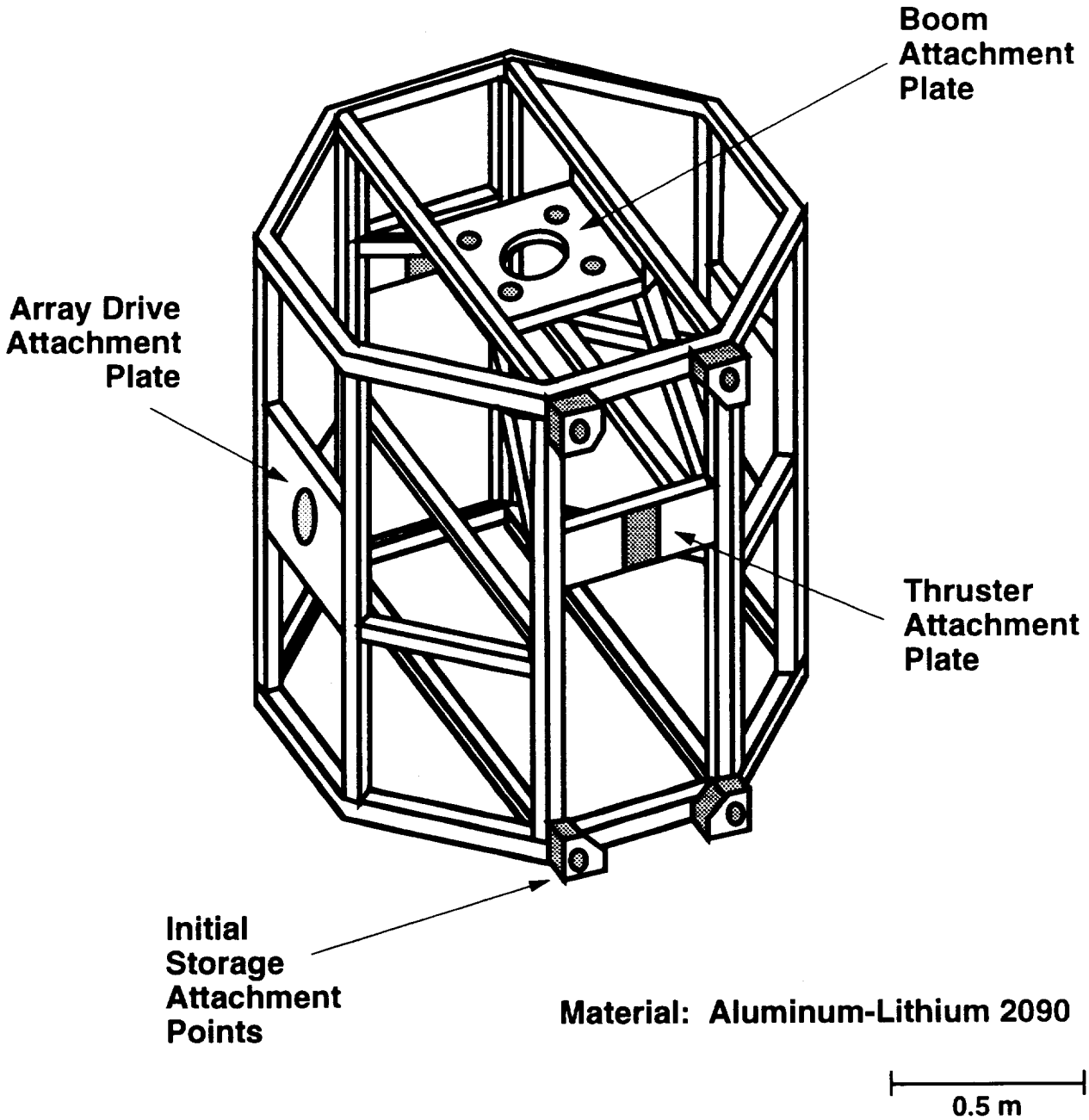

Fig. 9.7 SOCM structural layout.

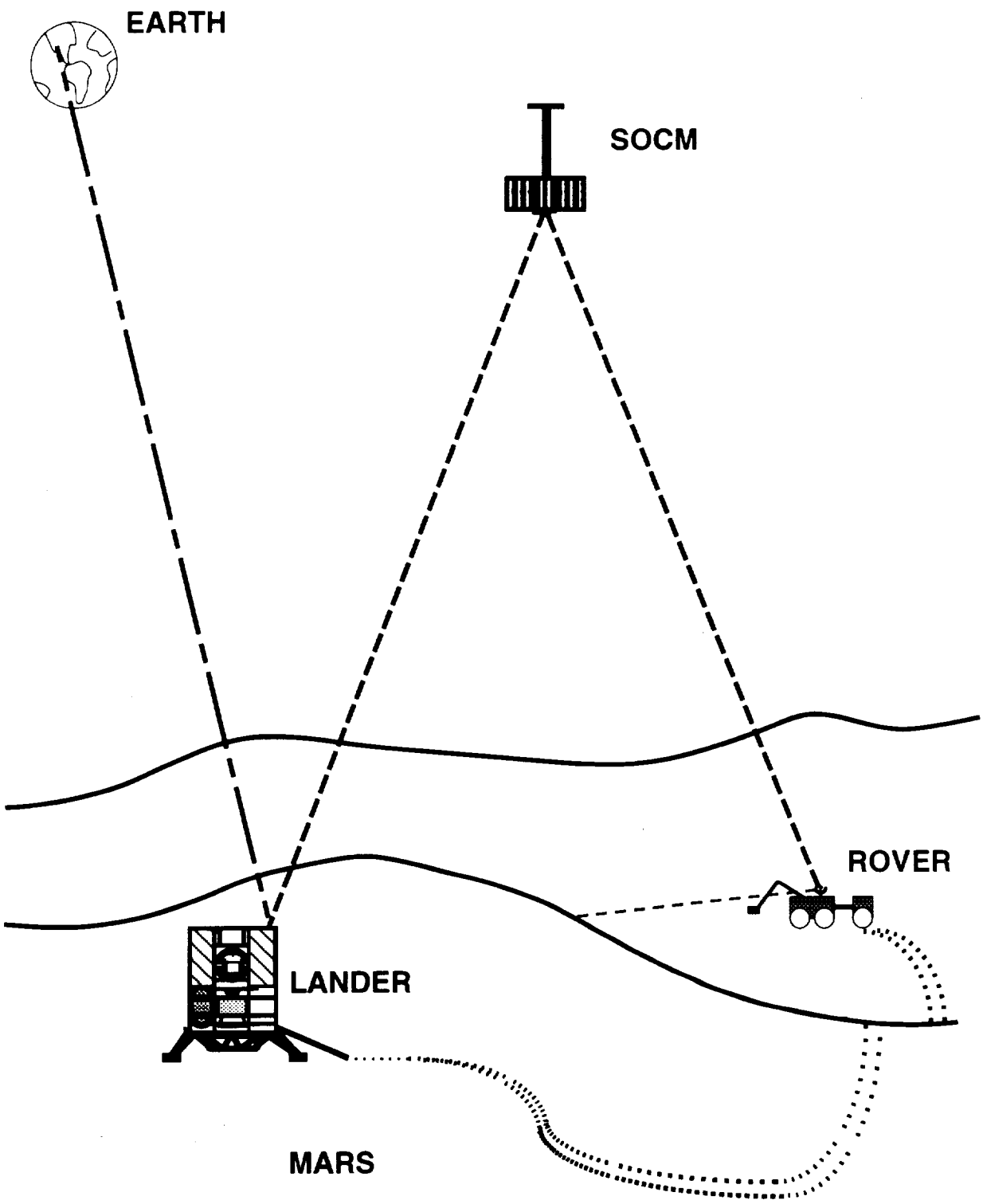

Fig. 9.8 Earth/Mars communications architecture

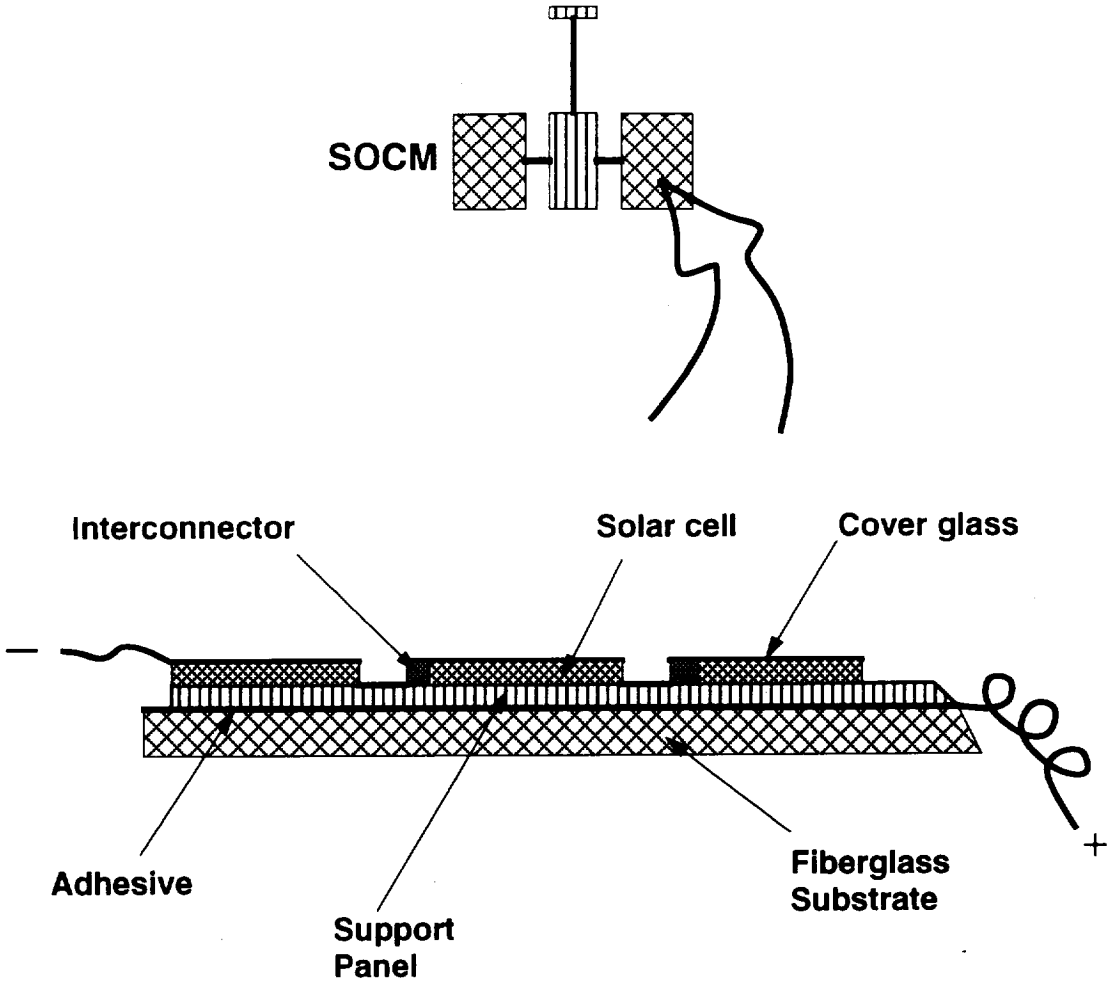

Fig. 9.9 SOCM flat type solar array mounting.

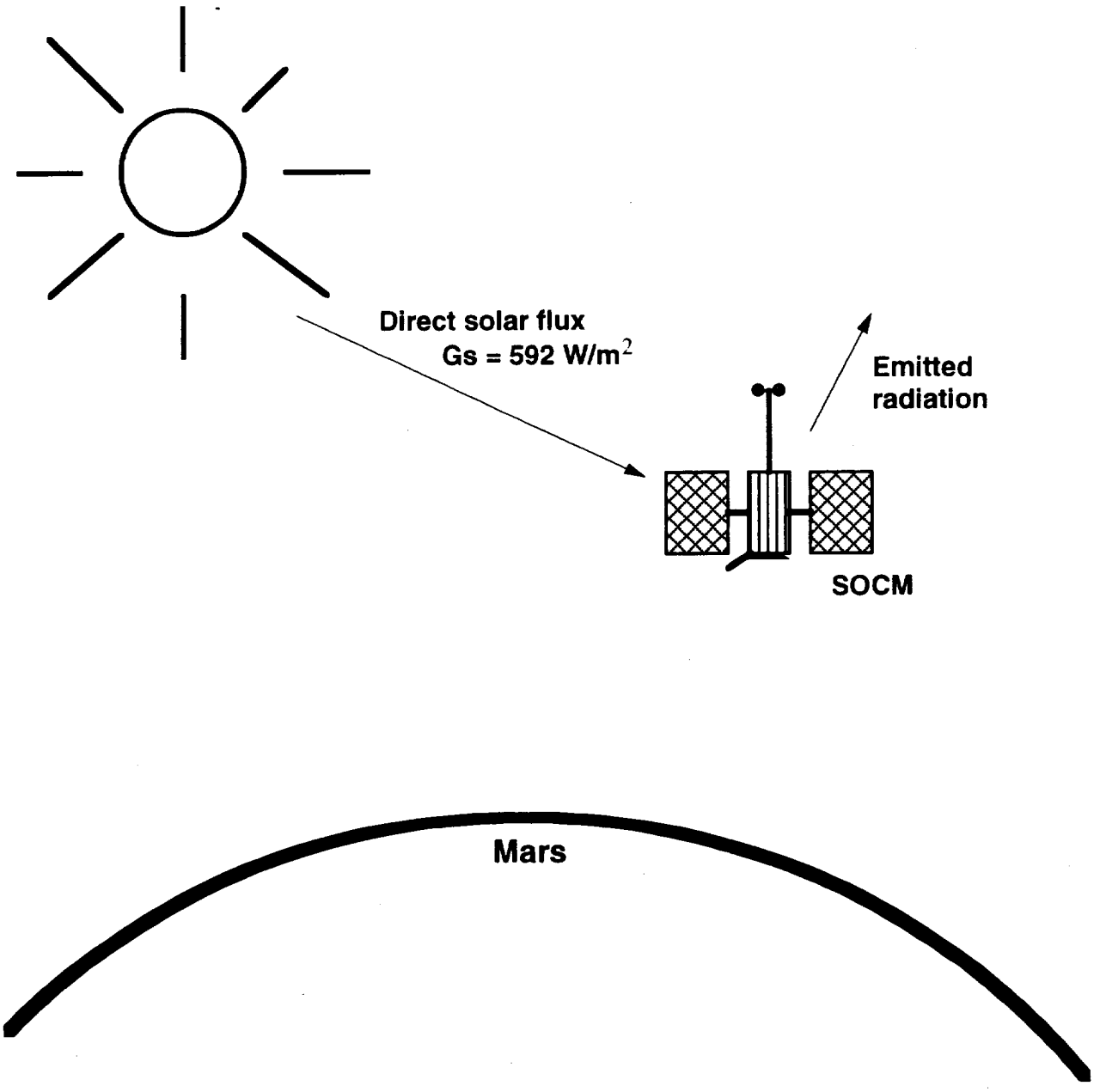

Fig. 9.10 Thermal-radiation environment for SOCM.

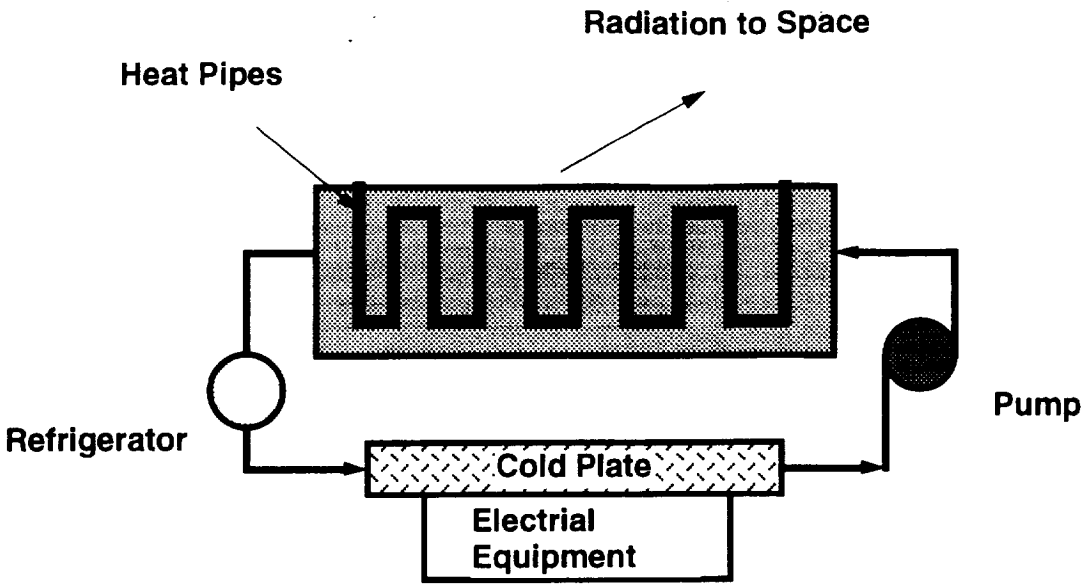

Active Thermal Control

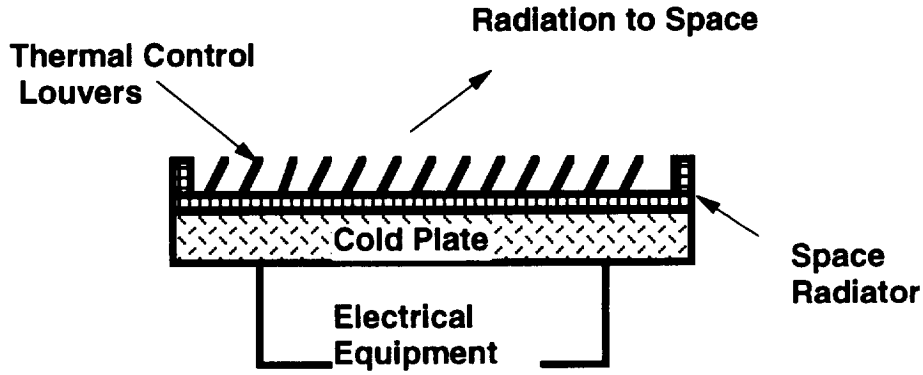

Passive Thermal Control

Fig. 9.11 Schematics of active and passive thermal control subsystems.

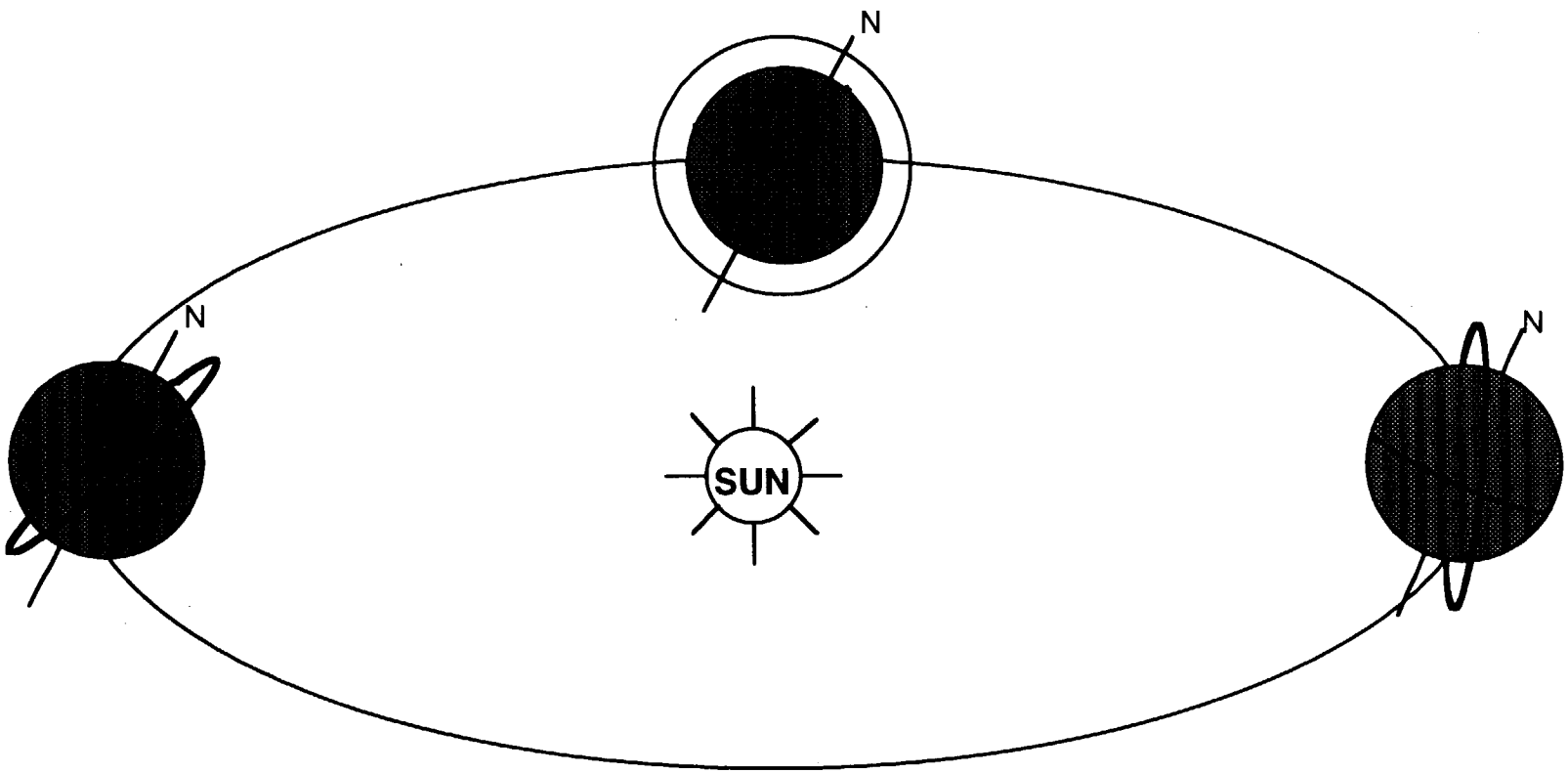

Fig. 9.12 Sun synchronous orbit

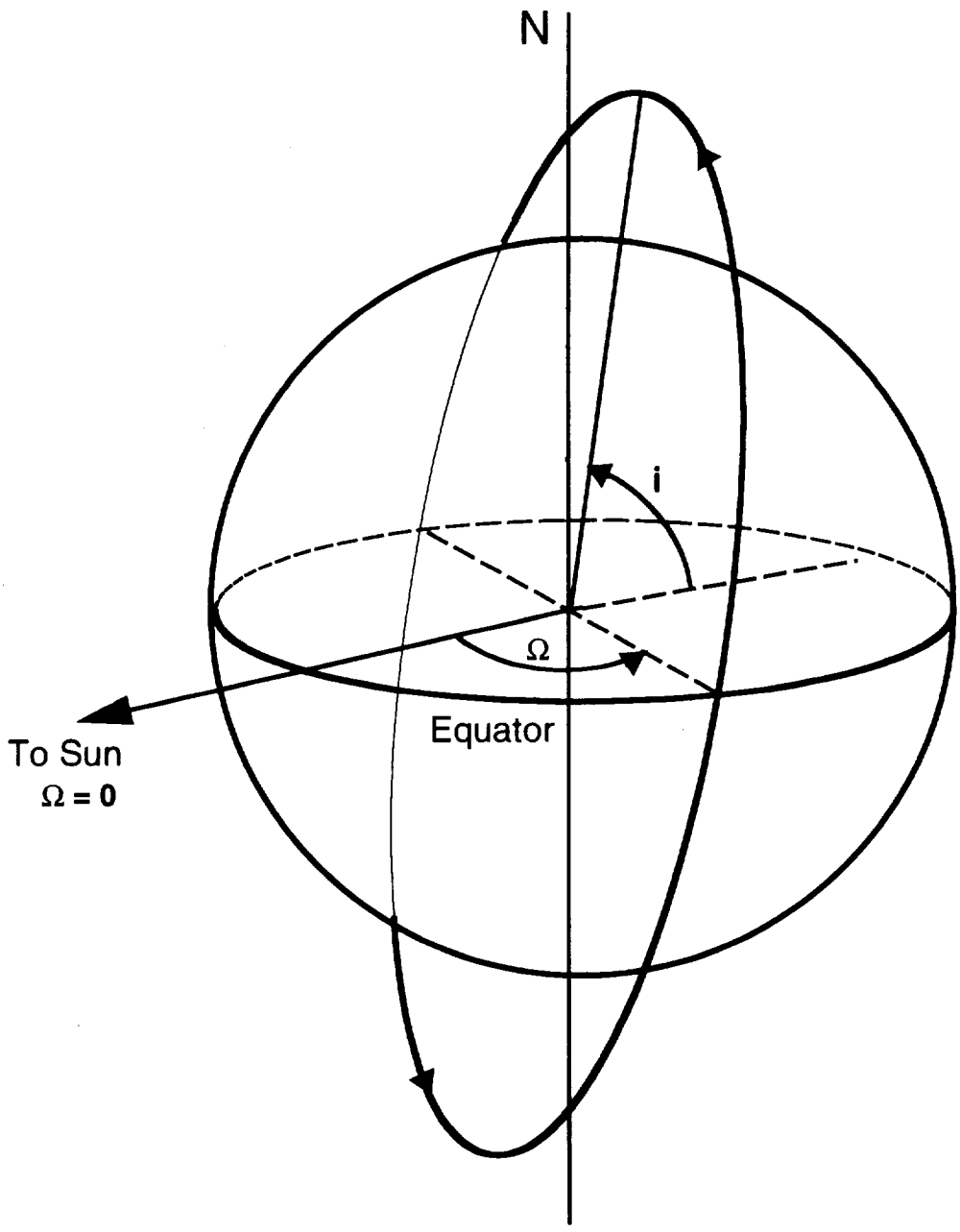

Altitude = 580 km
Period = 126 minutes
Inclination, i = 87°
Nodal precession rate, $\dot{\Omega}$ = 0.526°/day
Ω = 90°

Fig. 9.13 SOCM's Sun synchronous orbit.

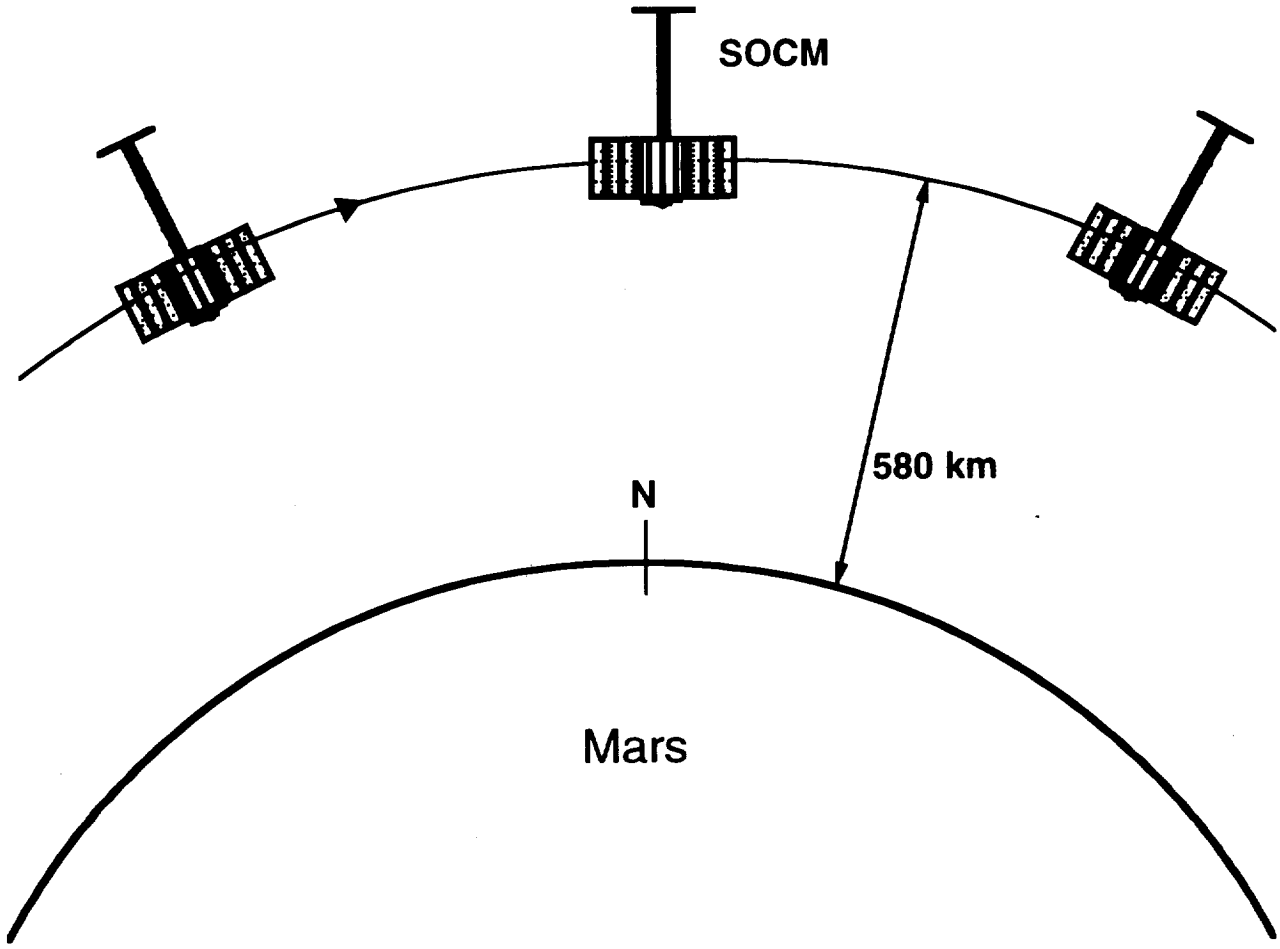

Fig. 9.14 SOCM's final operational orbit configuration.

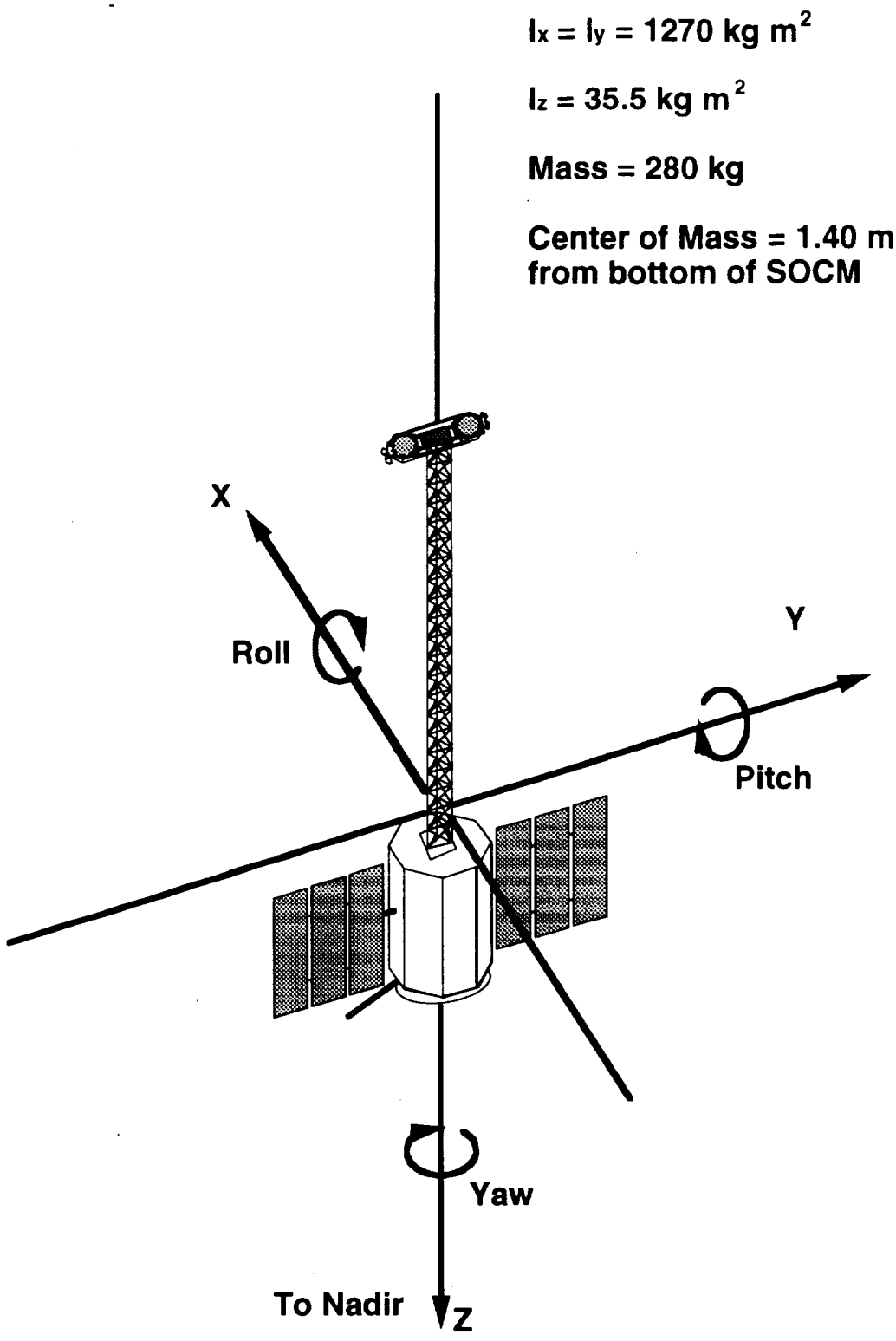

Fig. 9.15 SOCM attitude and orientation.

10.0 EARTH RETURN

Heather Nicholson

Laurie Nill

Heidi Schubert

Richard Warwick

TABLE OF CONTENTS

10.1 INTRODUCTION 10.1

10.2 EARTH RETURN SCENARIO 10.1

10.3 SAMPLE RETURN CAPSULE DESIGN 10.3

10.4 AEROBRAKING AT EARTH 10.4

REFERENCES 10.6

FIGURES 10.7

10.1 INTRODUCTION

(Richard Warwick)

A description of the Earth return scenario as well as the sample return capsule (SRC) is presented here. The samples must be stored at near Mars' ambient conditions. Mars launch and Earth aerocapture are described. In addition, SRC retrival and quaruntine matters are considered.

10.2 EARTH RETURN SCENARIO

Shortly before the launch window for return to Earth opens, the propellant plant ceases operation and the last samples are loaded aboard the ERV. When the launch window opens, the methane ascent engine ignites and the ERV lifts off the Martian surface.

Upon achieving a low Mars orbit of 300 km altitude, the ERV coasts until it reaches the burn point for the interplanetary transfer orbit injection. The methane engine fires again and boosts the ERV through the velocity increment required to send it to Earth. Once the ERV is in transit to Earth, the vehicle orients itself so that the small aerobrake on the Earth return capsule shades the sample container. This maneuver alleviates the need for a large and elaborate refrigeration system that would otherwise be required to reject the heat from the sample canister due to the solar flux. Temperature control is essential for maintaining Mars ambient conditions, in order to preserve the state of volatile components of the samples. The ΔV budget for the Mars launch and Earth return is given in Table 10.1.

When the ERV nears Earth, the Earth return capsule, which consists of the sample canister, an ablative aerobrake and a small control system, detaches from the rest of the ERV. The ERV then performs a contamination and collision avoidance maneuver (CCAM) which

moves it away from the Earth return capsule. During the CCAM, the ERV reorients itself so that the thrust vector is away from the Earth return capsule, yet the exhaust does not impinge on the capsule. The appropriate RCS thrusters fire to depletion and the ERV coasts away from the capsule for a brief time. When the ERV is a safe distance from the Earth return capsule, the remaining primary propellants are burned in the main engine. This should provide the small boost required to prevent the ERV from re-entering the Earth's atmosphere and burning up. The ERV will swing by Earth in a hyperbolic orbit and continue out to deep space.

Table 10.1 ΔV budget for Mars launch (m/s).

Velocity at parking orbit insertion	3412
Velocity penalty due to drag	< 5
Velocity penalty due to gravity	146
Transfer Orbit Injection ΔV	2693
ΔV gain from Mars rotation	– 232
TOTAL	6,024

The Earth return capsule, now powered by internal batteries, re-enters the Earth's Atmosphere at an entry angle of 11.8° and an entry velocity of 11.2 km/sec, using an Apollo style ablative heat shield for the aerocapture pass. The aerobraking pass will decelerate the capsule to a velocity of 7.8 km/sec. Once the aerobrake maneuver is completed, the orbit is circularized with a ΔV of 490 m/sec by a monopropellant thruster, and the capsule is reoriented to shade the sample container from sunlight. The container then awaits retrieval by the Space Shuttle in the circular orbit at an altitude of 340 km. As an alternative, the capsule could be picked up at either Space Station Freedom or Mir, provided one of them is in orbit at the time. Preliminary analysis of the samples can be conducted in orbit to

determine if they pose any danger. If deemed safe, the samples will be returned to Earth. If for some reason the decision is made not to return the samples to Earth's surface, the samples can either be sterilized and disposed of or the sample container can be attached to a Payload Assist Module (PAM) and boosted to a quarantine orbit or back into deep space.

10.3 SAMPLE RETURN CAPSULE DESIGN

(Laurie Nill, Heidi Schubert, Richard Warwick)

The sample return capsule consists of the sample containers, a heater/refrigerator unit, batteries, an ablative aerobrake, a monopropellant thruster to circularize the LEO, and a small, low gain antenna and controls unit. Figure 10.1 shows the layout of the SRC. The hydrazine monopropellant engine used to circularize the orbit in LEO is a Marquardt R-30B, which has an Isp of 228 sec. The engine and two propellant tanks are mounted on the underside of the sample container unit. The tanks were designed using the same method described in Section 2.0. Each tank is 35 cm in diameter and has a mass of 2 kg. The ΔV requirement of 490 m/s will consume 43 kg of monopropellant.

For the Earth return trip, a different type of aerobrake is needed, because the velocity of the vehicle is much larger with respect to Earth than it is on entry to Mars [1,2]. The entry velocity for Mars is 5.69 km/sec, whereas at Earth it is 11.2 km/sec. This means that radiative heating will be significant compared to convective heating, so an ablative heat shield will be necessary. The sample container requires an aerobrake that can withstand high heat transfer rates for a single pass through the atmosphere to attain an elliptical orbit around Earth. For this pupose, the aerobrake chosen is similar to the Apollo heat shield. It is a conical shpe with a half cone angle of 70°. The total area of the aerobrake is 2.26 m^2. An ablative material will be required for the 280 W/cm^2 stagnation point heating No non-ablative shielding materials exist yet which can withstand such high entry heating [3,4]. AVCO-5026 H/CG is the currently preferred ablator material, because it was used on the

Apollo Command Module and it has been extensively studied [5]. For these reasons it has been chosen for the SRC.

10.4 AEROBRAKING AT EARTH

(Heather Nicholson, Laurie Nill)

The aerobraking scenario that is used for aerocapture at Earth is a single pass scenario into an elliptical orbit around, followed by a burn at apogee to circularize the orbit at a 340 km altitude. The sample return capsule is equiped to stay in orbit to await shuttle retrieval or rendez-vous with a space station. The specific parameters of the Earth return aerobraking pass are as follows: once the sample return module has separated from the ERV, it enters Earth's atmosphere at an angle of 11.8° and aerobrakes to a velocity of 7.8 km/sec and an exit angle of 2.3° which defines the capture orbit as an ellipse with r_a = 6720 km (alt. = 340 km). A burn of 490 m/sec must be performed by the SRC at apogee point to circularize this orbit. This option allows the Martian samples to be quarantined in orbit before arrival at Earth.

In the event that no shuttle retrieval or space station retrieval is possible then an alternate method is to bring the sample container directly to the Earth's surface, first through aerobraking down to a low altitude and velocity and then to complete the deceleration via a parachute recovery system. This method is more cost-efficient, since it does not require a piloted space shuttle mission to complete the return. Its main disadvantage, however, is that it does not allow for a quarantine period during which further analysis of the samples can be done before entering the Earth's atmosphere.

The parachute recovery system used in this method will be a low weight, state of the art, nylon-Kevlar system, as used in the CL-289 surveillance drone recovery system [6]. The major components of this parachute system are the main parachute, the Webb chute (positioned within the mouth of the main canopy), and the drogue chute. The drogue chute is

a conventional nylon canopy with riser and riser connections made of MIL-C-87129 type Kevlar braided cord. The skirt band is also made of Kevlar.

The main parachute consists mostly of conventional low mass nylon. All lines and connections are made of Kevlar braided cord. The Webb chute, which is spiderlike in appearance, is also made of nylon with Kevlar lines and connections. The purpose of the Webb chute is to initially force open the main canopy, and then to provide a circular, consistent area for air inflow. The Webb chute stabilizes the main canopy during the inflation period.

When the sample return container enters the Earth's atmosphere, the drogue chute is deployed via explosive bolts on the parachute compartment door. After a six second deceleration phase, the drogue chute will automatically deploy the main parachute. The total mass of this parachute recovery system is 15 kg. The maximum mass that can be returned to Earth by this system is 205 kg.

REFERENCES

1. Tauber, M., et al, "Aerobraking Design Studies for Manned Mars Missions," 91-1344, AIAA ,*26th Thermophysics Conference*, Honolulu, HI, June 24-26, 1991.

2. Arnold, J. O., Tauber, M. E., and Goldstein, H. E. "Aerobraking Technology for Manned Space Transportation Systems," 43rd Congress of the International Astronautical Federation, Washington, DC, August 28-September 5, 1992.

3. Tauber, M. and Sutton, K., "Stagnation-Point Radiative Heating Relations for Earth and Mars Entries," *Journal of Spacecraft and Rockets*, Vol. 28, Number 1, January-February 1991, pp. 40-42.

4. Tauber, M.E.; Palmer, G.E.; Yang, L., "Earth Atmospheric Entry Studies for Manned Mars Missions," *Journal of Thermophysics and Heat Transfer*, Vol. 6, Number 2, April-June 1992, pp. 193-197.
5. Williams, S. D., Gietzel, M. M., Rochelle, W. C., and Curry, D. M., "TPS Design for Aerobraking at Earth and Mars," NASA TM 104739 Lyndon B. Johnson Space Center, August 1991.

6. Webb, D.B., Palm, L., "Development of a Nylon-Kevlar Recovery System for the CL-289 Surveillance Drone," *AIAA Paper*, 1981.

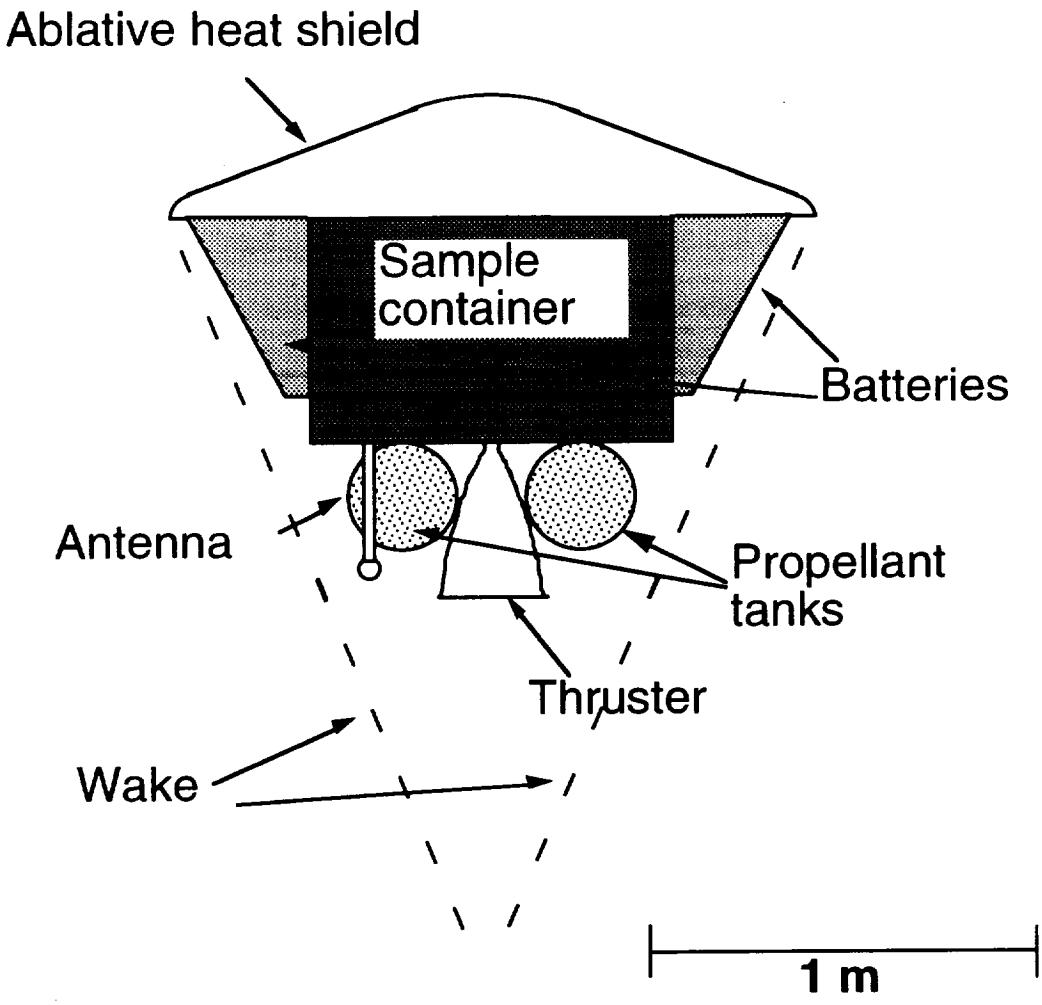

Fig. 10.1 Sample return capsule (SRC).

11.0 CONCLUSIONS

Lee Thrush

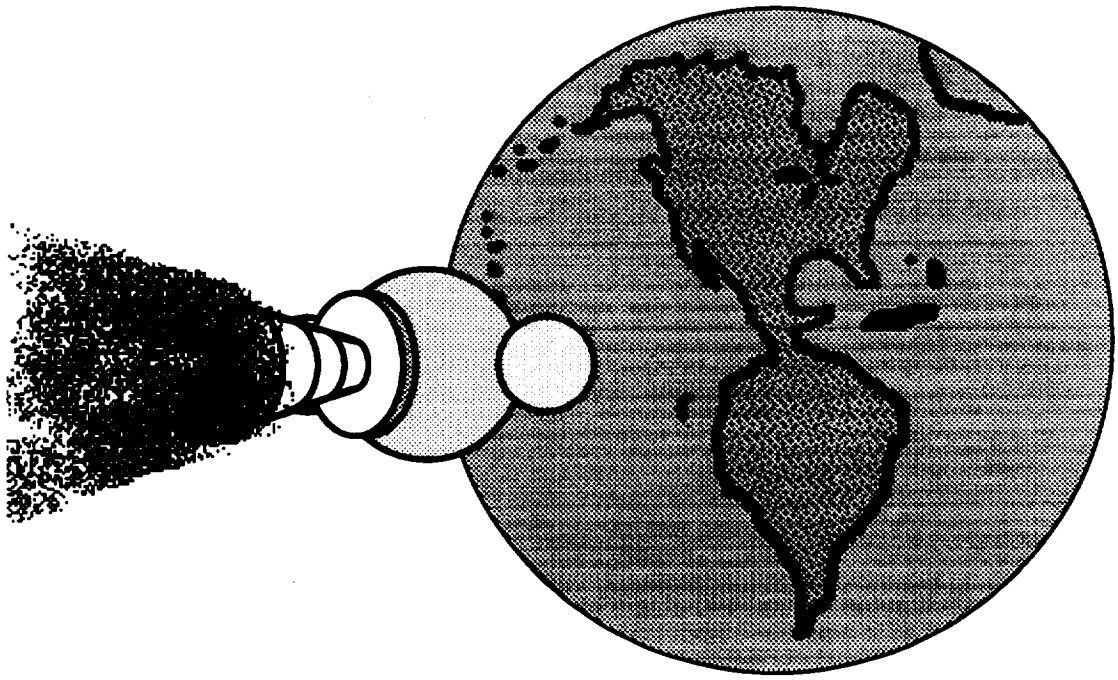

Nearly 200 years ago, the young American nation sent forth two courageous explorers by the names of Lewis and Clark to challenge the unknown western wilderness of the North American continent. Today, we stand at the threshold of a new, far more expansive, frontier. Very soon, the United States, either as an individual nation or as one joined in cooperation with the other peoples of the world, will be ready to send men and women to Mars. Like the explorers of 200 years past, astronauts of the twenty-first century will find their task much simplified if they are able to utilize their environment rather than compete against it. The surface of Mars is far less hospitable than the wild expanses of the untamed American West, but it too has resources that can be used to our benefit if we are smart enough to take advantage of them.

In 1992, the NASA / USRA design team from the University of Washington developed the Project Minerva proposal. This proposal called for a series of manned expeditions to Mars. The propellant for the Earth return voyages would be produced from carbon dioxide in the Martian atmosphere and a small supply of liquid hydrogen brought to Mars from Earth. A cost analysis of this mission architecture indicated that the cost of a Minerva-type mission would be approximately 10% of the similarly-sized, conventional missions that NASA has been studying. More scientific and exploration equipment could be carried to Mars, and complicated orbital assembly of the spacecraft would be unnecessary due to their smaller sizes.

It is important to note that even the much reduced cost of such a mission would represent a very large national investment, in terms of money, resources, time, and personnel. Therefore, a precursor mission should be performed to prove the viability of this mission architecture. Project Hyreus is our proposal for such a mission.

Project Hyreus combines many key features of various missions under consideration by NASA. The Hyreus mission will include a Mars-orbiting satellite that will make extended observations of the planet, using both an optical camera and a ground penetrating radar system. Rather than being a repetition of Mars Observer, this satellite will complement and build on that mission. A large rover will be carried by Hyreus. This vehicle will allow a variety of locations to be examined and give some diversity to the collected samples. As a sample return mission, Hyreus will deliver approximately 27 kg of Martian material to Earth. This represents a two order of magnitude increase over many other sample return missions currently being evaluated (Fig. 11.1). Such an increase is possible due to the innovative mission architecture of Project Hyreus. Finally, Hyreus relies on current technology. All the hardware used in this mission is either currently available or could easily be developed in time to meet the projected launch date in 2003.

In closing, Project Hyreus is a bridge to the future of the United States space program, the manned exploration of Mars. However, the Hyreus vehicle would not be just an expendable prototype developed to test mission hardware and then be discarded. Project Hyreus is a complete and worthwhile mission in its own right. Not only will this mission prove the viability of a mission architecture based on *in-situ* resource utilization, it will help us to define the goals of the manned missions that we will send later. Advance exploration by the Hyreus mission will be invaluable in selecting a landing site and determining what research equipment should be carried, and will build up experience with deep space missions of this kind. A manned mission to Mars is clearly needed, but in the age of shrinking budgets NASA must do as much as possible to ensure the success of such a mission. Hyreus will greatly expand our knowledge of Mars, and lead the way so that others may follow.

Conventional Mission Return Sample

Project Hyreus Return Sample

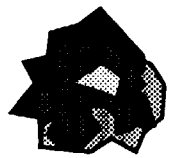

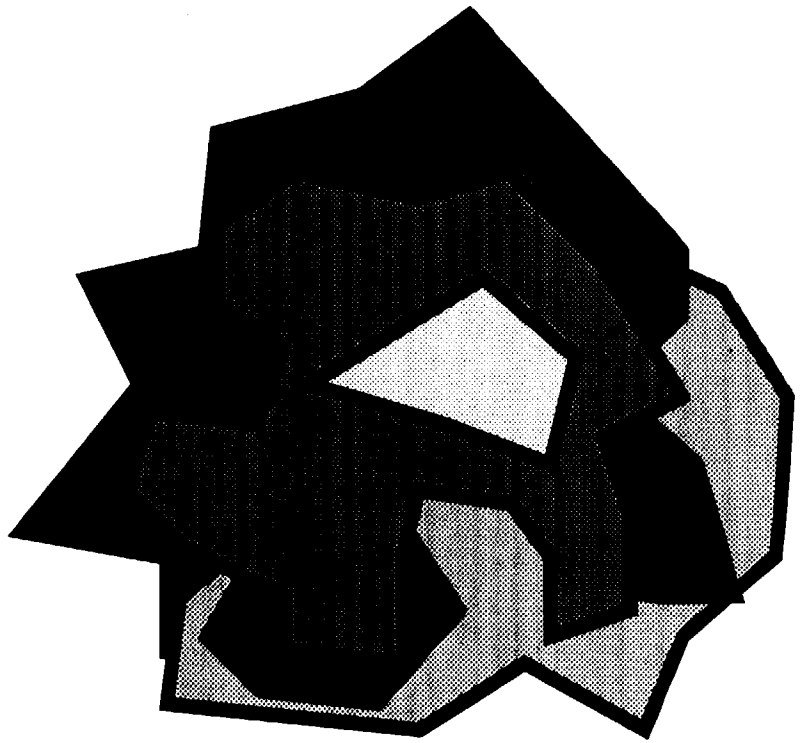

Approximately 1/4 kilogram

25 kilograms

Fig 11.1 Return sample mass comparison.

APPENDIX A:

THE TALE OF HYREUS

Lee Thrush

Hyreus* was born as a mortal in the Greek city-state of Sparta. As a young man, he was apprenticed to the local bronze smith, where he learned the ways of the forge. He excelled at the trade, particularly at weapons smithing. Hyreus studied for many years, and took a wife to start a family. When he had learned all he needed, he set out to find work on his own merits. Unfortunately for the bronze smiths of Sparta, the Greek city-states were in a period of peace. Hyreus was unable to find work due to the lull in the industry, and in his despair he dared to blame the gods for his plight.

The gods were angered by the blasphemy of Hyreus, and sought divine retribution. They banished Hyreus to the underworld, Hades, where he was to remain for four years. He was given only his bronze smith mallet and a handful of pomegranate seeds with which to survive. Hyreus was forced to live off the land; a rather difficult task in the desolate underworld.

Hyreus survived his ordeal, and the gods were impressed with his performance. Zeus himself decided to make Hyreus an immortal. Hyreus became a demi-god, and went on to serve as an attendant of Hephaistos, the Greek god of the forge. From that time on Hyreus became known as the God of Gainful Employment.

* The correct pronunciation of Hyreus is "hire-us".

APPENDIX B:

MATERIAL SELECTION

Ross Kruse

Keith Stokke

B.1 INTRODUCTION
(Ross Kruse, Keith Stokke)

Like aircraft structures, space structures require light materials so as to maximize payload capability. The propulsion system mass is fixed for the most part, thus a decrease in structure mass leads to a noticeable improvement in payload capability. If this were the only underlying factor, it would be easy to pick a material but there are many other constraints to consider. Materials with high specific strength and elastic modulus, low coefficient of thermal expansion, low thermal distortion, and high stiffness are prime candidates. Other factors such as thermal and electrical conductivity, long-term stability under vacuum and space radiation, low outgassing, manufacturability, and cost are also important.

The spacecraft structure has many components, and materials must exhibit acceptable compatibility. That is, each material must exhibit relatively the same properties. Materials should also have good weldablity. In other words the weld should exhibit nearly the same tensile properties as the material itself, otherwise the weld could fail before the material does.

In what follows, the components of the structure are broken down and the candidate materials applicable to them are discussed. Also covered are the materials needed for radiation shielding of the spacecraft. Table B.1 lists the advantages and disadvantages of commonly used materials for aerospace applications [1].

B.2 STRUCTURAL MATERIALS
(Ross Kruse, Keith Stokke)

The truss structure is the backbone of the spacecraft. It supports all other spacecraft subsystems and attaches the spacecraft to the launch vehicle. It must be able to withstand the dynamic loading of the vehicle and yet be as light as possible. Aluminum-lithium 2090 offers

high specific strength and elastic modulus, along with a lower density than most aluminum alloys, and shows increasing strength with decreasing temperature. Aluminum-lithium 2090 is widely available and is currently used on some aircraft. Table B.2 shows some properties of this alloy at room temperature.

Table B.1 Advantages and disadvantages of commonly used materials.

Material	Advantages	Disadvantages
Aluminum	• High specific strength • Ductile • Easy to machine	• Relatively low strength vs. volume • Low hardness • High coefficient of thermal expansion
Steel	• High strength • Wide range of strength, hardness and ductility obtained by treatment	• Magnetic • High Density
Magnesium	• Low density	• Low strength vs. volume
Titanium	• High specific strength • Low coefficient of thermal expansion	• Difficult to machine • Poor fracture toughness if solution treated and aged
Beryllium	• High stiffness vs. density	• Low ductility and fracture toughness • Toxic
Composite	• Can be tailored for high stiffness, high strength, and extremely low coefficient of thermal expansion	• Costly; requires development program • Strength depends on workmanship • Requires individual proof testing

B.2.1 Truss Frame Materials

The truss frame is composed of aluminum-lithium 2090. Although composites were considered due to their high specific strength and modulus of elasticity, along with a possible mass savings of up to 30% over aluminum alloys, they offer compatibility problems with other materials, and little information is available on their actual performance in many space applications. Therefore, for ease of manufacturing and homogeneity of the spacecraft, Al-Li 2090 was chosen.

Table B.2 Properties of aluminum-lithium 2090 at room temperature.

Density g/cm^3	Thermal Conductivity W/(m*K)	Modulus of Elasticity GPa / psi	Ultimate Strength MPa / ksi	Yield Strength MPa / ksi
2.57	84-92.3	76 / 11.0×10^6	517 / 75	483 / 70

B.2.2 Support Strut Materials

Support struts are what actually connect the various subsystems to the truss. They must endure highly concentrated areas of stress and fatigue. Shear stress is also important. Here again aluminum-lithium 2090 is the material of choice.

B.2.3 Tank Materials

The material for the propellant tanks must be reliable at cryogenic temperatures and be able to withstand the "g" forces of the spacecraft. Materials with the highest strength to density ratios are ideal. For pressure vessels the ultimate strength of the vessel is related to the ultimate usable strength of the material. Table B.3 shows some of the properties of aluminum alloys. Aluminum-lithium is the prime candidate, specifically Weldalite™ 049 (2195). Compared to the alloy used for cryogenic tanks on the space shuttle (2219-T87), Weldalite™ 049 has a 60% higher yield strength at 75 K and has a 4.5% lower density. Weldalite also has a 45% higher fracture stress than 2219 at liquid oxygen operating temperatures and it exhibits the same damage tolerance as 2219 welds [2]. Therefore, based on these facts, Weldalite™ 049 is the material of choice.

Table B.3 Some Properties of Al 2195 and 2219-T87 at Different Temperatures

Material	Density Kg/m^3	Yield Strength MPa / ksi	Ultimate Strength MPa / ksi
2195 (Weldalite)	$2.7x10^3$		
@ 75K		670 / 99	730 / 107
@ 300K		600 / 88	650 / 96
2219	$2.83x10^3$		
@ 75K		420 / 62	520 / 76
@ 300K		360 / 53	460 / 68

B.3 RADIATION SHIELDING

(Ross Kruse, Keith Stokke)

The radiation environment consists of solar flares, galactic cosmic rays and particle radiation trapped in Earth's magnetic field. Solar flares have a composition of mainly protons, with some helium and heavier ions, and solar flares are periodic and decrease in intensity as the spacecraft travels farther from the sun on its way to Mars. Galactic cosmic rays have the same composition as solar flares and are believed to originate from supernovae outside our galaxy [1]. Trapped particle radiation consists of protons and electrons trapped in Earth's magnetic field, i.e. the Van Allen Belts, and is only of concern during a short time following departure from Earth's orbit. For the most part radiation shielding is not a major problem, because of the unpiloted nature of this mission. Some sensitive electronic components need to be shielded and this is done using sheet aluminum.

REFERENCES

1. Larson, W.J., and Wertz, J.R., *Space Mission Analysis and Design*, Second Edition, Microcosm, Inc. and Kluwer Academic Publishers, 1992, pp 430-468, 646, 657.

2. Loechel, L.W., Roberts, M.O., and Scholz, E.F., "Advanced Cryogenic Tank Development Status," AIAA Paper No. 92-3707, July, 1992.

APPENDIX C:
LAUNCH SYSTEM ANALYSIS TABLES

Richard Warwick

C.1 INTRODUCTION

The following pages show the results of the analysis for each launch vehicle. The data in the left column are the performance parameters of each stage. The next column to the right shows the flight sequence analyzed segment by segment, each new segment determined by an event such as stage shutdown, fairing jettison, etc. The column farthest to the right shows various performance results. The top row shows the payload mass used and the row beneath that shows the total ΔV capability of that system for that payload mass. Also included in the right column are estimated drag and gravity losses, as well as the velocity gain due to the Earth's rotation. All units in these tables are MKS.

Each segment was analyzed using the rocket equation and the sea level or vacuum I_{sp}, whichever was appropriate. Parallel burns were also evaluated (these are the unlabeled numbers in some of the tables). The drag losses were approximated by using the known drag loss to orbit values of the Titan IV and scaling them to the cross sectional area of each vehicle. The gravity losses were estimated by scaling total burn time to orbit of each vehicle to the known Titan IV values. Rotational gains were determined from launch site latitude and parking orbit inclinations available from each launch site.

C.2 RESULTS

C.2.1 Titan IV/Centaur

SINGLE TITAN IV			Duration
Stage 0			136.6
Mgross	352396.4		
Mprop	315270.3		
Mfin	37126.08		
Burn t	136.6		
Isp	249.32	284.6	12
Stage 1			
Mgross	169457.6		
Mprop	154449.6		
Mfin	15008.01		98
Burn t	187.73		
Mass Flow	822.7218		
Isp	301.45		
Mfair	10400		77.73
Stage 2			
Mgross	38999.42		
Mprop	34636.31		
Mfin	4363.105		226.91
Burn t	226.91		
Mass Flow	152.6434		
Isp	316.55		

Upper Stage	Centaur	IUS
Mgross	23724	23724	10965
Mprop	21000	21000	9710
Mfin	2724	2724	1255
Burn t	600	600	153
Isp	444.4	444.4	292.9
2nd Half Upper Stage if any			IUS
Mgross	0		3900
Mprop	0		2750
Mfin	0		1150
Burn t	104		104
Isp	300.9		300.9

Segment 1	
Minit	952023.7
Mfin	321483.2
Isp	249.32
Delta V	2652.595
Segment 2	
Minit	321483.2
Mfin	311610.5
Isp	301.45
Delta V	92.14523
Segment 3	
Minit	237358.3
Mfin	156731.6
Isp	301.45
Delta V	1226.104
Segment 4	
Minit	146331.6
Mfin	82381.43
Isp	302
Delta V	1700.335
Segment 5	
Minit	67373.42
Mfin	32737.11
Isp	316.55
Delta V	2238.979
Segment 6	
Mflow	35
Time	600
Mpused	21000
Minit	28374
Mfin	7374
Isp	444.4
Delta V	5868.581
Segment 7 (if IUS)	
Mflow	0
Time	0
Mpused	0
Minit	4650
Mfin	4650
Isp	300.9
Delta V	0

TITAN IV CH4	
Payload	4650
Total dV	13778.74
Upstg Brn	600
X-Sectional Area	
Stage 0	16.08495
Fairing	55.18044
Total	71.2654
Time to Parking	
Orbit	558
gt	5468.4
Grav Loss	822.6552
Drag Loss	68.2752
Orb Incl	28.6
Rot Gain	407.2272
Net dV	13295.04

C.2.2 Titan IIIE/TOS

TITAN III			Duration			TITAN IIICH4	
Stage 0		SRM	108	Segment 1		Payload	4650
Mgross	247000			Minit	671850	Total dV	11055.06
Mprop	210000			Mfin	280815.5	Upstg Brn	150
Mfin	37000			Isp	238	TOS	
Burn t	116			Delta V	2034.639		
Isp	238		8	Segment 2			
Stage 1				Minit	280815.5	X-Sectional Area	
Mgross	122000			Mfin	245428.2	Stage 0	15.1929
Mprop	118000			Isp	255.8173	Fairing	55.18044
Mfin	4000			Delta V	337.6776		
Burn t	147		139	Segment 3		Total	70.37334
Mass Flow	802.7211			Minit	171428.2		
Isp	296	255.8173		Mfin	59850	Drag Loss	67.55841
				Isp	296		
Mfair	10400			Delta V	3052.579	Time to Parking	
			10	Segment 4		Orbit	510
Stage 2				Minit	55850	gt	4998
Mgross	30000			Mfin	54366.48	Grav Loss	749.7
Mprop	27000			Isp	316.55		
Mfin	3000			Delta V	83.51615	Orb Incl	28.6
Burn t	182		172	Segment 5		Rot Gain	407.2272
Mass Flow	148.3516			Minit	43966.48		
Isp	316.55			Mfin	18450	Net dV	10645.03
				Isp	316.55		
Upper Stage		TOS	Transtage	Delta V	2693.828		
Mgross	10800	10800	13510	Segment 6			
Mprop	9710	9710	10380	Mflow	64.73333		
Mfin	1090	1090	3130	Time	150		
Burn t	150	150	449	Mpused	9710		
Isp	294	294	309.1	Minit	15450		
				Mfin	5740		
				Isp	294		
				Delta V	2852.82		

C.2.3 Space Shuttle/IUS

SPACE SHUTTLE			Duration
Stage 0			123
Mgross	590000		
Mprop	502000		
Mfin	88000		
Burn t	123		
Isp	236.3386	267.3	399
		268.4161	
Stage 1			
Mgross	750000		
Mprop	721000		
Mfin	29000		
Burn t	522		
Mass Flow	1381.226		
Isp	363.2	455.2	
Morbiter	94000		

Upper Stage	Centaur	IUS
Mgross	10965	23724	10965
Mprop	9710	21000	9710
Mfin	1255	2724	1255
Burn t	153	600	153
Isp	292.9	444.4	292.9

2nd Half Upper Stage if any		IUS
Mgross	3900	3900
Mprop	2750	2750
Mfin	1150	1150
Burn t	104	104
Isp	300.9	300.9

Segment 1	
Minit	2043515
Mfin	869624.2
Isp	268.4161
Delta V	2247.39
Segment 2	
Minit	693624.2
Mfin	142515
Isp	455.2
Delta V	7059.394
Segment 3	
Mflow	63.46405
Time	153
Mpused	9710
Minit	19515
Mfin	9805
Isp	292.9
Delta V	1975.684
Segment 4	
Mflow	26.44231
Time	104
Mpused	2750
Minit	8550
Mfin	5800
Isp	300.9
Delta V	1144.359

SHUTTLE CH4	
Payload	4650
Total dV	12426.83
IUS brn 1	153
IUS brn 2	104
X-Sectional Area	
Stage 0	89.39706
Tank	55.41769
Orbiter	24.27948
Total	169.0942
Drag Loss	162.3305
Time to Parking Orbit	522
gt	5115.6
Grav Loss	767.34
Orb Incl	28.6
Rot Gain	407.2272
Net dV	11904.38

C.2.4 Delta 7925

DELTA			Duration			DELTA	CH4
Stage 0				Segment 1		Payload	4650
Mgross	13000	13100		Minit	233829.4	Tot dV	9369.759
Mprop	11700	11700	63	Mfin	140806.8	Upstg Brn	600
Mfin	1300	1400		Isp	252.2448		
Isp	63	63		Delta V	1253.806		
Burn t	245.7	273.8		Segment 2			
Mass Flow	185.7143	252.2448		Minit	140806.8	X-Sectional Area	
Stage 1		292.3106	3	Mfin	139720	Stage 0	4.712389
Mgross	101900			Isp	301.8	Fairing	55.18044
Mprop	96000			Delta V	22.91658		
Mfin	5900			Segment 3		Total	59.89283
Burn t	265			Minit	131920		
Mass Flow	362.2642		63	Mfin	73997.33	Drag Loss	57.49712
Isp	255.6	301.8		Isp	292.3106		
				Delta V	1656.241	Time to Parking	
Mfairing	841			Segment 4		Orbit	600
				Minit	73997.33	gt	5880
Stage 2			3	Mfin	72910.54	Grav Loss	882
Mgross	6997			Isp	301.8		
Mprop	6076			Delta V	43.76075	Orb Incl	51.6
Mfin	921			Segment 5		Rot Gain	288.1015
Burn t	439.7			Minit	68710.54		
Mass Flow	13.81851		133	Mfin	20529.41	Net dV	8718.363
Isp	319.4			Isp	301.8		
				Delta V	3572.96		
Stage 3				Segment 6			
Mgross	2141.41	2141.41		Minit	14629.41		
Mprop	2009.414	2009.414	24	Mfin	14297.77		
Mfin	131.9954	131.9954		Isp	319.4		
Burn t	54.8	54.8		Delta V	71.77555		
Isp	292.6	292.6		Segment 7			
			415.7	Minit	13456.77		
			415.7	Mfin	7712.41		
Mgross	0	1149		Isp	319.4		
Mprop	0	1080.06		Delta V	1742.385		
Mfin	0	68.94		Segment 8			
Burn t	104			Minit	6791.41		
Isp	300.9	291		Mfin	4781.995		
				Isp	292.6		
				Delta V	1005.914		

C.2.5 Ariane V

ARIANE V			Duration			ARIANE V CH4	
Stage 0			123	Segment 1		Payload	4650
Mgross	265000			Minit	723561.9	Tot dV	11825.26
Mprop	230000			Mfin	231248.3	Upstg Bur	800
Mfin	35000			Isp	245.4485		
Burn t	123			Delta V	2743.82		
Isp	239.148	245	58	Segment 2			
Stage 1				Minit	161248.3	X-Sectional Area	
Mgross	170000			Mfin	146011	Stage 0	28.84265
Mprop	155000			Isp	335.1387	Fairing	55.18044
Mfin	15000			Delta V	326.0166		
Burn t	590		406	Segment 3		Total	84.02309
Mass Flow	262.7119			Minit	135611		
Isp	335.1387	430		Mfin	28950	Drag Loss	80.66217
				Isp	430		
Mfair	10400			Delta V	6507.345	Time to Parking	
			800	Segment 4		Orbit	590
Upper Stage				Mflow	9	gt	5782
Mgross	9300			Time	800	Grav Loss	867.3
Mprop	7200			Mpused	7200		
Mfin	2100			Mgross	13950	Orb Incl	5.2
Burn t	800			Mfin	6750	Rot Gain	461.9123
Mass Flow	9			Isp	316		
Isp	316			Delta V	2248.082		
						Net dV	11339.21

C.2.6 Energia

ENERGIA			Duration			ENERGIA	CH4
Stage 0			145	Segment 1		Payload	4650
Mgross	355000			Minit	2434050	Tot dV	19046.66
Mprop	320000			Mfin	906341.7	Upstg Brn	680
Mfin	35000			Isp	316.2965		
Burn t	145			Delta V	3062.185		
Isp	309	316	105	Segment 2		X-Sectional Area	
Stage 1				Minit	766341.7	Stage 0	47.78362
Mgross	905000			Mfin	586966.7	Stage 1	50.26548
Mprop	820000			Isp	354	Fairing	55.18044
Mfin	85000			Delta V	925.0971		
Burn t	480		230	Segment 3		Total	153.2296
Mass Flow	1708.333			Minit	576566.7	Drag Loss	147.1004
Isp	354	453		Mfin	183650		
				Isp	452.5	Burn to Parking	
Mfairing	10400			Delta V	5073.331	Orbit	480
			??	Segment 4		gt	4704
EUS				Minit	98650	Grav Loss	705.6
Mgross	77000			Mfin	28650		
Mprop	70000			Isp	490	Orb Incl	51.6
Mfin	7000			Delta V	5937.312	Rot Gain	288.1015
Burn t	??	approx 343		Segment 5			
Mass Flow	ERR			Mflow	22.05882	Net dV	18482.06
Isp	490			Time	680		
				Mpused	15000		
RCS				Minit	21650		
Mgross	17000			Mfin	6650		
Mprop	15000			Isp	350		
Mfin	2000			Delta V	4048.733		
Burn t	680						
Isp	350						

C.2.7 Proton

PROTON		Duration			PROTON	CH4
Stage 1		130	Segment 1		Payload	4650
Mgross	455600		Minit	711800	Upstg Brn	680
Mprop	410200		Mfin	301600	Total dV	12319.21
Mfin	45400		Isp	285		
Isp	285		Delta V	2398.336		
Burn t	130				X-Sectional Area	
		212	Segment 2		Stage 1	43.0084
Stage 2			Minit	256200	Fairing	55.18044
Mgross	165600		Mfin	106200		
Mprop	150000		Isp	316	Total	98.18885
Mfin	15600		Delta V	2727.148		
Isp	316				Drag Loss	94.26129
Burn t	212	29	Segment 3			
			Minit	90600	Time to Parking	
Stage 3			Mfin	86457.14	Orbit	600
Mgross	55600		Isp	316	gt	5880
Mprop	50000		Delta V	144.9469	Grav Loss	882
Mfin	5600					
Isp	316	321	Segment 4		Orb Incl	51.6
Burn t	350		Minit	76057.14	Rot Gain	288.1015
Mass Flow	142.8571		Mfin	30200		
			Isp	316	Net dV	11631.05
Fairing	10400		Delta V	2860.338		
Stage 4		680	Segment 5			
Mgross	19950		Minit	24600		
Mprop	17300		Mass Used	17300		
Mfin	2650		Mfin	7300		
Isp	351.8		Isp	351.8		
Burn t	680		Delta V	4188.442		
Mass Flow	25.44118					

C.2.8 Zenit

ZENIT		Duration			ZENIT CH4	
Stage 1		150	Segment 1		Payload	4650
Mgross	352700		Minit	477600	Upstg Brn	660
Mprop	318800		Mfin	158800	Total dV	11045.66
Mfin	33900		Isp	309		
Isp	309		Delta V	3334.436		
Burn t	150				X-Sectional Area	
		315	Segment 2			
Stage 2			Minit	124900	Fairing	55.18044
Mgross	89900		Mfin	44300		
Mprop	80600		Isp	350	Total	55.18044
Mfin	9300		Delta V	3555.294		
Isp	350				Drag Loss	52.97323
Burn t	315		Segment 3			
			Minit	35000	Time to Parking	
Stage 3		29	Mfin	34239.85	Orbit	600
Mgross	19950		Isp	351.8	gt	5880
Mprop	17300		Delta V	75.70306	Grav Loss	882
Mfin	2650					
Isp	351.8		Segment 4		Orb Incl	12
Burn t	660		Minit	23839.85	Rot Gain	453.6856
Mass Flow	26.21212	631	Mfin	7300		
			Isp	351.8	Net dV	10564.37
Fairing	10400		Delta V	4080.227		

APPENDIX D:
CARBON MONOXIDE PRODUCTION

Richard Warwick

As an alternative to methane, carbon monoxide has been considered as a fuel choice. Because of its lower I_{sp} of 290 s versus methane's 370 s, a considerably larger quantity of carbon monoxide will be required. The carbon monoixde plant must produce 3600 kg of CO and 1800 kg of O_2. The plant design used here is adapted from a design from the University of Arizona. A schematic is shown in figure D.1 Carbon monoxide and oxygen can be produced directly from the Martian atmosphere using the reaction:

$$2CO_2 \rightarrow 2CO + O_2 \qquad \Delta H = -280.7 \text{ kJ/kg} \qquad (1)$$

This reaction can be carried out by passing a potential across a solid oxide electroyte. Zirconia electrolytic cells are used to produce O_2 from atmospheric CO_2. The O_2 is produced relatively free of impurities and is liquefied and stored. Due to inefficiencies, the exhaust stream from the electrolyzer will contain both CO and CO_2. Research conducted at the University of Arizona has identified a method for separating the CO and CO_2. Catalytic disproportionation is used to separate the CO from the CO_2 by the following reaction:

$$2CO \rightarrow C + CO_2 \qquad \Delta H = -44 \text{ kJ/kg} \qquad (2)$$

The plant will actually require two catalyst beds. One unit is used to disproportionate CO while the other is heated to gasify the deposited carbon and produce relatively pure CO from the reverse reaction. When sufficient carbon has been deposited in one bed, the two reversre roles. In this manner, steady state production can be achieved. The CO_2 stream from the catalyst bed is recycled to reduce the CO_2 intake requirement. The total production rate is 10.8 kg/day of propellant, 7 kg/day of CO, and 3.8 kg/day of O_2.

The CO plant uses a hydrocyclone filter similar to the one used in the methane plant. Again, the dust is retained in a sample canister for return to Earth. Because the zirconia cells operate at high temperatures, the filtered atmospheric gases are not condensed to remove the

nitrogen, argon, and other trace gases. Small amounts of these impurities do not adversely affect the reaction, as was confirmed by computer analysis of CO/O_2 reaction with trace impurities present. The zirconia cells should also not be affected by the trace gases. The plant is designed to allow these gases to be vented at a later stage.

The CO_2 enters the zirconia electrolyzer unit at 1270 K. The zirconia cells require 250 mA/cm^2. Experimentally determined efficiencies of 60% result in a power requirement of 193 W_e per kilogram of O_2 produced per day. This translates into 140 A/(kg O_2)day and 2128 cm^2 of cell surface area. The standard Westinghouse zirconia cell is 2.54 cm in diameter with a maximum lenght of 61 cm. Thus a single cell has a surface areaof 486 cm^2. The CO plant requires five cells of 54 cm length to produce 3.8 kg/day O_2. This translates into a total power requirement of 733 W_e for the zirconia cells. Using five cells also increases the conversion efficiency. If the cells are cascaded, the gases from the previous cell are further electrolyzed producing more O_2 and CO.

Once the mixture exits the electrolyzer, sufficient quantities of CO_2 are still present to require a separation device as noted above. Two catalyst beds are used to separate the CO_2 from the CO. One unit operates at 700 K and rejects heat while disproportioning CO into C and CO_2. The other bed requires heat input, which is nearly equal to the heat output of the first unit, and passes CO_2 over the deposited carbon to form relatively pure CO. The CO is then liquefied and stored in a cycle similar to the methane plant. When one catalyst bed has accumulated a large amount of carbon, the flow over the beds is reversed and they reverse roles. The excess CO_2 is recirculated back the zirconia electrolyzer for further electrolysis. This recirculation greatly reduces the intake requirement of the plant, resulting in a much smaller intake nozzle.

Start-up can be facilitated by filling a tank with atmospheric CO_2 and then using that gas to start the plant. Periodically, the recirculating CO_2 can be vented, since it will eventually become rich in trace gases. If the small start-up storage tank were refilled with

fresh atmospheric CO_2 during normal operation, then that gas can be used to replenish the vented CO_2.

When other requirements such as pumps and refrigeration are included, the plant will have a total electrical power requirement of 1180 W_e. Although additional thermal power is required, this can be supplied by the radioisotope power source used to power the propellant plant. Since the power supply operates at an efficiency of around 20% and has a total thermal output of nearly 8 kW, more than sufficient heat energy will be available from the power supply coolant to add the additional 230 W of thermal energy required. Although mass estimates for the CO plant are less reliable, the CO plant is expected to have a mass of 300 kg, or about 100 kg less than the methane plant.

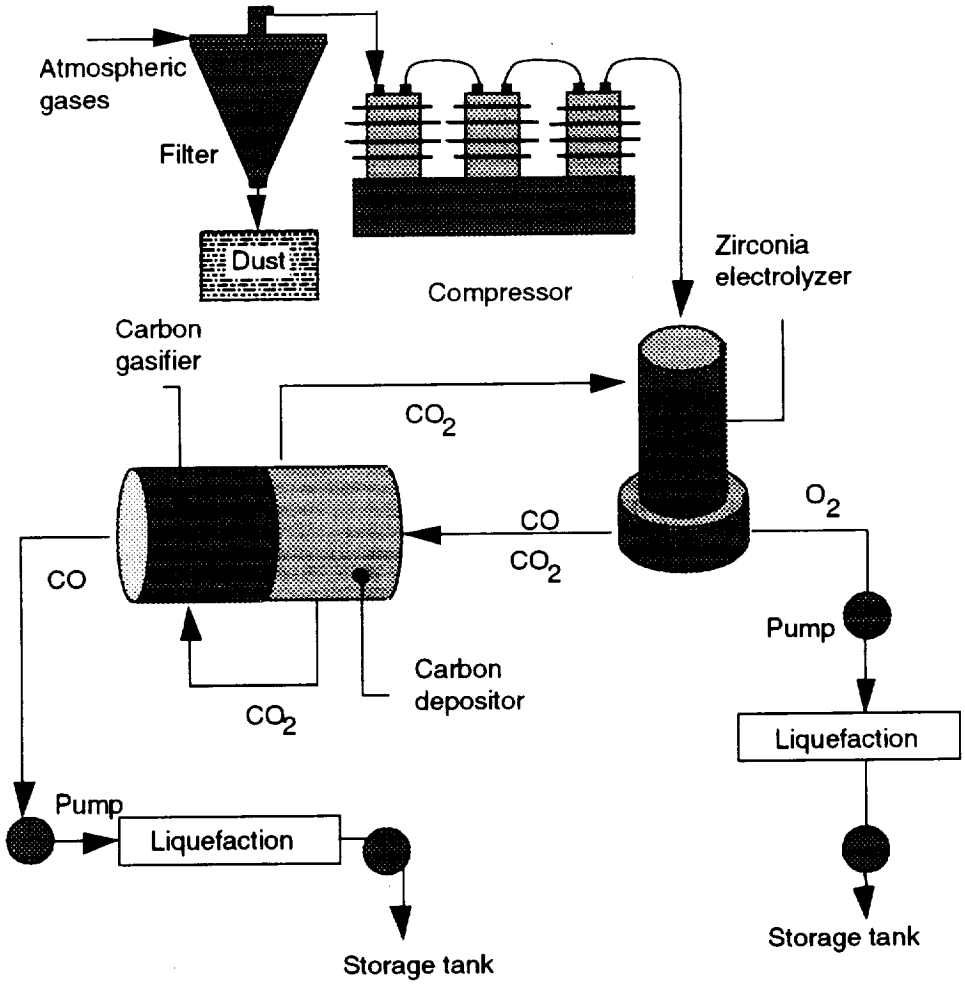

Figure D.1 Carbon monoxide plant schematic.

APPENDIX E:
MARS BALLOON

Gretchen Swanson

Patrick Sweeney

The second rover design, which is not a rover in the traditional sense, is a Mars Balloon. For the sample collection mission as proposed in Section 7, the balloon cannot be used as the primary "vehicle." In order to calculate the mass that a Mars balloon could carry, the Martian atmosphere was assumed to consist solely of CO_2, and to behave as an ideal gas.

Using the equations below, and assuming that the balloon can carry the same amount of mass as the mass of atmosphere displaced, a balloon 10 m in diameter could carry approximately 7.7 kg. This payload is large enough for a free floating balloon with rudimentary experiments, but provides little utility as an actual exploration vehicle.

$$\begin{aligned} \text{Mass of air displaced} &= \rho V \\ V &= 4/3\pi r^3 \\ r &= \text{balloon radius} \\ \rho &= P/RT \\ P = \text{pressure} &= 6 \text{ mbar} \\ R = \text{gas constant} &= 188.95 \text{ kJ/kg K} \\ T = \text{temperature} &= 215 \text{ K} \end{aligned}$$

Advantages and disadvantages of a Mars Balloon have been considered. The ability of the balloon to navigate into hard to reach places, such as valleys, makes the balloon an attractive idea. A major problem arises when the winds on Mars are taken into consideration. These winds may create enough dynamic pressure that the balloon would be uncontrollable. If a specific location is desired for sample collecting, the balloon starts looking much less attractive. Not of minor importance is the problem of guidance and control of the balloon. Propellers and other control surfaces will not be effective in the low pressure Martian atmosphere, so other alternatives must be found.

Rather than using the balloon as a sample collection vehicle, it may be possible to use it in conjunction with the wheeled rover. In this scenario, the balloon would be tethered to the rover, and would travel wherever the rover goes. A camera could be installed to

provide a "bird's eye" view of the Martian landscape. This view would be helpful not only from an information standpoint, but also the scenes viewed could also be used to aid in the control and navigation of the rover. There would be two cameras mounted for stereo vision. These cameras would be the same as used on the rover, charge coupled device (CCD) cameras weighing only 0.25 kg and requiring only 10 W of power each. Data transmission would have to occur through the tether. With this constraint, the cameras could draw power directly from the rover or possibly from a small solar cell array approximately 0.5 m by 0.5 m.

APPENDIX F:

AIAA 93-2242
MARS ROVER SAMPLE RETURN MISSION UTILIZING IN SITU PRODUCTION OF THE RETURN PROPELLANTS

AIAA 93-2242

Mars Rover Sample Return Mission Utilizing In Situ Production of the Return Propellants

A.P. Bruckner, L. Nill, H. Schubert,
B. Thill, R. Warwick
Department of Aeronautics and Astronautics
University of Washington
Seattle, WA 98195

AIAA/SAE/ASME/ASEE
29th Joint Propulsion Conference and Exhibit
June 28-30, 1993 / Monterey, CA

MARS ROVER SAMPLE RETURN MISSION UTILIZING *IN SITU* PRODUCTION OF THE RETURN PROPELLANTS

A.P. Bruckner,* L. Nill,† H. Schubert,† B. Thill,§ and R. Warwick†
Department of Aeronautics and Astronautics
University of Washington, FS-10
Seattle, WA 98195

ABSTRACT

This paper presents an unmanned Mars sample return mission that utilizes propellants manufactured *in situ* from the Martian atmosphere for the return trip. A key goal of the mission is to demonstrate the considerable benefits that can be realized through the use of indigenous resources and to test the viability of this approach as a precursor to manned missions to Mars. Two *in situ* propellant combinations, methane/oxygen and carbon monoxide/ oxygen, are compared to imported terrestrial hydrogen/ oxygen within a single mission architecture, using a single Earth launch vehicle. The mission is assumed to be launched from Earth in 2003. Upon reaching Mars, the landing vehicle aerobrakes, deploys a small satellite, and lands on the Martian surface. Once on the ground, the propellant production unit is activated, and the product gases are liquefied and stored in the empty tanks of the Earth Return Vehicle (ERV). Power for these activities is provided by a dynamic isotope power system. A semi-autonomous rover, powered by the indigenous propellants, gathers between 25 and 30 kg of soil and rock samples which are loaded aboard the ERV for return to Earth. After a surface stay time of approximately 1.5 years, the ERV leaves Mars for the return voyage to Earth. When the vehicle reaches the vicinity of Earth, the sample return capsule detaches, and is captured and circularized in LEO via aerobraking maneuvers.

INTRODUCTION

In recent years a number of proposals have been made for using Martian *in situ* resources to enhance or enable manned Mars missions. Zubrin of Martin Marietta, has proposed a direct-to-Mars manned mission based on indigenous resource utilization.[1,2] Both Ramohalli at University of Arizona, and Ash at Old Dominion University, have studied *in situ* propellant production and have built laboratory scale devices that have demonstrated its feasibility.[3,4] At the University of Washington the authors and their colleagues have developed both manned and unmanned missions to Mars utilizing *in situ* propellant production.[5,6]

This paper presents the results of a recent study of an unmanned Mars sample return mission that utilizes propellants manufactured *in situ* from the Martian atmosphere for the return trip. Two types of fuel, methane and carbon monoxide, are considered here for use in the sample return mission. The advantages and disadvantages of each propellant are compared for each aspect of the mission. These results are also compared with a scenario that utilizes imported terrestrial hydrogen and oxygen. The goals of this mission are to demonstrate the considerable scientific and technological benefits that can be realized through the use of indigenous resources, and to test the viability of this approach as a precursor to manned missions to Mars. Scientific goals as recommended by the U.S. National Academy of Sciences Committee on Planetary Exploration (COMPLEX) are implemented in the mission, e.g., locate water/ice deposits, investigate volcanic activity, and investigate the existence of life on Mars.[7] In addition, a large sample, between 25-30 kg is returned to Earth. The mission is accomplished using a single existing Earth launch vehicle.

MISSION SCENARIO

As shown in Fig. 1, the mission begins with the launch of the Mars Landing Vehicle (MLV) and upper stage into low Earth orbit (LEO). The upper stage then injects the MLV into a transfer orbit to Mars, where it is captured into orbit through aerobraking maneuvers. Additional aerobraking maneuvers are used to decelerate the MLV into a lower orbit, where a satellite is deployed, and to initiate the MLV's descent to Mars. After aerobraking down to a low altitude, parachutes and retro-rockets are used to bring the vehicle to a soft landing on the surface of Mars. For present purposes, the Mangala Valles region was selected as the primary landing site.

Once the MLV is in place, the Mars surface portion of the mission begins. The methane or carbon monoxide propellant production plant is activated and begins producing fuel and oxidizer for the return trip and for the rover. The liquefied propellants are stored in the initially empty tanks of the Earth Return Vehicle (ERV). Rover surface missions begin once sufficient amounts of the propellants have been

---

* Professor. Associate Fellow AIAA.
† Undergraduate. Student Member AIAA.
§ Graduate Student. Student Member AIAA.

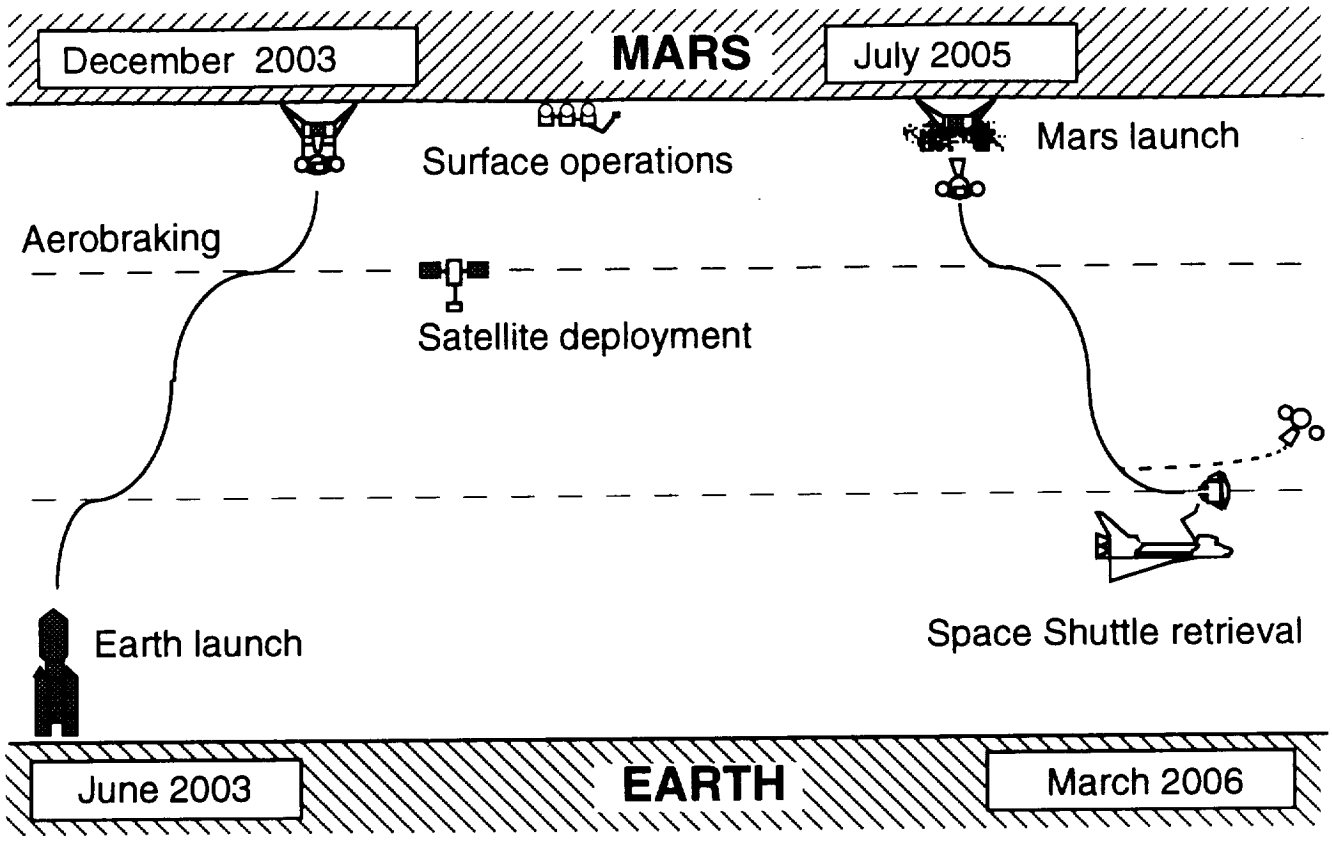

Fig. 1 Mission architecture

produced to meet the needs of the rover's power system. The rover then explores the Martian surface, gathering rock and soil samples and creating a map of the area. Scientific experiments are conducted both from the Martian surface and from the satellite.

Approximately 1.5 years after arrival, the ERV launches from the MLV support structure and returns to Earth. The ERV is a single-stage vehicle which first ascends into Low Mars Orbit (LMO) and then performs the burn for injection into the Earth transfer orbit. Once the vehicle reaches the vicinity of Earth, the Sample Return Capsule (SRC) detaches and performs an aerocapture maneuver in the atmosphere. The ERV continues on a hyperbolic trajectory out to deep space. The SRC's orbit is circularized in LEO by performing a burn. It is subsequently retrieved by the Space Shuttle.

REQUIREMENTS

There are several basic requirements for the Mars sample return mission discussed here. Orbital mechanics for the voyage to and from Mars must be calculated, including the use of aerobraking at Mars and upon return at Earth. A propellant plant and a power system must be designed based on the type of propellant chosen for the return mission. Engines for Mars ascent which use the selected propellant are required. An additional requirement is a rover large enough to explore and collect a variety of samples over a wide area. Communication links between the MLV and the rover must be considered in the satellite design. Finally, a launch system must be chosen which is capable of launching the MLV from the Earth's surface. The design of both the MLV and the ERV depends on the choice of propellant.

IN SITU PROPELLANT PRODUCTION PLANT

Two different *in situ* propellant combinations are considered: CH_4/O_2 and CO/O_2. The plants needed to produce each propellant combination are considerably different, though they share some similar components. Both propellants have advantages and disadvantages as a result of different chemical processes involved. Other propellant combinations that have been proposed for Mars' applications are not addressed in this paper.[2]

Methane Plant

The sample return portion of this mission requires 490 kg of methane and 1,960 kg of oxygen to be produced during the 1.5 year stay on the surface of Mars. An additional 100 kg of methane and 200 kg oxygen are needed to power the rover. These propellants are manufactured in the Propellant Production Plant (PPP), using carbon dioxide found in the Martian atmosphere and seed hydrogen imported from Earth.

The production of methane is performed through the Sabatier reaction:

$$CO_2 + 4H_2 \rightarrow CH_4 + 2H_2O \quad (1)$$

Many reactors exist which perform this reaction reliably.[8] The methane plant described here is based on a Sabatier reactor currently available through Hamilton Standard.

The oxygen is produced through two means. The first is the electrolysis of the water produced in the Sabatier reaction.[9] The electrolysis breaks the water down into hydrogen and oxygen:

$$2H_2O \rightarrow 2H_2 + O_2 \quad (2)$$

The hydrogen is recycled into the Sabatier reaction, to minimize the amount imported from Earth. However, the Sabatier and electrolysis reactions produce only half of the required oxygen. Thus, oxygen production is supplemented using the reverse water-gas shift (RWGS)[10] reaction:

$$CO_2 + H_2 \rightarrow CO + H_2O \quad (3)$$

This reaction produces carbon monoxide as a waste product which is released into the Martian atmosphere.

The methane PPP, shown in Fig. 2, is designed to produce the needed propellant in approximately 1.4 years. Because the total stay time is 1.5 years, the excess time allows for any delays in the landing sequence at Mars and any necessary plant shutdowns which may occur due to severe dust storms. Methane is produced at a rate of 1.15 kg/day and oxygen at 4.62 kg/day. Martian atmospheric gas is drawn into the PPP at a rate of 9.6 kg/day.

The Martian atmosphere is composed of 95.3% carbon dioxide, 2.7% nitrogen and 1.6% argon.[11] Dust is also present. The filter system, composed of a hydrocyclone and a membrane filter in series, is designed to remove the dust. The hydrocyclone removes particles as small as 5 μm and the membrane filter removes the remaining fine particulates. Dust particles removed via the hydrocyclone are collected to

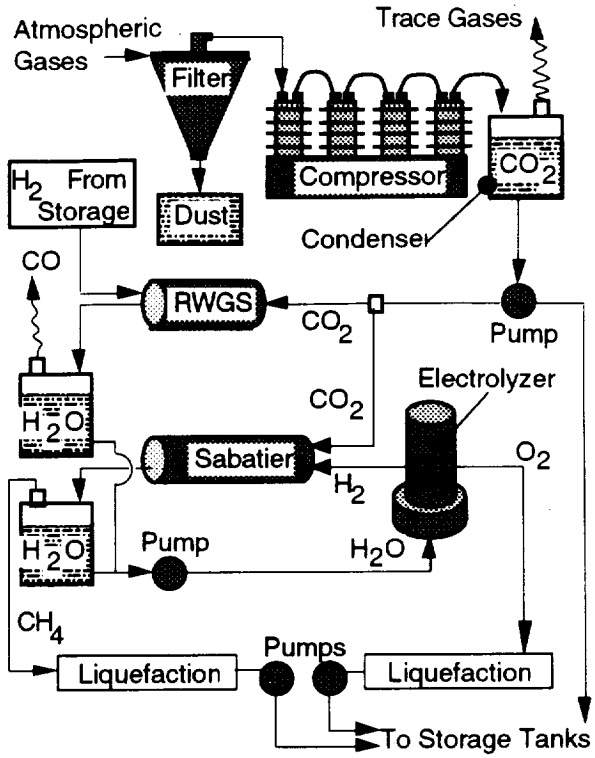

Fig. 2 Methane propellant plant schematic

be returned to Earth. Following filtration, the carbon dioxide is purified by removing nitrogen and argon. This is accomplished by compressing the atmospheric gases to 1.3 MPa, condensing the carbon dioxide at ambient Martian temperatures, and bleeding off the trace gases. A portion of the liquefied carbon dioxide is stored at 1.3 MPa and ambient temperature for use on the rover as a diluent.

The purified carbon dioxide is pumped to the Sabatier reactor and the RWGS reactor. The Sabatier reactor produces methane and water and the RWGS reactor produces carbon monoxide and water. The water is separated from each gas mixture by condensation and is pumped to the electrolyzer. The carbon monoxide is vented to the atmosphere, and the methane is pumped to the liquefaction cycle. The hydrogen produced from the electrolyzer is pumped to the Sabatier reactor and the oxygen is pumped to the liquefaction cycle.

In the liquefaction cycle, the methane and oxygen are compressed, cooled in heat exchangers and liquefied through Joule-Thompson expansion. Methane is pumped into two tanks to be stored at 10 atm and 135 K. Oxygen is pumped into a tank to be stored at 7.1 atm and 108 K. The storage tanks and the seed hydrogen tank are all insulated by Multi-Layer Insulation (MLI).[12] The MLI reduces the heat flux into the tanks to a total of 8 W. To prevent boiloff and propellant loss, the heat is removed from the tanks by a refrigerator.

With a mass of 140 kg and a power requirement of 500 W_e, the pumps and compressors are the largest part of the methane PPP. Other notable masses include 60 kg for tank insulation, 43 kg each for the Sabatier and RWGS reactors, and 30 kg each for liquefaction and refrigeration. In addition, liquefaction and refrigeration each require 300 W_e. The total power requirement is 1215 W_e.

Carbon Monoxide Plant

As an alternative to methane, carbon monoxide has been considered as a fuel choice. Because of its lower I_{sp} of 290 sec versus methane's 370 sec, a much larger quantity of carbon monoxide is required. The carbon monoxide plant must produce 3440 kg of CO and 1960 kg of O_2. Carbon monoxide and oxygen can be produced directly from the Martian atmosphere using the reaction:

$$2CO_2 \rightarrow 2CO + O_2 \qquad (4)$$

This reaction is carried out within a zirconia electrolytic cell. The almost pure O_2 that is produced is liquefied and stored. Due to incomplete reaction, the other exhaust stream will contain both CO and CO_2. Catalytic disproportionation[13] is used to separate CO from the CO_2 by the following reaction:

$$2CO \rightarrow C + CO_2 \qquad (5)$$

The plant actually requires two catalyst beds. One unit is used to break the CO into solid C and gaseous CO_2 while the other is heated to gasify the deposited carbon and produce CO from the reverse reaction. By using two catalyst beds, steady state production can be achieved.

The CO plant, shown in Fig. 3, is derived from a plant designed at the University of Arizona.[14] As in the methane case, the necessary propellant is produced in 1.4 years. The total production rate is 10.8 kg/day of propellant: 6.87 kg/day of CO and 3.93 kg/day of O_2.

The CO plant uses a hydrocyclone and membrane filter similar to the ones used in the methane plant. Again, the dust is retained in a sample canister for return to Earth. Because the zirconia cells operate at very high temperatures, the filtered atmospheric gases are not condensed to remove the nitrogen, argon, and other trace gases. Small amounts of these impurities do not adversely affect combustion, as was confirmed by computer analysis of CO/O_2 combustion with trace impurities present.[15] The zirconia cells should also not be affected by the trace gases.[14] The plant is designed to allow these gases to be vented at a later stage.

The CO_2 is heated and enters the zirconia electrolyzer unit at 1270 K. The zirconia cells require 250 mA/cm^2 of

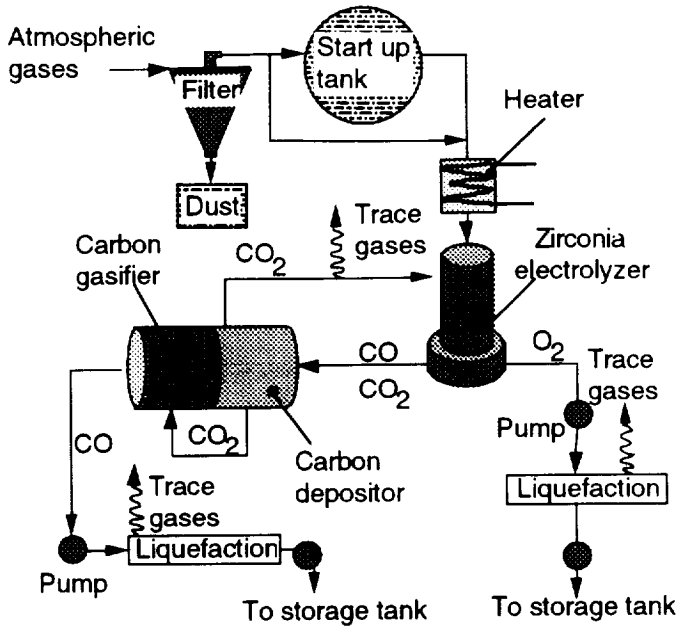

Fig. 3 Carbon monoxide propellant plant schematic

cell surface area. Experimentally determined efficiencies of 60% result in a power requirement of 193 W_e per kilogram of O_2 produced per day.[16] This translates into 140 A/kg(O_2)/day and 2128 cm^2 of cell surface area. The standard Westinghouse zirconia cell is 2.54 cm in diameter with a maximum length of 61 cm. Thus a single cell has a surface area of 486 cm^2. The CO plant requires five cells cut to a length of 54 cm to produce 3.93 kg/day O_2. The total power requirement for the zirconia cells is 733 W_e. Using five cells in series increases the conversion efficiency. If the cells are cascaded, the residual CO_2 from the previous cell is further electrolyzed producing more O_2 and CO.

Once the mixture exits the electrolyzer, enough CO_2 is still present to require a separation device. Two catalyst beds are used to separate the CO_2 from the CO. One unit operates at 700 K and rejects heat while breaking CO into C and CO_2. The other bed requires heat input, nearly equal to the heat output of the first unit, and gasifies the deposited C which combines with the CO_2 to form CO. The CO is then liquefied and stored. When one catalyst bed has accumulated a large amount of carbon, the flow over the beds is reversed and they reverse roles. The excess CO_2 is recirculated back to the zirconia electrolyzer for further electrolysis. Recirculation greatly reduces the intake requirement of the plant, resulting in a much smaller inlet nozzle area.

Start-up can be facilitated by filling a tank with atmospheric CO_2 and then using that gas to start the plant. Periodically, the recirculating CO_2 can be vented, since it will eventually become rich in trace gases. The small start-

up storage tank is refilled with fresh atmospheric CO_2 during normal operation, and that gas is used to replenish the vented CO_2.

When other requirements such as pumps and refrigeration are included, the plant has a total electrical power requirement of 1120 W_e. Although additional thermal power is required, this can be supplied by the radioisotope power source used to power the propellant plant. Because the power supply, described in the next section, operates at an efficiency of around 20% and has a total thermal output of nearly 8 kW, more than adequate heat energy is available from the power supply coolant to add the additional thermal energy required by the CO plant. Although the mass estimates for the CO plant are less refined, fewer components, such as pumps and compressors, as well as greater simplicity, give the CO plant an expected mass of 300 kg, roughly 100 kg less than the methane plant.

Power Supply

The propellant production plant requires slightly different power levels for the two scenarios. The methane plant requires about 1,215 W_e of steady state power while the carbon monoxide plant requires a slightly smaller 1,120 W_e. This relatively small difference allows for identical power supplies to be used in both propellant options.

For the two *in situ* propellant cases, power is supplied by a single Dynamic Isotope Power Supply (DIPS) derived from the Rockwell design.[17] The DIPS used for each mission contains two fuel canisters of 16 General Purpose Heat Source modules and supplies over 1,600 W_e of power. This power level is sufficient to run the plant for either scenario, in addition to other MLV operations such as communications equipment and science experiments. High power MLV operations, such as the MLV's remote manipulator arm, are run one at a time.

For the hydrogen case, using propellant exclusively imported from Earth eliminates the need for a PPP and therefore its power requirements. However, 780 W_e of power is needed for refrigeration of the stored hydrogen, therefore the same power system is used. An advantage of the hydrogen scenario is that more insulation could be added to reduce the power requirements, possibly enabling the use of existing RTGs and resulting in a small reduction in mass.[18]

MARS ASCENT ENGINES

No rocket engines currently in use utilize either methane or carbon monoxide as fuel, although oxygen is widely used as an oxidizer. Extensive research has been conducted using methane as a rocket fuel.[19-25] Carbon monoxide has only recently been researched as a rocket fuel, primarily at NASA Lewis Research Center.[26-31] Initial results have been promising. When considered as a rocket propellant, methane appears to be the fuel of choice because it has a higher I_{sp}, approximately 370 sec compared to about 290 sec for carbon monoxide.

Although a survey of existing engines was conducted to see if any could be converted for use with either fuel choice, the expansion ratios required are such that it is unlikely that any existing engine could be sufficiently modified for use with either methane or carbon monoxide. Methane has been tested in Pratt & Whitney's RL-10 engine.[19,20] However, the thrust of the RL-10 is several times higher than that required by this mission and would subject the smaller methane Earth Return Vehicle to very high accelerations. In addition, the RL-10 is more massive than an engine of this type need be. Because of these considerations, new designs for both a methane and a carbon monoxide engine were developed.

Because CO has a lower I_{sp}, considerably more propellant is required by a carbon monoxide based system than a methane based system. Thus, because of the resulting greater Mars launch mass of a CO system, a CO engine must have a higher thrust than its methane counterpart.

It should be noted that because Mars' ambient pressure is exceedingly low, any ascent engine will likely require an under-expanded nozzle to optimize the design. To expand the flow to Mars' ambient pressure would need an area ratio that is likely to require excessively large nozzle exit areas. Also, the thrust should be such as to limit the ascent to a reasonable flight time while not generating unduly high accelerations. Gravity losses increase with increasing flight time, consequently, minimizing time of ascent is also a priority. These considerations were taken into account when designing both engines. Table 1 shows the operating parameters determined for each propellant. Both engines operate on the expander cycle, which is known for its simplicity and proven technology.

The masses of both engines were estimated by comparing the characteristics to those of existing engines. Such a comparison suggested that both engines would have a mass of approximately 100 kg.

Both *in situ* scenarios require development of a new engine, although more research has been conducted using methane as a rocket fuel. Successful injector and chamber designs have been studied, and existing technology for such components as oxygen coolant pumps should make the design of a methane rocket substantially easier. Carbon monoxide is currently being studied as a rocket propellant at NASA Lewis Research Center. These studies will greatly

Table 1 Engine operating parameters

Characteristics	Methane	Carbon Monoxide
Mixture Ratio (O/F)	4:1	0.57:1
Fuel Inlet Temperature (K)	135	128
Oxidizer Inlet Temperature (K)	150	150
Chamber Pressure (MPa/psi)	6.9/1,000	6.9/1,000
Chamber Temperature (K)	3,600	3,470
Exhaust Molecular Weight (g/mole)	22.9	37.5
Specific Heat Ratio (Combusted)	1.146	1.140
I_{sp} (s)	370	292
Thrust (N)	29,000	42,000
Mass Flow Rate (kg/s)	7.78	14.6
Nozzle Exit Velocity (m/s)	3,633	2,862
Nozzle Exit Pressure (Pa)	2,200	1,245
Area Ratio	225	375
Throat diameter (cm)	5.1	6.1
Exit diameter (m)	0.76	1.18

add to the database of knowledge for carbon monoxide rockets.

For the imported hydrogen/oxygen case, the same engine is used for both Mars landing and ascent. A currently available engine that could be used is Pratt & Whitney's RL10A-3-3A. This engine is flight qualified and currently used on the Centaur. Although the RL-10 produces a greater thrust than required by the hydrogen ERV, it is used to land the much more massive Mars Landing vehicle. As a result, the maximum thrust required by the hydrogen engine is greater than that of either the methane or the carbon monoxide engine

VEHICLE / SYSTEMS INTEGRATION

The MLV is comprised of a structural frame, an aerobrake, and payload elements, which are arranged according to several constraints:

- Center of mass envelope
- Aerobrake envelope
- Proximity of components
- Size of launch fairing

It is necessary to maintain the center of mass close to the centerline, and relatively low for launch vehicle considerations.[32] Also, to reduce heat loading on the MLV, the structural frame and payload must remain entirely inside the wake of aerobrake while passing through the atmosphere of Mars. In addition, some components are located close together to reduce piping, wiring, etc. Finally, the MLV and its aerobrake must fit within the payload fairing.

Figures 4 and 5 show the configuration of the MLV for the methane/oxygen scenario. The MLV is divided into two main sections. The upper section, seen in cut-away A-A, Fig. 5, contains the ERV and the DIPS with its radiators. The parachutes and support structure above the ERV are separated from the vehicle before landing. The lower section holds the MLV experiment package, the surface rover, the propellant plant, the undeployed satellite, and the seed hydrogen. The overall design of the MLV is similar for the CO and H_2 options; however, the dimensions differ slightly.

Structure

The MLV's structural frame is broken down into the central truss frame, the thrust structure, and the Centaur adapter. All structural members are 4 cm OD by 3.6 cm ID tubes, and are made of aluminum-lithium 2090-T83. Connections are made with titanium tube end fittings and pins, where welding is not practical.

The central truss frame holds all of the payload elements, and consists of four octagonal rings connected by vertical beams and other cross-members. At the bottom of the central truss frame, the thrust structure forms a fifth ring which is based on a Boeing stiffened web construction.[33] The upper stage adapter lies below the thrust structure, and is disconnected with pyrotechnic bolts once the upper stage has separated from the MLV. The parachute support structure also separates using pyrotechnic bolts just before the MLV begins retro-firing its landing engines.

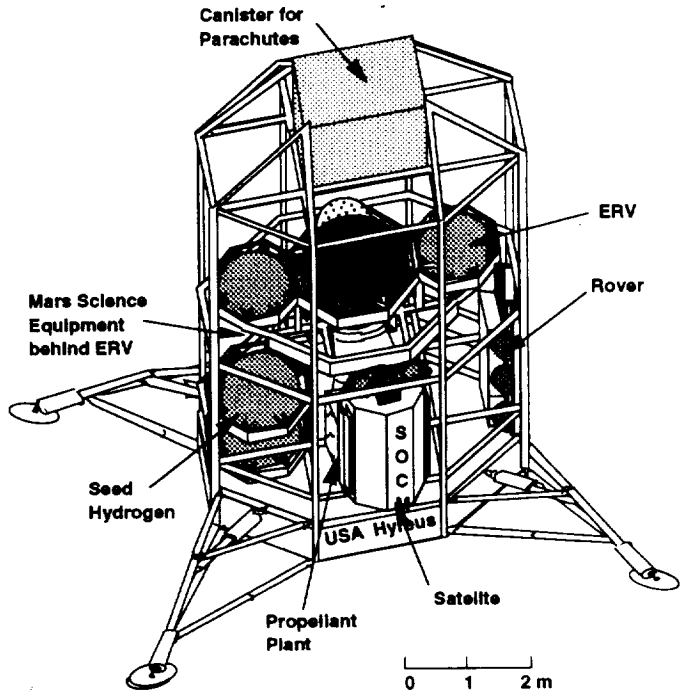

Fig. 4 Methane MLV isometric view. Not all components shown. (CO and H_2 MLVs are similar)

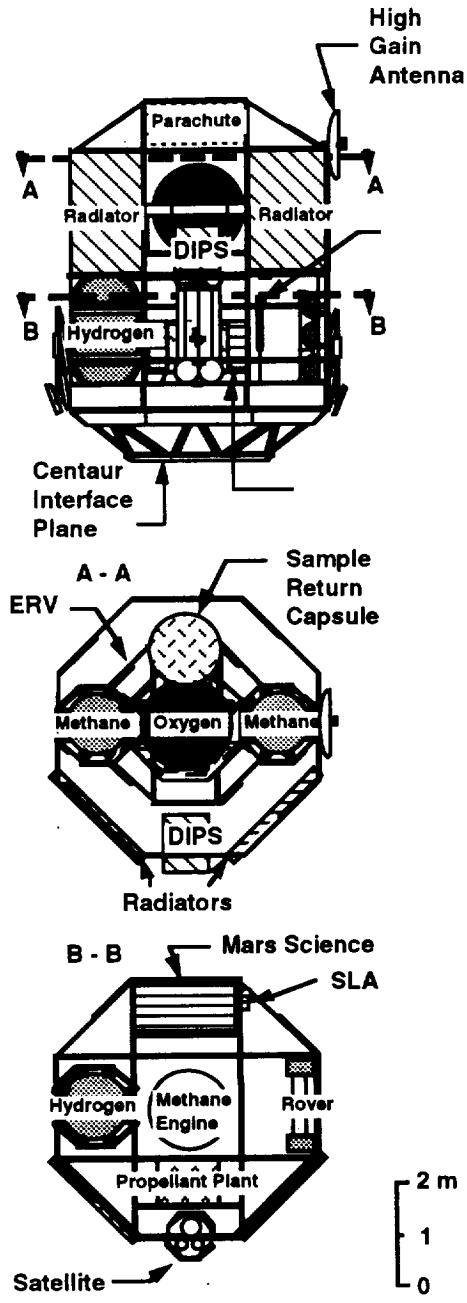

Fig. 5 MLV layout. Aerobrake shell is not shown. (CO and H_2 MLVs are similar)

- Propellant must be easily storable.
- Engines must be simple and reliable.
- Must have sufficient net thrust for a landing thrust/weight ratio of ~1.2
- Low mass and high specific impulse.
- Use same propellant in retro engine as in RCS (except in H_2 MLV).

With these requirements in mind, the Marquardt R-40B and R-4D engines were selected for the CH_4 and CO MLV options. Both are currently in production and both use the same propellants. With a nominal thrust of 4,000 N, four Marquardt R-40B engines (I_{sp} = 303 sec) are needed to meet the required net thrust for the CH_4 and CO MLV options. These four engines are spaced evenly on the bottom of the MLV. The R-4D thrusters (nominal thrust = 400 N, I_{sp} = 312 sec) are mounted on the MLV as shown in Fig. 6, to complete the RCS. Their location and thrust provide a maximum angular acceleration of 5 deg/sec^2.

In the H_2 MLV scenario the RL10A-3-3A H_2/O_2 ascent engine is used for landing because of the much greater mass of the MLV for this option. The RCS is similar to that of the other two MLV options.

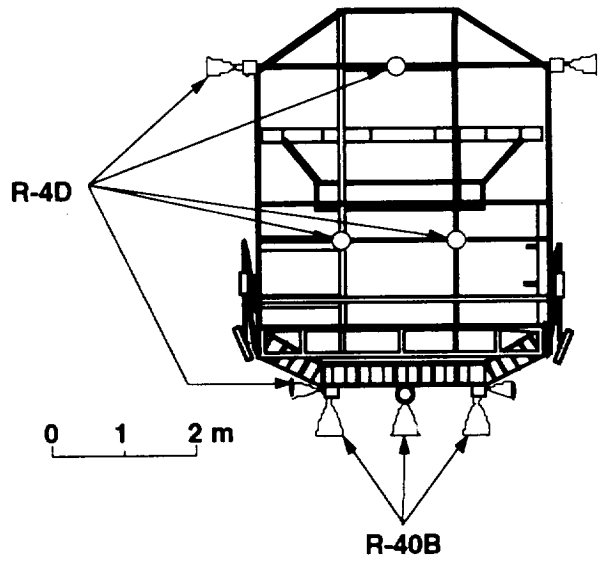

Fig. 6 Side view of CH_4 MLV, showing placement of engines for RCS. (Similar for CO MLV)

Landing Engines and Reaction Control System

Several different types of rocket engines were examined for the retrorocket system and the reaction control system (RCS). The criteria used in selecting an appropriate package were:

MLV Aerobrake Design

The geometry of the Mars aerobrake for the methane fuel case (see Fig. 7) is the raked-sphere cone design, which provides the L/D requirement of 0.4 to perform skip maneuvers in the Martian atmosphere.[34] For the methane

case, the dimensions of the aerobrake are 11.3 m by 9.4 m in order for the MLV to be shielded from the wake, and have the proper aspect ratio for providing the required L/D. Its mass is 735 kg. Because the width of the aerobrake is larger than the diameter of existing launch vehicle fairings, the aerobrake must be hinged to allow it to fold around the MLV. The aerobrake for the carbon monoxide fuel case is slightly smaller (10.4 m x 8.7 m) and thus lighter in weight (635 kg) than for the methane case. When the CO aerobrake is hinged, it easily fits into an existing launch vehicle fairing. The aerobrake for the hydrogen fuel case is much larger and heavier (14.7 m x 12.2 m, 1250 kg) than any existing fairing and may require in-orbit assembly.

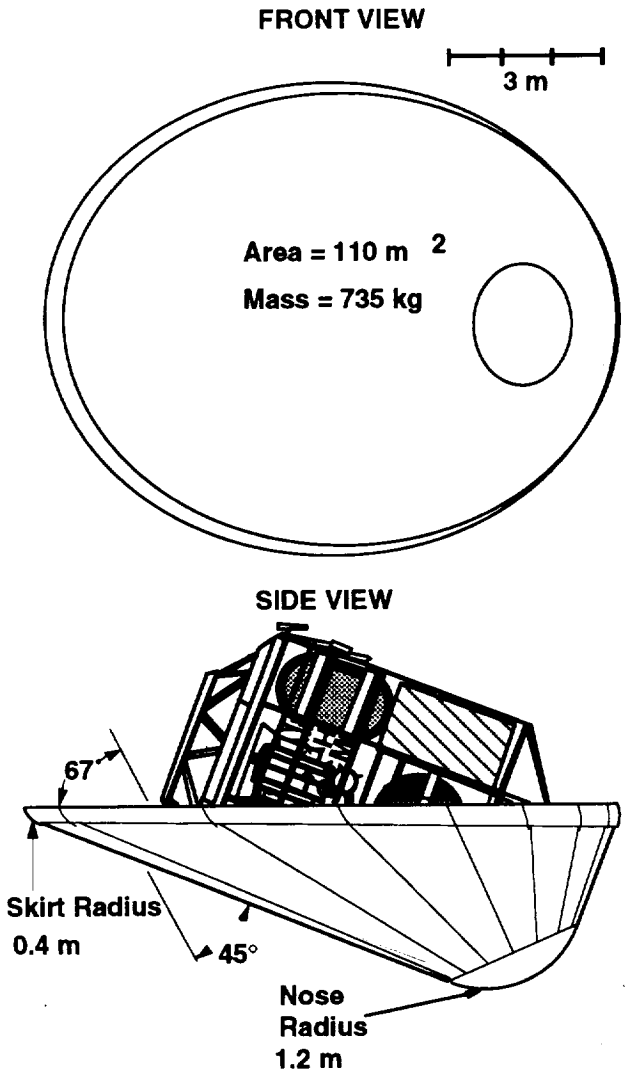

Fig. 7 Mars aerobrake configuration for methane case. (Configuration for other cases is similar; dimensions are different)

The thermal protection system (TPS) for the aerobrake consists of an ablative material (advanced carbon/carbon composite material) for the stagnation region and a non-ablative material (Fibrous Refractory Composite Insulation-FRCI-12) for the rest of the aerobrake.[35] A layer of reaction cured glass (RCG), a high emissivity glass material, coats the surface of the aerobrake. The TPS is mounted on an Aluminum honeycomb core structure with graphite epoxy face sheets.[36] The TPS is the same for each propellant case, because, although the area changes, the ballistic coefficient is the same. The aerobrake is affixed to the MLV by a set of struts similar to the structure of the vehicle.

The ERV

Nested inside the MLV is the ERV, which mainly consists of a thrust frame, a gimbaled ascent engine, propellant tanks, and sample return capsule (SRC). Figure 8 shows the ERV designs for all three scenarios considered here. The main difference between the two ERVs based on *in situ* resource utilization is the greater mass of propellant required for the carbon monoxide option. Therefore the carbon monoxide ERV has four large cylindrical fuel tanks instead of the two smaller spherical tanks on the methane ERV.

The MLV and ERV are both different for the imported hydrogen and oxygen scenario. The hydrogen MLV has no propellant production plant, and the ERV contains a large imported hydrogen tank, as well as an imported oxygen tank. Also, as noted earlier, the ascent engine on the hydrogen ERV is used for retro-firing the MLV when landing, which requires that the hydrogen ERV sit much lower in its MLV and that the engine have higher thrust capability. The hydrogen and oxygen for descent, rover operations, and ascent are stored in the same large tanks on the hydrogen ERV, thereby reducing the refrigeration and tank mass requirements.

For each case, the ERV is made of aluminum-lithium 2090-T83 4 cm OD x 3.6 cm ID structural tubing, and its basic truss structure is comprised of one octagonal ring with its thrust frame welded to the inside. The propellant tanks, however, are made of Weldalite™ due to its higher welding strength. The tanks are held in place as shown in Fig. 8.

The SRC consists of the sample container, an aerobrake for slowing down at Earth, an engine for circularizing the orbit after aerobraking, a small solar array, batteries to provide power after aerobraking, and a low-gain antenna for telemetry. The SRC is mounted on the ERV beside the propellant tanks, as shown in Fig. 8. The slight lateral displacement of the center of mass of the ERV resulting from this placement is compensated by gimbaling the ascent engine.

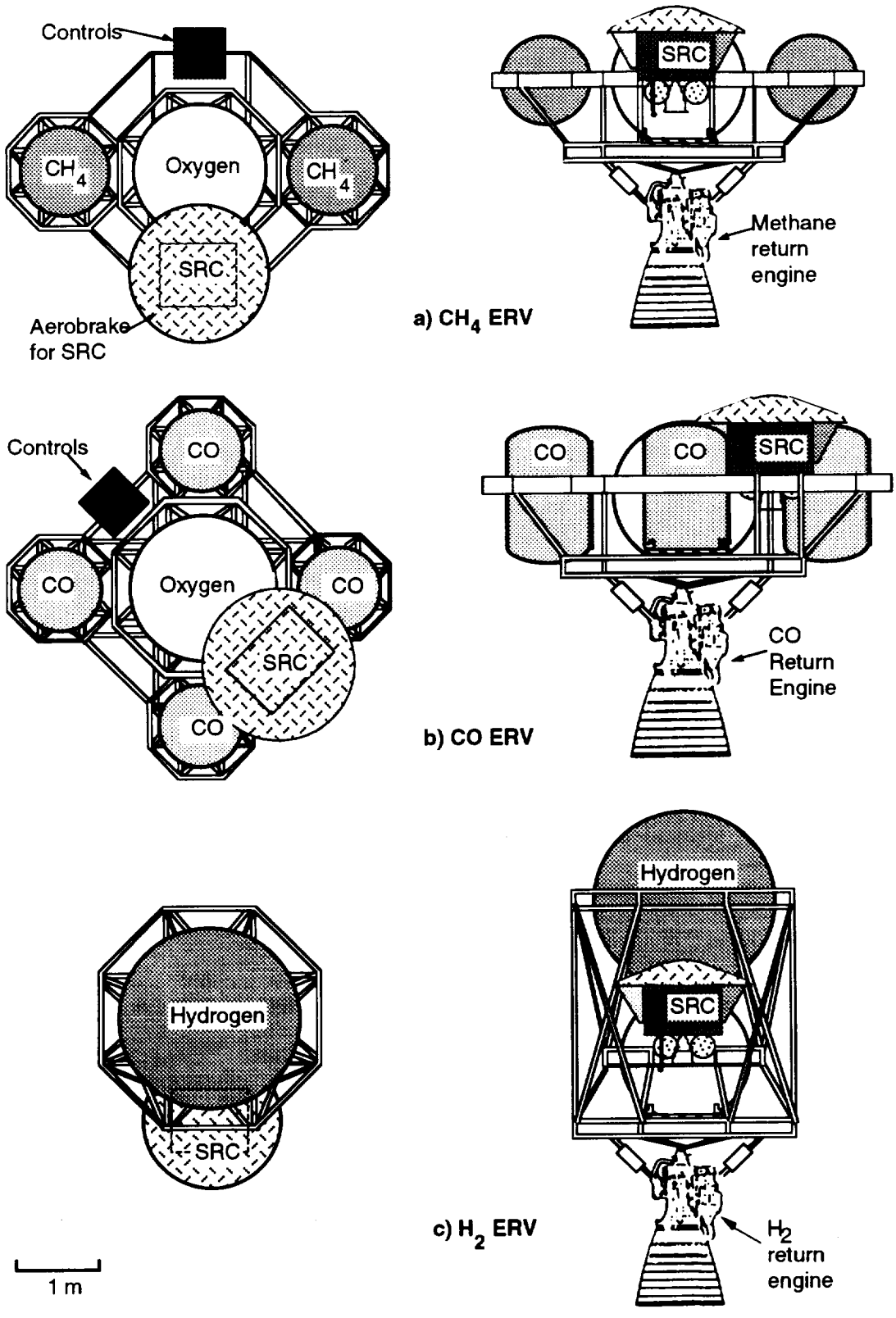

Fig. 8 ERV configuration for the three propellant scenarios

Rover

Sample collection on the Martian surface is accomplished by a robotic rover vehicle that is also powered by indigenous propellants (see Fig. 9). This is a semi-autonomous vehicle equipped with a remote manipulator arm, drills, and tools for sample collection. With a maximum speed of 3 kph, the rover has a range of 45 km and a mass of 185 kg. The material for the rover's primary chassis is Al 7079-T6; composites are used for secondary structures. The rover is a six-wheeled vehicle with three individual sections joined together by swivel joints. Each section's frame is 1 m wide and 0.44 m long, and has a wheel attached to each side via a wishbone suspension. The rover's tires are similar to those on the Apollo LRV but are smaller, with a diameter of 0.5 m and a mass of 4 kg.[36] During its stay on Mars, the rover is designed to perform a total traverse of ~150 km, which is the approximate lifetime of its tires.

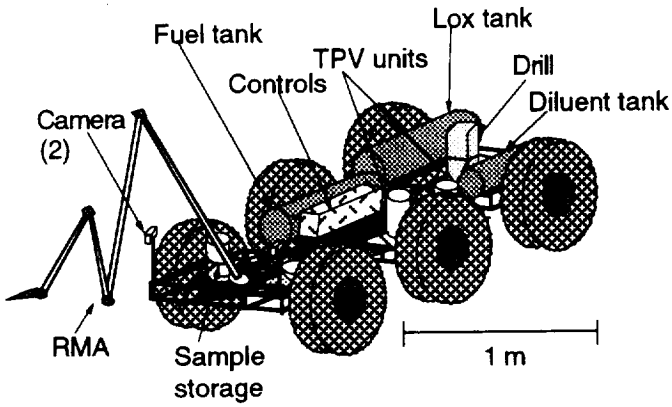

Fig. 9 Layout of rover. (Radiator not shown, for clarity)

Power Source. For present purposes, the power generating system selected for the rover is a thermophotovoltaic (TPV) generator producing 1 kW_e of power. This unit utilizes two-junction GaAs/GaSb tandem photovoltaic cells, in conjunction with an infrared emitter burning a mixture of the *in situ* propellant and oxygen. The TPV unit is currently being developed by the Vehicle Research Institute (VRI) at Western Washington University in Bellingham, WA, for use in automobiles, but it is an ideal generator for use on the rover, as it has no moving parts.[37] The TPV can burn any of the three propellant combinations considered here.

Combustion occurs inside a 2 cm dia. x 50 cm long tungsten tube at a pressure of 1 atm and a temperature of approximately 2,150 K, well within the material limits of the tube. The flame temperature is limited to this value by adjusting the O/F ratio and using stored atmospheric CO_2 as a diluent. Approximately 3.3 kW of radiant energy are emitted from the tube walls to the thermophotovoltaic cells, which are arrayed symmetrically around the tube on a 7.5 cm radius.[6] The photovoltaic cells, which operate at 373 K, are 30% efficient. Thus ~2.3 kW of waste heat must be radiated using fins having a total surface area of 2.5 m^2 (convective contributions to heat rejection were ignored). The output of the TPV unit can be fed directly to the wheel motors and/or to onboard nickel metal hydride storage batteries.

The size of the radiator may be problematic, particularly in the presence of high winds. Therefore, alternatives to the TPV power source should be considered. One potentially attractive power source is a gas generator turbine driving an alternator, which supplies electricity to the wheel motors directly and to the storage batteries. Such a device would be compact, lightweight, and flexible, and would not require a radiator. However, it does involve a rotating component.

Satellite

A small satellite, illustrated in Fig. 10, is placed in a sun synchronous orbit around Mars by the MLV. The primary mission objective of the orbiter is to look for subsurface water deposits (ice) using a ground penetrating radar (GPR) system. Also, the satellite is equipped with a weather monitoring system (wide-angle camera) to warn the rover of impending Martian dust storms. In addition, the orbiter provides a communication link between the rover and the MLV.

The Sun-synchronous orbit is almost polar, with an inclination of approximately 87°, therefore, most of the planet's surface is covered by the satellite's camera and GPR. The satellite is deployed from the MLV before the spacecraft performs its final aerobraking maneuver for landing. Deployment occurs at the apoapsis of the landing orbit (580 km). A small burn (ΔV = 100 m/sec) with the satellite's hydrazine control thrusters is required to circularize its orbit.

After orbital insertion, solar panels are deployed, and for gravity gradient control, a lattice type extendible boom separates two sections of the satellite. Gravity gradient stabilization is the primary method of control, but a three-axis stabilization system is used for occasional orbital maintenance and for orbital insertion. The total wet mass of the satellite is 280 kg, and the dry mass is 260 kg. The GaAs solar panels provide 350 W_e of power to the satellite, most of which is required by the GPR system.

The satellite does not communicate directly with Earth. Instead, it dumps data to the MLV, which relays the information to Earth. The ERV is equipped with a low-gain antenna for in-transit communication on both the incoming trip to Mars and the return to Earth voyage. Upon landing on the Martian surface, the MLV deploys a high-gain antenna for Mars/Earth communications. Both the rover and the satellite have low-gain antennas for communication with

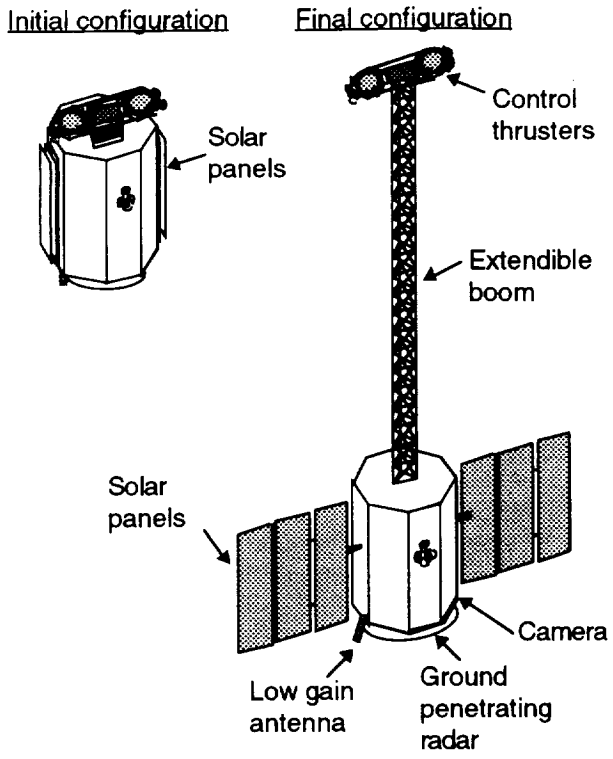

Fig. 10 Satellite configuration and boom deployment

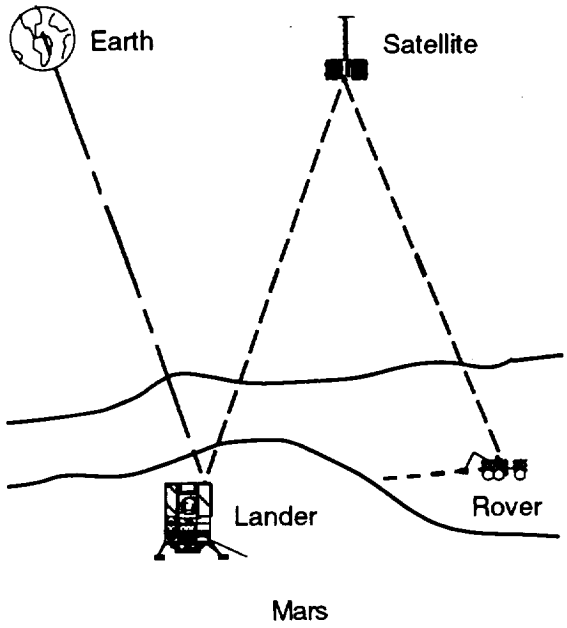

Fig. 11. Communication architecture

the MLV. If the rover/MLV communication link is blocked by terrain, the rover can still communicate with the MLV via the satellite.

Overall Mass Inventory

A complete list of system masses for all three scenarios considered is presented in Table 2. Note that the carbon monoxide option has a nearly 10% lower Earth launch mass than the methane scenario. This lower mass requirement stems from the fact that seed hydrogen is not needed, and from the lower aerobrake mass required by the slightly smaller MLV. Not surprisingly, the imported hydrogen/oxygen option is much more massive than either of the two indigenous propellant options. In particular, it is more than twice as heavy as the carbon monoxide option.

Table 2 Mission mass comparison

Component	CH_4/O_2 system mass (kg)	CO/O_2 system mass (kg)	H_2/O_2 system mass (kg)
H_2/O_2 propellant	–	–	3000
Seed H_2 & tank	210	–	–
Propellant plant	400	300	–
Power & control	300	300	300
MLV structure	980	835	1625
Aerobrake	735	635	1250
Parachutes	250	210	480
Landing propellant & tank	310	260	–
Landing engines/RCS	75	75	100
Science equipment	230	230	230
Satellite	280	280	280
Rover	185	185	185
Earth return vehicle	540	720	720
TOTAL	4495	4030	8170

EARTH LAUNCH SYSTEMS

In-situ resource utilization permits the use of a wider variety of existing launch vehicles. Elements considered when evaluating launch systems include:

- C3 capability
- Availability
- Reliability
- Existing hardware (i.e. payload fairings, launch facilities, upper stages, etc.)
- Cost

Several launch systems were considered.[38] The American systems evaluated include the Titan III, the Titan IV, the Space Shuttle, and the Delta. Three Russian launch vehicles, the Energia, the Proton, and the Zenit, were

also considered, as was the European Space Agency Ariane V.

The Delta and the Zenit do not have the ΔV capability to launch any of the three systems. The Titan III, the Proton, and the Ariane V could launch a carbon monoxide-based system. However, these three vehicles do not meet the ΔV requirements of a methane or hydrogen based system. As a result, the use of a Titan III, a Proton, or an Ariane V with a methane-based system is possible only by reducing the scientific payloads, such as the rover, the satellite, or the science package. The hydrogen-based system cannot be handled by these three launchers under any circumstances. The Space Shuttle, the Energia, and the Titan IV/Centaur are all capable of launching either *in situ* propellant system. Only the Titan IV/Centaur and the Energia have the lift capability to be used with the hydrogen system. The Titan system would require the Centaur structural upgrade and a large fairing, which would increase the launch mass sufficiently to bring this launch system close to the limits of its capability. Any significant mass growth in final design and construction of the spacecraft would render the Titan IV/Centaur system incapable of launching the hydrogen based option.

The Titan III and Titan IV, as well as the Proton, are all readily available. The Space Shuttle has a considerable backlog but could be used if desired; however, its limited payload bay diameter would predicate in-orbit assembly of the aerobrake. Only two Energia vehicles currently exist, with a third partially completed.[39] The Ariane V is not scheduled for first launch until 1995 or later.

Table 3 shows the success rate of the capable launch systems.[40] The reliability, R, is defined as the number of successful launches divided by the total number of launches. To date, the Titan IV has the highest success rate at 6 for 6. The Energia has only flown twice, the first flight an unsuccessful test of the cargo carrier version and the second a successful unmanned test of the Buran space shuttle. The Ariane V has yet to fly, making evaluation of its reliability impossible. The Proton has the lowest success rate of all, except for the Energia, and is thus questionable as a candidate launch vehicle. The Space Shuttle has only had one unsuccessful flight.

With the exception of the Ariane V, all the capable launch vehicles currently exist. None of the existing vehicles has a payload fairing large enough to enclose the spacecraft designed, although McDonnell Douglas has made proposals to the Air Force for a variable diameter fairing for the Titan IV that could enclose the spacecraft as currently designed.[41] The smaller aerobrake of the carbon monoxide system would require the least amount of modification to the fairing. Minimal modifications to the launch vehicle would be required. The methane system would require a fairing over 7.5 m in diameter. When dynamic envelope and manufacturing considerations are included, the five segment

Table 3 Launch vehicle comparison

Vehicle	Launches (Successful/ Total)	Reliability (R)	Cost (M $1992)
Titan IV	6/6	1.000	200-400
Titan III*	144/155	.929	150-225
Space Shuttle	54/55	.982	300-500
Energia	1/2	.500	110
Proton	164/187	.877	35-70
Ariane+V	--/--	--	>110 (?)

* Titan III launch cost includes the price of a TOS upper stage

\+ Ariane V planned to cost no more than 90% of the Ariane 44L

fairing required would have a mass of over 10,000 kg. Such a fairing would require enlargement of the core of the Titan launch vehicle. The hydrogen option's aerobrake, the largest of the three, would be even more difficult to enclose within an existing fairing. It is likely that it would have to be assembled onto the MLV in LEO.

Russian launch systems are somewhat less than ideal for this mission. The upper stage used with the first Energia launch, a cargo carrier vehicle that failed, is not powerful enough. Two new upper stages were supposed to have been built by 1992. Construction or testing of these upper stages has not been confirmed as of this writing. Another problem with any of the Russian systems is that Russian launch vehicles are integrated and fueled horizontally. The structural design of the spacecraft does not take into account the lateral loads involved with horizontal integration. Such structural upgrades would doubtless raise the mass of all three systems, possibly placing the carbon monoxide-based system out of the capability range of the Proton.

Table 3 also shows the cost of each system.[42] The cost of the upper stage of the Ariane V was not available at the time of writing. As a result, the final cost of this system will doubtless be higher than that listed in Table 3. It is interesting to note that the American launch vehicles are much more costly than the Russian or European systems. Thus, should the political climate allow, serious consideration of a foreign vehicle is warranted, if cost is a determining factor.

Based on the above arguments, determination of the best launch vehicle suited for this mission is problematic. While the Titan IV/Centaur appears to be a good choice in terms of capability, reliability, and availability, it is one of the most expensive systems available. If mission success is determined to be of the utmost importance, then cost may be less of a concern than reliability. Such considerations must be carefully weighed by mission planners.

FLIGHT SEQUENCE

The orbital mechanics for this mission are not dependent on the propellant selected. They are based on a launch in the early 21st century (2003) to allow about ten years for development. Using an aerobrake greatly reduces the mass launched from Earth.

Astrodynamics

To maximize the payload, the transfer trajectory energy is minimized using the lowest energy launch opportunities and trajectories, minimizing the velocity increment needed on arrival at Mars or Earth. The transfer trajectory variables which define the transfer orbit were obtained from Jet Propulsion Laboratory publication 82-43.[43]

The Earth to Mars transfer is a Type I trajectory, with the launch window defined by a maximum departure energy value of $C_3 = 10\ km^2/sec^2$ and a Mars arrival date of December 25, 2003. The launch window opens on May 22, 2003 and closes on June 20, 2003 with the optimal launch date on June 7, 2003. The velocity increment required for injection from LEO to Mars ranges from 3.60 km/sec to 3.65 km/sec. The time of flight ranges from 188 days to 217 days.

The Mars to Earth transfer is a Type II trajectory. The launch window, defined by a maximum C_3 of $14\ km^2/sec^2$ and an Earth arrival date of March 31, 2006, opens on June 25, 2005 and closes on July 21, 2005 with an optimal launch date on July 8, 2005. The total velocity increment required for injection from LMO to Earth ranges from 2.63 km/sec to 2.69 km/sec. The time of flight ranges from 253 to 280 days.

The total mission time is approximately 2.8 years with a Martian surface stay time of about 1.5 years.

Aerobraking Scenario At Mars

Aerobraking was chosen for capture and entry at Mars as well as capture at Earth, over all-propulsive braking, because this significantly reduced the ΔV requirements of the propulsion systems. Consequently, the launch mass decreases because of a reduction in propellant needed to decelerate the vehicle at Mars. For example, aerobraking saves over 5,000 kg for the hydrogen case. The basic aerobraking scenario is the same for each of the three cases.

Instead of a single entry to landing scenario, the MLV performs a multi-pass scenario with a parking orbit before entry and landing at Mars.[34,44] This scenario allows for deployment of the satellite and for the rotation of Mars to bring the landing site into proper alignment. The sequence begins with the MLV arriving from Earth in a hyperbolic transfer trajectory and making its first atmospheric pass for aerocapture at Mars.[45] This pass places the vehicle into an elliptical polar orbit around Mars. A small burn of 55 m/sec at apoapsis is performed to raise the periapsis out of the atmosphere. As soon as the landing site is in proper alignment, the MLV performs another burn at apoapsis to lower the periapsis and enter the atmosphere for a second aerobraking pass. Table 4 below gives a summary of the two aerobraking passes.

Table 4 Summary of aerobraking passes at Mars

	First Pass	Parking Orbit	Second Pass
Entry Velocity (km/sec)	5.69	–	3.91
Exit Velocity (km/sec)	3.90	–	3.59
Exit Angle, γ (deg)	7.47	–	5.13
Apoapsis Burn (m/sec)	–	56.5	36
Periapsis Altitude (km)	-20	250	-97
Apoapsis Altitude (km)	2,470	2,470	600

The second atmospheric pass is a skip maneuver that lowers the apoapsis to an altitude of 580 km on exit from the atmosphere. At the apoapsis point, the satellite is deployed by the MLV and performs its own circularization burn while the MLV re-enters the atmosphere for final descent and landing. For final descent, the vehicle aerobrakes to an altitude of 10 km, whereupon the aerobrake is jettisoned and a cluster of three parachutes is deployed for continued braking. The parachutes will differ in total area depending on the mass of the system being considered (CO, CH_4, or H_2). Finally, retro-firing is required in the final phase of descent to bring the MLV down to a soft landing on the Martian surface.[36]

Earth Return Scenario

Shortly before the launch window for return to Earth opens, the propellant plant ceases operation in the CH_4 and CO scenarios, and the last samples are loaded aboard the SRC on the ERV. When all systems are ready, the ascent engine ignites and the ERV lifts off the Martian surface. The ΔV budget for the Mars launch and Earth return is given in Table 5.

The DIPS provides the power for launch via an umbilical. The batteries on the SRC provide power for the ERV on the Mars ascent. Upon achieving a low Mars orbit of 300 km altitude, the ERV coasts until it reaches the burn

Table 5 ΔV budget for Mars launch (m/sec)

Velocity at parking orbit insertion	3412
Velocity penalty due to drag	< 5
Velocity penalty due to gravity	146
Transfer Orbit Injection ΔV (max)	2693
ΔV gain from Mars rotation	– 232
TOTAL	6,024

point for the interplanetary transfer orbit injection. The ascent engine fires again and boosts the ERV through the velocity increment required to send it to Earth. Once the ERV is in its heliocentric transfer trajectory, the solar array deploys and begins recharging the SRC's batteries. The 0.34 m^2 GaAs solar array also provide 40 W for maintaining the Martian samples at regular Mars surface temperatures and for operating the SRC's low-gain antenna. The vehicle orients itself so that the small aerobrake on the Earth return capsule shades the sample container. This maneuver alleviates the need for a large and elaborate refrigeration system that would otherwise be required to reject the heat from the sample canister due to the solar flux. Temperature control is essential for maintaining Mars ambient conditions in order to preserve the state of volatile components of the samples.

When the ERV reaches the Earth's sphere of influence, the SRC, which consists of the sample canister, an ablative aerobrake, and a small propulsive and control system, detaches from the rest of the ERV. The ERV then performs a contamination and collision avoidance maneuver (CCAM) which moves it away from the SRC. During the CCAM, the ERV reorients itself so that the thrust vector is away from the Earth return capsule, yet the exhaust does not impinge on the capsule. The appropriate RCS thrusters fire to depletion. The ERV coasts away from the capsule for a brief time. When the ERV is a safe distance from the Earth return capsule, the remaining primary propellants are burned in the main engine. This provides the small boost required to prevent the vehicle from re-entering the Earth's atmosphere and burning up. The ERV swings by Earth in a hyperbolic orbit and continues back out to deep space.

The sample return capsule, now powered by its internal batteries, re-enters the Earth's atmosphere at an entry angle of 11.8° and an entry velocity of 11.2 km/sec, using an Apollo style ablative heat shield for the aerocapture pass. This maneuver decelerates the capsule to a velocity of 7.27 km/sec. Once the aerobraking is completed, the orbit is circularized at 340 km with a ΔV of 490 m/sec, provided by a small monopropellant engine. The capsule is then reoriented to shade the sample container from sunlight, and awaits retrieval by the Space Shuttle. As an alternative, the capsule could be picked up at either Space Station Freedom or Mir, provided one of them is in orbit at the time. Preliminary analysis of the samples can be conducted in orbit to determine if there is any danger of biological contamination. If deemed safe, the samples can be returned to Earth. If for some reason the decision is made not to return the samples to Earth's surface, the samples can either be sterilized and disposed or the sample container can be attached to a payload assist module and boosted to a quarantine orbit or back into deep space.

CONCLUSIONS

Two different *in situ* propellant combinations, CH_4/O_2 and CO/O_2, have been compared to importing H_2/O_2 for use as the return propellant in a Mars rover sample return mission. Clearly, *in situ* resource utilization (ISRU) offers a significant mass savings over importing terrestrial propellants. When considering space operations in terms of cost per kilogram of payload, ISRU appears quite attractive, as it reduces costs by a factor of two. With only a modest investment, engines and propellant plants for either of the ISRU systems can be developed. The decision of what *in situ* propellant is the correct choice is much less clear. A more careful evaluation is necessary.

The components and reactions used in the methane plant are well developed and understood. The Sabatier reactor has been in use in industry for over a hundred years. The water electrolyzer has been used extensively on submarines for many years. On the other hand, the Sabatier reactor only produces methane in an oxidizer to fuel ratio of 2:1. Because the rocket engine requires a mixture ratio of 4:1 to achieve the Isp of 370 sec (only 340 sec is possible at 2:1 ratio), the Sabatier reactor must be coupled with a reverse water gas shift reactor to produce the additional oxygen. The greatest disadvantage of methane is that the procedure relies on seed hydrogen which must be imported. This increases the mass, complexity, and failure modes of the mission. The plant also produces CO as a by product, which is vented directly to the Martian environment.

In contrast, the carbon monoxide plant does not rely on imported hydrogen, thus reducing Earth launch mass and eliminating failure modes. Because the plant requires only Martian CO_2 as an input, the amount of propellant that can be produced is limited only by the lifetimes of the components of the plant and the power source. The CO plant is also less complex, smaller, and requires less power. However, the components of the carbon monoxide plant are less well developed. A possible failure point is the unit used to separate the CO from the other gases, which requires periodic flow reversal. The basic reaction used in the CO plant is endothermic, requiring thermal input that must be supplied by a heater or taken from the power supply coolant.

Selection of one in-situ propellant scenario over the other is difficult. Although methane would reduce the amount of propellant required, as well as the Mars launch mass, carbon monoxide alleviates the need for importing seed hydrogen from Earth, thus reducing Earth launch mass

and complexity. On the other hand, a methane fueled rocket would most likely require less research investment, because considerable work has already been completed.

Other considerations must also be taken into account. Although carbon monoxide offers a mass savings over methane, the lower I_{sp} makes it uninteresting for most other applications. A CO system would require prohibitively large amounts of propellants for use on Venus, for example. Methane, on the other hand, has been studied for Earth-to-orbit engines and could be used for other, higher energy applications. Another concern is the high toxicity of CO. The use of such a toxic propellant in future manned missions may prove undesirable.

The simplicity of the CO system warrants consideration. By using only one gas for input, the CO system eliminates the reliance on hydrogen. Multiple lander relocation and continued rover operation after the departure of the ERV are some of the possibilities not available with methane. Other studies indicate that CO would offer substantial mass and power savings with manned missions as well.[46]

Ultimately, the choice of which in situ propellant to use will reside with the mission planners. Regardless of the choice, however, it is clear that ISRU offers considerable savings. In the current atmosphere of tight budgets and low funding, ISRU offers a less expensive alternative to planetary exploration.

ACKNOWLEDGMENTS

This work was funded by a grant from the NASA/USRA Advanced Design Program.

Our sincerest thanks go to Diane Linne and Mary Wadel of NASA Lewis Research Center; Tom Callahan, Phil Ginser, David Roldness, Steve Seus, and Mike Holquin of General Dynamics; Ed Parsons of the Air Force Public Affairs Office; Captain Kevin Klonoski and Lt. Tim Dickinson of the Titan IV Program Office; Peter Nolan of the University of Arizona; Dana Andrews, Jeff Cannon, and John Jordan of Boeing; Robert Hartmann of General Electric; Clarence Quan of McDonnell Douglas; and Tim Voght of Martin Marietta; Mike Tauber of NASA Ames Research Center; Don Rethke of Hamilton Standard Division of United Technologies; Mike Duke, Tom Sullivan, Dwayne Weary, and David Weaver of Johnson Space Center.

We are also indebted to everyone else who provided assistance on this project, in particular the students who participated in an earlier study and A. Hertzberg for his support and encouragement.

REFERENCES

1. Zubrin, R.M., Baker, D., and Gwynne, O., "Mars Direct: A Simple, Robust, and Cost Effective Architecture for the Space Exploration Initiative," AIAA Paper No. 91-0326, 29th Aerospace Sciences Meeting, Reno, NV, Jan 7-10, 1991.

2. Zubrin, R.M., "In-Situ Propellant Production: The Key Technology Required for the Realization of a Coherent and Cost-Effective Space Exploration Initiative," Paper No. AIAA 91-668, 42nd Congress of the International Astronautical Federation, Montreal, Canada, October 5-11, 1991.

3. Ash, R.L., Dowler, W.L., and Varsi, G. "Feasibility of rocket propellant production on Mars," *Acta Astronautica*, 1978, Vol. 5, pp. 705-724.

4. Ramohalli, K., Dowler, W., French, J., and Ash, R., "Novel Extraterrestrial Processing for Space Propulsion," *Acta Astronautica*, Vol. 8, N0 5-6, 1987, pp. 511-526.

5. Bruckner, A.P., Cinnamon, M., Hamling, S., Mahn, K., Phillips, J., and Westmark, V., "Low-Cost Manned Mars Mission Based on Indigenous Propellant Production," AIAA Paper 93-1010, February 1993.

6. Bruckner, A.P. et al., "Project Hyreus: Mars Sample Return Mission Utilizing *In Situ* Propellant Production," *Proceedings of the 9h NASA/USRA Advanced Design Program Summer Conference*, Houston, TX, June 14-18, 1993, in press.

7. COMPLEX, Strategy for Exploration of the Inner Planets: 1977-1987, National Academy of Sciences, Washington, DC., 1978.

8. Kleiner, G.N. and Cusick, R.J., "Development of an Advanced Sabatier CO_2 Reduction Subsystem," ASME publication 81-ENAs-11, 1981, pp. 1-7.

9. McElroy, J.F., "The Status of SPE Water Electrolyzers in Support of Space Energy Systems," Hamilton Standard Division, United Technologies Corporation, April 1992.

10. Keiski, R.L., *The Water-Gas Shift Reaction in Nonisothermal Conditions Over an Iron Oxide/Chromium Oxide Catalyst*, University of Oulu Printing Center, Oulu, Finland, 1991, pp. 2-13.

11. Carr, M.H., *The Surface of Mars*, Yale University Press, New Haven, CT, 1981.

12. Kaganer, M.G., *Thermal insulation in cryogenic engineering*, Israel Program for Scientific Translations Ltd., Jerusalem, 1969, pp. 117-120.

13. Nolan, P.E., "Separating Carbon Monoxide from Carbon Dioxide For Mars Oxygen Production Using Catalytic Disproportionation of Selective Adsorption," M.S. Thesis, Materials Science and Engineering Department, University of Arizona, Tucson, AZ, 1992.

14. Kaloupis, P., Nolan, P.E., and Cutler, H., "Martian Resource Utilization," *Space Power*, in press.

15. Pratt, B.S. and Pratt, D.T., "An Interactive Code for Calculation of Gas-Phase Chemical Equilibrium: EQLBRM", NASA CR-168337, Department of Mechanical Engineering, University of Washington, April 1984.

16. Isenberg, A.O., "Three Man Solid Electrolyte Carbon Dioxide Electrolysis Breadboard," Final Report, Contract No. NAS9-17590, Science and Technology Center, Westinghouse Electric Corporation, Pittsburgh, PA, 1989.

17. "Dynamic Isotope Power Systems (DIPS) for Space Exploration - Technical Information," Rockwell International, Rocketdyne Division, August 1992,

18. Hartman, R.F., "Modular RTG Technology Status," *Proceedings, 25th Intersociety Energy Conversion Engineering Conference*, August 12-17, 1990, Vol. 1, pp. 235-238.

19. Masters, A.I., "Investigation of Light Hydrocarbon Fuels with Flox Mixtures as Liquid Rocket Propellants," Final Report, NASA CR-54445, Pratt & Whitney Aircraft, Sept. 1, 1965.

20. Masters, A.I., Visek, W.A., and Carroll, R.G., "Survey of LOX/Hydrocarbon Combustion and Cooling," NASA TR N89-126471, Pratt & Whitney Aircraft/ United Technologies Corp., p. 445.

21. Kramer, R. and Martin, J., "Undeveloped Rocket Cycle Applications to Advanced Earth-to-Orbit Transportation," AIAA Paper No. 90-2438, 26th AIAA/SAE/ASME/ASEE Joint Propulsion Conference, Orlando, FL, July 16-18, 1990.

22. Cook, R.T. and Kirby, F.M., "LOX/Hydrocarbon Combustion and Cooling Survey," NASA Technical Report N89-12648, Rockwell International/Rocketdyne Division, 1989, pp. 472-473.

23. Mercer, S.D., and Rousar, D.C., "Aerojet Tech Systems Company Contribution to LOX/HC Combustion and Cooling Technology," NASA TR N89-12646, Aerojet Tech Systems Company, 1989, pp. 396, 398, 404-405.

24. Nielson, C.E. and Csomor, A., "Advanced Launch System Propulsion Focused Technology Liquid Methane Turbopump Technical Implementation Plan, "NASA CR-183681, Rockwell International/ Rocketdyne Division, May 25, 1989.

25. Martin, J.A., "Hydrocarbon Rocket Engines for Earth-to-Orbit Vehicles," *Journal of Spacecraft and Rockets*, Vol. 20, 1983, pp. 249-256.

26. Linne, D.L., "Performance and Heat Transfer Characteristics of a Carbon Monoxide/Oxygen Rocket Engine," NASA Lewis Research Center, Cleveland, OH, 1992.

27. Linne, D.L., "Carbon Monoxide and Oxygen Combustion Experiments: A Demonstration of Mars *In Situ* Propellants," AIAA Paper 91-2443, June 1991.

28. Linne, D.L., and Meyer, M.L., "Technical Prospects for Utilizing Extraterrestrial Propellants for Sapce Exploration," NASA-TM-105263, NASA Lewis Research Center, 1991.

29. Wadel, M.F., and Roncace, E.A., "Propulsion Systems Using *In Situ* Propellants for a Mars Ascent Vehicle," AIAA Paper 92-3445, July 1992.

30. Armstrong, E.S., "Cooling of *In Situ* Propellant Rocket Engines for Mars Missions," NASA-TM-103729, NASA Lewis Research Center, Cleveland, OH, 1991.

31. Roncace, E.A., "In Situ Propellant Rocket Engines for Mars Mission Ascent Vehicle," AIAA Paper 91-2445, June 1991.

32. *Titan IV/Centaur User's Guide*, General Dynamics, Oct. 1992.

33. Cannon, J., Boeing Defense and Space Group, Seattle, WA, Personal Communication, April 1993.

34. Arnold, J.O.; Tauber, M.E.; and Goldstein, H.E.; "Aerobraking Technology for Crewed Space Transportation Systems," Paper No. IAF-92-0764, 43rd Congress of the International Astronautical Federation, Washington D.C., Aug. 28- Sept.5, 1992

35. Williams, S.D., Gietzel, M. M., Rochelle, W.C., and Curry, D.M., "TPS Design for Aerobraking at Earth and Mars," NASA TM 104739, Lyndon B. Johnson Space Center, August 1991.

36. NASA News, Release No. 71-119K, Project: Apollo 15, July 15, 1971, pp. 77-85.

37. Seal, M., Automotive Engineering Department, Western Washington University, Bellingham, WA, Personal Communication, March, 1993.

38. Isakowitz, S.J., *International Reference Guide to Space Launch Systems*, American Institute of Aeronautics and Astronautics, Washington, DC, 1991.

39. Jordan, J., Boeing Defense and Space Group, Seattle, WA, Personal Communication, March, 1993.

40. Larson, W.J., and Wertz, J.R., eds., *Space Mission Analysis and Design*, Second Edition, Microcosm Inc. and Kluwer Academic Publishers, 1992, pp. 672-673.

41. Quan, C., McDonnell Douglas Space Systems Company, Huntington Beach, CA, Personal Communication, April, 1993.

42. Farliss, D., Jet Propulsion Laboratory, Pasadena, CA, Personal Communication, June 1993.

43. Sergeyevsky, A.B., Snyder, G.C., and Cunniff, R.A., *Earth to Mars Ballistic Mission Opportunities, 1990-2007*, Publication 82-43, Jet Propulsion Laboratory, Pasadena, CA, 1983.

44. Tauber, M., et al., "Aerobraking Design Studies for crewed Mars Missions," AIAA Paper 91-1344, June 1991.

45. Regan, F.J., *Vehicle Re-Entry Dynamics*, American Institute of Aeronautics and Astronautics, Washington, DC, 1984, pp. 100-1.

46. Clapp, M., "Comparison of Mars-Produced Methane and Carbon Monoxide," AIAA Paper 91-2442, June 1991.